

NOVEL APPROACHES IN MODELING INTEGRATED POWER  
TRANSMISSION AND DISTRIBUTION SYSTEM WITH DISTRIBUTED  
ENERGY RESOURCES AND CONTROLS

by

Arun Suresh

A dissertation submitted to the faculty of  
The University of North Carolina at Charlotte  
in partial fulfillment of the requirements  
for the degree of Doctor of Philosophy in  
Electrical Engineering

Charlotte

2021

Approved by:

---

Dr. Sukumar Kamalasan

---

Dr. Yogendra Kakad

---

Dr. Abasifreke Ebong

---

Dr. Ertunga Ozelkan



## ABSTRACT

ARUN SURESH. Novel Approaches in Modeling Integrated Power Transmission and Distribution System with Distributed Energy Resources and Controls. (Under the direction of DR. SUKUMAR KAMALASADAN)

In recent years the grid modernization and rapid growth in distributed energy resources due to environmental consciousness have resulted in distribution grids becoming more active which has led to significant interaction between transmission and distribution grids. In this dissertation, novel approaches in modeling and management tools are proposed considering integrated power transmission and distribution systems with Distributed Energy Resources (DERs). First, new power methods for power distribution system considering DERs is proposed in a single-phase, three-phase, and three sequence domain. Second, an integrated transmission and distribution (T&D) grid model where transmission and distribution systems are considered as a single unit is proposed. A coalescing Ybus approach is used to obtain the bus admittance matrix of the combined T&D system. Further, to successfully capture the effect of unbalances in the system at the same time reducing computational burden owing to the larger size, a three-sequence modeling framework is used for a unified system. A three-sequence-based multi-period power flow method is used to accurately capture the time-varying aspects of the system. Next, a three-sequence fault analysis method capable of conducting short circuit analysis on a DER integrated unbalanced distribution system is developed. All these sequence-based methods are then used for steady-state analysis of the integrated T&D system. Finally, a sensitivity-based coordinated voltage control scheme using reactive power support from DERs is proposed which can lead to reduced voltage regulator operations and tighter voltage profiles. The proposed methods have been validated using large-scale IEEE T&D feeders to prove the real-life implementation capabilities of the models and tools.

## DEDICATION

This dissertation is wholeheartedly dedicated to my loving mother Asha for being my first teacher and my father Suresh for being a pillar of strength with his wise words of wisdom. I am thankful to their prayers and blessings of the Almighty which enabled me to pursue this research, and will undoubtedly continue to inspire my contributions to the world. This dissertation is also dedicated to my wife Greeshma and my sister Amrutha.

## ACKNOWLEDGEMENTS

I would like to express my sincere gratitude and appreciation to the wisest and kindest people who have generously extended their expertise and support all through the completion of this dissertation, and those of whom I was tremendously fortunate enough to have crossed paths with at the most crucial, yet right times;

First, foremost and throughout, my advisor, mentor and guide Dr. Sukumar Kamalasan, a man of principles, and whose genius has been the inspiration and motivation all these years, who convincingly instills the spirit of research in the lives of his students, whose mentorship is deeply indebted for and, under whose valuable guidance this dissertation was completed; I would like to express my sincere gratitude to the committee members of Dr. Yogendra Kakad, Dr. Abasifreke Ebong, and Dr. Ertunga Ozelkan. I would also like to express my sincere gratitude to Dr. Sumit Paudyal of Florida International University for his valuable guidance. I would also like to acknowledge fellow students in Power Energy and Intelligent System Laboratory (PEISL) for their constant support throughout this study. The graduate assistantships provided by the Graduate School, and funded by Duke Energy, National Science Foundation (NSF) and Department of Energy (DOE) are sincerely appreciated. Finally, I would like to express my sincere thanks to my parents, sister and wife for their time and support and inspiration through out this journey.

## TABLE OF CONTENTS

LIST OF TABLES	xii
LIST OF FIGURES	xv
CHAPTER 1: INTRODUCTION	1
1.1. General Background	1
1.2. Motivation	4
1.3. Objectives and Contribution of the Dissertation	6
1.4. Dissertation outline	9
CHAPTER 2: INJECTION CURRENT SENSITIVITY BASED SINGLE PHASE DISTRIBUTION SYSTEM LOAD FLOW	12
2.1. Introduction	12
2.2. Research Contribution	15
2.3. Single Phase Distribution System Modeling	15
2.3.1. Power Delivery Elements	15
2.3.2. Power Conversion Elements	16
2.4. Injected Current Sensitivity based Single Phase Power Flow	18
2.5. State of the art methods	21
2.5.1. Forward-Backward Sweep Power Flow	21
2.5.2. Z-bus Approach - Fixed-point Iteration	23
2.6. Single-phase Test Distribution Systems	25
2.6.1. Small Test Feeder-123 node	25
2.6.2. Large Test Feeder - 2522-node	25

2.7. Simulation Results	25
2.7.1. 123-node test system	25
2.7.2. 2522-node test system	29
2.8. Single Phase Distribution Load Flow Tool	30
2.9. Summary	31
CHAPTER 3: INJECTION CURRENT SENSITIVITY BASED THREE PHASE AND THREE SEQUENCE LOAD FLOW	33
3.1. Introduction	33
3.2. Research Contribution	34
3.3. Three Phase Distribution System Modeling	35
3.3.1. Distribution Lines	36
3.3.2. Load Tap Changers and Voltage Regulators	38
3.3.3. Transformers	40
3.3.4. Load Models	42
3.4. Injected Current Sensitivity based Three Phase Power Flow	44
3.4.1. ICS based Power Flow without DERs	45
3.4.2. ICS based Power Flow with DERs	49
3.4.3. Simulation Results	55
3.5. Three Sequence Based Steady State Analysis	61
3.5.1. Advantages of Sequence Based Methods	62
3.5.2. Sequence Components	63
3.5.3. Time Complexity and Computational Improvement	65
3.6. Three Sequence Load Flow Analysis	67

3.7. Three Sequence Continuation Power Flow	72
3.7.1. CPF Formulation	72
3.8. Three Phase Distribution Load Flow Tool	77
3.9. Summary	79
CHAPTER 4: MULTI-PERIOD POWER FLOW OF THREE PHASE DISTRIBUTION SYSTEM	80
4.1. Introduction	80
4.2. Research Contribution	82
4.3. Modeling of Control Devices	82
4.3.1. Voltage Regulators	83
4.4. Proposed MPF with DERs	87
4.5. Applications of Multi-Period Power Flow	87
4.5.1. Impact of load and DER variation on grid voltage	89
4.5.2. Impact of DER location on operation of voltage regu- lators	90
4.5.3. Approximate Voltage Stability Margin Assessment	94
4.6. Three Phase Time Series Analysis Tool	97
4.7. Summary	98
CHAPTER 5: FAULT ANALYSIS OF UNBALANCED DISTRIBUTION SYSTEM USING SEQUENCE COMPONENTS	99
5.1. Introduction	99
5.2. Research Contribution	102
5.3. Power System Modeling	103
5.3.1. Formation of Sequence Bus Impedance Matrix	105

5.3.2.	Buses with Missing Phases	106
5.4.	State of the Art Fault Analysis Methods	107
5.4.1.	Phase based fault Analysis	107
5.4.2.	Existing Sequence based fault Analysis	108
5.5.	Proposed Sequence based fault Analysis	109
5.5.1.	Sequence Components	109
5.5.2.	Single Line to ground fault	112
5.5.3.	Line to Line fault	114
5.5.4.	Double Line to Ground fault	116
5.5.5.	Three Phase to Ground fault	121
5.5.6.	Bus Voltages during fault	121
5.5.7.	Faults with B and C phase as Reference	121
5.6.	Simulation Results	122
5.6.1.	Comparison of Proposed Method with Existing Sequence based method and Phase based method	122
5.6.2.	Validation of Proposed Method with state-of-the-art Fault Analysis results	125
5.6.3.	Fault analysis on buses with missing phases	127
5.6.4.	Fault analysis with B and C phase as Reference	127
5.7.	Three Phase Fault Analysis Tool	129
5.8.	Three Sequence Based Distribution System Analysis Tool	129
5.9.	Summary	129

CHAPTER 6: THREE-SEQUENCE UNIFIED TRANSMISSION AND DISTRIBUTION STEADY STATE ANALYSIS	131
6.1. Introduction	131
6.2. Research Contribution	134
6.3. Methods of modeling Transmission busloads in Integrated T&D framework	134
6.3.1. Multiplication Factor(MF) Based Methods	135
6.3.2. Non Multiplication Factor Based Methods	139
6.4. State of the art method in Integrated T&D load flow	144
6.4.1. Decoupled Approach of T&D System	144
6.5. Proposed Unified Approach of T&D System	147
6.5.1. Stacked Ybus Approach for Unified Ybus	149
6.5.2. Challenges and Solutions	151
6.6. Power Flow Analysis	153
6.6.1. Single Phase Integrated T&D System	153
6.6.2. Three Phase Integrated T&D System	156
6.7. Voltage Stability Assessment	161
6.7.1. Integrated T&D Multi-Period Power Flow Model(MPF)	162
6.7.2. Integrated T&D Continuation Power Flow Model	169
6.8. Fault Analysis	173
6.9. Sequence Based Integrated T&D System Analysis Tool	174
6.10. Summary	175

CHAPTER 7: SENSITIVITY BASED DYNAMIC COORDINATED CONTROL FOR GRID SUPPORT USING DISTRIBUTED ENERGY RESOURCES	177
7.1. Introduction	177
7.2. Research Contribution	179
7.3. Realtime DER Integrated Distribution System Modeling	179
7.3.1. Voltage Regulators	179
7.3.2. Realtime Implementation with OPAL-RT	181
7.3.3. DER Integration to Distribution Grid	183
7.3.4. Control of DERs	185
7.4. Voltage Control using ADMM	186
7.4.1. ADMM based Transfer Function Identification	187
7.4.2. Kalman Filter based State Estimation	190
7.4.3. Discrete Linear Quadratic Regulator Control	191
7.4.4. Simulation Results	191
7.5. Summary	199
CHAPTER 8: CONCLUSIONS AND FUTURE WORK	200
REFERENCES	205
APPENDIX A: Fault Analysis on IEEE Test Distribution Feeders	216

## LIST OF TABLES

TABLE 2.1: Size of Jacobian	22
TABLE 2.2: Case 1:123 bus system - Power Flow with capacitor ON and voltage regulators (taps = 0,0,0,0)	27
TABLE 2.3: Case 2:123 bus system - Power Flow with capacitor ON and voltage regulators (taps = 0,1,2,-1)	28
TABLE 2.4: Case 1 - Power Flow with capacitor ON and voltage regulators (taps = 0,0,0,0)	29
TABLE 2.5: Case 2 - Power Flow with capacitor ON and voltage regulators (taps = 0,6,6,0)	30
TABLE 3.1: Y-bus for Various Transformer Connections from [1]	41
TABLE 3.2: Test Systems	55
TABLE 3.3: Comparison of NR and ICS for various loading	57
TABLE 3.4: Comparison of NR and ICS for various R/X	57
TABLE 3.5: Summary of load flow using ICS	58
TABLE 3.6: Summary of PV bus in 123 bus system	58
TABLE 3.7: No of mathematical operations.	66
TABLE 3.8: Total No of computations for a phase method.	66
TABLE 3.9: Total No of computations for a positive sequence method.	66
TABLE 3.10: Total No of computations for a negative and zero sequence method.	67
TABLE 3.11: Improvement in computation.	67
TABLE 3.12: Substation Power.	71
TABLE 3.13: Size of matrices.	76
TABLE 3.14: Iterations to converge.	78

TABLE 4.1: Impact of DER location on operation of voltage regulators	93
TABLE 5.1: Comparison of Per Unit Voltage during LLLG Fault	122
TABLE 5.2: Comparison of Fault Current (Amps) for Buses with missing phases	127
TABLE 5.3: Comparison of LLG Fault on CA phase on IEEE 13 bus system	128
TABLE 6.1: Multiplication Factor per phase	136
TABLE 6.2: Transmission boundary bus load distribution using M1	136
TABLE 6.3: Net Load on 3 distribution system	137
TABLE 6.4: Transmission boundary bus load distribution using M2	137
TABLE 6.5: Net Load on 3 distribution system	138
TABLE 6.6: Transmission boundary bus load distribution using M3	139
TABLE 6.7: Transmission boundary bus load distribution using M4	140
TABLE 6.8: Transmission boundary bus load distribution using M5	141
TABLE 6.9: Transmission boundary bus load distribution using M6	142
TABLE 6.10: Loading Factor per phase	143
TABLE 6.11: Transmission boundary bus load distribution using M7	143
TABLE 6.12: Comparison of merits and demerits of each method	144
TABLE 6.13: Average Computational Time for Convergence	169
TABLE 6.14: Iterations to converge.	169
TABLE 6.15: Fault Currents in Amps for 9-123 T&D System.	175
TABLE 7.1: PV integration to Test Feeders	184
TABLE A.1: LLLG and SLG Fault currents in Amps for IEEE 13 bus system	217

TABLE A.2: LL Fault currents in Amps for IEEE 13 bus system	217
TABLE A.3: LLG Fault currents in Amps for IEEE 13 bus system	218
TABLE A.4: LLLG and SLG Fault currents in Amps for IEEE 34 bus system	219
TABLE A.5: LL Fault currents in Amps for IEEE 34 bus system	220
TABLE A.6: LLG Fault currents in Amps for IEEE 34 bus system	221
TABLE A.7: LLLG and SLG Fault currents in Amps for IEEE 123 bus system	222
TABLE A.8: LLLG and SLG Fault currents in Amps for IEEE 123 bus system(cont.)	223
TABLE A.9: SLG Fault currents in Amps for IEEE 123 bus system	224
TABLE A.10: LL Fault currents in Amps for IEEE 123 bus system	225
TABLE A.11: LL Fault currents in Amps for IEEE 123 bus system(cont.)	226
TABLE A.12: LLG Fault currents in Amps for IEEE 123 bus system	227
TABLE A.13: LLG Fault currents in Amps for IEEE 123 bus system(cont.)	228

## LIST OF FIGURES

FIGURE 1.1: Dissertation Outline.	9
FIGURE 2.1: Constant Voltage type DGs	18
FIGURE 2.2: Flowchart of Proposed load flow	21
FIGURE 2.3: Single-phase representation of the IEEE-123 node system	26
FIGURE 2.4: Single-phase representation of the IEEE-8500 node system	26
FIGURE 2.5: Voltage profile with and without PV DG	28
FIGURE 2.6: Load Flow Graphical User Interface	30
FIGURE 2.7: Graphical User Interface flow.	31
FIGURE 3.1: Schematic representation of three phase distribution line .	35
FIGURE 3.2: Schematic representation of Voltage Regulator	38
FIGURE 3.3: Block diagram representation of three phase transformer.	40
FIGURE 3.4: Load modeling (a)Star Connected (b)Delta Connected	43
FIGURE 3.5: Injected Current Sensitivity Based Load Flow	50
FIGURE 3.6: Three phase distribution system with DGs modeled as PV bus	51
FIGURE 3.7: Validation of LF results	59
FIGURE 3.8: Validation of LF results and % Error Plots	60
FIGURE 3.9: DER in 123 bus	61
FIGURE 3.10: PV Bus in 123 bus system	61
FIGURE 3.11: Sequence Components	63
FIGURE 3.12: Distribution line	64
FIGURE 3.13: Sequence component of admittance submatrices	68

FIGURE 3.14: Grouping of Sequence admittance submatrices	69
FIGURE 3.15: Grouping of Sequence current and voltage submatrices	69
FIGURE 3.16: Three Sequence Load Flow.	70
FIGURE 3.17: (a) Comparison of Sequence Load Flow-Phase A (b) Comparison of Sequence Load Flow-Phase B	71
FIGURE 3.18: Comparison of Sequence Load Flow-Phase C	72
FIGURE 3.19: Three sequence distribution continuation power flow.	77
FIGURE 3.20: Comparison of three phase and three sequence CPF.	78
FIGURE 3.21: Distribution Load Flow Tool	78
FIGURE 4.1: Schematic representation of Voltage Regulator	83
FIGURE 4.2: Compensator Circuit (Source: [2])	84
FIGURE 4.3: Operation of voltage regulator	85
FIGURE 4.4: Proposed QSTS Simulation	86
FIGURE 4.5: (a) Load Profile (b) Three phase voltage at node 8 with regulator control OFF	88
FIGURE 4.6: (a) Tap Operation (b) Three phase voltage at node 8 with regulator control ON	88
FIGURE 4.7: (a) Irradiance Profile (b) Three phase voltage at node 8 with regulator control OFF	89
FIGURE 4.8: (a) Tap Operation (b) Three phase voltage at node 8 with regulator control ON	90
FIGURE 4.9: (a) DER far from Sub station (b) A phase voltage profile with and without DER	91
FIGURE 4.10: (a) B phase voltage profile with and without DER (b) C phase voltage profile with and without DER.	91

FIGURE 4.11: (a) DER near to Sub station (b) A phase voltage profile with and without DER	92
FIGURE 4.12: (a) B phase voltage profile with and without DER (b) C phase voltage profile with and without DER.	92
FIGURE 4.13: Location of DERs	93
FIGURE 4.14: B phase voltage profile for case 2-9 with DERs far from substation	95
FIGURE 4.15: A phase voltage profile for case 2-9 with DERs near to substation	96
FIGURE 4.16: Approximate Voltage Stability Margin using MPF.	97
FIGURE 4.17: Distribution Times Series Analysis Tool	97
FIGURE 5.1: Sequence component of impedance submatrices.	104
FIGURE 5.2: Grouping of Sequence impedance submatrices.	104
FIGURE 5.3: Grouping of Sequence current and voltage submatrices.	105
FIGURE 5.4: Formation of sequence impedance matrix for system having nodes with missing phases.	107
FIGURE 5.5: Sequence Components.	109
FIGURE 5.6: Short circuit Analysis with Mutual Coupling.	110
FIGURE 5.7: Single Line to Ground Fault.	112
FIGURE 5.8: Line to Line Fault.	114
FIGURE 5.9: Double Line to Ground Fault.	116
FIGURE 5.10: Double Line to Ground Fault with separate fault impedance.	120
FIGURE 5.11: Three Phase to Ground Fault.	122
FIGURE 5.12: Flow chart of Proposed Fault Analysis.	123

FIGURE 5.13: Fault Current at Bus 4 for LLG and LLLG fault.	124
FIGURE 5.14: Negative sequence Voltage during LLLG fault.	125
FIGURE 5.15: Comparison of Maximum % error for IEEE 13 Bus.	125
FIGURE 5.16: Comparison of Fault Analysis with Benchmark.	126
FIGURE 5.17: (a) A phase Fault current for LLLG Fault on IEEE 34 bus system. (b) B phase Fault current for LLLG Fault on 123 bus system.	126
FIGURE 5.18: SLG fault on phase C.	128
FIGURE 5.19: Distribution Fault Analysis Tool	129
FIGURE 5.20: Sequence Based Distribution System Analysis Tool.	130
FIGURE 6.1: Modelling load at boundary bus in transmission system.	135
FIGURE 6.2: Per phase MF method.	136
FIGURE 6.3: Three phase MF with balanced shunt load.	138
FIGURE 6.4: Three phase MF with unbalanced shunt load.	139
FIGURE 6.5: Balanced shunt load compensation.	140
FIGURE 6.6: Unbalanced shunt load compensation.	141
FIGURE 6.7: Unbalanced shunt load compensation with phase balancing loads.	143
FIGURE 6.8: Multiple Distribution System in detail.	144
FIGURE 6.9: Integrated T&D Decoupled System.	145
FIGURE 6.10: Integrated T&D Unified System.	147
FIGURE 6.11: (a)T&D Unified system (b) Renumbered T&D Unified System.	150
FIGURE 6.12: T&D Unified Ybus	152

FIGURE 6.13: Flowchart of Unified T&D Simulation.	154
FIGURE 6.14: One line diagram of 47-bus T&D system.	155
FIGURE 6.15: Voltage solution and error on transmission circuits.	155
FIGURE 6.16: (a) Voltage solution (b) Angle solution (and error) of 47-bus T&D system obtained from decoupled and unified approaches.	156
FIGURE 6.17: Two configuration of 113-bus T&D system.	157
FIGURE 6.18: (a) Voltage solution (b) Angle solution (and error) of 113-bus T&D system (Case a) obtained from decoupled and unified approaches.	157
FIGURE 6.19: (a) Voltage solution (b) Angle solution (and error) of 113-bus T&D system (Case b) obtained from decoupled and unified approaches.	158
FIGURE 6.20: One line diagram of 3phase T&D system.	158
FIGURE 6.21: Phase Voltage solution of Transmission system with spot load and distribution system	159
FIGURE 6.22: (a) Phase A Voltage (b) Phase B Voltage solution (and error) of T&D system obtained from decoupled and unified approaches	159
FIGURE 6.23: (a) Phase C Voltage (b) Phase A Angle solution (and error) of T&D system obtained from decoupled and unified approaches	160
FIGURE 6.24: (a) Phase B Angle (b) Phase C Angle solution (and error) of T&D system obtained from decoupled and unified approaches	160
FIGURE 6.25: Comparison of Unified Sequence T&D Load Flow with state of the art T&D load flow method	161
FIGURE 6.26: Distribution load flow with different swing bus voltage.	162
FIGURE 6.27: Proposed Integrated T&D Load flow.	164
FIGURE 6.28: One line diagram of T&D system.	165
FIGURE 6.29: (a) PV curves using Positive Sequence T&D method (b) PV curves using Proposed Three Phase T&D method	167

FIGURE 6.30: (a) PV curves of T&D system with constant power load (b) PV curves of T&D system with ZIP load	167
FIGURE 6.31: Maximum loading factor.	168
FIGURE 6.32: Three sequence T&D continuation power flow.	170
FIGURE 6.33: Comparison of CPF and MPF.	171
FIGURE 6.34: VSM with Regulator Control.	172
FIGURE 6.35: PV Curves of 14-8500 T&D System.	173
FIGURE 6.36: IEEE 9-123 T&D system	174
FIGURE 6.37: Comparison of different faults currents at bus 7 Distribu- tion system	174
FIGURE 6.38: Sequence Based Distribution System Analysis Tool.	175
FIGURE 7.1: Voltage comparison at test node.	180
FIGURE 7.2: Voltage Regulator Control	180
FIGURE 7.3: Regulator Taps	181
FIGURE 7.4: Real Time Implementation using OP 5707	182
FIGURE 7.5: IEEE 123 Bus Distribution Test Feeder	183
FIGURE 7.6: PV farm design	184
FIGURE 7.7: Control Topology	184
FIGURE 7.8: Closed-loop control architecture.	187
FIGURE 7.9: Overall algorithm flowchart.	189
FIGURE 7.10: IEEE 123 Bus Distribution Test Feeder with DERs.	192
FIGURE 7.11: Voltage at test node.	193
FIGURE 7.12: (a) Load variation(b) Voltage variation with load variation.	193

FIGURE 7.13: (a) $\Delta V$ at target node (b) Reactive power reference of DER1.	194
FIGURE 7.14: Taps operation of Regulator 160-67.	194
FIGURE 7.15: Voltage comparison at test node.	195
FIGURE 7.16: Location of DERs for different test cases.	196
FIGURE 7.17: Voltage error at target node for case 1.	196
FIGURE 7.18: Voltage error area comparison for different cases.	197
FIGURE 7.19: (a) Reactive power of each DER (b) Total Reactive power of DERs.	197
FIGURE 7.20: Voltage comparison at test node.	198
FIGURE A.1: IEEE 13 Bus Distribution Test Feeder	216
FIGURE A.2: IEEE 34 Bus Distribution Test Feeder	216
FIGURE A.3: IEEE 123 Bus Distribution Test Feeder	218

## CHAPTER 1: INTRODUCTION

### 1.1 General Background

With new grid edge technologies like advanced inverters, demand response (DR), and Advanced Distribution Management Systems (ADMS), the power distribution circuits are becoming more active. The high proliferation of distributed energy resources (DERs) has resulted in an increased coupling between distribution and transmission networks. The dynamic and intermittent nature of DERs will lead to the increased interaction of transmission and distribution system operators. The resources in the LV/MV grid will have a significant impact on the operations of bulk transmission systems. There has been a sudden growth of research interest in co-simulation platforms for solving transmission and distribution (T&D) systems simultaneously for steady-state and dynamic analysis. An integrated grid modeling approach combining transmission and distribution (T&D) can help capture these unprecedented interactions between distribution and transmission systems.

The transmission and distribution circuits are analyzed independently in existing steady-state analysis tools. While analyzing the transmission system, all the distribution systems connected are reduced to lumped loads representing total loads and losses of distribution systems. On the other hand, the transmission system is represented using a constant voltage source with infinite capacity while solving distribution systems [3]. The existing electromagnetic transient (EMT) simulators can be used to solve a combination of transmission and distribution systems as one unit. But due to computational complexities, it may not be scalable for large-scale systems. Therefore, to reduce the computational burden of EMT simulations, co-simulation platforms were developed that can combine EMT simulation and transient stability

analysis. Recently co-simulation platforms capable of solving transmission and distribution Systems (T&D) in the phasor domain is developed for several applications like power flow [4, 5], contingency analysis [6] and dynamic simulation [4].

Load flow(LF) analysis for power system planning and analysis is used to determine voltage magnitude and phase angle at each bus, the injected power by each generator, power flowing through each branch, and also the total active and reactive power losses in the system [2,7]. A power distribution system consists of various components classified generally into 2 categories, the power delivery components, and the power conversion components [8]. The power delivery components are those which transport energy from one point to another such as distribution lines, voltage regulators, transformers. The power conversion components convert energy from the electrical domain to other forms and vice versa such as loads and distributed energy resources, and energy storage devices. To perform load flow analysis of the distribution system, models of these components should be developed in detail.

The existing three-phase power flow approaches require the solution of a set of  $6N$  nonlinear simultaneous equations, for an  $N$  bus system. This can lead to a huge computational burden for larger systems. A method based on the sequence components frame can be used to solve a three-phase unbalanced power flow. The power flow problem is decomposed into sub-problems where the positive sequence sub-problem is solved by using a nonlinear iterative scheme and the other sub-problems are formulated into two sets of linear simultaneous equations [9, 10]. This would reduce the size of the Jacobian from  $6N \times 6N$  to  $2N \times 2N$  and can lead to huge computational advantages.

The distribution system planning analysis was traditionally focused on steady-state power flow simulations and protection studies. But with new grid edge technologies photovoltaic (PV), battery energy storage (BES), electrical vehicles (EVs) advanced inverters, there has been a shift in distribution system planning [11]. To analyze

the interactions of new grid edge technologies such as snapshot analysis may not be adequate as only considering peak periods can lead to over-estimation of normal operating issues. With the high proliferation of distributed energy resources, it is indispensable to extend steady-state analysis to a multi-period analysis to capture the time-dependent variations in the active distribution system. A multi-period power flow analysis (MPF) is required to accurately capture the time-varying aspects of the system. Using accurate load and generation time-series data, an MPF simulation can be used to quantify the magnitude and duration of the impact of DERs accurately. MPF can also be used to conduct vulnerability analysis where the strength of DERs and how much vulnerable the grid would be in an event of loss of DERs can be analyzed.

Short circuit analysis or fault analysis constitutes a significant part of power system study and is used for obtaining the proper ratings of the protection elements like relays and circuit breakers. The last decade has seen a rapid growth of inverter-based DERs and this has led to a change in the dynamics of short circuit current on the bulk power systems. This also leads to new issues for consideration while setting relay elements. In contrast to conventional generators which have universal short-circuit response characteristics, the inverter fault response is based on specific inverter control system designs [12]. During faults, the inverter restricts the maximum short-circuit current to limit thermal overloads of power electronics. In a vast majority of the software packages made use of today by the industry, it is the sequence components based fault analysis algorithm that is employed. If the existing sequence components methodology which assumes a balanced system is used for fault analysis in a distribution system that has untransposed lines, multi-phase laterals, and many other sources of unbalances, it will result in deviations from actual current and voltage values during fault. Accurate sequence voltages at DER terminals during fault will be required to find the amount of fault current that DER should inject during fault

to support the grid.

For a distribution network, being in direct contact with the user, the power supply reliability and quality is of prime importance. The reactive power compensation in the distribution network can lead to improved power quality of users, a better utilization rate of the power transformer, and reduced network losses. The penetration level of DERs can be fairly increased if voltage profiles can be optimally balanced. Moreover, if the voltage profile is kept at an optimal level, the losses in the distribution network can be reduced as well. As the integration of DERs causes bidirectional power flow, conventional voltage and reactive power management may not be effective at all operating conditions. The two main control methods for DER units are decentralized control and centralized control [13]. The local control is achieved by controlling the reactive power of the DG unit locally, without coordination with other DGs connected in the grid. Centralized control on the other hand is taken into account optimum sharing of reactive power between different DG units. A coordinated control architecture for multiphase DERs using a sensitivity-based method can be used for coordinating DERs to achieve a common objective.

## 1.2 Motivation

With distribution systems becoming more active, the interactions between transmission and distribution systems are increasing. It is important to have a better understanding of the coupling of transmission and distribution systems to maintain secure operations of the power system. The efficient way to examine such interactions in smart grid systems is to establish a simulation process that integrates transmission and distribution systems. In the existing state-of-the-art approaches, there is an absence of an appropriate benchmark to validate the results. Currently, electromagnetic transient (EMT) simulators are used to check the validity of results. A unified co-simulation approach in the phasor domain can serve as a benchmark for existing approaches. Also, single-phase PV-based DG can aggravate imbalance in the

power system due to the asymmetrical placement of DG on the three phases. It is extremely critical to have an integrated T&D framework with both transmission and distribution modeled in three-phase detail in the existing decoupled approach of T&D modeling.

The steady-state response of power systems (power flow analysis) using Integrated T&D is challenging because numerical methods used for power flow analysis which are stable for transmission networks may not work as required for distribution networks. For example, the Newton Raphson method that is efficient for transmission systems may fail if used in the distribution system and the Forward Backward sweep would fail (or require system-dependent modifications) when used for transmission system analysis. A Current Injection based method is a promising candidate that can solve weakly meshed systems as well as radial systems effectively. But the Jacobian size and the elements updated per load flow iteration in the case of traditional current injection-based approaches depends on the number of DERs (modeled as PV bus). A current sensitivity-based approach can be utilized for modeling multiphase DERs with voltage control capability. Any three-phase power flow approaches require a solution of  $6N$  nonlinear simultaneous equations where  $N$  is the total number of buses. To reduce this computational complexity, a method based on the sequence components frame can be utilized. The three-phase unbalanced power flow is decomposed into sub-problems (positive, negative, and zero sequences sub-problems) of which only positive sequence sub-problems should be solved iteratively. This would reduce the size of the Jacobian from  $6N \times 6N$  in a 3 phase power flow to a  $2N \times 2N$ . This is extended to continuation power flow can be used to analyze voltage stability of unbalanced distribution systems with a considerably less computational burden.

The steady-state analysis is executed at snapshots in time with an extreme condition, such as the peak load period. With the advent of new grid edge technologies like DERs, smart inverters, EVs such snapshot analysis may not be adequate as only

considering peak periods can lead to over-estimation of normal operating issues. A multi-period analysis is indispensable to capture the time-dependent variations in active distribution systems with high penetration of distributed energy resources.

Short circuit analysis or fault analysis is used to derive ratings of protection devices is conventionally conducted based on the symmetrical sequence networks. The basic assumption is that the system is balanced which is not true in the case of distribution systems. Therefore the application of existing sequence components methodology for distribution fault analysis will result in deviations from actual values. Phase-based methods are prominently used for fault analysis for distribution systems, but with the proliferation of DERs which only inject positive sequence current during a fault, it is better to have a sequence-based fault analysis procedure. Therefore, a sequence-based fault analysis method that can take care of all unbalances in the distribution system is indispensable for DER integrated power systems.

The intermittent nature of DERs can affect the reliability and quality of power. The frequent use of control devices like voltage regulators and SVCs can lead to more cost of operation even though the cost of generation from a DER is minimal. The penetration level of DERs can be increased if the voltage profile is maintained at an optimal level which also leads to lower power losses in the distribution network. A coordinated voltage control scheme using reactive power support from DERs itself can result in reduced voltage regulator operations and tighter voltage profiles.

### 1.3 Objectives and Contribution of the Dissertation

Based on the above discussions, this dissertation aims to answer the following research questions:

- Is there a way to have an integrated T&D framework that can accurately capture the interaction between transmission and distribution system?
- What frame is best suited, phase or sequence in order to efficiently conduct the

steady state analysis of the T&D system?

- Are there numerical methods for power flow analysis that are stable for both transmission and distribution systems?
- Are these methods computationally efficient considering the bigger size of T&D systems with a large number of DERs integrated into them?
- How would the voltage stability of an integrated T&D system vary when a positive sequence transmission system is replaced by three phase transmission system?
- Are there computationally efficient methods that can be used to conduct voltage stability analysis of the T&D system.
- There has been a recent trend towards DERs supporting the grid during an abnormal condition. Is the present sequence-based short circuit analysis capable of efficiently handling this?
- The intermittent nature of DERs can affect the quality of power in a DER integrated grid. Can these DERs themselves be efficiently used to enhance the reliability of the grid?

The major contributions from this dissertation can be summarized as follows:

- A novel injected current sensitivity-based load flow method for distribution system is proposed which can be used to model DERs with voltage control capability.
- A load flow tool for single-phase distribution system is developed which can be used to solve any distribution system load flow using state-of-the-art methods and the proposed method.

- A generalized bus admittance matrix (Y-bus) is formulated which includes distribution lines voltage regulators, and different transformer connections.
- A new injected current sensitivity-based three phase load flow method is developed which can cater to multi-phase distribution lines connected to Delta/Star ZIP loads. Multi-phase DERs with voltage control capability is modeled as PV bus using a reactive power sensitivity based approach.
- A three sequence based load flow and continuation power flow to solve unbalanced three phase distribution system is developed.
- A multi-period load flow method with detailed modeling of voltage regulating devices and distributed energy resources is proposed to analyze the influence of DERs on control devices and how their operation impacts the grid.
- A three sequence based fault analysis(TSFA) of distribution system considering mutual coupling is proposed which can be used to analyze all shunt faults in an unbalanced distribution system. It can also be extended to conduct short circuit analysis on DER integrated distribution system.
- An integrated T&D model where transmission and distribution systems are modeled considering all the three phases including unbalances and all load types are proposed.
- The steady-state load flow and fault analysis of integrated T&D system is conducted using three sequence methods developed.
- A multi-period integrated T&D load flow approach is proposed that can provide insights on voltage stability margin. Also, the three sequence CPF developed is used to analyze voltage stability of T&D system

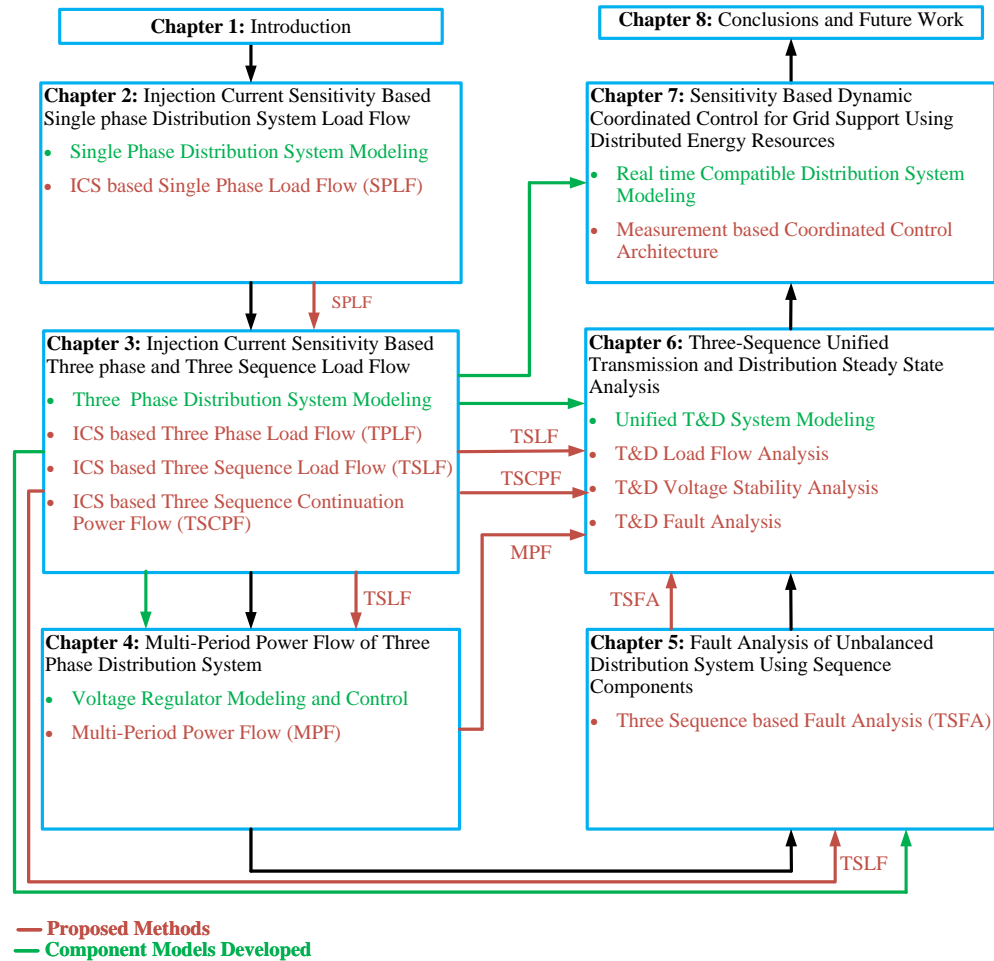


Figure 1.1: Dissertation Outline.

- A coordinated control architecture for multiphase DERs using measurement-based transfer function identification is proposed which can be used for dynamic DER selection and voltage support.

#### 1.4 Dissertation outline

The dissertation outline is as follows and summarized in Fig. 1.1:

In Chapter 2 a comprehensive literature review of the state-of-the-art distribution power flow methods is done. The modeling of distribution components in single-phase detail is illustrated. The DER is modeled in power factor control mode as well as in voltage control mode. A computationally efficient single phase load flow (SPLF)

algorithm based on injected current sensitivity (ICS) for distribution systems with high penetration of DERs is proposed where the DERs can be modeled using voltage control capability.

Chapter 3 extends the proposed method to the three-phase distribution network (TPLF). Models for distribution lines, capacitors, voltage regulators, load models, and relevant transformer connections are derived and a stacked bus admittance matrix (Y-bus) is formulated. Multiphase DER with voltage control capability is modeled as PV bus using a reactive power sensitivity based approach. The three sequence component framework is introduced and an unbalanced power flow (TSLF) and continuation power flow (TPCPF) based on the three sequence components is proposed where three-phase unbalanced power flow is decomposed into three separate subproblems. The single phase load flow (SPLF) derived in the first chapter is used for the positive sequence subproblem.

In Chapter 4 a multi-period power flow (MPF) based on three sequence is proposed to accurately capture the time-varying aspects of the system. A QSTS framework with detailed modeling of discrete control devices and distributed energy resources is proposed to analyze the influence of DERs on control devices and how their operation impacts the grid. MPF is also used to find how DER location affects regulator operation and steady-state grid voltage.

In chapter 5 a three sequence based fault analysis(TSFA) of distribution system considering mutual coupling is proposed. Pre-fault voltages are calculated using TSLF. The method is suitable to be used for steady-state fault analysis of DER integrated power distribution systems and can also be used for short circuit analysis on integrated transmission and distribution systems. A tool to perform sequence based steady state analysis of distribution system is developed.

In chapter 6 a unified transmission and distribution modeling considering all the three phases is proposed. Three sequence load flow approaches are used to conduct

load flow analysis. A multi-period integrated T&D load flow approach is proposed which aids in obtaining insights on voltage stability margin. Also, the three sequence CPF developed is used to get a more accurate voltage stability margin. Finally, the steady state short circuit analysis of the T&D system is conducted using the three sequence based fault analysis developed. A tool to perform sequence based steady state analysis of integrated T&D system is developed.

In Chapter 7 distribution systems are modeled to run in real-time in the OPAL-RT real-time simulator. A coordinated control architecture for multiphase DERs using measurement-based transfer function identification is proposed. ADMM based transfer function identification scheme is used to obtain sensitivity between voltage deviation at a node and the reactive power injection of DERs. The algorithm is utilized for voltage support and also to analyze scenarios like the loss of one or more DERs during operation.

## CHAPTER 2: INJECTION CURRENT SENSITIVITY BASED SINGLE PHASE DISTRIBUTION SYSTEM LOAD FLOW

### 2.1 Introduction

Load flow (LF) analysis or steady-state analysis for distribution system (DS) are used to determine voltage magnitude and phase angle at each bus, the injected power by each generator, power flowing through each branch, and also the total active and reactive power losses in the system [2, 7]. Also, load flow helps to determine proper settings and locations for devices such as voltage regulators and reactive power compensating devices. Conventional methods of LF such as Gauss-Seidel [7], Newton-Raphson [14], fast decoupled [15–17], that are widely used for transmission systems (TS) exhibit poor convergence behavior when applied to DS. Therefore conventional load flow methods that were used to do the steady-state analysis of transmission systems have been modified to work for Distribution systems. Various attempts have been made to modify the Newton methods to make them applicable for load flow analysis on the distribution system.

One efficient method among those, called current injection method CIM, is based on the nodal current injections written in rectangular coordinates [18–22]. Another approach that uses complex bus admittance matrix and equivalent current injections called Gauss Implicit methods is presented in [23–25]. Using Ohm's law, voltage solutions at each iteration are obtained by inverting the  $Y - Bus$  resulting in a set of  $3n$  equations for an  $n$  bus 3 phase system which leads to less computational complexity and memory usage compared to Newton Raphson methods which require computation of Jacobian in each iteration. The convergence of the Zbus method is dependent upon the number of PV buses in the system. The rate of convergence

is comparable to the Newton-Raphson approach when there are no PV buses in the system and deteriorates as the number of PV buses increases.

Another type of distribution system load flow algorithm is based on backward-forward sweep (BFS) approach [26–34]. The BFS based algorithm consists of two steps, backward sweep for branch current computations and forward sweep for bus voltage computations. Kirchhoff’s current law is the backbone for the backward sweep and Kirchhoff’s voltage law is the base for the forward sweep. All of these LF methodologies are having enough potential to compute precise LF solutions. However, there are certain computational limitations are associated with these approaches [35,36]. All the prevailing BFS based approach in the literature utilizes time-consuming branch and bus numbering schemes to compute the branch currents and bus voltages. Inclusion of the mathematical model of distributed system components such as transformer, regulators, and capacitor in such sweep based approach is also a complicated task. Also, in the conventional BFS technique, computation of receiving end bus voltage is dependent upon the corresponding sending end bus voltage. This sequential computation requires considerably large computation time.

The matrix-based BFS based methods have addressed the complexity associated with primitive BFS based approaches [26–34]. The bus injection to branch current matrix (BIBC), branch current to bus voltage matrix (BCBV), and direct load flow (DLF) matrix have been developed by the authors in [37, 38] to acquire the load flow solution of the distribution system. The backward sweep is performed using the BIBC matrix for branch current computations and the forward sweep is performed using BCBV and DLF matrix to compute the bus voltage. But, the involvement of two direct multiplications, between BIBC and BCBV, and between DLF and current injection matrix increases the computational burden and also provides a research scope for further improvement. The load flow methodology developed [39] in is also an advanced direct load flow method utilizing the network topology based approach.

This solution technique requires direct multiplication between (a) transpose of branch current to bus current matrix and impedance matrix (let's assume that the resultant matrix is represented by the symbol say NCNV), (b) NCNV, and branch current to bus current matrix. This multiplication operation requires considerably large processing time. In [35, 40], authors have formulated the loads beyond branch matrix, load current matrix and branch current matrix for computing the load current and branch current (this step is backward sweep). In the forward sweep, the path impedance matrix, path drop matrix, slack bus to other buses drop matrix and load flow matrix have been developed to compute the bus voltage. There is no direct multiplication required between all the relevant matrices developed in the aforementioned work. Hence, this algorithm is computationally much more efficient than the direct load flow algorithm. Furthermore, these load flow approaches have not considered transformers and regulators models in their study. Several other methods of load flow based on BFS based methods are formulated in [36].

It is evident from the literature review that the prevailing load flow algorithms in the literature have their limitation in handling the modern distribution network. Some of the load flow algorithms provide load flow solution for radial distribution system only. In the case of the load flow solution of a weakly meshed distribution system, those load flow methodologies perform poorly. Some of the load flow approaches provide load flow solution of balanced or single-phase distribution network only. It is also noticed from the literature review that some of the prevailing load flow algorithms display poor convergence behavior. Some of the algorithms are capable of providing the load flow solution of both radial and meshed distribution system, but, not flexible enough to incorporate any new changes in the prevailing topology of the distribution network. The transformers, regulators, shunt element, and voltage-controlled model of distributed generations (PV bus model) have not been taken into considerations in various load flow studies existing in the literature.

## 2.2 Research Contribution

- A novel injected current sensitivity based load flow method for distribution system is proposed which can be used to model DERs with voltage control capability.
- Two state of art distribution load flow methods were developed
- A load flow tool for single-phase distribution system is developed which can be used to solve any distribution system load flow using state of the art methods and proposed method.

## 2.3 Single Phase Distribution System Modeling

This section describes the mathematical modeling of power distribution system equipment. The discussion is categorized into power delivery elements and power conversion elements. Power delivery elements such as distribution lines, transformers are responsible for power transmission in the distribution networks. Power conversion elements such as load, DGs, capacitor banks generate or consume electrical power following energy conversion principles.

### 2.3.1 Power Delivery Elements

#### 2.3.1.1 Distribution Lines and Transformers

The distribution lines and transformers are modeled as a two-terminal devices with fixed impedance. For each branch  $(i, j) \in \mathcal{E}$ , we model the complex impedance as  $z_{ij} = r_{ij} + jx_{ij}$ , where,  $r_{ij}$  and  $x_{ij}$  represent per-unit resistance and reactance, respectively. Other models for different transformer configurations are detailed in later sections (See Section V).

#### 2.3.1.2 Voltage Regulators

A 32-step voltage regulator with a voltage regulation range of  $\pm 10\%$  is assumed. The series and shunt impedance of the voltage regulator are ignored as these have

very small value. Let,  $a$  be the turn ratio for the voltage regulator connected to line  $(i, j)$ . Then  $a$  can take values between 0.9 to 1.1 with each step resulting in a change of 0.00625 pu. The control for regulator is defined using binary variables. Let, for  $u_{tap,i} \in \{0, 1\}$  be a binary variable defined for each regulator step position i.e.  $i \in (1, 2, \dots, 32)$ . Also define a vector  $b_i \in \{0.9, 0.90625, \dots, 1.1\}$ . Then  $V_i, V_j, I_{ii'}$ , and  $I_{i'j}$  are given as follows:

$$V_j = V_{i'} = aV_i \text{ and } I_{ii'} = aI_{i'j} \quad (2.1)$$

where,  $a = \sum_{i=1}^{32} b_i u_{tap,i}$  and  $\sum_{i=1}^{32} u_{tap,i} = 1$ .

### 2.3.2 Power Conversion Elements

#### 2.3.2.1 Loads

The most widely acceptable load model is the ZIP model which is a combination of constant impedance (Z), constant current (I) and constant power (P) characteristics of the load [41]. The mathematical representation of the ZIP model for the load connected at bus  $i$  is given by (18)-(19).

$$p_{L,i} = p_{i,0} \left[ k_{p,1} \left( \frac{V_i}{V_0} \right)^2 + k_{p,2} \left( \frac{V_i}{V_0} \right) + k_{p,3} \right] \quad (2.2)$$

$$q_{L,i} = q_{i,0} \left[ k_{q,1} \left( \frac{V_i}{V_0} \right)^2 + k_{q,2} \left( \frac{V_i}{V_0} \right) + k_{q,3} \right] \quad (2.3)$$

where,  $k_{p,1} + k_{p,2} + k_{p,3} = 1$ ,  $k_{q,1} + k_{q,2} + k_{q,3} = 1$ ,  $p_{i,0}$  and  $q_{i,0}$  are load consumption at nominal voltage,  $V_0$ .

#### 2.3.2.2 Distributed Generation

A per-phase model for reactive power support from smart inverter connected to DGs is developed. The DGs are modeled as constant power factor(PQ) type DG or constant voltage(PV) type DG. The constant power factor type DGs are modelled as

negative loads with a known active power generation equal to the forecasted value. The reactive power support from DG depend upon the rating of the smart inverter. Let, the rated per-phase apparent power capacity for smart inverter connected to  $i^{th}$  DG be  $s_{DG,i}^{rated}$  and the forecasted active power generation be  $p_{DG,i}$ . The available reactive power,  $q_{DG,i}$  from the smart inverter is given by

$$-\sqrt{(s_{DG,i}^{rated})^2 - (p_{DG,i})^2} \leq q_{DG,i} \leq \sqrt{(s_{DG,i}^{rated})^2 - (p_{DG,i})^2} \quad (2.4)$$

In this work, the PQ type DGs are installed at the 10%, 30%, and 50% of the load nodes. The rated power of each DG is equal to the rated power of the load connected to that node. It is assumed that all the DGs are interfaced with the smart inverters and its kVA rating is equal to the 120% of the rated active power.

The constant voltage type DGs or PV type DGs are modelled using a PV sensitivity impedance matrix (PVSIM). Consider a system as shown in Fig. 2.1. The sensitivity matrix for computing net reactive current injections by the DGs can be written as:

$$Z^{PV} = \begin{bmatrix} Z_{11} & Z_{12} \\ Z_{21} & Z_{22} \end{bmatrix} \quad (2.5)$$

The PV sensitivity impedance matrix is obtained using the procedure described. From input data, a graph is created using network topology information of the distribution system. The path from the substation bus to each PV bus is obtained. Dijkstra's algorithm is used to find the shortest path from a source node to any node in a graph. Since distribution systems are generally radial, there will be only 1 path between the source node and the target node. A modified Dijkstra's algorithm is used since we are only interested to find a path from the swing bus to each PV bus and not every bus in the system. Using the path obtained, the total impedance for each path is calculated. Once all diagonal blocks are calculated, the common path shared between 2 PV nodes with substation is found using a common path algorithm and

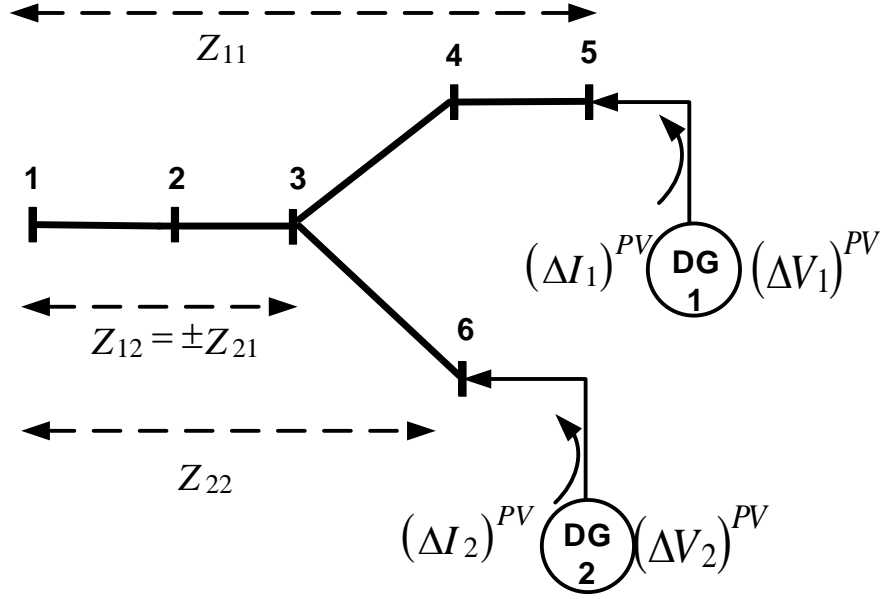


Figure 2.1: Constant Voltage type DGs

off-diagonal blocks of PVSIM are obtained using R, X, B values of line components in the common path.

#### 2.4 Injected Current Sensitivity based Single Phase Power Flow

The proposed method is a modified version of current injection based power flow as in [18]. In current injection-based power flow, the complex current injection equations are expressed in terms of rectangular coordinates, and the bus admittance matrix is represented in terms of its real (G) and imaginary values (B). The Jacobian matrix is formed from the bus admittance matrix where each element in the bus admittance matrix is replaced with  $2 \times 2$  blocks. The off-diagonal blocks obtained in the Jacobian are fixed over iterations and diagonal blocks are updated at every iteration based on the type of load model connected to that bus. In an electric power network with N buses the complex current mismatch at a bus  $i$  can be expressed as:

$$\Delta I_i = (I_i^{sp}) - (I_i^{calc}) \quad (2.6)$$

Eq (2.6) can be expanded as

$$\Delta I_i = \frac{(P_i^{sp}) - j(Q_i^{sp})}{(V_i^*)} - \sum_{j=1}^n Y_{ji} V_j \quad (2.7)$$

where  $P_i^{sp}$  is active component of scheduled power at bus i and  $Q_i^{sp}$  is reactive component of scheduled power at bus i.

Eq (2.7) which is in complex form can be represented in terms of real and imaginary component as

$$\Delta I_{ri} = \frac{P_i^{sp} V_{ri} + Q_i^{sp} V_{mi}}{V_{ri}^2 + V_{mi}^2} - \sum_{j=1}^N (G_{ij} V_{rj} - B_{ij} V_{mj}) \quad (2.8)$$

$$\Delta I_{mi} = \frac{P_i^{sp} V_{mi} - Q_i^{sp} V_{ri}}{V_{ri}^2 + V_{mi}^2} - \sum_{j=1}^N (G_{ij} V_{mj} - B_{ij} V_{rj}) \quad (2.9)$$

The power flow formulation using current injections can be solved using (2.10) as

$$\begin{bmatrix} \Delta I_{m1} \\ \Delta I_{r1} \\ \vdots \\ \Delta I_{mn} \\ \Delta I_{rn} \end{bmatrix} = \begin{bmatrix} \frac{\partial I_{m1}}{\partial V_{r1}} & \frac{\partial I_{m1}}{\partial V_{m1}} & \dots & \frac{\partial I_{m1}}{\partial V_{rn}} & \frac{\partial I_{m1}}{\partial V_{mn}} \\ \frac{\partial I_{r1}}{\partial V_{r1}} & \frac{\partial I_{r1}}{\partial V_{m1}} & \dots & \frac{\partial I_{r1}}{\partial V_{rn}} & \frac{\partial I_{r1}}{\partial V_{mn}} \\ \vdots & \vdots & \vdots & \vdots & \vdots \\ \frac{\partial I_{mn}}{\partial V_{r1}} & \frac{\partial I_{mn}}{\partial V_{m1}} & \dots & \frac{\partial I_{mn}}{\partial V_{rn}} & \frac{\partial I_{mn}}{\partial V_{mn}} \\ \frac{\partial I_{rn}}{\partial V_{r1}} & \frac{\partial I_{rn}}{\partial V_{m1}} & \dots & \frac{\partial I_{rn}}{\partial V_{rn}} & \frac{\partial I_{rn}}{\partial V_{mn}} \end{bmatrix} \begin{bmatrix} \Delta V_{r1} \\ \Delta V_{m1} \\ \vdots \\ \Delta V_{rn} \\ \Delta V_{mn} \end{bmatrix} \quad (2.10)$$

The elements of Jacobian can be obtained as in [19]. The voltage mismatch can be represented in compact form as

$$\begin{bmatrix} \Delta V \end{bmatrix} = \begin{bmatrix} J \end{bmatrix}^{-1} \begin{bmatrix} \Delta I \end{bmatrix} \quad (2.11)$$

The updated voltage is given by

$$\begin{bmatrix} V \end{bmatrix}^{k+1} = \begin{bmatrix} V \end{bmatrix}^k + \begin{bmatrix} \Delta V \end{bmatrix} \quad (2.12)$$

In order to model PV type DERs in current injection based power flow, at each iteration, the deviation of magnitude of voltage at PV bus  $k$  from its specified values is calculated and given by

$$|\Delta V_k^{PV}| = |V_k^{spec}| - |V_k^s|, \quad (2.13)$$

where  $V_k^{spec}$  and  $V_k$  are specified and calculated values of voltage at PV node  $k$ . If the voltage deviation of bus  $k$  is not within the acceptable tolerance, reactive power compensation is required to maintain voltage to a specified value. Assuming that the voltage variation due to active power is minimal, the reactive current injection required by at all PV nodes are given by

$$\begin{bmatrix} \Delta I_m^{PV} \end{bmatrix} = \begin{bmatrix} Z^{PV} \end{bmatrix}^{-1} \begin{bmatrix} \Delta V^{PV} \end{bmatrix} \quad (2.14)$$

where  $Z^{PV}$  is the PV sensitivity impedance matrix (PVSIM). The reactive current injection is then added to current mismatch vector of respective buses. The voltage mismatch equation considering PV type DG at bus  $k$  is given by (2.15)

$$\begin{bmatrix} \Delta V_{r1} \\ \Delta V_{m1} \\ \vdots \\ \Delta V_{rk} \\ \Delta V_{mk} \\ \vdots \\ \Delta V_{rn} \\ \Delta V_{mn} \end{bmatrix} = \begin{bmatrix} \frac{\partial I_{m1}}{\partial V_{r1}} & \frac{\partial I_{m1}}{\partial V_{m1}} & \dots & \frac{\partial I_{m1}}{\partial V_{rn}} & \frac{\partial I_{m1}}{\partial V_{mn}} \\ \frac{\partial I_{r1}}{\partial V_{r1}} & \frac{\partial I_{r1}}{\partial V_{m1}} & \dots & \frac{\partial I_{r1}}{\partial V_{rn}} & \frac{\partial I_{r1}}{\partial V_{mn}} \\ \vdots & \vdots & \vdots & \vdots & \vdots \\ \frac{\partial I_{mk}}{\partial V_{r1}} & \frac{\partial I_{mk}}{\partial V_{m1}} & \dots & \frac{\partial I_{mk}}{\partial V_{rn}} & \frac{\partial I_{mk}}{\partial V_{mn}} \\ \frac{\partial I_{rk}}{\partial V_{r1}} & \frac{\partial I_{rk}}{\partial V_{m1}} & \dots & \frac{\partial I_{rk}}{\partial V_{rn}} & \frac{\partial I_{rk}}{\partial V_{mn}} \\ \vdots & \vdots & \vdots & \vdots & \vdots \\ \frac{\partial I_{mn}}{\partial V_{r1}} & \frac{\partial I_{mn}}{\partial V_{m1}} & \dots & \frac{\partial I_{mn}}{\partial V_{rn}} & \frac{\partial I_{mn}}{\partial V_{mn}} \\ \frac{\partial I_{rn}}{\partial V_{r1}} & \frac{\partial I_{rn}}{\partial V_{m1}} & \dots & \frac{\partial I_{rn}}{\partial V_{rn}} & \frac{\partial I_{rn}}{\partial V_{mn}} \end{bmatrix}^{-1} \begin{bmatrix} \Delta I_{m1} \\ \Delta I_{r1} \\ \vdots \\ \Delta I_{mk} + \Delta I_{mk}^{PV} \\ \Delta I_{rk} \\ \vdots \\ \Delta I_{mn} \\ \Delta I_{rn} \end{bmatrix} \quad (2.15)$$

A flow chart of proposed method is shown in Fig. 2.1. Thus the PV bus inclusion in LF is achieved without updating any additional elements (for each PV bus) in

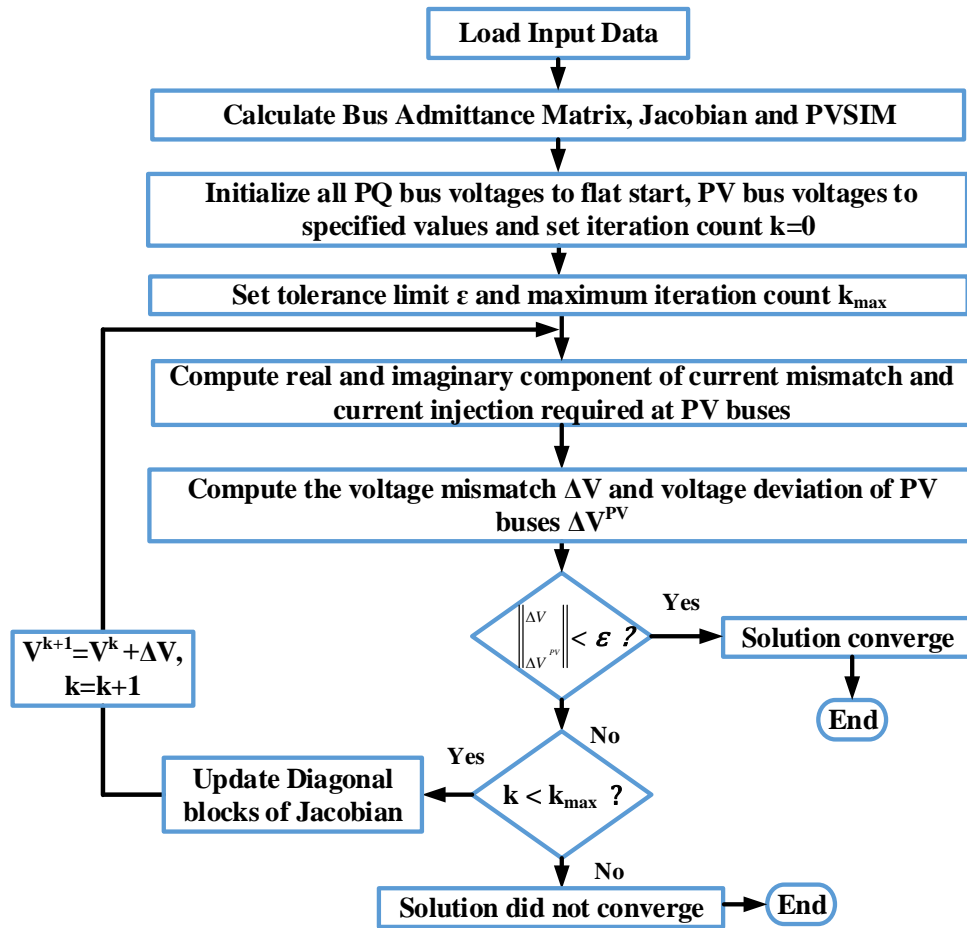


Figure 2.2: Flowchart of Proposed load flow

Jacobian. This would lead to a large computational advantage especially with large DER penetration in the distribution system. A table showing size and number of elements updated in Jacobian per iteration for an  $n$  bus system with  $m$  PV buses is shown in Table. 2.1. Values for the IEEE 14 bus system with 4 PV buses are shown.

## 2.5 State of the art methods

### 2.5.1 Forward-Backward Sweep Power Flow

The Forward-Backward Sweep method exploits radial nature and overcome the challenges related to ill-conditioned nature of distribution networks. The algorithm consists of a nodal current calculation, a backward sweep and a forward sweep. Con-

Table 2.1: Size of Jacobian

	Tradition NR	Current Injection [18]	Current Injection [20]	Proposed Method
Size of Jacobian	2n-m-2	2n-2	2n-2+m	2n-2
Size of Jacobian (14 bus system)	22	26	30	26
Elements Updated per Iteration	146	74	60	52

sider a power network with  $N$  buses and  $L$  branches, nodal current equation can be expressed At iteration  $k$ , the nodal current injection at node  $i$  can be calculated as

$$I_i^k = \frac{P_i^{sp} - jQ_i^{sp}}{V_i^{k-1*}} \quad (2.16)$$

$$P_i^{sp} = P_{G_i} - P_{L_i} \quad (2.17)$$

$$Q_i^{sp} = Q_{G_i} - Q_{L_i} \quad (2.18)$$

where  $P_i^{sp}$ ,  $P_{G_i}$  and  $P_{L_i}$  are active component of scheduled, generated and load power at bus  $i$  respectively and  $Q_i^{sp}$ ,  $Q_{G_i}$  and  $Q_{L_i}$  is reactive component of scheduled, generated and load power at bus  $i$  respectively.

During backward sweep, the branch currents are calculated (with initialized voltages for the first iteration). A current summation method is applied to start from nodes at the far end of the feeder towards the source bus. The current in-branch  $l$  connected between node  $f$  and  $t$  can be obtained as

$$I_l^k = -I_t^k + \sum(I_{tp}) \quad (2.19)$$

where  $I_{tp}$  is currents in all branches emanating from node  $t$ . If a voltage regulator with tap  $t$  is connected between node  $f$  and  $t$  the current in branch  $l$  is modified as

$$I_l^k = (1 + 0.00625t)I_l^k \quad (2.20)$$

The forward sweep calculates voltages using the calculated currents from backward sweep from the source bus till nodes at far end of feeder. The voltage at node  $t$  is obtained using current in branch  $l$  and updated voltage in node  $f$  as

$$V_t^k = V_f^k - Z_l * I_l^k \quad (2.21)$$

where  $Z_l$  is impedance of line  $l$ . If a voltage regulator with tap  $t$  is connected between node  $f$  and  $t$  voltage at node  $t$  is modified as

$$V_t^k = (1 + 0.00625t)V_t^k \quad (2.22)$$

The voltages obtained using forward sweep are used for the next iteration in the backward sweep. The voltage mismatch is calculated as

$$\Delta V = V^k - V^{k-1} \quad (2.23)$$

The load flow iterations are repeated until voltage mismatches is lesser than a convergence tolerance.

### 2.5.2 Z-bus Approach - Fixed-point Iteration

In an electric power network with  $N$  buses, nodal current equation can be expressed according to the following matrix form:

$$\mathbf{I} = \mathbf{YV} = \sum_{j=1}^N Y_{ji} V_j \quad (2.24)$$

where

$$\mathbf{I} = \begin{bmatrix} I_1 \\ I_2 \\ \vdots \\ I_n \end{bmatrix}, \mathbf{V} = \begin{bmatrix} V_1 \\ V_2 \\ \vdots \\ V_n \end{bmatrix}, \mathbf{Y} = \begin{bmatrix} Y_{11} & Y_{12} & \cdots & Y_{1n} \\ Y_{21} & Y_{22} & \cdots & Y_{2n} \\ \vdots & \vdots & \ddots & \vdots \\ Y_{n1} & Y_{n2} & \cdots & Y_{nn} \end{bmatrix} \quad (2.25)$$

are the nodal injection current vector, bus voltage vector, and the bus admittance matrix of the network, respectively. Partitioning the matrices into slack and non-slack buses eq (2.24) can be expressed as

$$\begin{bmatrix} I_s \\ I_n \end{bmatrix} = \begin{bmatrix} Y_{ss} & Y_{sn} \\ Y_{ns} & Y_{nn} \end{bmatrix} \begin{bmatrix} V_s \\ V_n \end{bmatrix} \quad (2.26)$$

where  $I_s$  is the current injection at slack bus and  $V_s$  is the voltage at the slack bus and  $I_n$  is the current injection for all other buses and  $V_n$  is the voltage at all other buses. Therefore

$$I_n = Y_{ns} \cdot V_s + Y_{nn} \cdot V_n \quad (2.27)$$

At iteration  $k$ , the nodal current injection at node  $i$  can be calculated as

$$I_i^k = \frac{(P_i^{sp}) - j(Q_i^{sp})}{(V_i^*)} \quad (2.28)$$

where  $P_i^{sp}$  is active component of scheduled power at and  $Q_i^{sp}$  is reactive component of scheduled power at bus  $i$ . A fixed-point equation for voltages  $V_n$  can be obtained as

$$V_n^{k+1} = Y_{nn}^{-1} \cdot (I_n^k - Y_{ns} \cdot V_s^k) \quad (2.29)$$

The voltage mismatch is calculated as

$$\Delta V = V^k - V^{k-1} \quad (2.30)$$

The load flow iterations are repeated until voltage mismatches is lesser than a convergence tolerance.

## 2.6 Single-phase Test Distribution Systems

### 2.6.1 Small Test Feeder-123 node

This test system is developed by converting the three-phase IEEE-123 node distribution system into an equivalent single-phase system (using OpenDSS). The system has four voltage regulators and four capacitor banks as shown in Fig.2.3. The transformers in the system are converted into a line with an equivalent line impedance. Also, the line capacitance of the system is ignored. All loads were converted into wye connected constant power loads.

### 2.6.2 Large Test Feeder - 2522-node

This test system is developed by converting the three-phase IEEE-8500 node distribution system into an equivalent single-phase system (using OpenDSS) by ignoring the secondary lines and combining the secondary loads and shifting it to the primary. Due to this conversion, the resultant number of nodes in the system is 2522. The original system has four voltage regulators and four capacitor banks which is intact at the same position in the derived model as shown in Fig.2.4.

## 2.7 Simulation Results

### 2.7.1 123-node test system

Two cases are simulated: (1) capacitor ON and voltage regulators (taps = 0,0,0,0) and (2) capacitor ON and voltage regulators (taps = 0,1,2,-1). The rationale is to evaluate the performance of the algorithms for two different operational scenarios characterized by the setpoints of the discrete voltage control devices. DGs considered being of PQ type. The base case power flow is solved using the power flow algorithms proposed method. The results are then validated using a benchmark power flow solver tool named OpenDSS [42] and also compared with the state of the art methods like

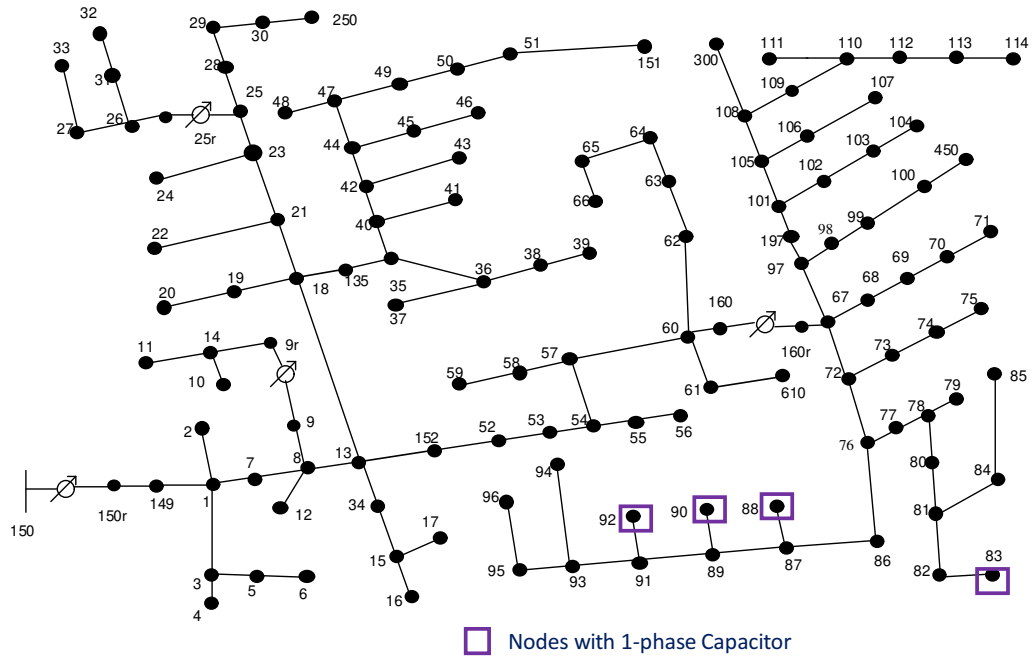


Figure 2.3: Single-phase representation of the IEEE-123 node system

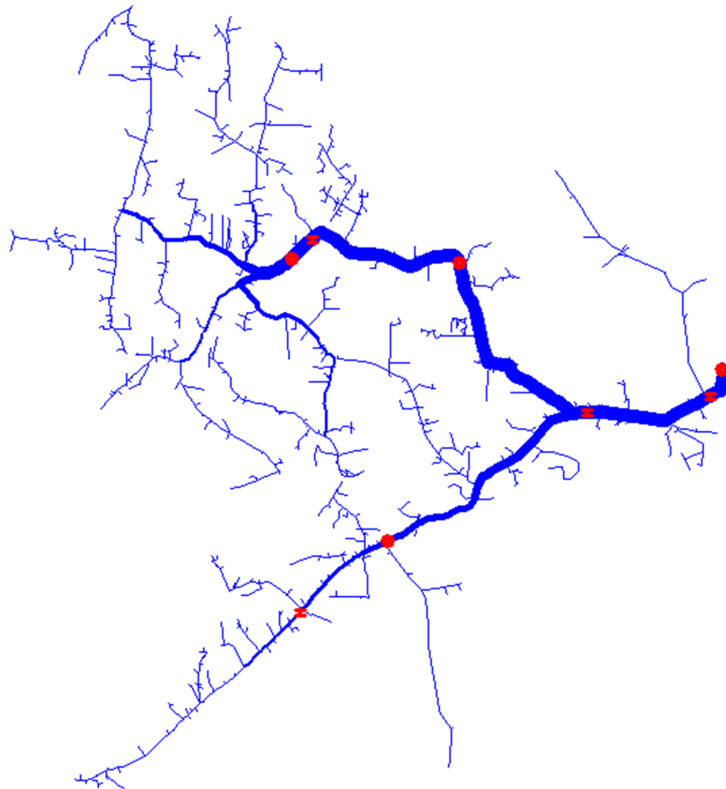


Figure 2.4: Single-phase representation of the IEEE-8500 node system

forward-backward sweep and Z-bus. The apparent power flow in the system for the base case is 1.273 MVA. It can be observed from the Table.2.2, all the nonlinear power flow results are similar to that obtained by solving the power flow in OpenDSS. Next, with the increase in DG penetration from 10% to 50% there is a reduction in power flow from the substation to 1.016 MVA to 0.660 MVA. The maximum error in the voltage magnitude(PU) and the angle (in radian) for the proposed method at the base case is 0.0008 pu, and it decreases with the increase in DG penetration. Also, the maximum difference in the voltage angle is 0.00014 rad.

Table 2.2: Case 1:123 bus system - Power Flow with capacitor ON and voltage regulators (taps = 0,0,0,0)

<b>Apparent Power flow from substation (MVA)</b>				
<b>% DG penetration</b>	<b>OpenDSS</b>	<b>Proposed Method</b>	<b>FB Sweep</b>	<b>Z-bus method</b>
0	1.273	1.273	1.273	1.273
10	1.016	1.016	1.016	1.016
30	0.840	0.840	0.840	0.840
50	0.660	0.660	0.660	0.660
<b>Maximum error in pu voltage with respect to OpenDSS solutions</b>				
0	-	0.0008	0.0008	0.0008
10	-	2.53e-05	2.53e-05	2.53e-05
30	-	2.45e-05	2.45e-05	2.79e-05
50	-	2.79e-05	2.79e-05	2.79e-05
<b>Maximum error in voltage angle with respect to OpenDSS solutions</b>				
0	-	0.0001415	0.0001458	0.000141
10	-	5.502e-05	5.760E-05	5.501e-05
30	-	5.142e-05	5.359E-05	5.142e-05
50	-	3.455e-05	3.601E-05	3.454e-05

The power flow comparison by changing the tap positions of the voltage regulators from 0,0,0,0 is change to 0,1,2,-1 and the all the capacitor switch ON is shown in Table.2.3. This validates that the power flow algorithm is not affected by changing the tap position of the voltage regulators. Next 2 PV type DGS are used to maintain a 1pu voltage at bus number 40 and 60. It can be seen from Fig. 2.5 that proposed algorithm is able to successfully model voltage controlled DGs and maintain voltage

Table 2.3: Case 2:123 bus system - Power Flow with capacitor ON and voltage regulators (taps = 0,1,2,-1)

Apparent Power flow from substation (MVAR)				
% DG penetration	OpenDSS	Proposed Method	FB Sweep	Z-bus method
0	1.273	1.273	1.273	1.273
10	1.0163	1.0164	1.0164	1.0164
30	0.8401	0.8402	0.8402	0.8402
50	0.6601	0.6602	0.6602	0.6602
Maximum error in pu voltage with respect to OpenDSS solutions				
0	-	3.068e-05	3.059e-05	3.062e-05
10	-	9.372e-05	9.379e-05	9.365e-05
30	-	7.505e-05	7.498e-05	7.502e-05
50	-	6.381e-05	6.385e-05	6.378e-05
Maximum error in voltage angle with respect to OpenDSS solutions				
0	-	0.000140	8.783e-05	0.00014065
10	-	5.466e-05	8.528e-05	5.465e-05
30	-	5.135e-05	8.217e-05	5.135e-05
50	-	3.447e-05	5.743e-05	3.447e-05

at specified value.

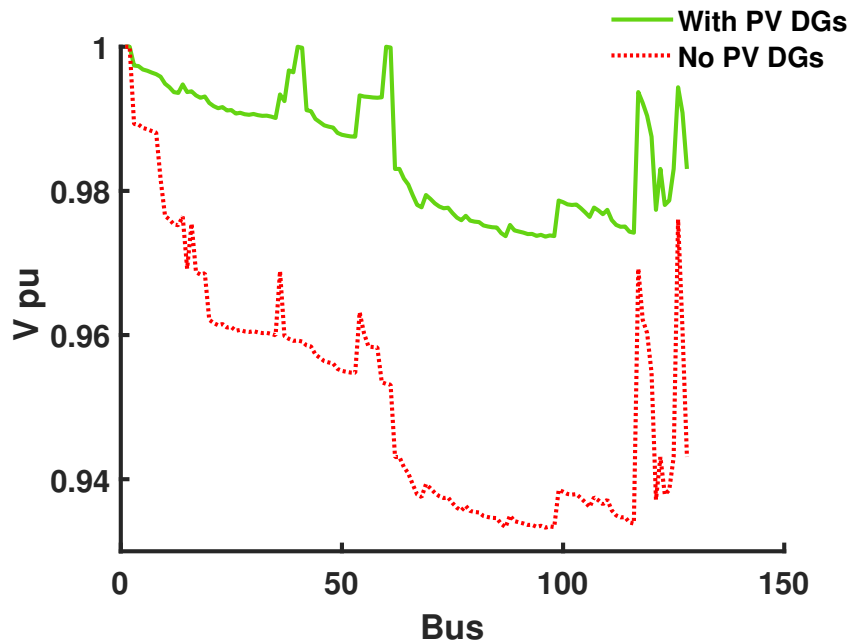


Figure 2.5: Voltage profile with and without PV DG

## 2.7.2 2522-node test system

A larger test feeder is required to validate the performance of the algorithms. The performance of algorithms are evaluated using two test cases, viz. case (1)- all the capacitor switch ON and all the voltage regulators taps at 0 and case (2) all the capacitor switch ON and all the voltage regulators taps at 0,6,6,0. The comparison of

Table 2.4: Case 1 - Power Flow with capacitor ON and voltage regulators (taps = 0,0,0,0)

<b>Apparent Power flow from substation (MVA)</b>				
<b>% DG penetration</b>	<b>MatPower</b>	<b>Proposed Method</b>	<b>FB Sweep</b>	<b>Z-bus method</b>
0	3.7493	3.749	3.750	3.749
10	3.277	3.278	3.277	3.277
30	2.394	2.394	2.394	2.394
50	1.669	1.669	1.670	1.669
<b>Maximum error in pu voltage with respect to MATPOWER solutions</b>				
0	-	0.0002	0.0002	0.0001
10	-	0.0001	0.0001	0.0001
30	-	0.00013	0.00016	0.00012
50	-	9.15e-05	9.06e-05	9.06e-05
<b>Maximum error in voltage angle with respect to MATPOWER solutions</b>				
0	-	0.00015	0.00015	0.00014
10	-	0.00012	0.00012	0.00012
30	-	7.9e-05	7.9e-05	7.9e-05
50	-	4.3e-05	4.38e-05	4.38e-05

the power flow variables obtained by solving different power flow algorithms for case (1) is shown in the Table.2.4. The solution in this case is validated using a standard power flow solver named MATPOWER. It can be observed from the table that the apparent power flow from substation is exactly equal for all algorithms and for all level of DG penetration. As the DG penetration increases the line losses will decrease, this is due to increase in the number of nodes with net zero power consumption ( $P_L - P_G$ ). Further, it can be observed from the table that the maximum error in the voltage angle for all the algorithms with respect to MATPOWER angle is almost equal.

The power flow comparison for the the 2522 node system for Case 2, is shown in Table.2.5.

Table 2.5: Case 2 - Power Flow with capacitor ON and voltage regulators (taps = 0,6,6,0)

<b>Apparent Power flow from substation (MVA)</b>				
<b>% DG penetration</b>	<b>MatPower</b>	<b>Proposed Method</b>	<b>FB Sweep</b>	<b>Z-bus method</b>
0	3.735	3.735	3.736	3.735
10	3.267	3.267	3.267	3.267
30	2.388	2.388	2.388	2.388
50	1.667	1.667	1.667	1.667
<b>Maximum error in pu voltage with respect to MATPOWER solutions</b>				
0	-	0.0002	0.00015	8.99e-05
10	-	0.00011	0.00013	9.44e-05
30	-	7.79e-05	8.04e-05	7.29e-05
50	-	4.13e-05	4.17e-05	4.10e-05
<b>Maximum error in voltage angle with respect to MATPOWER solutions</b>				
0	-	0.0049	0.0038	0.00017
10	-	0.00012	0.0034	0.00011
30	-	7.31e-05	0.0023	7.4e-05
50	-	4.04e-05	0.0014	4.06e-05

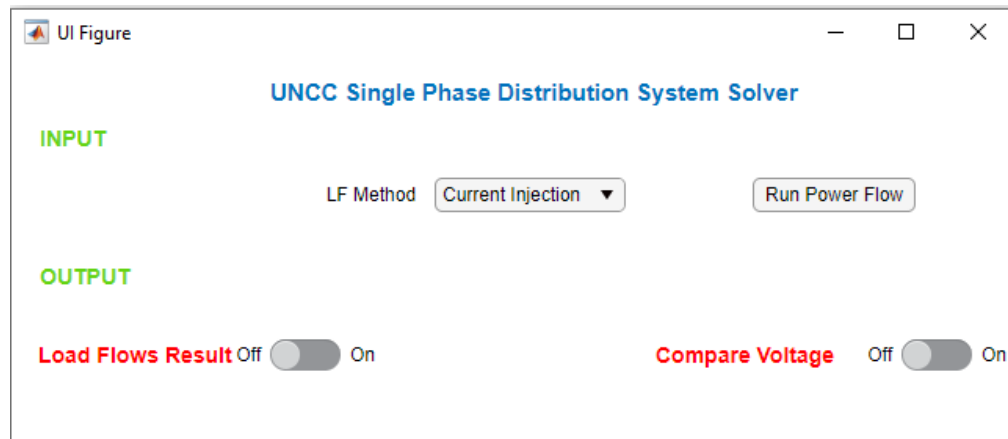


Figure 2.6: Load Flow Graphical User Interface

## 2.8 Single Phase Distribution Load Flow Tool

A Graphical User Interface for the single phase distribution load flow tool as shown in Fig. 2.6 is developed. The tool is universal and can be used to analyze any

distribution system. The user can select the load flow method from a drop-down list which will display the list of all load flow methods. An option to plot voltage magnitude as well as to compare results with a benchmark is provided.

Then once the user clicks on the RunPF button, a window appears from which the user can select the interested test system. The complete flow of the tool is shown in Fig. 2.7.

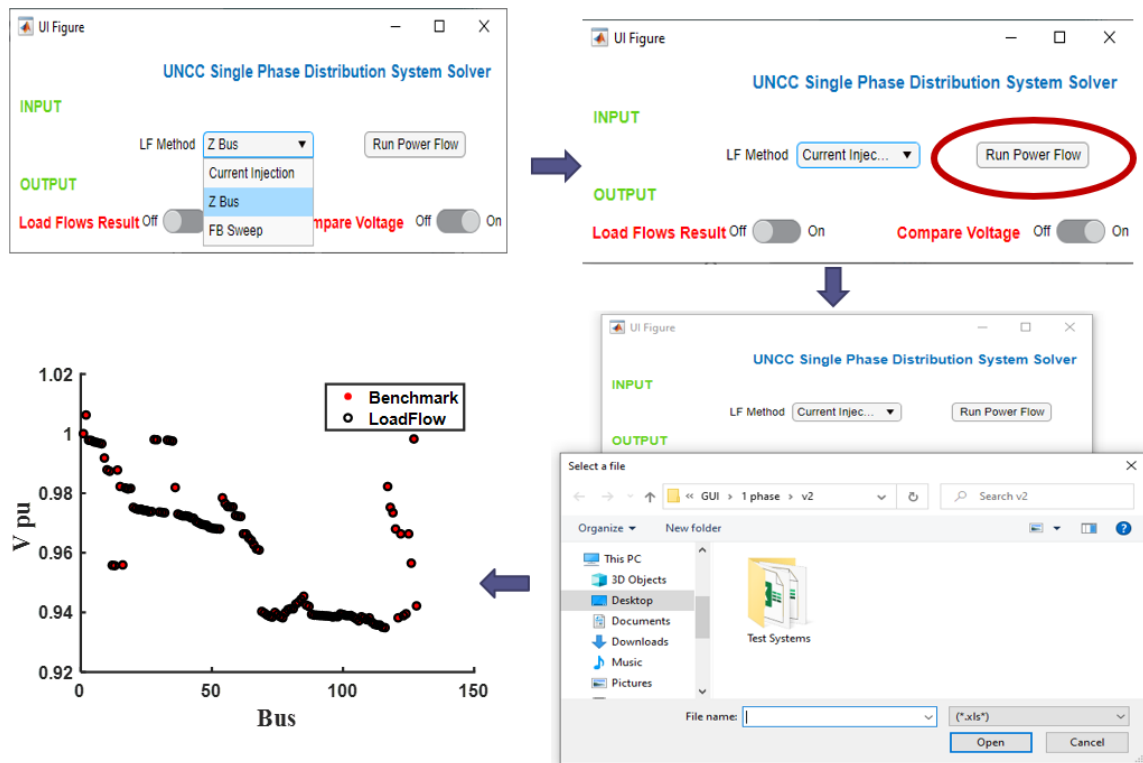


Figure 2.7: Graphical User Interface flow.

## 2.9 Summary

A load flow algorithm based on current injection is proposed which can cater to distribution systems with high penetration of DERs has been introduced in this chapter. The DGs are modeled as constant power factor type(PQ) treating them as negative load in the proposed LF studies. The DGs which have voltage control capability is modeled as constant voltage type(PV) bus using a reactive power sensitivity based approach. Unlike conventional current injection type load flow, the Jacobian size and

elements to be updated per iteration will not be affected because of the PV bus in the proposed method. case studies on IEEE-123 bus test distribution systems show the accuracy and robustness of the proposed approach. The scalability of the approach is validated using the IEEE-8500 node system. Finally, a universal load flow tool with a graphical user interface for the single-phase distribution load flow is developed which can be used to analyze any distribution systems.

## CHAPTER 3: INJECTION CURRENT SENSITIVITY BASED THREE PHASE AND THREE SEQUENCE LOAD FLOW

### 3.1 Introduction

Conventional Load flow (LF) analysis methods that are widely used for transmission systems may exhibit poor convergence behavior when applied to Distribution Systems. The transmission networks are generally having a meshed structure, while distribution systems are generally radial. The lines in the transmission system are assumed to be transposed which results in no coupling between phases. The loads are treated as balanced loads and therefore the three phase load flow can be reduced to a single phase or positive sequence load flow. But the distribution systems are highly unbalanced in nature. The lines are modeled as untransposed lines and hence mutual coupling effects are prominent. There will be combinations of three phase, two phase, and single phase line sections. The loads are generally unbalanced and due to the presence of a large number of single phase loads. Another important feature of the distribution system is its higher R/X ratio compared to the transmission system. The high R/X ratio of distribution lines makes the distribution system ill-conditioned. Finally, a larger number of nodes in the distribution system leads to higher time for calculation and inversion of the Jacobian matrix at each iteration which makes the load flow more time-consuming and computationally complex. Due to the above-mentioned reasons, conventional load flow methods have been modified to work for DS.

A three-phase form of current injection method (TCIM) has been demonstrated earlier [19] and found to be numerically robust with quadratic convergence and efficient in solving radial as well as highly meshed systems. The complex current injection equations in phase coordinates are represented in rectangular form resulting in a set

of  $6n$  equations for a  $n$  bus system. The Jacobian matrix composed of  $6 \times 6$  block matrices have the same structure as the admittance matrix and only needs updating of the diagonal elements depending on the type of loads. Even though the framework is computationally efficient, TCIM does not consider different load connection types such as delta-connected loads. Also, with multiple PV buses (as becoming a normal due to high penetration of DERs), more number of off-diagonal blocks in Jacobian needs iterative update making the Jacobian computation more complex and time-consuming especially while treating a large number of control devices [22]. The Gauss Implicit methods [23–25] has less computational complexity and memory usage compared to Newton Raphson methods which require computation of Jacobian in each iteration. But the rate of convergence is comparable to the Newton-Raphson deteriorates as the number of PV increases.

### 3.2 Research Contribution

- A new injection current sensitivity based load flow method is proposed in this chapter which can cater to distribution lines with missing phases connected to Delta/Star ZIP loads.
- Models for distribution lines, capacitors, voltage regulators, and relevant transformer connections are derived and a generalized bus admittance matrix (Y-bus) is formulated.
- Generalised Jacobian matrix have been formulated which embeds the properties or features of the distribution system components mentioned above.
- Multiphase DERs with voltage control capability is modeled as PV bus using a reactive power sensitivity based approach. The additional injection will be suitably updated in the current injection vector. Thus, the jacobian matrix will not be affected. Whereas, in the case of traditional Newton- Raphson and current injection based approaches size and elements of the Jacobian matrix

will be highly affected due to PV bus inclusion.

- A three sequence load flow and continuation power flow for unbalanced three phase distribution system is developed.

### 3.3 Three Phase Distribution System Modeling

A power distribution system consists of various components classified generally into 2 categories, the power delivery components, and the power conversion components [8]. The power delivery components that transport energy from one point to another such as distribution lines, voltage regulators, transformers. The power conversion components convert energy from the electrical domain to other forms and vice versa such as loads and distributed energy resources, and energy storage devices. To perform load flow analysis on the system, models of these components should be developed. This section explains the modeling of various components and obtaining the bus admittance matrix corresponding to each of them.

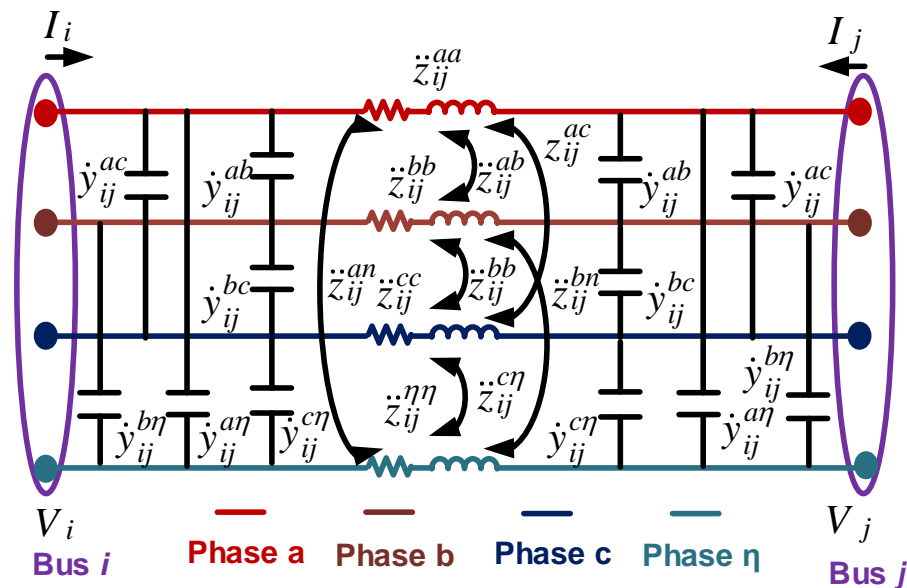


Figure 3.1: Schematic representation of three phase distribution line .

### 3.3.1 Distribution Lines

A distribution network is represented by a set of  $\mathbb{K}$  buses, and a set of  $\mathbb{L}$  lines connecting these buses as shown in Fig. 3.1. For a three-phase line segment connected between bus  $i$  and  $j$  with neutral (Fig. 3.1), the primitive impedance matrix corresponding to its series elements is symmetric and can be written as per [43]:

$$\mathbb{Z}_{ij}^{prim} = \begin{bmatrix} z_{ij}^{aa} & z_{ij}^{ab} & z_{ij}^{ac} & z_{ij}^{a\eta} \\ z_{ij}^{ba} & z_{ij}^{bb} & z_{ij}^{bc} & z_{ij}^{b\eta} \\ z_{ij}^{ca} & z_{ij}^{cb} & z_{ij}^{cc} & z_{ij}^{c\eta} \\ z_{ij}^{\eta a} & z_{ij}^{\eta b} & z_{ij}^{\eta c} & z_{ij}^{\eta\eta} \end{bmatrix} \quad (3.1)$$

In this matrix, diagonal elements represent the self-inductance of the corresponding phase and off-diagonal elements depict mutual impedance between corresponding phases of the line segment connected between bus  $i$  and  $j$ .

Since, most of power flow analysis only uses phase impedance matrix representation of the distribution lines. Hence, primitive impedance matrix of distribution line segment can be transformed into phase impedance matrix by suitably applying Kron's reduction algorithm on  $\mathbb{Z}_{ij}^{prim}$  thus merging the effect of neutral conductor ( $\eta$ ) into the three phase conductors. The phase impedance matrix corresponding to series element of the distribution line connected between bus  $i$  and  $j$  is given by

$$\mathbb{Z}_{ij} = \begin{bmatrix} z_{ij}^{aa} & z_{ij}^{ab} & z_{ij}^{ac} \\ z_{ij}^{ba} & z_{ij}^{bb} & z_{ij}^{bc} \\ z_{ij}^{ca} & z_{ij}^{cb} & z_{ij}^{cc} \end{bmatrix} \quad (3.2)$$

The phase admittance matrix corresponding to series element of distribution line

segment  $ij$  is computed using equation below:

$$\mathbb{Y}_{ij}^{ser} = \mathbb{Z}_{ij}^{-1} \quad (3.3)$$

Similarly, the phase admittance matrix corresponding to shunt element of distribution line segment  $ij$  is computed following the similar procedure as described above and the resultant equation is written as:

$$\mathbb{Y}_{ij}^{sh} = \frac{1}{2} \mathbb{B}_{ij}^{sh} \quad (3.4)$$

where,  $\mathbb{B}_{ij}^{sh}$  is total three phase shunt admittance matrix of the line connecting bus  $i$  and  $j$ .

The current injections at terminals  $i$  and  $j$  in complex form can be obtained as

$$\mathbf{I}_i = (\mathbb{Y}_{ij}^{ser} + \mathbb{Y}_{ij}^{sh}) \mathbf{V}_i - \mathbb{Y}_{ij}^{ser} \mathbf{V}_j \quad (3.5)$$

$$\mathbf{I}_j = -\mathbb{Y}_{ij}^{ser} \mathbf{V}_i + (\mathbb{Y}_{ij}^{ser} + \mathbb{Y}_{ij}^{sh}) \mathbf{V}_j \quad (3.6)$$

where

$$\mathbf{V}_i = \begin{bmatrix} V_i^a & V_i^b & V_i^c \end{bmatrix}^T \quad \mathbf{V}_j = \begin{bmatrix} V_j^a & V_j^b & V_j^c \end{bmatrix}^T \quad (3.7)$$

$$\mathbf{I}_i = \begin{bmatrix} I_i^a & I_i^b & I_i^c \end{bmatrix}^T \quad \mathbf{I}_j = \begin{bmatrix} I_j^a & I_j^b & I_j^c \end{bmatrix}^T \quad (3.8)$$

Therefore, the detailed Y-bus matrix of the three phase distribution line shown in

Fig. 3.1 is given by:

$$\mathbf{Y}_{bus} = \begin{bmatrix} \mathbb{Y}_{ij}^{ser} + \mathbb{Y}_{ij}^{sh} & -\mathbb{Y}_{ij}^{ser} \\ -\mathbb{Y}_{ij}^{ser} & \mathbb{Y}_{ij}^{ser} + \mathbb{Y}_{ij}^{sh} \end{bmatrix} = \begin{bmatrix} Y_{ii} & Y_{ij} \\ Y_{ji} & Y_{jj} \end{bmatrix} \quad (3.9)$$

### 3.3.2 Load Tap Changers and Voltage Regulators

Load Tap Changers and Voltage Regulators are used to regulated the feeder voltage and maintain it within acceptable limits. Load tap changer (LTC) are installed at substation and step voltage regulator(SVR) are installed along the feeder. For load flow solutions, the SVRs are modeled as an admittance  $\mathbb{Y}_t^{reg}$  in series with an ideal autotransformer as shown in Fig. 4.1 The relationship between voltage and current

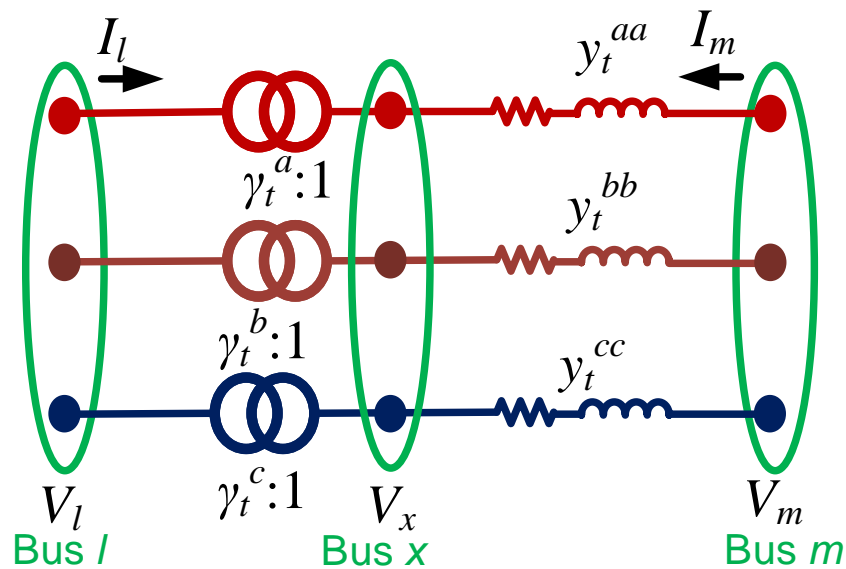


Figure 3.2: Schematic representation of Voltage Regulator

of the auto transformer for phase  $\phi$  can be given by

$$\frac{V_x^\phi}{V_l^\phi} = \frac{1}{\gamma_t^\phi} \quad (3.10)$$

$$\frac{I_l^\phi}{I_m^\phi} = -\gamma_\phi^s \quad (3.11)$$

where,  $V_x^\phi$  and  $V_l^\phi$  are line to neutral voltages of nodes  $x$  and  $l$  respectively.  $I_l^\phi$  and  $I_m^\phi$  are current injections into phase  $\phi$  of nodes  $l$  and  $m$  respectively.

$$\gamma_t^\phi = 1 \mp \frac{N_2}{N_1} = 1 \mp d_v * tp \quad (3.12)$$

where  $tp$  is the tap setting and  $d_v$  is the per unit voltage change per tap. The current injections at terminals  $l$  and  $m$  can be obtained as

$$I_l^\phi = \frac{y_t^{\phi\phi}}{(\gamma_t^\phi)^2} V_l^\phi - \frac{y_t^{\phi\phi}}{\gamma_t^\phi} V_m^\phi \quad (3.13)$$

$$I_m^\phi = -\frac{y_t^{\phi\phi}}{\gamma_t^\phi} V_s(l) + y_t^{\phi\phi} V_s(m) \quad (3.14)$$

The Y-bus matrix considering only single phase of the distribution network depicted in Fig.3 can be written as:

$$Y_{bus} = \begin{bmatrix} \frac{y_t^{\phi\phi}}{(\gamma_t^\phi)^2} & -\frac{y_t^{\phi\phi}}{\gamma_t^\phi} \\ -\frac{y_t^{\phi\phi}}{\gamma_t^\phi} & y_t^{\phi\phi} \end{bmatrix} \quad (3.15)$$

The same analysis can be extended to 3 phase system, with  $y_t^{\phi\phi}$  replaced by 3- $\phi$  admittance matrix of regulator t i.e  $Y_t^{reg}$ .

$$Y_t^{reg} = \begin{bmatrix} y_t^{aa} & 0 & 0 \\ 0 & y_t^{bb} & 0 \\ 0 & 0 & y_t^{cc} \end{bmatrix} \quad (3.16)$$

Following the similar procedure, Y-bus matrix of the three phase distribution system with regulator only can be obtained as,

$$\mathbf{Y}_{bus} = \begin{bmatrix} \mathbf{F}_t \mathbf{Y}_t^{reg} \mathbf{F}_t^T & \mathbf{F}_t (-\mathbf{Y}_t^{reg}) \\ (-\mathbf{Y}_t^{reg}) \mathbf{F}_t^T & \mathbf{Y}_t^{reg} \end{bmatrix} = \begin{bmatrix} Y_{ll} & Y_{lm} \\ Y_{ml} & Y_{mm} \end{bmatrix} \quad (3.17)$$

where

$$\mathbf{F}_t = \begin{bmatrix} \frac{1}{\gamma_t^a} & 0 & 0 \\ 0 & \frac{1}{\gamma_t^b} & 0 \\ 0 & 0 & \frac{1}{\gamma_t^c} \end{bmatrix}. \quad (3.18)$$

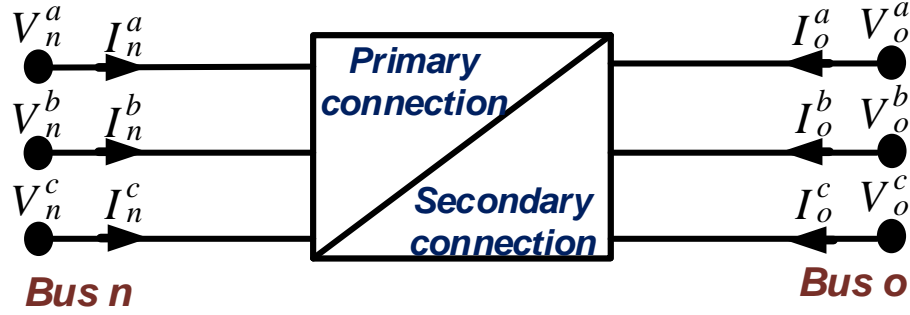


Figure 3.3: Block diagram representation of three phase transformer.

### 3.3.3 Transformers

A three-phase transformer can be represented by a series block representing the per unit leakage admittance, and a shunt block modeling transformer core losses. The nodal current injection matrix for a three-phase distribution transformer shown in Fig. 3.3 can be written as:

$$\begin{bmatrix} \mathbf{I}_n \\ \mathbf{I}_o \end{bmatrix} = \mathbf{Y}_{bus} \begin{bmatrix} V_n \\ V_o \end{bmatrix} \quad (3.19)$$

In a generalized form  $\mathbf{Y}_{bus}$  can be represented as

$$\mathbf{Y}_{bus} = \begin{bmatrix} Y_{nn} & Y_{no} \\ Y_{on} & Y_{oo} \end{bmatrix} \quad (3.20)$$

where

$$Y_1 = \begin{bmatrix} y_d & 0 & 0 \\ 0 & y_d & 0 \\ 0 & 0 & y_d \end{bmatrix}, Y_2 = \frac{1}{3} \begin{bmatrix} 2y_d & -y_d & -y_d \\ -y_d & 2y_d & -y_d \\ -y_d & -y_d & 2y_d \end{bmatrix} \quad (3.21)$$

$$Y_3 = \frac{1}{\sqrt{3}} \begin{bmatrix} -y_d & y_d & 0 \\ 0 & -y_d & y_d \\ y_d & 0 & -y_d \end{bmatrix} \quad (3.22)$$

where  $y_d$  is the leakage admittance of transformer  $d$  and  $\alpha, \beta$  are the off-nominal tap ratios on the primary and second sides respectively. The nodal admittances of different types of transformer are discussed in [1] and shown in Table. 3.1 The

Table 3.1: Y-bus for Various Transformer Connections from [1]

Node n	Node 0	$Y_{nn}$	$Y_{no}$	$Y_{on}$	$Y_{oo}$
Wye-G	Wye-G	$Y_1/(\alpha)^2$	$-Y_1/(\alpha\beta)$	$-Y_1/(\alpha\beta)$	$Y_1/(\beta)^2$
Wye-G	Wye	$Y_2/(\alpha)^2$	$-Y_2/(\alpha\beta)$	$-Y_2/(\alpha\beta)$	$Y_2/(\beta)^2$
Wye	Wye-G	$Y_2/(\alpha)^2$	$-Y_2/(\alpha\beta)$	$-Y_2/(\alpha\beta)$	$Y_2/(\beta)^2$
Wye	Wye	$Y_2/(\alpha)^2$	$-Y_2/(\alpha\beta)$	$-Y_2/(\alpha\beta)$	$Y_2/(\beta)^2$
Wye-G	Delta	$Y_1/(\alpha)^2$	$Y_3/(\alpha\beta)$	$Y_3^T/(\alpha\beta)$	$Y_2/(\beta)^2$
Wye	Delta	$Y_2/(\alpha)^2$	$Y_3/(\alpha\beta)$	$Y_3^T/(\alpha\beta)$	$Y_2/(\beta)^2$
Delta	Delta	$Y_2/(\alpha)^2$	$-Y_2/(\alpha\beta)$	$-Y_2/(\alpha\beta)$	$Y_2/(\beta)^2$
Delta	Wye-G	$Y_2/(\alpha)^2$	$Y_3/(\alpha\beta)$	$Y_3^T/(\alpha\beta)$	$Y_1/(\beta)^2$
Delta	Wye	$Y_2/(\alpha)^2$	$Y_3/(\alpha\beta)$	$Y_3^T/(\alpha\beta)$	$Y_2/(\beta)^2$

rank deficiency of  $Y_2$  and  $Y_3$  would lead to singular  $\mathbf{Y}_{bus}$ . A method to surpass this

problem is presented in [44] where a small shunt admittance is added from the isolated transformer sides to the ground. This is achieved by adding small shunt admittance (compared to  $y_d$ ) to  $Y_2$ . Based on linear algebra, [45] shows how connecting small shunt admittance aids in restoring invertibility of  $\mathbf{Y}_{bus}$ .

An algorithm of Stacked  $\mathbf{Y}_{bus}$  formation of a given distribution system including distribution lines, regulators, and transformers is shown in Algorithm1. Such a stacked  $\mathbf{Y}_{bus}$  approach provides a huge computational advantage. In case of a re-configuration or a tap change in the voltage regulator, only  $\mathbf{Y}_{bus}$  related to those respective components are calculated instead of recalculation full system  $\mathbf{Y}_{bus}$  which improves adaptability and operational ability of the proposed LF method.

---

**Algorithm 1:** Stacked Y bus Calculation

---

- 1: Get data for line configuration data (RLC values), transformer data(leakage impedance, type) and regulator data(taps).
  - 2: Find total number of buses ( $N$ ) and renumber system with slack bus as initial bus.
  - 3: Create a "topology" vector that consists of from bus, to bus, length of line, configuration and line component. Size of topology vector is ( $N_L$ ).
  - 4: Initialize  $Y_{bus}$ ,  $Y_{bus}^{dl}$ ,  $Y_{bus}^{reg}$ ,  $Y_{bus}^{trf}$  with a zero vector of dimension( $3N \times 3N$ ).
  - 5: **while**  $k < N_L$  **do**
    - 6: **if** *line component is "distribution line"* **then**
      - ┌ Get R, L C values of respective distribution line and calculate  $Y_{bus}^{dl}$  as
      - └ in section 3.3.1
    - 7: **if** *line component is "voltage regulator"* **then**
      - ┌ Get taps of respective regulator and RLC values of transmission line in
      - └ series with it and calculate  $Y_{bus}^{reg}$  as in section 3.3.2
    - 8: **if** *line component is "transformer"* **then**
      - ┌ Get leakage impedance values and type of respective transformer and
      - └ calculate  $Y_{bus}^{trf}$  as in section 3.3.3
  - 9:  $Y_{bus} = Y_{bus}^{dl} + Y_{bus}^{reg} + Y_{bus}^{trf}$
- 

### 3.3.4 Load Models

The important features that must be accounted while modelling loads in a distribution system are unbalanced nature and voltage dependence. The voltage sensitive loads can be modelled as a combination of constant power, constant current, and

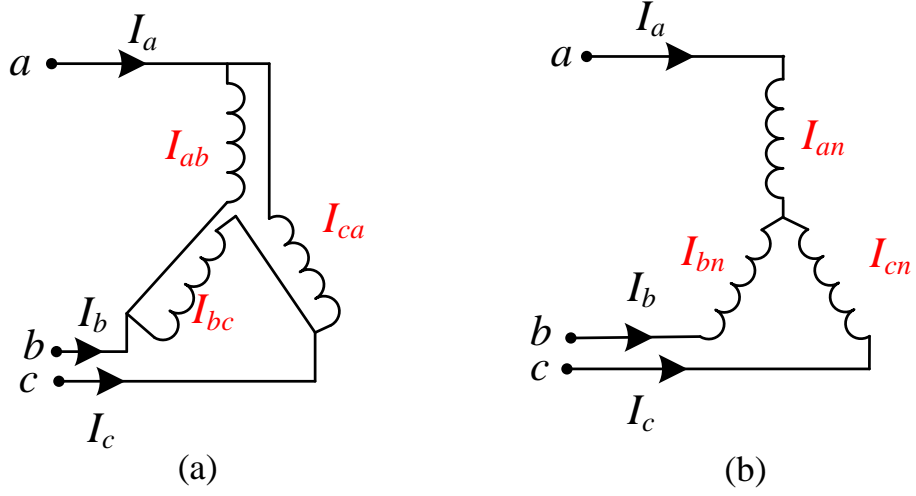


Figure 3.4: Load modeling (a)Star Connected (b)Delta Connected

constant impedance loads (ZIP). A three phase load can either be a star connected load or a delta connected load as shown in Fig. 3.4. The load at bus  $i$  associated with phase  $\phi$  can be modelled as [46].

$$P_{L_i}^\phi = (P_{L_i}^\phi)^0 (K_1 |V_i^\phi|^2 + K_2 |V_i^\phi| + K_3) \quad (3.23)$$

$$Q_{L_i}^\phi = (Q_{L_i}^\phi)^0 (K_4 |V_i^\phi|^2 + K_5 |V_i^\phi| + K_6) \quad (3.24)$$

where  $(P_{L_i}^\phi)^0$  and  $(Q_{L_i}^\phi)^0$  are nominal values of the active power and reactive power of load associated with phase  $\phi$  of node  $i$  respectively. Also

$$K_1 + K_2 + K_3 = 1 \quad (3.25)$$

$$K_4 + K_5 + K_6 = 1 \quad (3.26)$$

Considering the voltage dependence, the nodal current injection at node  $i$  becomes a function of nodal voltages  $V_i$ . With ZIP load modeling, the net specified nodal current injection will be composed of currents from constant power loads  $I_i^{PQ}$ , constant

current loads  $I_i^I$  and constant impedance loads  $I_i^Z$ .

$$(I_i^{sp})^s = -((I_i^{PQ})^s + (I_i^I)^s + (I_i^Z)^s) \quad (3.27)$$

For a constant power load, the injected current is given by

$$(I_i^{PQ})^s = \left( \frac{S_i^s}{V_i^s} \right)^* = \left( \frac{|S_i^s| \angle \theta^s}{|V_i^s| \angle \delta^s} \right)^* \quad (3.28)$$

where  $\delta$  is the voltage angle and  $\theta$  is the power factor angle. For a constant impedance load, the nominal voltage  $V_{0i}$  and specified power is first used to obtain impedance of load.

$$Z_i^s = \frac{|(V_{0i}^s)|^2}{(S_i^s)^*} \quad (3.29)$$

The injected current is given by

$$(I_i^Z)^s = \left( \frac{V_i^s}{Z_i^s} \right) \quad (3.30)$$

For a constant current load, the magnitude of the current is held constant and the angle of current is calculated using voltage angle and power factor angle.

$$(I_i^I)^s = \left( \frac{|S_i^s|}{|V_{0i}^s|} \right) \angle (\delta^s - \theta^s) \quad (3.31)$$

### 3.4 Injected Current Sensitivity based Three Phase Power Flow

In this section a new injected current sensitivity based LF method is proposed for multi-phase unbalanced power distribution system with multiple DERs. The main features of the proposed method are as follows.

### 3.4.1 ICS based Power Flow without DERs

In current injection-based power flow, the complex current injection equations are expressed in terms of rectangular coordinates. The complex values in the bus admittance matrix ( $\mathbf{Y}$ ) are represented in terms of real( $G$ ) and imaginary values( $B$ ). The Jacobian matrix is formed from the bus admittance matrix where each element in the bus admittance matrix is replaced with  $2 \times 2$  blocks in case of 1 phase system and each  $3 \times 3$  matrix in the bus admittance matrix is replaced with  $6 \times 6$  blocks in case of 3 phase system. The off-diagonal blocks obtained in the Jacobian are fixed over iterations and diagonal blocks are updated at every iteration based on the type of load model connected to that bus.

In an electric power network with  $N$  buses, nodal current equation can be expressed according to the following matrix form:

$$\mathbf{I}_{bus} = \mathbf{Y}_{bus} \mathbf{V}_{bus} = \sum_{i=1}^N \sum_{j=1}^N Y_{ij} \mathbf{V}_j \quad (3.32)$$

where:

$$\mathbf{I}_{bus} = \begin{bmatrix} \mathbf{I}_1 \\ \mathbf{I}_2 \\ \vdots \\ \mathbf{I}_N \end{bmatrix}, \mathbf{V}_{bus} = \begin{bmatrix} \mathbf{V}_1 \\ \mathbf{V}_2 \\ \vdots \\ \mathbf{V}_N \end{bmatrix} \quad (3.33)$$

$$\mathbf{Y}_{bus} = \begin{bmatrix} Y_{11} & Y_{12} & \cdots & Y_{1N} \\ Y_{21} & Y_{22} & \cdots & Y_{2N} \\ \vdots & \vdots & \ddots & \vdots \\ Y_{N1} & Y_{N2} & \cdots & Y_{NN} \end{bmatrix} \quad (3.34)$$

are the nodal injection current vector, bus voltage vector, and the bus admittance matrix of the network, respectively.

The current injection in a phase say  $\phi$  of bus  $i$  is computed using equation below:

$$I_i^\phi = \sum_{j \in \xi} \sum_{\varphi \in \sigma} Y_{ij}^{\phi\varphi} V_j^\varphi = I_{i(r)}^\phi + \mathbf{j} I_{i(q)}^\phi \quad (3.35)$$

$$V_j^\varphi = V_{j(r)}^\varphi + \mathbf{j} V_{j(q)}^\varphi \quad (3.36)$$

$$Y_{ij}^{\phi\varphi} = G_{ij}^{\phi\varphi} + \mathbf{j} B_{ij}^{\phi\varphi} \quad (3.37)$$

where,  $\xi = (1, 2, \dots, N)$ ,  $\sigma = (a, b, c)$ ,  $i = (1, 2, \dots, N)$

The phase current injection can be represented in terms of real and imaginary component as

$$I_{i(r)}^\phi = \sum_{j \in \xi} \sum_{\varphi \in \sigma} G_{ij}^{\phi\varphi} V_{j(r)}^\varphi - B_{ij}^{\phi\varphi} V_{j(q)}^\varphi \quad (3.38)$$

$$I_{i(q)}^\phi = \sum_{j \in \xi} \sum_{\varphi \in \sigma} G_{ij}^{\phi\varphi} V_{j(q)}^\varphi + B_{ij}^{\phi\varphi} V_{j(r)}^\varphi \quad (3.39)$$

The phase complex current mismatch in phase  $s$  of the bus  $i$  is given by:

$$\Delta I_i^\phi = (I_i^\phi)^{spf} - (I_i^\phi)^{calc} \quad (3.40)$$

where

$$(I_i^\phi)^{calc} = \sum_{j \in \xi} \sum_{\varphi \in \sigma} Y_{ij}^{\phi\varphi} V_j^\varphi \quad (3.41)$$

$$(I_i^\phi)^{spf} = \frac{(P_i^\phi)^{spf} - \mathbf{j}(Q_i^\phi)^{spf}}{(V_i^\phi)^*} \quad (3.42)$$

where

$$(P_i^\phi)^{spf} = P_{DG_i}^\phi - P_{L_i}^\phi \quad (Q_i^\phi)^{spf} = Q_{DG_i}^\phi - Q_{L_i}^\phi \quad (3.43)$$

$$V_i^\phi = V_{i(r)}^\phi + \mathbf{j} V_{i(q)}^\phi \quad (3.44)$$

where  $(P_i^\phi)^{spf}$ ,  $P_{DG_i}^\phi$ , and  $P_{L_i}^\phi$  is active component of scheduled, generated power and

net load respectively at bus  $i$  and  $(Q_i^\phi)^{spf}$ ,  $Q_{DG_i}^\phi$ , and  $Q_{L_i}^\phi$  is reactive component of scheduled, generated power and net load respectively at bus  $i$ . Thus, (3.40) can be expanded as:

$$\Delta I_i^\phi = \frac{(P_i^\phi)^{spf} - \mathbf{j}(Q_i^\phi)^{spf}}{(V_i^\phi)^*} - \sum_{j \in \xi} \sum_{\varphi \in \sigma} Y_{ij}^{\phi\varphi} V_j^\varphi \quad (3.45)$$

The (3.40) which is in complex form can be represented in terms of the real and imaginary component as

$$\begin{aligned} \Delta I_{i(r)}^\phi &= \frac{(P_i^\phi)^{spf} V_{i(r)}^\phi + (Q_i^\phi)^{spf} V_{i(q)}^\phi}{(V_{i(r)}^\phi)^2 + (V_{i(q)}^\phi)^2} \\ &\quad - \sum_{j \in \xi} \sum_{\varphi \in \sigma} G_{ij}^{\phi\varphi} V_{j(r)}^\varphi - B_{ij}^{\phi\varphi} V_{j(q)}^\varphi \end{aligned} \quad (3.46)$$

$$\begin{aligned} \Delta I_{i(q)}^\phi &= \frac{(P_i^\phi)^{spf} V_{i(q)}^\phi - (Q_i^\phi)^{spf} V_{i(r)}^\phi}{(V_{i(r)}^\phi)^2 + (V_{i(q)}^\phi)^2} \\ &\quad - \sum_{j \in \xi} \sum_{\varphi \in \sigma} G_{ij}^{\phi\varphi} V_{j(q)}^\varphi + B_{ij}^{\phi\varphi} V_{j(r)}^\varphi \end{aligned} \quad (3.47)$$

Therefore the power flow formulation using current injections can be solved using (3.48) as

$$\begin{bmatrix} \Delta \mathbf{V}_{1(r)} \\ \Delta \mathbf{V}_{1(q)} \\ \vdots \\ \Delta \mathbf{V}_{N(r)} \\ \Delta \mathbf{V}_{N(q)} \end{bmatrix} = \begin{bmatrix} \frac{\partial I_{1(q)}}{\partial V_{1(r)}} & \frac{\partial I_{1(q)}}{\partial V_{1(q)}} & \cdots & \frac{\partial I_{1(q)}}{\partial V_{N(r)}} & \frac{\partial I_{1(q)}}{\partial V_{N(q)}} \\ \frac{\partial I_{1(r)}}{\partial V_{1(r)}} & \frac{\partial I_{1(r)}}{\partial V_{1(q)}} & \cdots & \frac{\partial I_{1(r)}}{\partial V_{N(r)}} & \frac{\partial I_{1(r)}}{\partial V_{N(q)}} \\ \vdots & \vdots & \vdots & \vdots & \vdots \\ \frac{\partial I_{N(q)}}{\partial V_{1(r)}} & \frac{\partial I_{N(q)}}{\partial V_{1(q)}} & \cdots & \frac{\partial I_{N(q)}}{\partial V_{N(r)}} & \frac{\partial I_{N(q)}}{\partial V_{N(q)}} \\ \frac{\partial I_{N(r)}}{\partial V_{1(r)}} & \frac{\partial I_{N(r)}}{\partial V_{1(q)}} & \cdots & \frac{\partial I_{N(r)}}{\partial V_{N(r)}} & \frac{\partial I_{N(r)}}{\partial V_{N(q)}} \end{bmatrix}^{-1} \begin{bmatrix} \Delta \mathbf{I}_{1(q)} \\ \Delta \mathbf{I}_{1(r)} \\ \vdots \\ \Delta \mathbf{I}_{N(q)} \\ \Delta \mathbf{I}_{N(r)} \end{bmatrix} \quad (3.48)$$

The elements of Jacobian can be obtained

$$\frac{\partial \mathbf{I}_{i(q)}}{\partial V_{i(r)}} = B_{ii} - \text{diag}(La_i) \quad \frac{\partial \mathbf{I}_{i(q)}}{\partial V_{i(r)}} = B_{ij}, \quad i \neq j \quad (3.49)$$

$$\frac{\partial \mathbf{I}_{i(q)}}{\partial V_{i(q)}} = G_{ii} - \text{diag}(Lb_i) \quad \frac{\partial \mathbf{I}_{i(q)}}{\partial V_{i(q)}} = G_{ij}, \quad i \neq j \quad (3.50)$$

$$\frac{\partial \mathbf{I}_{i(r)}}{\partial V_{i(r)}} = G_{ii} - \text{diag}(Lc_i) \quad \frac{\partial \mathbf{I}_{i(r)}}{\partial V_{i(r)}} = G_{ij}, \quad i \neq j \quad (3.51)$$

$$\frac{\partial \mathbf{I}_{i(r)}}{\partial V_{i(q)}} = -B_{ii} - \text{diag}(Ld_i) \quad \frac{\partial \mathbf{I}_{i(r)}}{\partial V_{i(q)}} = -B_{ij}, \quad i \neq j \quad (3.52)$$

where  $B_{ii}$  and  $G_{ii}$  are  $3 \times 3$  imaginary and real parts of admittance element corresponding to node  $i$ . The elements  $La$ ,  $Lb$ ,  $Lc$ ,  $Ld$  depends on type of load connected [19] and can be calculated as below.

$$\begin{aligned} La_i^\phi &= \frac{K_6(Q_{L_i}^\phi)^0 [(V_{i(r)}^\phi)^2 - (V_{i(q)}^\phi)^2] - 2V_{i(r)}^\phi V_{i(q)}^\phi K_3(P_{L_i}^\phi)^0}{((V_{i(r)}^\phi)^2 + (V_{i(q)}^\phi)^2)^4} \\ &+ \frac{V_{i(r)}^\phi V_{i(q)}^\phi K_2(P_{L_i}^\phi)^0 + (V_{i(q)}^\phi)^2 K_5(Q_{L_i}^\phi)^0}{((V_{i(r)}^\phi)^2 + (V_{i(q)}^\phi)^2)^3} + K_4(Q_{L_i}^\phi)^0 \end{aligned} \quad (3.53)$$

$$\begin{aligned} Lb_i^\phi &= \frac{K_3(P_{L_i}^\phi)^0 [(V_{i(r)}^\phi)^2 - (V_{i(q)}^\phi)^2] + 2V_{i(r)}^\phi V_{i(q)}^\phi K_6(Q_{L_i}^\phi)^0}{((V_{i(r)}^\phi)^2 + (V_{i(q)}^\phi)^2)^4} \\ &- \frac{V_{i(r)}^\phi V_{i(q)}^\phi K_5(P_{L_i}^\phi)^0 + (V_{i(r)}^\phi)^2 K_2(P_{L_i}^\phi)^0}{((V_{i(r)}^\phi)^2 + (V_{i(q)}^\phi)^2)^3} - K_1(P_{L_i}^\phi)^0 \end{aligned} \quad (3.54)$$

$$\begin{aligned} Lc_i^\phi &= \frac{K_3(P_{L_i}^\phi)^0 [(V_{i(q)}^\phi)^2 - (V_{i(r)}^\phi)^2] - 2V_{i(r)}^\phi V_{i(q)}^\phi K_6(Q_{L_i}^\phi)^0}{((V_{i(r)}^\phi)^2 + (V_{i(q)}^\phi)^2)^4} \\ &+ \frac{V_{i(r)}^\phi V_{i(q)}^\phi K_5(Q_{L_i}^\phi)^0 - (V_{i(q)}^\phi)^2 K_2(P_{L_i}^\phi)^0}{((V_{i(r)}^\phi)^2 + (V_{i(q)}^\phi)^2)^3} - K_1(P_{L_i}^\phi)^0 \end{aligned} \quad (3.55)$$

$$\begin{aligned} Ld_i^\phi &= \frac{K_6(Q_{L_i}^\phi)^0 [(V_{i(r)}^\phi)^2 - (V_{i(q)}^\phi)^2] - 2V_{i(r)}^\phi V_{i(q)}^\phi K_3(P_{L_i}^\phi)^0}{((V_{i(r)}^\phi)^2 + (V_{i(q)}^\phi)^2)^4} \\ &+ \frac{V_{i(r)}^\phi V_{i(q)}^\phi K_2(P_{L_i}^\phi)^0 - (V_{i(q)}^\phi)^2 K_5(Q_{L_i}^\phi)^0}{((V_{i(r)}^\phi)^2 + (V_{i(q)}^\phi)^2)^3} - K_4(Q_{L_i}^\phi)^0 \end{aligned} \quad (3.56)$$

The voltage mismatch can be represented in compact form as

$$\begin{bmatrix} \Delta V \end{bmatrix} = \begin{bmatrix} J \end{bmatrix}^{-1} \begin{bmatrix} \Delta I \end{bmatrix} \quad (3.57)$$

The updated voltage is given by

$$\begin{bmatrix} V \end{bmatrix}^{k+1} = \begin{bmatrix} V \end{bmatrix}^k + \begin{bmatrix} \Delta V \end{bmatrix} \quad (3.58)$$

### 3.4.2 ICS based Power Flow with DERs

The distributions system is generally unbalanced with non-transposed lines and is been fed from a single source. But with large DER integrations, the distribution system is becoming more active. The DGs in the distribution system can be modeled as PQ bus and PV bus. The PQ model of DG is incorporated in the proposed LF algorithm by treating the injections by the DG as the negative load. A DG can be modeled as a PV bus if its capacity is large enough and has the capability to control the bus voltage. Sensitivity matrix or breakpoint matrix has been developed and utilized for calculating injections by the voltage controlled buses (PV buses) in the distribution network. Sensitivity matrix parameters are determined by writing simple voltage magnitude mismatch equations in terms of  $Z$  parameters and PV bus current injections (called sensitivity equations or matrix). For the distribution system shown in Fig. 5, the sensitivity matrix for computing net reactive current injections by the DGs modeled as PV bus can be written as:

$$\begin{bmatrix} (\Delta \mathbf{V}_{\lambda_1})^x \\ (\Delta \mathbf{V}_{\lambda_2})^x \end{bmatrix} = \begin{bmatrix} Z_{11} & Z_{12} \\ Z_{21} & Z_{22} \end{bmatrix} \begin{bmatrix} (\Delta \mathbf{I}_{\lambda_1})^x \\ (\Delta \mathbf{I}_{\lambda_2})^x \end{bmatrix} \quad (3.59)$$

The elements of impedance matrix is given by:

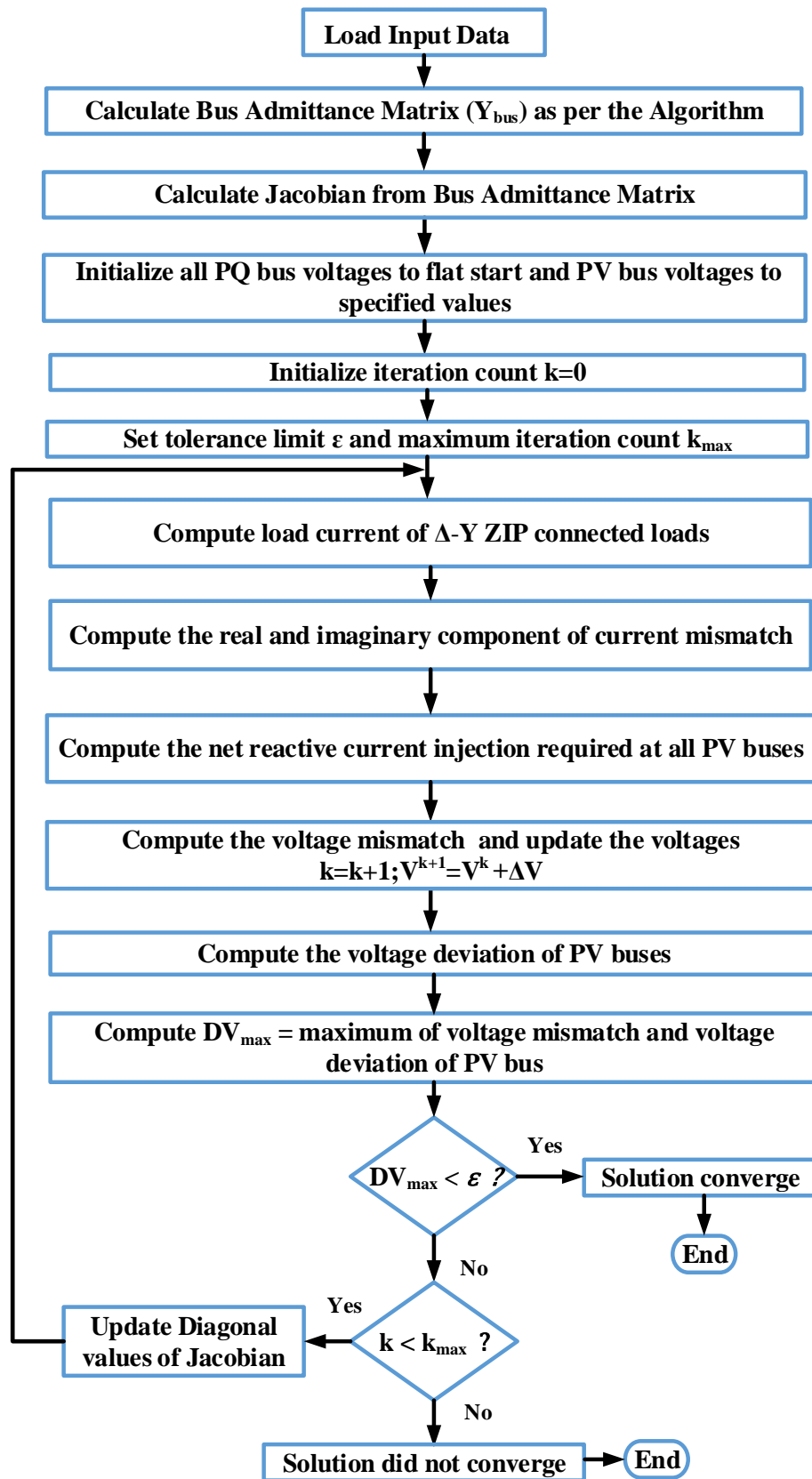


Figure 3.5: Injected Current Sensitivity Based Load Flow

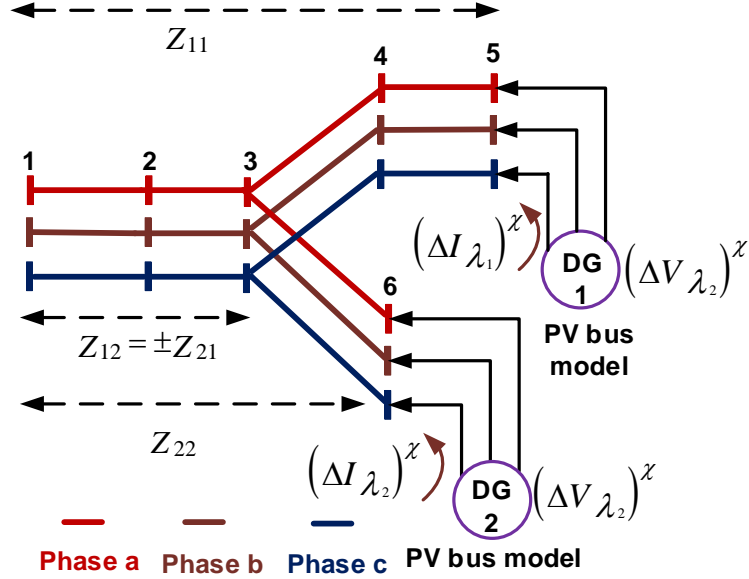


Figure 3.6: Three phase distribution system with DGs modeled as PV bus

$$Z_{11} = Z_{12}^{ser} + Z_{23}^{ser} + Z_{34}^{ser} + Z_{45}^{ser} = R_{11} + \mathbf{j}X_{11} \quad (3.60)$$

$$= (\mathbb{R}_{12}^{ser} + \mathbb{R}_{23}^{ser} + \mathbb{R}_{34}^{ser} + \mathbb{R}_{45}^{ser}) + \mathbf{j}(\mathbb{X}_{12}^{ser} + \mathbb{X}_{23}^{ser} + \mathbb{X}_{34}^{ser} + \mathbb{X}_{45}^{ser})$$

$$Z_{12} = Z_{21} = Z_{12}^{ser} + Z_{23}^{ser} = R_{12} + \mathbf{j}X_{12} = R_{21} + \mathbf{j}X_{21} \quad (3.61)$$

$$= (\mathbb{R}_{12}^{ser} + \mathbb{R}_{23}^{ser}) + \mathbf{j}(\mathbb{X}_{12}^{ser} + \mathbb{X}_{23}^{ser})$$

$$Z_{22} = Z_{12}^{ser} + Z_{23}^{ser} + Z_{36}^{ser} = R_{22} + \mathbf{j}X_{22} \quad (3.62)$$

$$= (\mathbb{R}_{12}^{ser} + \mathbb{R}_{23}^{ser} + \mathbb{R}_{36}^{ser}) + \mathbf{j}(\mathbb{X}_{12}^{ser} + \mathbb{X}_{23}^{ser} + \mathbb{X}_{36}^{ser})$$

The additional current injection required at the PV bus to compensate the difference between specified and computed PV bus voltage can be represented in terms of its real and reactive components:

$$(\Delta \mathbf{I}_{\lambda_1})^x = (\Delta \mathbf{I}_{\lambda_1(r)})^x - \mathbf{j} \Delta \mathbf{I}_{\lambda_1(q)}^x \quad (3.63)$$

$$(\Delta \mathbf{I}_{\lambda_2})^x = (\Delta \mathbf{I}_{\lambda_2(r)})^x - \mathbf{j} \Delta \mathbf{I}_{\lambda_2(q)}^x \quad (3.64)$$

The voltage mismatch equation can be written as:

$$(\Delta \mathbf{V}_{\lambda_1})^x = (\Delta \mathbf{V}_{\lambda_1(r)})^x + \mathbf{j} \Delta \mathbf{V}_{\lambda_1(q)}^x \quad (3.65)$$

$$(\Delta \mathbf{V}_{\lambda_2})^x = (\Delta \mathbf{V}_{\lambda_2(r)})^x + \mathbf{j} \Delta \mathbf{V}_{\lambda_2(q)}^x \quad (3.66)$$

Using (3.60)-(3.66) in (3.59) and splitting the resultant equation into real and imaginary parts:

$$\begin{bmatrix} (\Delta \mathbf{V}_{\lambda_1(r)})^x \\ (\Delta \mathbf{V}_{\lambda_2(r)})^x \end{bmatrix} = \begin{bmatrix} X_{11} & X_{12} & R_{11} & R_{12} \\ X_{21} & X_{22} & R_{12} & R_{22} \end{bmatrix} \begin{bmatrix} (\Delta \mathbf{I}_{\lambda_1(q)})^x \\ (\Delta \mathbf{I}_{\lambda_2(q)})^x \\ (\Delta \mathbf{I}_{\lambda_1(r)})^x \\ (\Delta \mathbf{I}_{\lambda_2(r)})^x \end{bmatrix} \quad (3.67)$$

$$\begin{bmatrix} (\Delta \mathbf{V}_{\lambda_1(q)})^x \\ (\Delta \mathbf{V}_{\lambda_2(q)})^x \end{bmatrix} = \begin{bmatrix} -R_{11} & -R_{12} & X_{11} & X_{12} \\ -R_{21} & -R_{22} & X_{12} & X_{22} \end{bmatrix} \begin{bmatrix} (\Delta \mathbf{I}_{\lambda_1(q)})^x \\ (\Delta \mathbf{I}_{\lambda_2(q)})^x \\ (\Delta \mathbf{I}_{\lambda_1(r)})^x \\ (\Delta \mathbf{I}_{\lambda_2(r)})^x \end{bmatrix} \quad (3.68)$$

Since the real power supply by the DER modeled as PV bus is constant and thus additional real power injections in the iteration  $k$  by distributed generations will be 0. Thus,

$$(\Delta \mathbf{I}_{\lambda_1(r)})^x = \begin{bmatrix} (\Delta I_{\lambda_1(r)}^a)^x \\ (\Delta I_{\lambda_1(r)}^b)^x \\ (\Delta I_{\lambda_1(r)}^c)^x \end{bmatrix} = \begin{bmatrix} \mathbf{0} \\ \mathbf{0} \\ \mathbf{0} \end{bmatrix} \quad (3.69)$$

$$(\Delta \mathbf{I}_{\lambda_2(r)})^x = \begin{bmatrix} (\Delta I_{\lambda_2(r)}^a)^x \\ (\Delta I_{\lambda_2(r)}^b)^x \\ (\Delta I_{\lambda_2(r)}^c)^x \end{bmatrix} = \begin{bmatrix} \mathbf{0} \\ \mathbf{0} \\ \mathbf{0} \end{bmatrix} \quad (3.70)$$

The voltage mismatch can be computed using following equation:

$$\begin{bmatrix} (\Delta \mathbf{V}_{\lambda_1})^x \\ (\Delta \mathbf{V}_{\lambda_2})^x \end{bmatrix} = \begin{bmatrix} |\mathbf{V}_{\lambda_1^{pv}}| - |(V_{\lambda_1})^k| \\ |\mathbf{V}_{\lambda_2^{pv}}| - |(V_{\lambda_2})^k| \end{bmatrix} \quad (3.71)$$

Thus, on splitting the above equation into real and imaginary parts it is evident that the voltage mismatch equation does not have any imaginary components. Hence,

$$(\Delta \mathbf{V}_{\lambda_1(q)})^x = \begin{bmatrix} (\Delta V_{\lambda_1(q)}^a)^x \\ (\Delta V_{\lambda_1(q)}^b)^x \\ (\Delta V_{\lambda_1(q)}^c)^x \end{bmatrix} = \begin{bmatrix} \mathbf{0} \\ \mathbf{0} \\ \mathbf{0} \end{bmatrix} \quad (3.72)$$

$$(\Delta \mathbf{V}_{\lambda_2(q)})^x = \begin{bmatrix} (\Delta V_{\lambda_2(q)}^a)^x \\ (\Delta V_{\lambda_2(q)}^b)^x \\ (\Delta V_{\lambda_2(q)}^c)^x \end{bmatrix} = \begin{bmatrix} \mathbf{0} \\ \mathbf{0} \\ \mathbf{0} \end{bmatrix} \quad (3.73)$$

Using (3.69)-(3.73) in (3.67) and (3.68), the additional reactive current injection can be computed using equation below:

$$\begin{bmatrix} (\Delta \mathbf{V}_{\lambda_1(r)})^x \\ (\Delta \mathbf{V}_{\lambda_2(r)})^x \end{bmatrix} = \begin{bmatrix} X_{11} & X_{12} \\ X_{21} & X_{22} \end{bmatrix} \begin{bmatrix} (\Delta \mathbf{I}_{\lambda_1(q)})^x \\ (\Delta \mathbf{I}_{\lambda_2(q)})^x \end{bmatrix} \quad (3.74)$$

In compact form (3.74) can be written as:

$$\Delta V^r = X \Delta I^q \quad (3.75)$$

The total reactive current injections by the DERs modeled as PV buses at iteration  $k$  is computed using the equation below:

$$\mathbf{I}_{\lambda_1 \mathbf{q}}^{\chi} = \Delta \mathbf{I}_{\lambda_1(\mathbf{q})}^{\chi} + \sum_{\mathbf{f}=1}^{\chi-1} (\Delta \mathbf{I}_{\lambda_1(\mathbf{q})})^{\mathbf{f}} \quad (3.76)$$

$$\mathbf{I}_{\lambda_2 \mathbf{q}}^{\chi} = \Delta \mathbf{I}_{\lambda_2(\mathbf{q})}^{\chi} + \sum_{\mathbf{f}=1}^{\chi-1} \Delta \mathbf{I}_{\lambda_2(\mathbf{q})}^{\mathbf{f}} \quad (3.77)$$

Once the net reactive current injections are computed and reflected in the current injections vector/matrix, the LF solution will be obtained without updating any elements of the Jacobian matrix. The reactive current injection is then added to current mismatch vector of respective buses. The voltage mismatch equation in (3.48) is modified considering PV bus at bus  $p$  and is given by (3.78).

$$\begin{bmatrix} \Delta \mathbf{V}_{1(r)} \\ \Delta \mathbf{V}_{1(q)} \\ \vdots \\ \Delta \mathbf{V}_{p(r)} \\ \Delta \mathbf{V}_{p(q)} \\ \vdots \\ \Delta \mathbf{V}_{N(r)} \\ \Delta \mathbf{V}_{N(q)} \end{bmatrix} = \begin{bmatrix} \frac{\partial I_{1(q)}}{\partial V_{1(r)}} & \frac{\partial I_{1(q)}}{\partial V_{1(q)}} & \cdots & \frac{\partial I_{1(q)}}{\partial V_{N(r)}} & \frac{\partial I_{1(q)}}{\partial V_{N(q)}} \\ \frac{\partial I_{1(r)}}{\partial V_{1(r)}} & \frac{\partial I_{1(r)}}{\partial V_{1(q)}} & \cdots & \frac{\partial I_{1(r)}}{\partial V_{N(r)}} & \frac{\partial I_{1(r)}}{\partial V_{N(q)}} \\ \vdots & \vdots & \vdots & \vdots & \vdots \\ \frac{\partial I_{p(q)}}{\partial V_{1(r)}} & \frac{\partial I_{p(q)}}{\partial V_{1(q)}} & \cdots & \frac{\partial I_{p(q)}}{\partial V_{N(r)}} & \frac{\partial I_{p(q)}}{\partial V_{N(q)}} \\ \frac{\partial I_{p(r)}}{\partial V_{1(r)}} & \frac{\partial I_{p(r)}}{\partial V_{1(q)}} & \cdots & \frac{\partial I_{p(r)}}{\partial V_{N(r)}} & \frac{\partial I_{p(r)}}{\partial V_{N(q)}} \\ \vdots & \vdots & \vdots & \vdots & \vdots \\ \frac{\partial I_{N(q)}}{\partial V_{1(r)}} & \frac{\partial I_{N(q)}}{\partial V_{1(q)}} & \cdots & \frac{\partial I_{N(q)}}{\partial V_{N(r)}} & \frac{\partial I_{N(q)}}{\partial V_{N(q)}} \\ \frac{\partial I_{N(r)}}{\partial V_{1(r)}} & \frac{\partial I_{N(r)}}{\partial V_{1(q)}} & \cdots & \frac{\partial I_{N(r)}}{\partial V_{N(r)}} & \frac{\partial I_{N(r)}}{\partial V_{N(q)}} \end{bmatrix}^{-1} \begin{bmatrix} \Delta \mathbf{I}_{1(q)} \\ \Delta \mathbf{I}_{1(r)} \\ \vdots \\ \Delta \mathbf{I}_{p(q)} + (\Delta \mathbf{I}_{\lambda_p(\mathbf{q})})^{\chi} \\ \Delta \mathbf{I}_{p(r)} \\ \vdots \\ \Delta \mathbf{I}_{N(q)} \\ \Delta \mathbf{I}_{N(r)} \end{bmatrix} \quad (3.78)$$

Special case: Consider a scenario in which the DGs modeled as PV bus are not three phase DGs. In this case, the sensitivity matrix computation will be based on the phases to which single phase DGs are connected. For example, consider the distribution system shown in Fig.5, the three phase DGs are replaced by single phase DGs and are connected with phase b and phase c of bus 5 and 6 respectively. The procedure of reduction of sensitivity matrix and when it is required is explained using

the scenario as below.

$$\begin{bmatrix} (\Delta V_{\lambda_1(r)}^b)^x \\ (\Delta V_{\lambda_2(r)}^c)^x \end{bmatrix} = \begin{bmatrix} X_{11}^{bb} & X_{12}^{bc} \\ X_{21}^{bc} & X_{22}^{cc} \end{bmatrix} \begin{bmatrix} (\Delta I_{\lambda_1(q)})^x \\ (\Delta I_{\lambda_2(q)})^x \end{bmatrix} \quad (3.79)$$

The reactive power required should be within lower and upper bounds of generator limits. If this is violated, reactive power generation is set to an extreme value, and the node is considered a PQ node. The reactive current injection is recalculated with this extreme value. A flowchart of the current injection-based load flow is shown in Fig. 3.5.

### 3.4.3 Simulation Results

The proposed modeling approach is assessed by using four IEEE test distribution systems. To test the efficacy of the proposed load flow algorithm for larger systems, two additional test systems are derived. All the systems are unbalanced consisting of different load types, voltage regulators, capacitor banks, and multi-phase laterals. A summary of characteristics of test systems used is depicted in Table 3.2. The accuracy of the proposed modeling approach is assessed by comparing load-flow voltage solutions obtained with benchmark solutions and existing algorithms in the literature.

Table 3.2: Test Systems

Sl No	Test System	No of Nodes	1 Ph VRegs	T/F	Shunt Caps	Avg R/X
1	IEEE 4 Bus	12	0	1	0	.2522
2	IEEE 13 Bus	32	3	1	2	0.3514
3	IEEE 34 Bus	86	6	1	4	0.2512
4	IEEE 123 Bus	256	9	1	4	0.2645
5	650 Bus	1950	12	0	4	0.2145
6	2500 Bus	6817	12	0	4	0.2145

### 3.4.3.1 Test System 1

The IEEE-4 bus system was used as a test system for verifying the different types of transformer connections. Five different transformer connections are tested. Load flow analysis with step up and step down operation of transformer with balanced and unbalanced loading conditions have been done and validated with benchmark values and error in all cases are less than 0.001%. The comparison of load flow results using the proposed method (ICS) with benchmark (BM) values for only Yg-Yg connected step down transformer with unbalanced loading are shown Fig.3.7(a)-Fig.3.7(c).

### 3.4.3.2 Test System 2

The IEEE 13 bus system is a highly loaded short feeder with a substation voltage regulator and one inline transformer. The loads are unbalanced with all combinations of load types (constant current, constant impedance, constant power). This feeder was mainly used to test the effectiveness of the algorithm in handling different types and connections of load viz star/delta ZIP loads. The comparison of load flow results using proposed method (ICS) with benchmark (BM) values are shown Fig.3.7(d)-Fig.3.7(f).

### 3.4.3.3 Test System 3

The IEEE 123 bus system contains a substation voltage regulator, three line voltage regulators, one inline transformer, and four shunt capacitor banks. This feeder was used to compare load-flow voltage solutions obtained with existing algorithms in the literature for various loading factors and R/X ratios. It was also used to analyze the inclusion of PV nodes using the proposed method. Two test cases were analyzed.

#### Case 1: Load Flow with PQ buses

The load flow results obtained using the proposed method are compared with load flow results obtained using a Newton Raphson(NR) load flow. The comparison for different loading conditions and various R/X ratios are depicted in Table 3.3 and

Table 3.3: Comparison of NR and ICS for various loading

Loading Factor	Newton Raphson		Current Injection	
	Iterations	NET	Iterations	NET
0.1	6	11.127	3	0.8533
0.3	5	9.4464	4	0.92326
0.5	5	9.4316	4	0.97507
0.7	4	7.9622	5	0.97144
0.9	4	7.8078	5	0.98544
1	4	7.8025	5	1
1.1	4	7.8794	5	1.00702
1.3	4	7.8722	6	1.02251
1.5	4	7.9329	6	1.03462
1.7	4	7.9039	7	1.06802
3	5	9.3924	13	1.58581

Table 3.4: Comparison of NR and ICS for various R/X

R/X Factor	Newton Raphson		Current Injection	
	Iterations	NET	Iterations	NET
0.125	4	9.70944	4	1.0877
0.25	4	9.6621	4	1.0513
0.5	5	8.0319	5	1
1	5	8.33466	5	1.1116
2	7	8.11662	6	1.1209
3	9	11.677	7	1.4984
5	NC	NC	10	1.654

Table 3.4. All the non-zero elements in the NR method are updated in each iteration whereas only diagonal elements are updated in the case of the proposed method. It is clear from the results that, the proposed approach is very much faster than the Newton Raphson method due to minimal Jacobian computation per iteration.

#### Case 2: Load Flow with PV buses

The test systems are modified by placing multi-phase DERs with voltage control capability at different locations. To show the effectiveness of the proposed method in dealing with multiphase DERs, a test case with 1-phase, 2-phase and 3-phase DERs in 123 bus systems has been used. The load flow result showing location, time, and

reactive power injection per phase is summarized in Table 3.6. The load flow results with and without PV buses are shown in Fig. 3.10.

Table 3.5: Summary of load flow using ICS

Sl	Test System	No. of Iter.	Time (sec)	Max Error Ph A (pu)	Max Error Ph B (pu)	Max Error Ph C (pu)
1	IEEE 4 Bus	3	0.0563	0.00019	0.00013	0.00022
2	IEEE 13 Bus	3	0.1727	0.0035	0.0014	0.00092
3	IEEE 34 Bus	4	0.2637	0.0065	0.0039	0.0069
4	IEEE 123 Bus	4	0.3133	0.00095	0.00064	0.00063
5	650 Bus	4	8.6779	0.00062	0.0014	0.00065
6	2500 Bus	4	100.21	0.0017	0.0018	0.0023

Table 3.6: Summary of PV bus in 123 bus system

Bus	No PV Bus			With PV Bus (1pu ref)					
	Voltage(pu)			Voltage(pu)			Q injection(Kvar)		
	Va	Vb	Vc	Va	Vb	Vc	Qa	Qb	Qc
151	0.9884			0.9998			49.57		
27	0.9952		1.0027	0.9999		0.9999	-27.72		-57.86
66	0.9850	1.025	0.9924	0.9999	1.0000	0.9999	73.38	-65.93	38.43

#### 3.4.3.4 Test System 4

Two custom test feeders (650 bus system and 2500 bus system) are derived from the IEEE 8500 node test feeder. These were used to test the efficacy of the proposed load flow algorithm for larger systems. The comparison of load flow results using proposed method (ICS) with Opends voltage (BM) values for 650 bus system are shown Fig.3.8(a)-Fig.3.8(c) and for 2500 bus system are shown Fig.3.8(d)-Fig.3.8f).

A complete summary of results including the number of iteration and total time taken is shown in table . 3.5. It is evident from results in Fig. 3.8(g)-Fig. 3.8(l) that the proposed method is accurate with a maximum error below 0.003% except for 34 bus system. The higher error in the 34 bus system is due to the larger number of distributed loads, which we approximate as spot loads on both the connecting nodes.

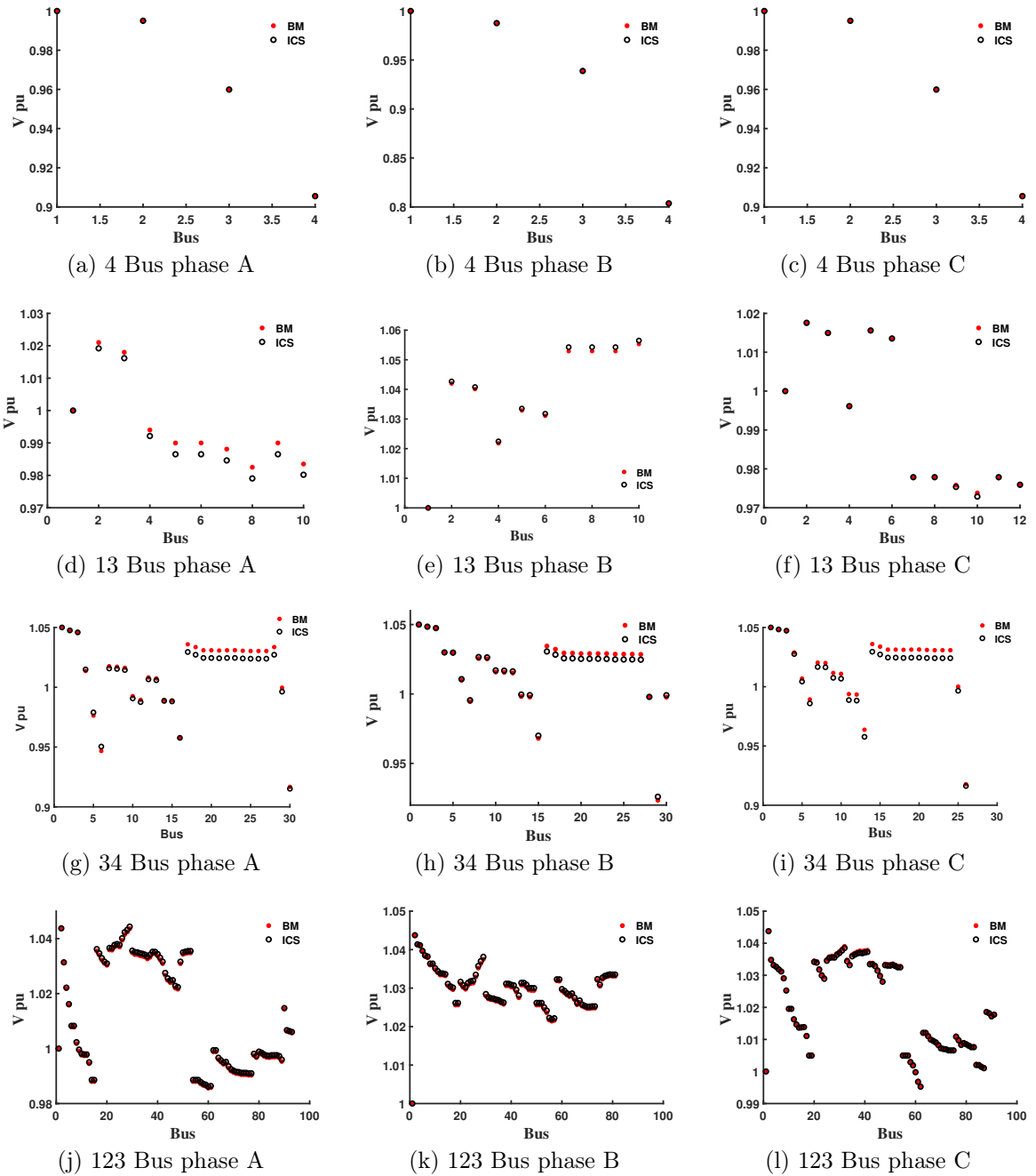


Figure 3.7: Validation of LF results

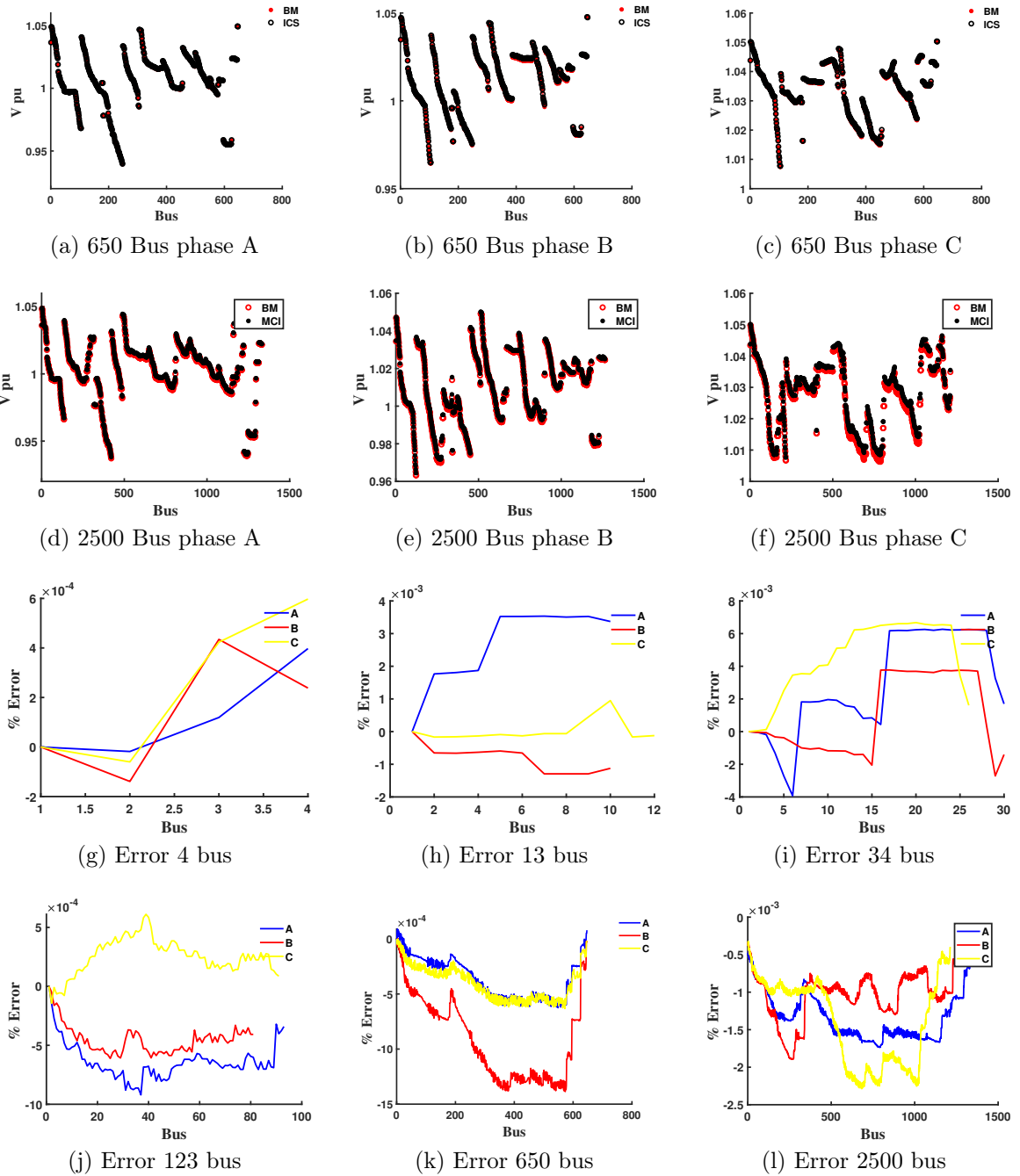


Figure 3.8: Validation of LF results and % Error Plots

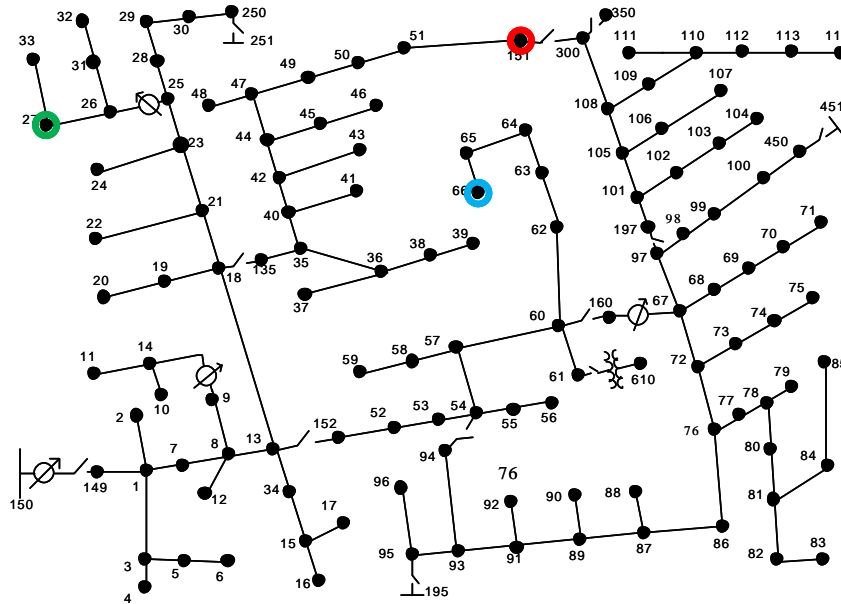


Figure 3.9: DER in 123 bus

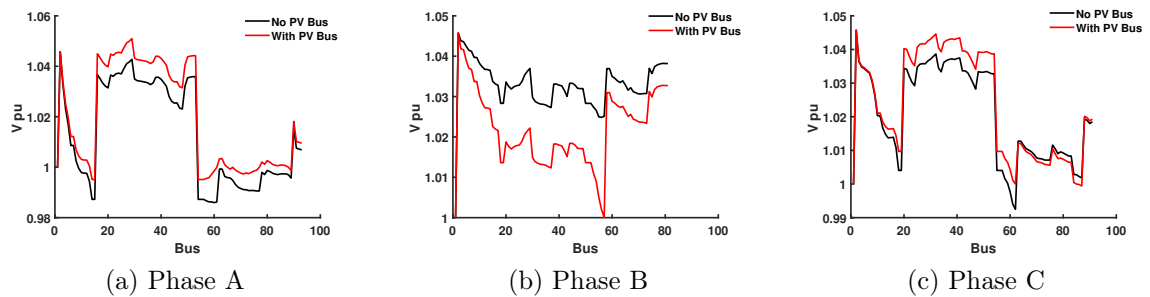


Figure 3.10: PV Bus in 123 bus system

### 3.5 Three Sequence Based Steady State Analysis

For an  $N$  bus system, the existing three-phase power flow approaches require solving a set of  $6N$  nonlinear simultaneous equations. This might be computationally unacceptable for relatively large systems. A method based on the sequence components frame can be utilized where a three-phase unbalanced power flow is decomposed into three separate sub-problems. The positive sequence subproblem is solved by using the injected current sensitivity iterative scheme and the other subproblems are formulated into two sets of linear simultaneous equations. This would reduce the size

of the Jacobian from  $6N \times 6N$  in case of a three phase power flow to a  $2N \times 2N$  in case of a positive sequence subproblem. Two sets of linear simultaneous equations would have a dimension of  $N \times N$

### 3.5.1 Advantages of Sequence Based Methods

The distribution systems generally consist of untransposed lines and single phase laterals. The proliferation of single phase DERs can aggravate the unbalance in the system. DERs capable of injecting negative sequence current during normal operating conditions can help reduce this unbalance. The level of unbalance in the voltage at PCC, or the negative sequence voltage at PCC could be used to determine the amount of negative sequence current a DER should produce during normal operation. With the existing phase based analysis, a phase to sequence conversion at each DER terminal is required to achieve this. Also, most of the power system data are available in terms of sequence values (for eg. data of distribution lines, transformers, generators) which are frequently transformed back to phase components to do analysis using phase coordinates methods [47]. In addition to that most of the inverter-based DGs produce only positive sequence current during a fault. This can be modeled easily if fault analysis is done in the sequence domain than the phase domain. There is a need for DER injecting negative sequence current during a fault which can reduce the overvoltage in unfaulted phases. Accurate negative sequence voltage at PCC during fault will be required to find the amount of negative sequence current that DER should inject during fault. Taking all of these factors into consideration and owing to its computational advantage, we can conclude that a method that can directly use sequence components to perform the steady analysis is more favorable in DER integrated power system.

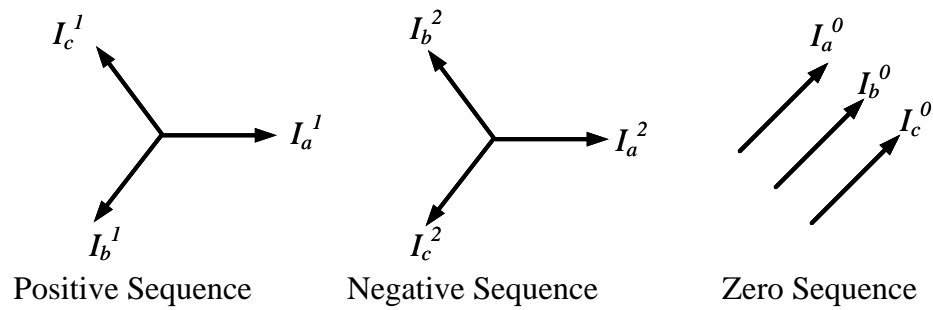


Figure 3.11: Sequence Components

### 3.5.2 Sequence Components

Symmetrical or sequence components allows us to represent an unbalanced vector using a set of 3 balanced vectors. Any unbalanced vector can be represented as a combination of 3 balanced vectors as shown in Fig. 5.5

$$\begin{aligned}
 I^a &= I_a^0 + I_a^1 + I_a^2 \\
 I^b &= I_b^0 + I_b^1 + I_b^2 \\
 I^c &= I_c^0 + I_c^1 + I_c^2
 \end{aligned} \tag{3.80}$$

According to fig Fig .5.5 we can write

$$\begin{aligned}
 I_a^0 &= I_a^0 & I_a^1 &= I_a^1 & I_a^2 &= I_a^2 \\
 I_b^0 &= I_a^0 & I_b^1 &= a^2 I_a^1 & I_b^2 &= a I_a^2 \\
 I_c^0 &= I_a^0 & I_c^1 &= a I_a^1 & I_c^2 &= a^2 I_a^2
 \end{aligned} \tag{3.81}$$

where  $\mathbf{a} = \mathbf{1} < 120$      $\mathbf{a}^2 = \mathbf{1} < 240$

Therefore

$$\begin{aligned}
 I^a &= I_a^0 + I_a^1 + I_a^2 \\
 I^b &= I_a^0 + a^2 I_a^1 + a I_a^2 \\
 I^c &= I_a^0 + a I_a^1 + a^2 I_a^2
 \end{aligned} \tag{3.82}$$

This can be written in matrix form as

$$\begin{bmatrix} I^a \\ I^b \\ I^c \end{bmatrix} = \begin{bmatrix} 1 & 1 & 1 \\ 1 & a^2 & a \\ 1 & a & a^2 \end{bmatrix} \begin{bmatrix} I^0 \\ I^1 \\ I^2 \end{bmatrix} \quad (3.83)$$

Therefore we can transform a current vector from sequence representation to phase representation as

$$\mathbf{I}^{abc} = \mathbf{C}\mathbf{I}^{012} \quad (3.84)$$

The sequence components can be obtained from phase components as

$$\mathbf{I}^{012} = \mathbf{C}^{-1}\mathbf{I}^{abc}$$

$$\mathbf{C}^{-1} = \frac{1}{3} \begin{bmatrix} 1 & 1 & 1 \\ 1 & a^2 & a \\ 1 & a & a^2 \end{bmatrix} \quad (3.85)$$

$$\begin{bmatrix} I^0 \\ I^1 \\ I^2 \end{bmatrix} = \frac{1}{3} \begin{bmatrix} 1 & 1 & 1 \\ 1 & a^2 & a \\ 1 & a & a^2 \end{bmatrix} \begin{bmatrix} I^a \\ I^b \\ I^c \end{bmatrix} \quad (3.86)$$

For a transmission line as shown in Fig. 3.12 we can write

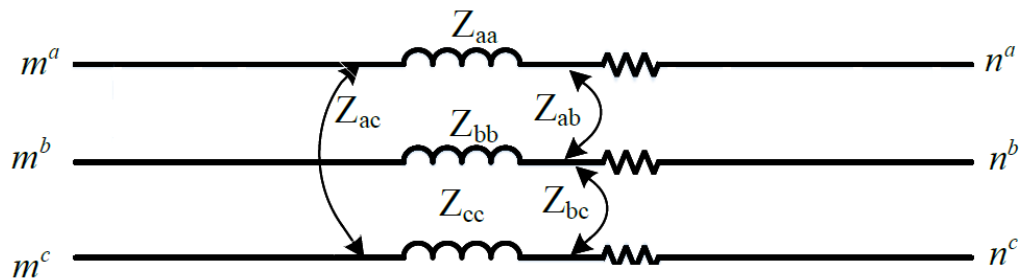


Figure 3.12: Distribution line

$$\begin{aligned}
V_{mn}^a &= z^{aa} I^a + z^{ab} I^b + z^{ac} I^c \\
V_{mn}^b &= z^{ab} I^a + z^{bb} I^b + z^{bc} I^c \\
V_{mn}^c &= z^{ca} I^a + z^{cb} I^b + z^{cc} I^c
\end{aligned} \tag{3.87}$$

$$\begin{bmatrix} V^a \\ V^b \\ V^c \end{bmatrix} = \begin{bmatrix} z^{aa} & z^{ab} & z^{ac} \\ z^{ba} & z^{bb} & z^{bc} \\ z^{ca} & z^{cb} & z^{cc} \end{bmatrix} \begin{bmatrix} I^a \\ I^b \\ I^c \end{bmatrix} \tag{3.88}$$

$$\mathbf{V}^{abc} = \mathbf{Z}^{abc} \mathbf{I}^{abc} \tag{3.89}$$

Converting to sequence component, we can write

$$\mathbf{C} \mathbf{V}^{012} = \mathbf{Z}^{abc} \mathbf{C} \mathbf{I}^{012} \tag{3.90}$$

Premultiplying by  $\mathbf{C}^{-1}$  we get

$$\begin{aligned}
\mathbf{V}^{012} &= \mathbf{C}^{-1} \mathbf{Z}^{abc} \mathbf{C} \mathbf{I}^{012} \\
\mathbf{V}^{012} &= \mathbf{Z}^{012} \mathbf{I}^{012}
\end{aligned} \tag{3.91}$$

where

$$\mathbf{Z}^{012} = \mathbf{C}^{-1} \mathbf{Z}^{abc} \mathbf{C} \tag{3.92}$$

$$\begin{bmatrix} z^{00} & z^{01} & z^{02} \\ z^{10} & z^{11} & z^{12} \\ z^{20} & z^{21} & z^{22} \end{bmatrix} = \frac{1}{3} \begin{bmatrix} 1 & 1 & 1 \\ 1 & a^2 & a \\ 1 & a & a^2 \end{bmatrix} \begin{bmatrix} z^{aa} & z^{ab} & z^{ac} \\ z^{ba} & z^{bb} & z^{bc} \\ z^{ca} & z^{cb} & z^{cc} \end{bmatrix} \begin{bmatrix} 1 & 1 & 1 \\ 1 & a^2 & a \\ 1 & a & a^2 \end{bmatrix} \tag{3.93}$$

### 3.5.3 Time Complexity and Computational Improvement

As mentioned in section 3.5, for an N bus system, the size of Jacobian will be reduced from 6Nx6N to 2Nx2N for positive sequence subproblem and NxN for two

Table 3.7: No of mathematical operations.

Operation	No of Operation
Divisions $N_d$	$N(N + 1)/2$
Multiplications $N_m$	$(2N^3 + 3N^2 - 5N)/6$
Subtractions $N_s$	$(2N^3 + 3N^2 - 5N)/6$
Total $N_T$	$2N^3/3$

Table 3.8: Total No of computations for a phase method.

No of Buses <b>n</b>	<b>N=6n</b>	$N_d$	$N_m$	$N_s$	$N_T$
4	24	300	4876	4876	10052
13	78	3081	161161	161161	325403
34	204	20910	2850526	2850526	5721962
123	738	272691	1.34E+08	1.34E+08	2.69E+08
650	3900	7606950	1.98E+10	1.98E+10	3.96E+10
2500	15000	1.13E+08	1.13E+12	1.13E+12	2.25E+12

sets of linear simultaneous equations for negative and zero sequence subproblem. To solve a system of  $N$  equations for  $N$  unknowns (by performing row operations on the matrix until it is in echelon form, and then solving for each unknown in reverse order) the total number of computations required [48] are shown in table 3.7. So arithmetic complexity is cubic and can be represented as  $\mathcal{O}(N^3)$ .

Table 3.9: Total No of computations for a positive sequence method.

No of Buses <b>n</b>	<b>N=2n</b>	$N_d$	$N_m$	$N_s$	$N_T$
4	8	36	196	196	428
13	26	351	6175	6175	12701
34	68	2346	107066	107066	216478
123	246	30381	4992365	4992365	10015111
650	1300	845650	7.33E+08	7.33E+08	1.47E+09
2500	5000	12502500	4.17E+10	4.17E+10	8.34E+10

Table 3.10: Total No of computations for a negative and zero sequence method.

No of Buses <b>n</b>	<b>N=n</b>	$N_d$	$N_m$	$N_s$	$N_T$
4	4	10	26	26	62
13	13	91	806	806	1703
34	34	595	13651	13651	27897
123	123	7626	627751	627751	1263128
650	650	211575	91752375	91752375	1.84E+08
2500	2500	3126250	5.21E+09	5.21E+09	1.04E+10

Table 3.11: Improvement in computation.

No of Buses <b>n</b>	Three phase $N_{Tp}$	Three Sequence $N_{Ts}$	Improvement $N_{Tp}/N_{Ts}$
4	10052	552	18.21014
13	325403	16107	20.20258
34	5721962	272272	21.01561
123	2.69E+08	12541367	21.43155
650	3.96E+10	1.83E+09	21.5677
2500	2.25E+12	1.04E+11	21.59158

### 3.6 Three Sequence Load Flow Analysis

The three-phase power flow equations in the phase frame are derived from the following bus voltage equations:

$$\begin{bmatrix} Y_{11}^{abc} & Y_{12}^{abc} & \dots & Y_{1N}^{abc} \\ Y_{21}^{abc} & Y_{22}^{abc} & \dots & Y_{2N}^{abc} \\ \vdots & \vdots & \ddots & \vdots \\ Y_{N1}^{abc} & Y_{N2}^{abc} & \dots & Y_{NN}^{abc} \end{bmatrix} \begin{bmatrix} \mathbf{V}_1^{abc} \\ \mathbf{V}_2^{abc} \\ \vdots \\ \mathbf{V}_N^{abc} \end{bmatrix} = \begin{bmatrix} \mathbf{I}_1^{abc} \\ \mathbf{I}_2^{abc} \\ \vdots \\ \mathbf{I}_N^{abc} \end{bmatrix} \quad (3.94)$$

where  $Y_{ii}^{abc}$  is  $3 \times 3$  submatrix of the self-admittance of bus  $i$  and  $Y_{ij}^{abc}$  is  $3 \times 3$  submatrix of the mutual-admittance between bus  $i$  and  $j$ . Each of the phase admittance submatrix in (3.94) can be converted to sequence submatrices using (3.95)

$$\mathbf{Y}^{012} = \mathbf{C}^{-1} \mathbf{Y}^{abc} \mathbf{C} \quad (3.95)$$

Converting voltage and current matrices in sequence form, bus voltage equations of

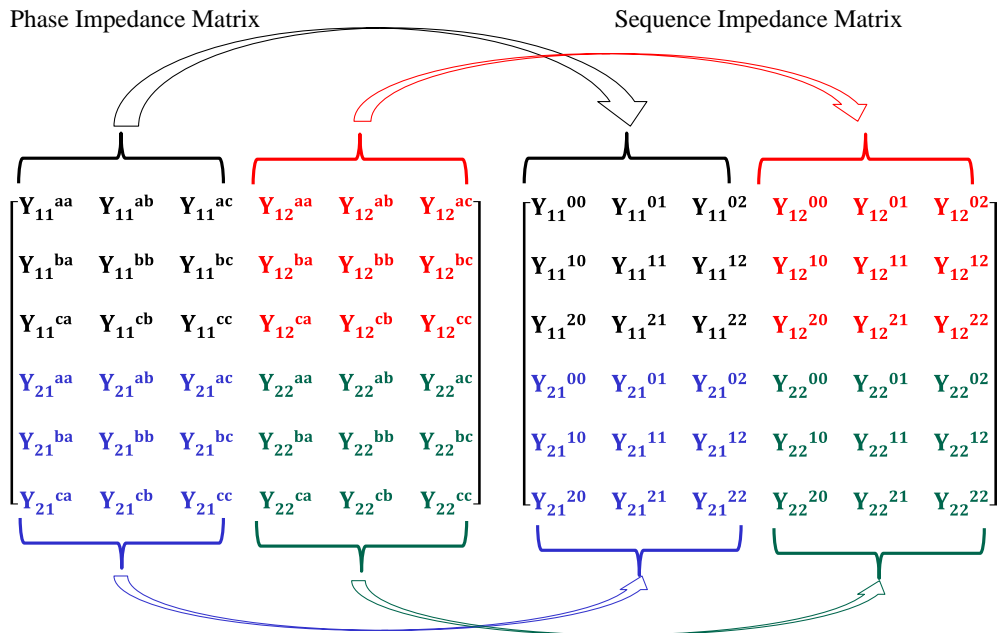


Figure 3.13: Sequence component of admittance submatrices

a power system in sequence component frame can be written as

$$\begin{bmatrix} Y^{00} & Y^{01} & Y^{02} \\ Y^{10} & Y^{11} & Y^{12} \\ Y^{20} & Y^{21} & Y^{22} \end{bmatrix} \begin{bmatrix} V^0 \\ V^1 \\ V^2 \end{bmatrix} = \begin{bmatrix} I^0 \\ I^1 \\ I^2 \end{bmatrix} \quad (3.96)$$

Since the magnitudes of  $V^1$  and  $I^1$  are much larger than those of  $V^2$ ,  $I^2$  and  $V^0, I^0$  respectively, and elements of  $Y_{km}$ , ( $k \neq m$ ) are smaller than those of  $Y_{kk}$  (3.96) can be decomposed into three independent equations [9] as

$$\mathbf{Y}^{00}V^0 = \mathbf{I}^0 - (Y^{01}V^1 + Y^{02}V^2) \quad (3.97)$$

$$\mathbf{Y}^{11}V^1 = \mathbf{I}^1 - (Y^{10}V^0 + Y^{12}V^2) = \mathbf{I}^{1T} \quad (3.98)$$

$$\mathbf{Y}^{22}V^2 = \mathbf{I}^2 - (Y^{20}V^0 + Y^{21}V^1) \quad (3.99)$$

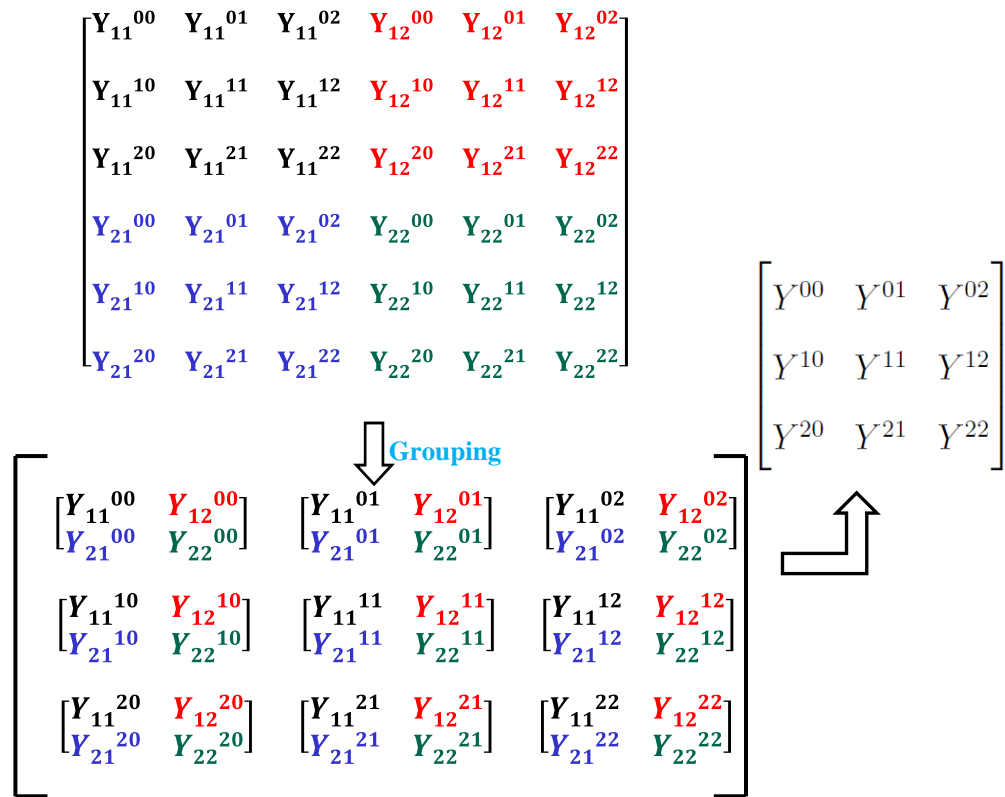


Figure 3.14: Grouping of Sequence admittance submatrices

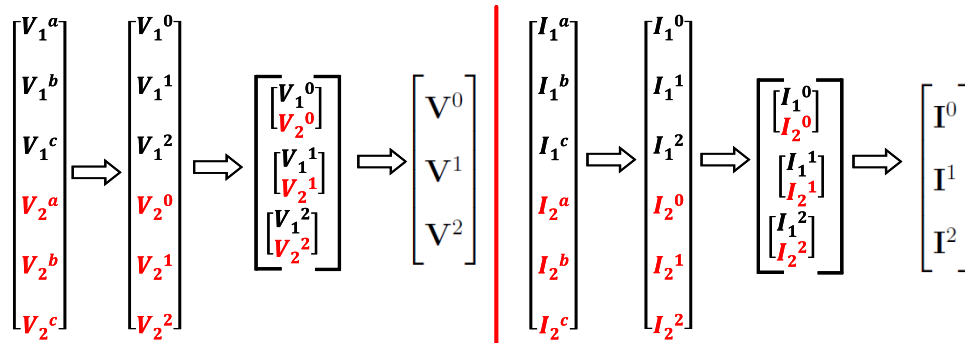


Figure 3.15: Grouping of Sequence current and voltage submatrices

The equations (3.97), (3.98) and (3.99) can be used to solve power flow in zero, positive and negative sequences respectively. Here the injected current in each sequence is modified using mutual admittance and voltage of other sequence. This modification aids in bringing in the effect of untransposed lines which is common in distribution

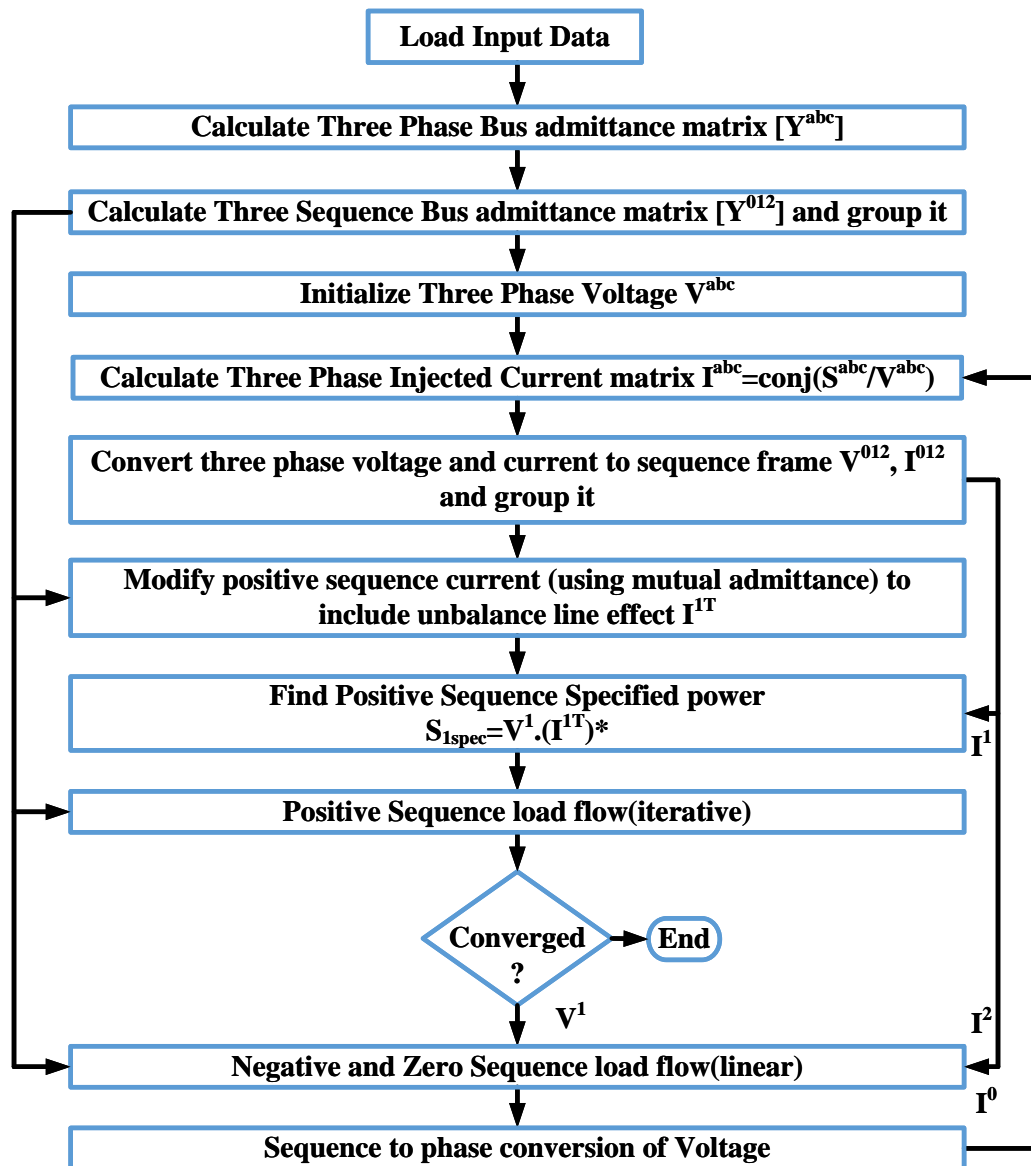


Figure 3.16: Three Sequence Load Flow.

systems. These equations can be used iteratively to solve three sequence power flow in (3.96). Normally, the magnitudes of positive sequence voltage and current will be much larger than those of negative and zero sequence and hence it can be justified that (3.98) corresponding to the positive sequence, is the main part of the three-phase power flow irrespective of the severity of system unbalance. The injected current sensitivity based power flow is used to solve positive sequence power flow.

Table 3.12: Substation Power.

	Phase Method			Sequence Method		
	Ph.a	Ph.b	Ph.c	Ph.a	Ph.b	Ph.c
P (KW)	1466.9	964.67	1198.4	1466.8	964.6	1198.6
Q (KVAR)	583.1	343.7	401.2	583	343.6	401.1

Different types of loads (ZIP) are considered and shunt capacitors are considered as constant impedance loads. A flowchart of sequence component load flow for an unbalanced distribution system is shown in Fig. 3.16. The IEEE 123 bus system was used to compare load-flow voltage solutions obtained using sequence components with the solution obtained using a three phase algorithm. It is clear from the results in Fig. 3.17, Fig. 3.18 and Table 3.12 that, proposed approach gives solution very much closer to the solution using a three phase algorithm. This proves the efficacy of the proposed sequence based method to perform load flow analysis on a distribution system in presence of unbalanced loads, untransposed lines, multiphase laterals voltage regulators, and distribution transformers.

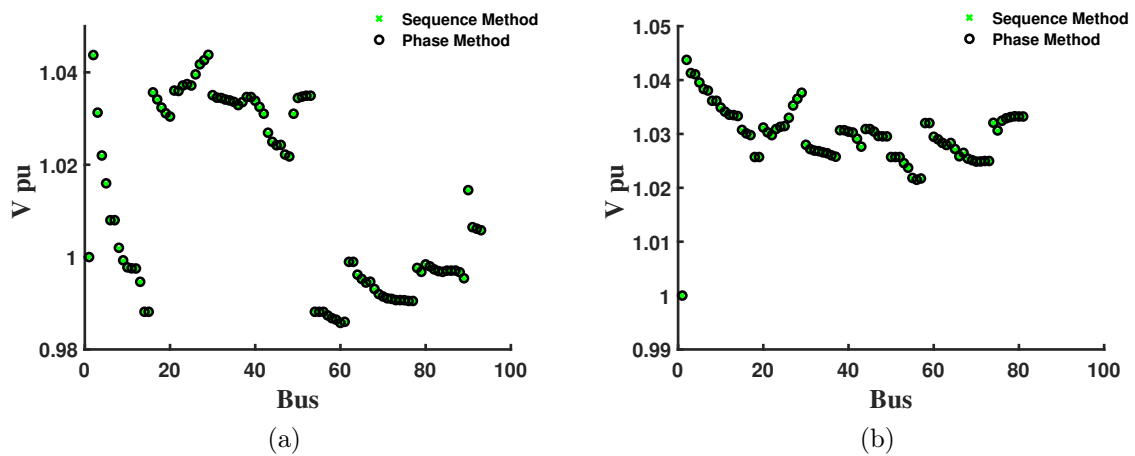


Figure 3.17: (a) Comparison of Sequence Load Flow-Phase A (b) Comparison of Sequence Load Flow-Phase B

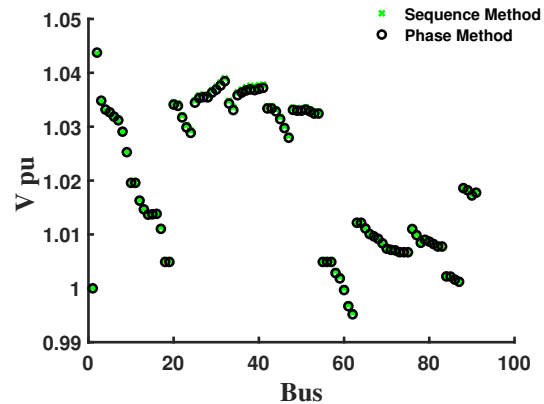


Figure 3.18: Comparison of Sequence Load Flow-Phase C

### 3.7 Three Sequence Continuation Power Flow

The continuation power flow (CPF) is a method based on a predictor-corrector scheme with a continuation parameter (voltage or power). It is generally used to trace the PV curve or nose curve which traces the voltage as the load is increased from base value until it reaches the loadability limit and then back to the base value. The Jacobian will become singular at the nose point and due to which the system becomes ill-conditioned. Therefore the normal power flow diverges at the nose point. This problem of ill-conditioning can be solved using continuation power flow. The continuation power flow introduces an additional parameter and an equation to the power flow equation so that the augmented Jacobian is not singular at the nose point. The basic approach in CPF is to first predict the power flow solution using a chosen continuation parameter. This is mostly accomplished using linear approximations. Then a corrector step is implemented where augmented power flow equations are solved using these predicted values as the initial condition.

#### 3.7.1 CPF Formulation

The non linear power flow equations from eq.(3.40)-(3.58) can be combined and represented by  $g(x) = 0$  where  $x = (V_r, V_m)$ . The current injection based equation to

solve this is given by

$$\mathbf{J}(\mathbf{x})\Delta\mathbf{x} = -g(x) \quad (3.100)$$

where  $J = \frac{\partial g(x)}{\partial x}$ . To apply continuation technique to power flow problem, a loading factor  $\lambda$  is introduced and power flow is reformulated. The generation and load variations are simulated using following modification.

$$P^{sp} = P_0^{sp}(1 + \lambda) \quad (3.101)$$

$$Q^{sp} = Q_0^{sp}(1 + \lambda) \quad (3.102)$$

where  $P^{sp} = P^g - P^l$  and  $Q^{sp} = Q^g - Q^l$ . Here  $\lambda = 0$  corresponds to base case and  $P_0^{sp}$  and  $Q_0^{sp}$  are total specified active and reactive powers of the base case. Therefore, the complex current mismatch in (2.7) can be reformulated as

$$\Delta I_i = \frac{P_{i0}^{sp}(1 + \lambda) - jQ_{i0}^{sp}(1 + \lambda)}{(V_i^*)} - \sum_{j=1}^n Y_{ji}V_j \quad (3.103)$$

Eq (3.103) can be represented in terms of real and imaginary component as

$$\Delta I_{ri} = \frac{P_{i0}^{sp}V_{ri} + Q_{i0}^{sp}V_{mi}(1 + \lambda)}{V_{ri}^2 + V_{mi}^2} - \sum_{j=1}^N (G_{ij}V_{rj} - B_{ij}V_{mj}) \quad (3.104)$$

$$\Delta I_{mi} = \frac{P_{i0}^{sp}V_{mi} - Q_{i0}^{sp}V_{ri}(1 + \lambda)}{V_{ri}^2 + V_{mi}^2} - \sum_{j=1}^N (G_{ij}V_{mj} - B_{ij}V_{rj}) \quad (3.105)$$

The non linear current mismatch equations in (3.104)-(3.105) can be combined and represented by

$$g(x, \lambda) = g(V_r, V_m, \lambda) = 0 \quad (3.106)$$

Linearizing (3.106), we have

$$dg(V_r, V_m, \lambda) = g_{V_r}dV_r + g_{V_m}dV_m + g_{\lambda}d\lambda = 0 \quad (3.107)$$

Here  $g_{V_r}$ ,  $g_{V_m}$  and  $g_\lambda$  are the derivatives of current mismatch equations in (3.108)-(3.109) with respect  $V_r$ ,  $V_m$  and  $\lambda$  respectively. The  $g_\lambda$  can be derived as

$$g_{\lambda r i} = \frac{P_{i0}^{sp} V_{ri} + Q_{i0}^{sp} V_{mi}}{V_{ri}^2 + V_{mi}^2} = I_{ri}^{sp} \quad (3.108)$$

$$g_{\lambda m i} = \frac{P_{i0}^{sp} V_{mi} - Q_{i0}^{sp} V_{ri}}{V_{ri}^2 + V_{mi}^2} = I_{mi}^{sp} \quad (3.109)$$

### 3.7.1.1 Predictor Process

The predictor step is used to provide an approximate point of the next solution. A prediction of the next solution is made by taking an appropriately sized step in the direction tangent to the solution path. The first task in the predictor process is to calculate the tangent vector. This can be obtained from

$$\begin{bmatrix} g_{V_r} & g_{V_m} & g_\lambda \end{bmatrix} \begin{bmatrix} dV_r \\ dV_m \\ d\lambda \end{bmatrix} = 0 \quad (3.110)$$

For a  $n$  bus system, the size of tangent vector  $[dV_r, dV_m, d\lambda]^T$  will be  $2n + 1$  in case of single phase (or positive sequence) and  $6n + 1$  in case of three phase system. To solve this equation, we need to balance known and unknown variables which is brought in using an additional equation. Therefore (3.110) can be modified as

$$\begin{bmatrix} g_{V_r} & g_{V_m} & g_\lambda \\ & E_k & \end{bmatrix} \begin{bmatrix} dV_r \\ dV_m \\ d\lambda \end{bmatrix} = \begin{bmatrix} 0 \\ \pm 1 \end{bmatrix} \quad (3.111)$$

where  $E_k$  is a row vector with all elements zero except the  $k^{th}$  element, which is equal to one. Therefore (3.111) can be represented in terms of Jacobian as

$$\begin{bmatrix} J & g_\lambda \\ & E_k \end{bmatrix} \begin{bmatrix} dV_r \\ dV_m \\ d\lambda \end{bmatrix} = \begin{bmatrix} 0 \\ \pm 1 \end{bmatrix} \quad (3.112)$$

This can be expanded as

$$\begin{bmatrix} \frac{\partial I_{m1}}{\partial V_{r1}} & \frac{\partial I_{m1}}{\partial V_{m1}} & \dots & \frac{\partial I_{m1}}{\partial V_{rn}} & \frac{\partial I_{m1}}{\partial V_{mn}} & I_{m1}^{sp} \\ \frac{\partial I_{r1}}{\partial V_{r1}} & \frac{\partial I_{r1}}{\partial V_{m1}} & \dots & \frac{\partial I_{r1}}{\partial V_{rn}} & \frac{\partial I_{r1}}{\partial V_{mn}} & I_{r1}^{sp} \\ \vdots & \vdots & \vdots & \vdots & \vdots & \vdots \\ \frac{\partial I_{mn}}{\partial V_{r1}} & \frac{\partial I_{mn}}{\partial V_{m1}} & \dots & \frac{\partial I_{mn}}{\partial V_{rn}} & \frac{\partial I_{mn}}{\partial V_{mn}} & I_{mn}^{sp} \\ \frac{\partial I_{rn}}{\partial V_{r1}} & \frac{\partial I_{rn}}{\partial V_{m1}} & \dots & \frac{\partial I_{rn}}{\partial V_{rn}} & \frac{\partial I_{rn}}{\partial V_{mn}} & I_{rn}^{sp} \\ \hline & & & E_k & & \end{bmatrix} \begin{bmatrix} dV_{r1} \\ dV_{m1} \\ \vdots \\ dV_{rn} \\ dV_{mn} \\ d\lambda \end{bmatrix} = \begin{bmatrix} 0 \\ 0 \\ \vdots \\ 0 \\ 0 \\ \pm 1 \end{bmatrix} \quad (3.113)$$

The predicted value is given by

$$\begin{bmatrix} V_r \\ V_m \\ \lambda \end{bmatrix}^{pred} = \begin{bmatrix} V_r \\ V_m \\ \lambda \end{bmatrix}^{old} + \sigma \begin{bmatrix} dV_r \\ dV_m \\ d\lambda \end{bmatrix} \quad (3.114)$$

where  $\sigma$  is a scalar that represents the step size.

### 3.7.1.2 Corrector Process

The corrector step is to solve the augmented power-flow equation with the predicted solution in (3.114) as the initial point. In the augmented power-flow algorithm an extra equation is included and is taken as a variable. The augmented power flow

Table 3.13: Size of matrices.

Matrix	Single Phase CPF	Three Phase CPF	Three Sequence CPF
Jacobian	$2n \times 2n$	$6n \times 6n$	$2n \times 2n$
Tangent Vector	$2n + 1$	$6n + 1$	$2n + 1$
Augmented Jacobian	$2n + 1 \times 2n + 1$	$6n + 1 \times 6n + 1$	$2n + 1 \times 2n + 1$

equation is given by

$$\begin{bmatrix} g(x, \lambda) \\ x_k - \eta \end{bmatrix} = \begin{bmatrix} 0 \\ 0 \end{bmatrix} \quad (3.115)$$

The current injection based power flow equation with augmented Jacobian is given by

$$\begin{bmatrix} \frac{\partial I_{m1}}{\partial V_{r1}} & \frac{\partial I_{m1}}{\partial V_{m1}} & \dots & \frac{\partial I_{m1}}{\partial V_{rn}} & \frac{\partial I_{m1}}{\partial V_{mn}} & I_{m1}^{sp} \\ \frac{\partial I_{r1}}{\partial V_{r1}} & \frac{\partial I_{r1}}{\partial V_{m1}} & \dots & \frac{\partial I_{r1}}{\partial V_{rn}} & \frac{\partial I_{r1}}{\partial V_{mn}} & I_{r1}^{sp} \\ \vdots & \vdots & \vdots & \vdots & \vdots & \\ \frac{\partial I_{mn}}{\partial V_{r1}} & \frac{\partial I_{mn}}{\partial V_{m1}} & \dots & \frac{\partial I_{mn}}{\partial V_{rn}} & \frac{\partial I_{mn}}{\partial V_{mn}} & I_{mn}^{sp} \\ \frac{\partial I_{rn}}{\partial V_{r1}} & \frac{\partial I_{rn}}{\partial V_{m1}} & \dots & \frac{\partial I_{rn}}{\partial V_{rn}} & \frac{\partial I_{rn}}{\partial V_{mn}} & I_{rn}^{sp} \\ \hline & & E_k & & & \end{bmatrix} \begin{bmatrix} \Delta V_{r1} \\ \Delta V_{m1} \\ \vdots \\ \Delta V_{rn} \\ \Delta V_{mn} \\ \Delta \lambda \end{bmatrix} = \begin{bmatrix} \Delta I_{m1} \\ \Delta I_{r1} \\ \vdots \\ \Delta I_{mn} \\ \Delta I_{rn} \\ 0 \end{bmatrix} \quad (3.116)$$

In the proposed sequence based CPF, positive sequence analysis is utilized during the prediction step. This positive sequence voltage is used as the initial condition to perform an augmented three sequence load flow in the correction step. A flow chart of three sequence based CPF for distribution system is shown in Fig. 3.19. A comparison of the size of Jacobian, prediction tangent vector and augmented Jacobian is depicted in table 3.13. It can be seen that the computational burden of the proposed sequence based CPF will be much lesser compared to three phase approach.

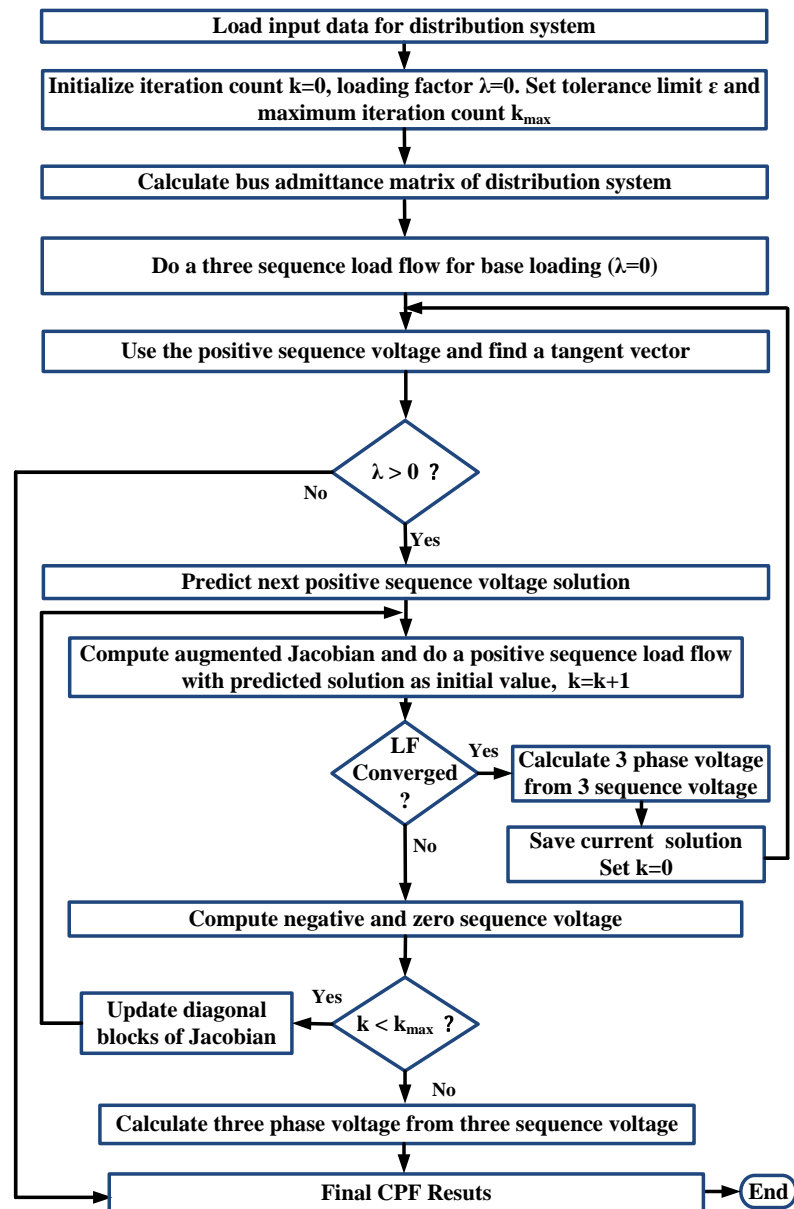


Figure 3.19: Three sequence distribution continuation power flow.

### 3.8 Three Phase Distribution Load Flow Tool

A Graphical User Interface for unbalanced three phase distribution systems utilizing the sequence method is developed as shown in Fig. 3.21. The tool is universal and can be used to analyze any distribution system. The user can select the load flow

Table 3.14: Iterations to converge.

$\lambda$	Sequence Power Flow (flat start)		Sequence Continuation Power Flow	
	Iteration	Time	Iteration	Time
0.1	4	4.2	2	2.8
0.3	5	5.1	3	3.4
0.5	9	8.2	5	5.6
0.8	14	15.4	8	9.2
0.9	50	30	15	25.
0.921	100	50	20	32.5

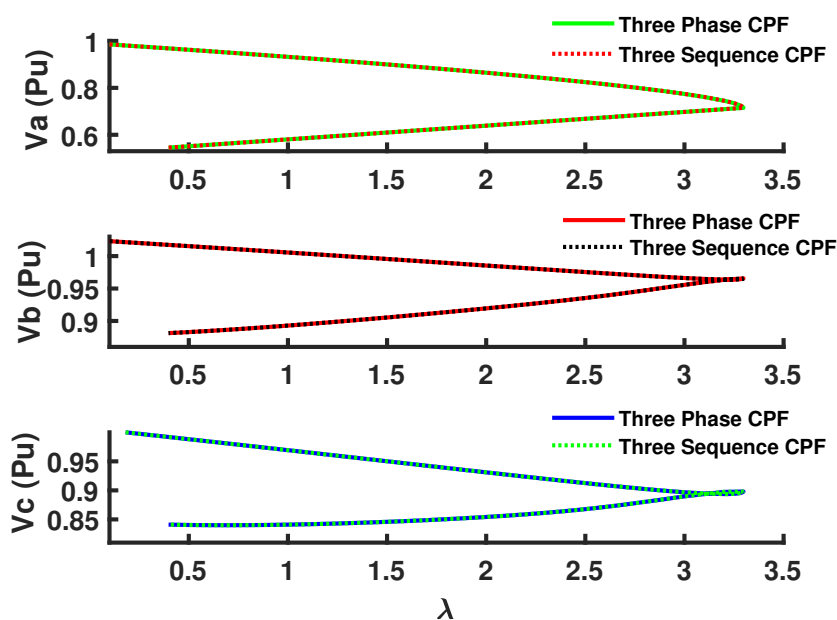


Figure 3.20: Comparison of three phase and three sequence CPF.

### Sequence Based Distribution System Analysis Tool

**Power Flow Analysis**

**Input**

Power Flow Method  Loading Factor

**Output**

Total Iterations  Computational Time

Figure 3.21: Distribution Load Flow Tool

method from a drop-down list which will display the list of all load flow methods. An option to plot voltage magnitude as well as to compare results with a benchmark is provided.

### 3.9 Summary

A computationally efficient load flow algorithm based on injected current sensitivity (ICS) for distribution systems with high penetration of DERs has been introduced in this chapter. Models for distribution lines, capacitors, voltage regulators, and relevant transformer connections are derived and a stacked bus admittance matrix (Y-bus) is formulated. A generalized Jacobian matrix has been formulated which embeds the properties or features of the distribution system components mentioned. All kinds of load models (ZIP) are also being taken care of. Various models of DERs have been incorporated in the proposed load flow studies. The DGs modeled as PQ type has been treated as negative PQ load in the proposed LF studies. Multiphase DERs with voltage control capability are modeled as PV bus using a reactive power sensitivity based approach. The proposed method has good convergence ability for a wide range of R/X ratio variations, load variations, and system size variations which have been clearly demonstrated through the test results. A three sequence based load flow and continuation power flow method to investigate voltage stability of unbalanced distribution system is proposed. Comprehensive numerical tests on IEEE-4, IEEE-13, IEEE-34, and IEEE-123 bus test distribution systems show the accuracy and robustness of proposed approaches for a system with missing phases, several voltage regulators, and transformer connections. The scalability of the approach is validated using two custom-built test systems derived from the IEEE-8500 node system. The result section elucidates the viability and authenticity of the proposed method.

## CHAPTER 4: MULTI-PERIOD POWER FLOW OF THREE PHASE DISTRIBUTION SYSTEM

### 4.1 Introduction

The distribution system analysis traditionally was focused on steady-state power flow simulations, harmonic analysis, and protection studies which were sufficient for the planning of a passive distribution system to design feeder layouts, determine upgrades, and control settings. But with new grid edge technologies like photovoltaic (PV), battery energy storage (BES), electrical vehicles (EVs) advanced inverters the paradigm for distribution system planning and operations has changed [11]. The steady state analysis was executed at snapshots in time with an extreme condition, such as the peak load period. To analyze the interactions of new grid edge technologies such snapshot analysis may not be adequate as only considering peak periods can lead to over-estimation of normal operating issues. A distributed energy resource must go through an interconnection study before connecting to the grid in order to identify its impacts on the system and find possible mitigation strategies. The generation capacity of these DERs varies from feeder to feeder and its distribution along feeder is often uneven which can have location-specific impacts. The inherent variability in PV power output can affect the operation of voltage regulation and protection devices and hence can interact with feeder operation in complex ways. [49]. With the high proliferation of distributed energy resources, it is indispensable to extend steady state analysis to a multi-period analysis to capture the time-dependent variations in the active distribution system. A multi-period power flow (MPF) analysis is required to accurately capture the time-varying aspects of the system.

Quasi-static time series simulation (QSTS) which can be considered as a subset

of multi-period power flow is a sequence of steady-state power flows conducted at a time step between 1sec to 1 hour where control devices like load tap changers, voltage regulators, switched capacitors, static var compensators, switches, and relays may change their state from one step to the other. In QSTS, there will not be any numerical integration of differential equations between time steps [50]. The converged state of the current iteration is used as the initial state for the next iteration thereby capturing time varying parameters such as loads, and time dependent states such as voltage regulator taps. The main feature of QSTS simulation is that solution of each time step relies on information like feeder state, regulator taps from the previous time step. These discrete control devices are specifically modeled and time-series simulations are executed to capture the time-dependent states of these control devices. Therefore potential impacts of DER integration, like an increase in voltage regulator operations due to voltages being not in the bandwidth, can be accurately analyzed with time-series analysis. Using accurate load and generation time-series data, a QSTS simulation can be used to quantify the magnitude and duration of an impact accurately. Generally, the recommended resolution for QSTS simulation is in the range of hours for energy impact analyses, in the range of minutes for steady-state overvoltage analysis, and in the range of seconds for voltage fluctuation studies. [51]. The requirements for the input data resolution, simulation time-step resolution, and duration of the simulation for QSTS analysis are discussed in [11]. Some of the applications of QSTS simulations discussed in the literature include impact studies of different DER [52–56], analyzing the operation of voltage regulating devices due to intermittent and fluctuating DER power [57, 58]. Other types of studies performed with QSTS analysis are the impact of power flow direction [59] and also study on system losses [60].

The location of DERs with respect to legacy voltage control devices can result in the erroneous operation of these devices and leads to a bad voltage profile. A multi-

period power flow analysis can also be used to find the impacts of DER location of voltage regulating device operation and resulting voltage profiles. Also, an approximate voltage stability margin of the power system can be obtained using MPF where a sequence of steady-state power flows with increasing loading is conducted until power flow diverges. This loading factor gives an approximate stability margin of the system.

## 4.2 Research Contribution

- Modeled regulating devices and their associated controls to execute a multi-period power flow analysis.
- Developed QSTS framework with detailed modeling of voltage regulating devices and distributed energy resources to analyze the influence of DERs and load variation on voltage profile.
- Developed MPF framework to analyze the impact of location of DERs on control devices and how their operation impacts the grid.
- Developed MPF framework to calculate approximate voltage stability margin of the system.

## 4.3 Modeling of Control Devices

The main motive of conducting a QSTS analysis on a system is to capture time dependent effects and controller actions. In order to accurately model the operation of a device with discrete controls through QSTS simulation, time resolution of simulation should be always lesser the fastest delay in any devices with discrete controls. [61]. To capture the impact of DERs on system using QSTS simulations, the regulating devices and their associated controls should be modelled. In this chapter, the load tap changers, voltage regulators and associated controls are modelled in detail.

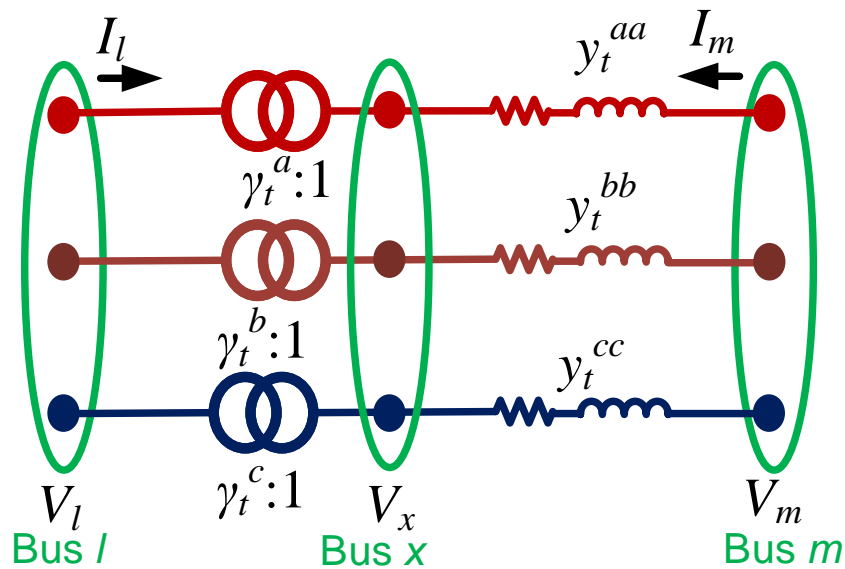


Figure 4.1: Schematic representation of Voltage Regulator

#### 4.3.1 Voltage Regulators

To maintain feeder voltages within acceptable limits, regulating devices are used. Load tap changers (LTC) are installed at the substation and step voltage regulators (SVR) are installed along the feeder. The LTC is built into the transformer by tapping the transformer winding in multiple locations and SVR is constructed as a separate unit from the transformer using an autotransformer winding with many taps [62]. In a three-phase system, the common practice is to install three, single-phase regulators so that, it can regulate each phase separately taking care of voltage unbalance. The regulators can be connected in grounded wye, closed delta, or open delta [2]. Standard step voltage regulators have a 10% voltage regulation range with a reversing switch with 32 steps (16 steps up and 16 steps down) which amounts to a 10/16% or 0.00625 per unit voltage change per step. Step voltage regulators can be connected in two different types which are type-A or type-B connection [63]. For QSTS analysis, the regulators are modeled as an admittance  $\Upsilon_t^{reg}$  in series with an ideal autotransformer

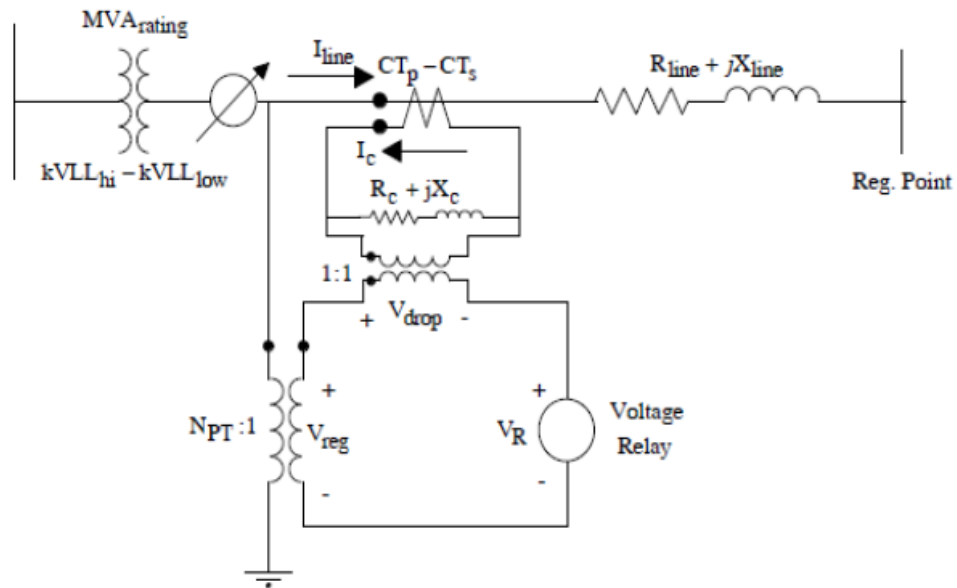


Figure 4.2: Compensator Circuit (Source: [2])

as shown in Fig. 4.1. The admittance matrix matrix of a three phase Yg-Yg type voltage regulator in series with a distribution line with admittance  $Y_{abc}(r)$  is given by

$$Y_{abc}^{reg} = \begin{bmatrix} RY_{abc}(r)R^T & -RY_{abc}(r) \\ -Y_{abc}(r)R^T & Y_{abc}(r) \end{bmatrix} \quad (4.1)$$

$$\text{where } R = \begin{bmatrix} \frac{1}{a_t} & 0 & 0 \\ 0 & \frac{1}{a_t^b} & 0 \\ 0 & 0 & \frac{1}{a_t^c} \end{bmatrix} \text{ and } a_t = 1 \mp \frac{N_2}{N_1} = 1 \mp d_V tp$$

where  $tp$  is the tap setting and  $d_V$  is the per unit voltage change per tap. Voltage regulators are assumed to be step-type and can be connected in the substation and/or to a specified line segment. The regulators can be three-phase or single phase. The changing of taps on a regulator is controlled by the line drop compensator(LDC). A simplified circuit of an analog compensator [64] and how it is connected to the feeder through the potential and current transformer is shown in Fig 7.2. Four settings are required for the compensator circuit. They are compensator impedance( $R, X$ )

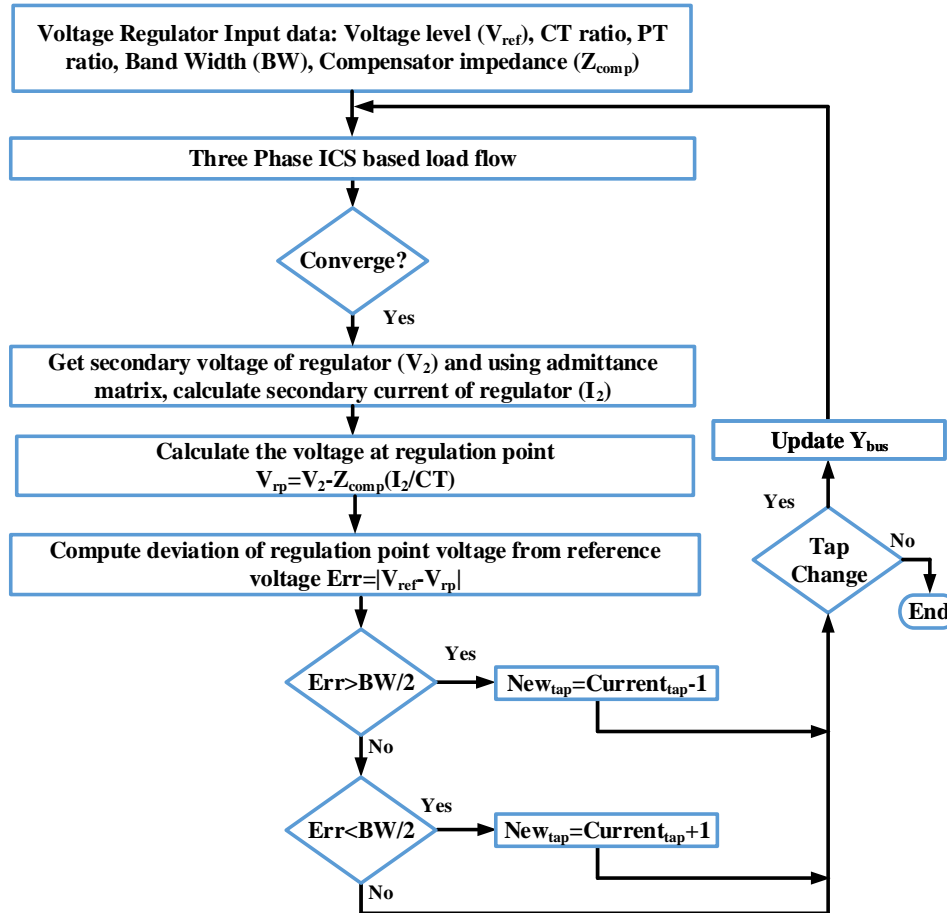


Figure 4.3: Operation of voltage regulator

settings, voltage Level setting, bandwidth setting, and time delay setting. The voltage setting gives the desired voltage to hold at the regulation point and bandwidth defines the allowed variance of the regulation point voltage centered at the desired Voltage Level. The time delay is the delay before a tap change is made when the voltage is not within the bandwidth. The goal of the compensator circuit is such that the voltage across the compensator voltage relay will be a scale model of the actual voltage at the regulation point. The per-unit voltage of the compensator voltage relay should be equal to the per-unit voltage at the regulation point. To make this happen, the per-unit R and X settings must be equal to the per-unit equivalent line impedance from the regulator output to the regulation point.

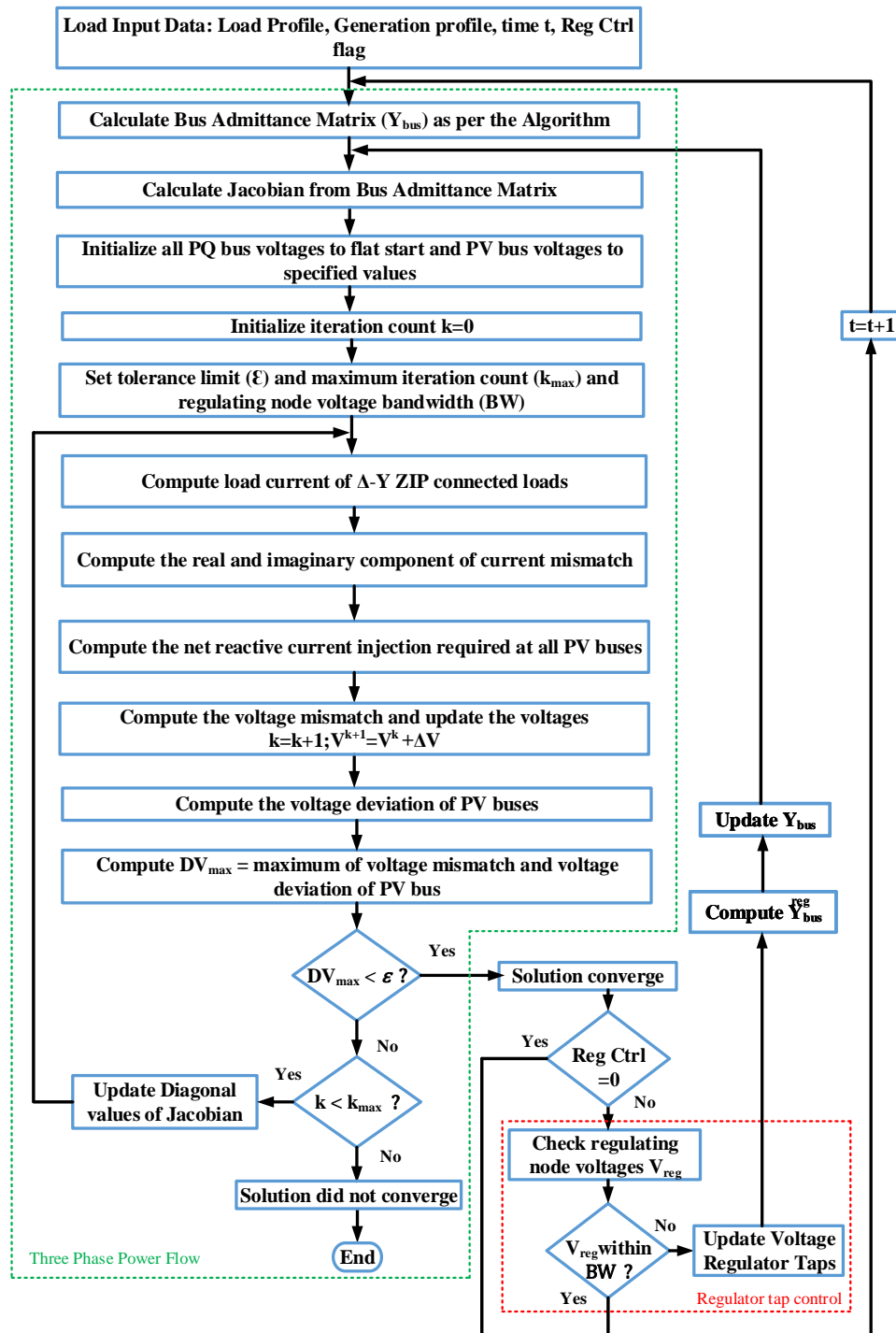


Figure 4.4: Proposed QSTS Simulation

#### 4.4 Proposed MPF with DERs

The MPF solves a series of power flow in a sequential manner where parameters of converged power flow are used as the initial parameters for the next power flow iteration. The MPF simulation on the distribution system is initiated with a three sequence load flow. Once the load flow converges, the regulating point voltage associated with a regulator is obtained from the load flow solution. This is then compared with the reference voltage of the respective regulator. If the voltage error between both is within a bandwidth (BW), load flow solution values are stored and load flow for next time instant is executed. If the error is not within the bandwidth (BW), a tap operation is initiated. If voltage is above the upper band, a tap down operation is initiated and if the voltage is below the lower band, a tap up operation is initiated. The effect of tap variation is brought in through the bus admittance matrix in the proposed three phase load flow. Therefore if there is a change in taps, the bus admittance matrix corresponding to regulators  $Y^{reg}$  is modified. A flowchart of the detailed operation of voltage regulator for a given LDC setting is shown in Fig. 4.3. With the updated system  $Y_{bus}$  load flow is executed for the same load and generation values. An option to switch off voltage regulator operation is also included. If Regulator control is switched off, then after a converged load flow iteration, load flow for next time instant is executed. A flowchart of the proposed MPF simulation is shown in Fig. 4.4.

#### 4.5 Applications of Multi-Period Power Flow

The proposed MPF framework is utilized to analyze the influence of DERs and load variation on voltage profiles. It is utilized to study how would the location of DERs affect the operation of legacy control devices. It is also used to calculate an approximate voltage stability margin of the system. The proposed modeling approach is assessed by using IEEE 123 bus distribution systems. The voltage regulator

operation due to time-varying aspects of the system is studied and its impacts on voltage are analyzed. The accuracy of the proposed modeling approach is assessed by comparing load-flow voltage solutions and tap operations obtained from solutions of Opends [42].

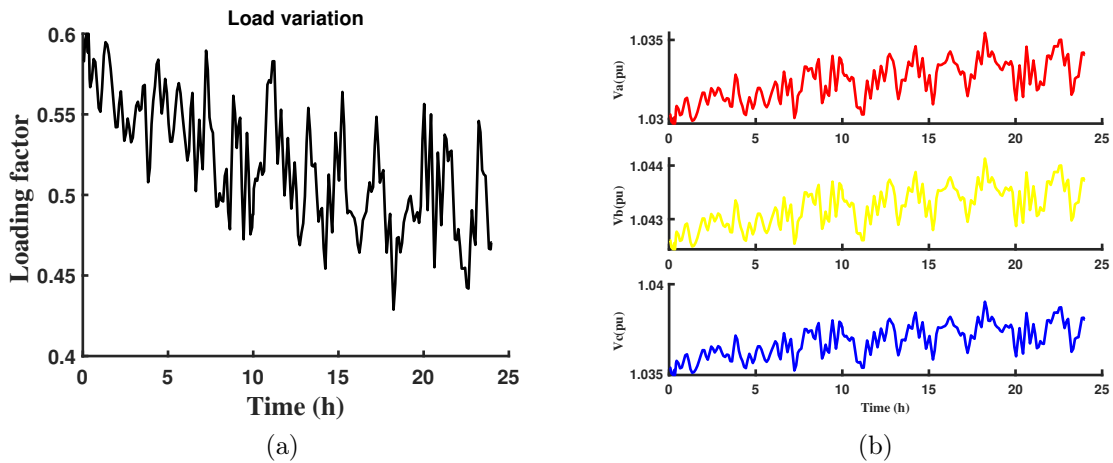


Figure 4.5: (a) Load Profile (b) Three phase voltage at node 8 with regulator control OFF

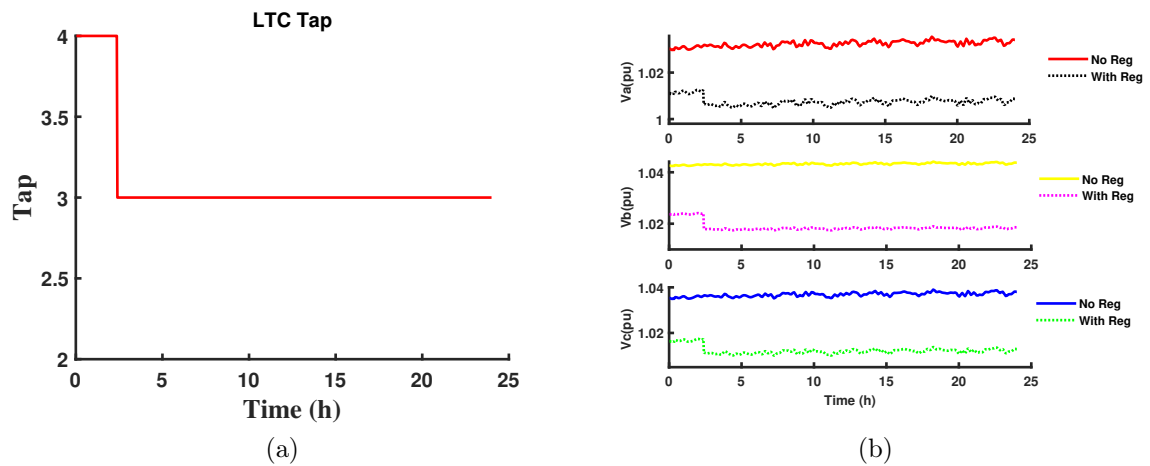


Figure 4.6: (a) Tap Operation (b) Three phase voltage at node 8 with regulator control ON

#### 4.5.1 Impact of load and DER variation on grid voltage

A time-varying load profile for 1 day with a 2-minute resolution is taken as shown in Fig. 4.5a. The QSTS simulation is first executed with Regulator off by setting Reg Ctrl flag to 0. The initial tap setting of LTC was 7. The voltage profile of each phase of node 8 is shown in Fig. 4.5b. It can be observed that, due to light loading conditions, voltages on all phases are higher (above 1.03 pu). Now QSTS simulation with Regulator on is executed. It can be seen from Fig. 4.6a that the taps are lowered to 4 from an initial value of 7. It is again lowered to 3 because of lighter loading and higher voltage around 3 hours. Fig. 4.6b shows the comparison of voltages with and without regulator action. It can be seen that, with the voltage regulator on, the grid voltages are close to 1 pu for phase A and below 1.02 pu for phase b and c. Since LTC is a ganged type, taps on all three phases are varied by only monitoring 1 phase (A phase in this case).

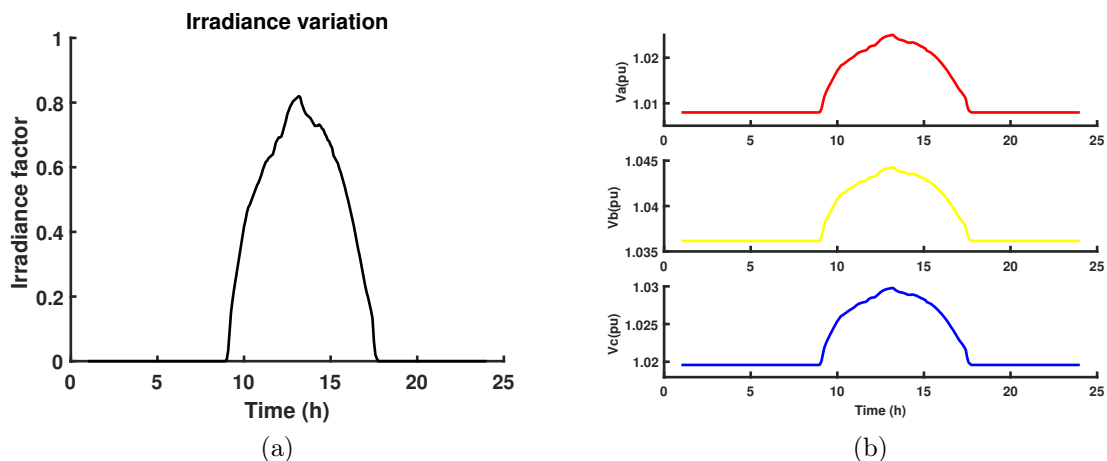


Figure 4.7: (a) Irradiance Profile (b) Three phase voltage at node 8 with regulator control OFF

A PV DER with a 4MVA rating operating on a unity power factor is connected to node 250 of the system. The time-varying PV irradiance profile for 1 day with a 5-minute resolution is shown in Fig. 4.7a. The QSTS simulation is first executed with Regulator off. The voltage profile of each phase of node 8 is shown in Fig. 4.7b.

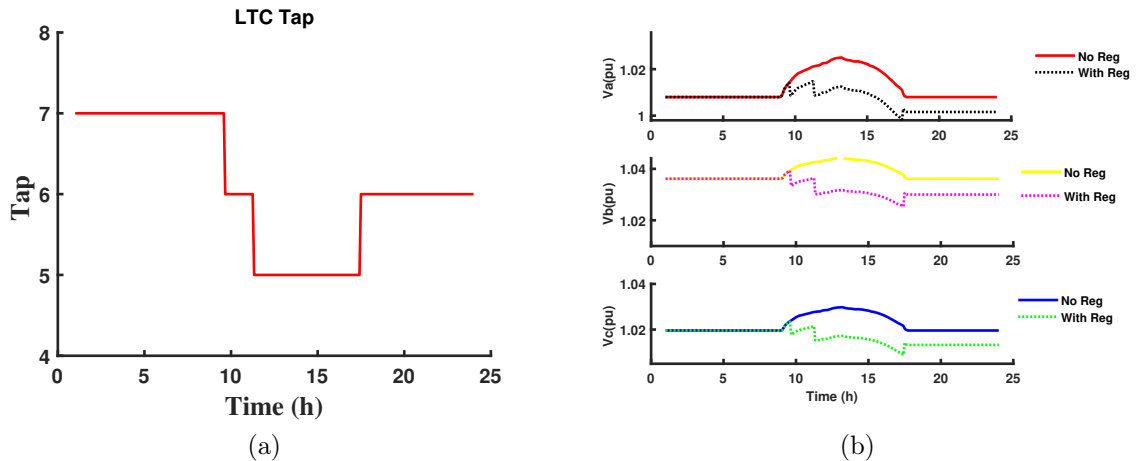


Figure 4.8: (a) Tap Operation (b) Three phase voltage at node 8 with regulator control ON

It can be observed that the variations in irradiance are reflected on voltages on all phases with high voltage on the lightly loaded b phase. Now QSTS simulation with Regulator on is executed. It can be seen from Fig. 4.8a that the taps are lowered to 6 from an initial value of 7 as soon as generation increases. It is again lowered to 5 because of higher generation and higher voltage around 12 hours. Fig. 4.8b shows the comparison of voltages with and without regulator action. It can be seen that, with the voltage regulator on, the grid voltages are close to 1pu for phase A and below 1.025 pu for phase b and c.

#### 4.5.2 Impact of DER location on operation of voltage regulators

The location of large DERs will have an impact on voltage regulating devices as well as grid voltages. In this study, the location of DERs from substation and how it impacts the operation of voltage regulating devices are studied. First, a 4MVA DER operating at unity power factor is connected to a remote node from substation (node 250) as shown in Fig. 4.9a. When 4MW of power is pushed, the voltage at the point of common coupling(PCC), as well as other nodes, would experience a high voltage. The voltage regulator operates and reduces the tap. But the voltage regulator will only lower the taps until the regulating point voltage is within the bandwidth. Even





to remote node is depicted in Fig. 4.11b, Fig. 4.12a and Fig. 4.12b. Therefore it can be concluded that, with high DER penetration at a node closer to the substation, node voltages towards the end of the feeder would have a low voltage profile after the voltage regulator operates.

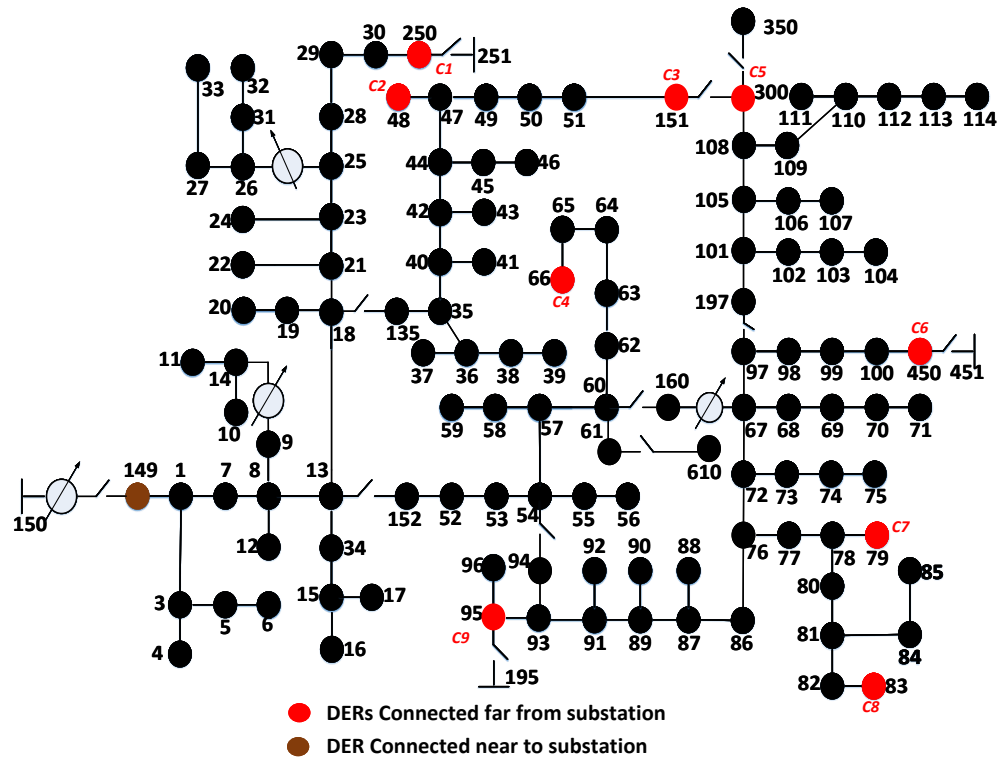


Figure 4.13: Location of DERs

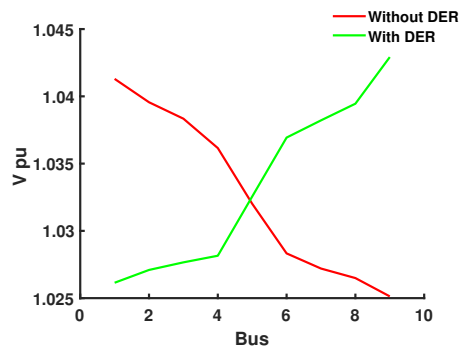
Table 4.1: Impact of DER location on operation of voltage regulators

Case	C1	C2	C3	C4	C5	C6	C7	C8	C9
Nodes considered for plotting voltage	1	1	1	1	1	1	1	1	1
	7	7	7	7	7	7	7	7	7
	8	8	8	8	8	8	8	8	8
	13	13	13	13	13	13	13	13	13
	18	18	18	52	52	52	52	52	52
	23	135	135	54	54	54	54	54	54
	25	40	42	57	57	57	57	57	57
	28	42	47	62	160	160	67	67	67
	30	45	50	64	101	98	76	78	87
	250	46	151	66	300	450	79	83	95

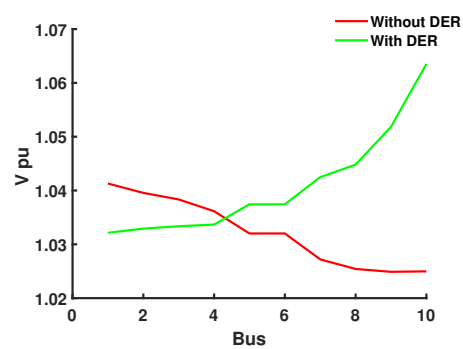
Additional test cases are used to analyze the effect of location of DERs on grid voltage. The location of DERs for each test case is shown in Fig. 4.13 and the nodes considered for analyzing voltage profile is shown in Table. 4.1. The phase B voltage profile of cases 2 to 8 with DERs located far from substation is plotted in Fig. 4.14. The trend remains same for all the cases where nodes towards end of the feeder experience higher voltage as large DER is connected at remote nodes of feeder. The phase A voltage profile of cases 2 to 8 is plotted in Fig. 4.15 with DERs located near to substation. It can be seen that for case 2 to case 4 the nodes towards end of the feeder experience lower voltage as large DER is connected towards beginning of feeder. For case 5 to case 9 the voltage towards end of feeder are at a higher voltage. This is due to the presence of a voltage regulator between node 60 and 160. But comparing the voltage with and without DER, it can be seen in all cases that, the voltage profile of all nodes with DER is lesser than the voltage without DER because of the tap down operation of voltage regulator due to wrong voltage estimation at remote node.

### 4.5.3 Approximate Voltage Stability Margin Assessment

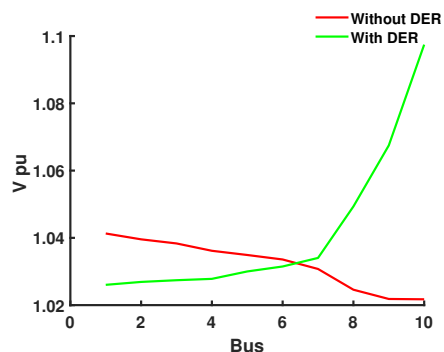
The voltage stability of a system is expressed in terms of voltage stability margin (VSM). VSM is defined as the difference between the critical loadability limit and the current operating load level. As the system state reaches near the maximum loading point the load flow diverges as the power flow Jacobian becomes singular. The proposed injection current sensitivity based multi-period power flow is used for solving distribution system power flow and finding approximate VSM of system. A series of load flows were performed using load increment factor  $\alpha$ . The loads were varied from baseload ( $\alpha = 0$ ) to a loading where load flow diverged ( $\alpha = \alpha_{max}$ ). The PV curve of phase A of node 1 of the 123 bus system is shown in Fig. 4.16. This  $\alpha_{max}$  is considered as the approximate voltage stability margin of the system.



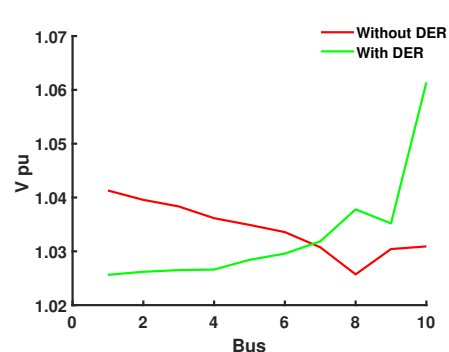
(a) Case 2



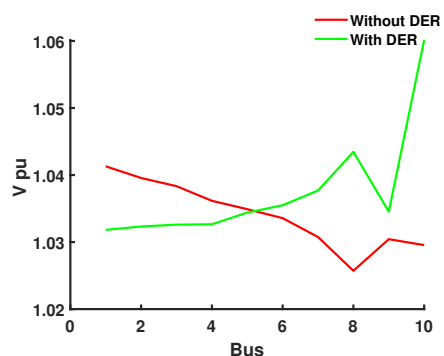
(b) Case 3



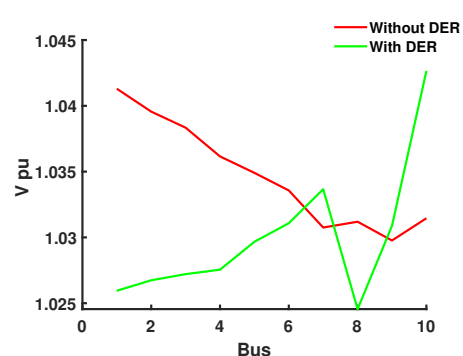
(c) Case 4



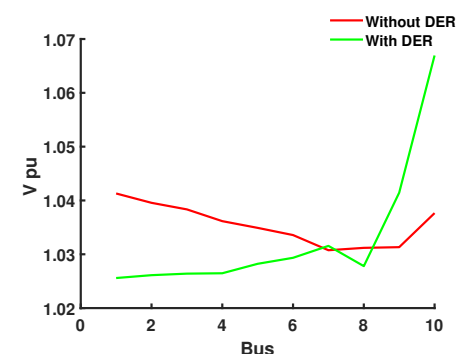
(d) Case 5



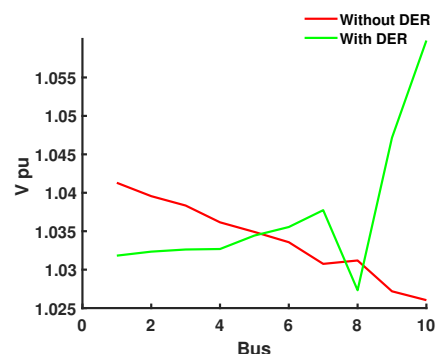
(e) Case 6



(f) Case 7

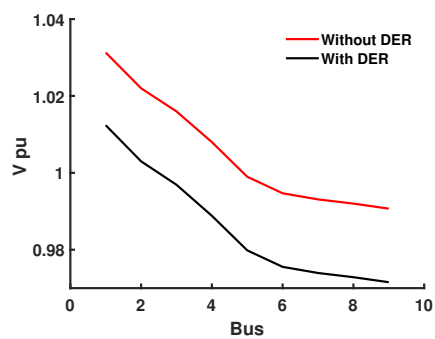


(g) Case 8

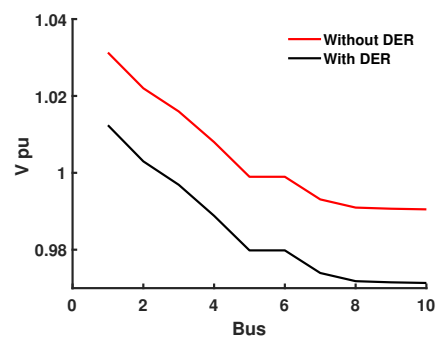


(h) Case 9

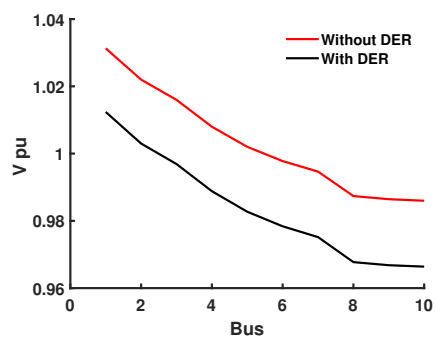
Figure 4.14: B phase voltage profile for case 2-9 with DERs far from substation



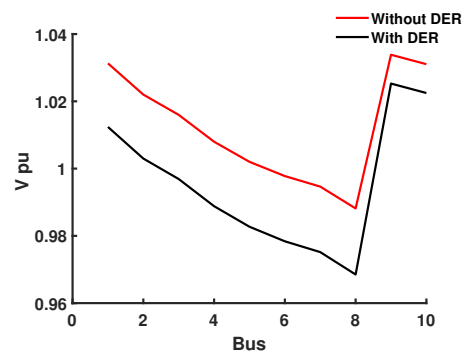
(a) Case 2



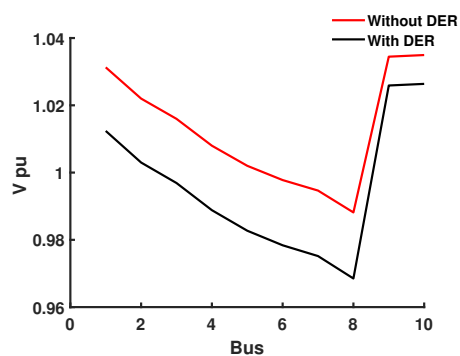
(b) Case 3



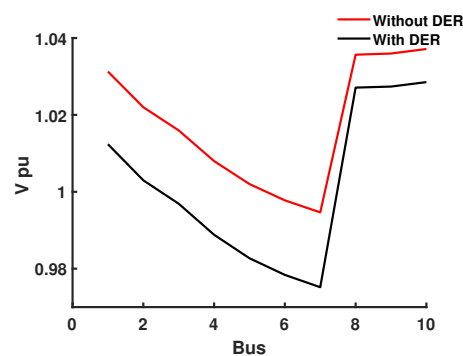
(c) Case 4



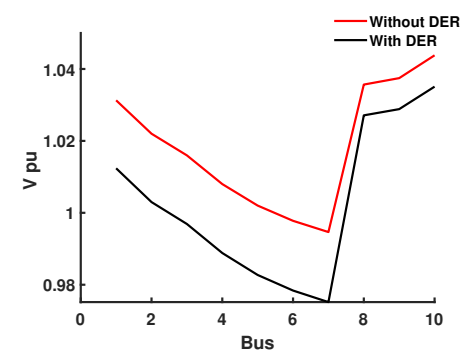
(d) Case 5



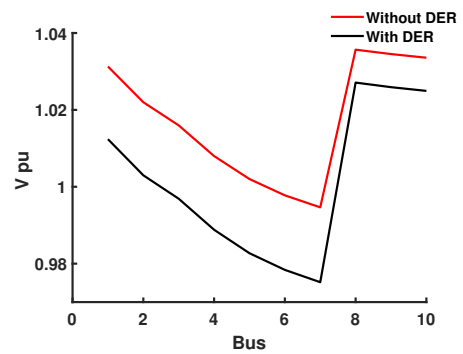
(e) Case 6



(f) Case 7



(g) Case 8



(h) Case 9

Figure 4.15: A phase voltage profile for case 2-9 with DERs near to substation

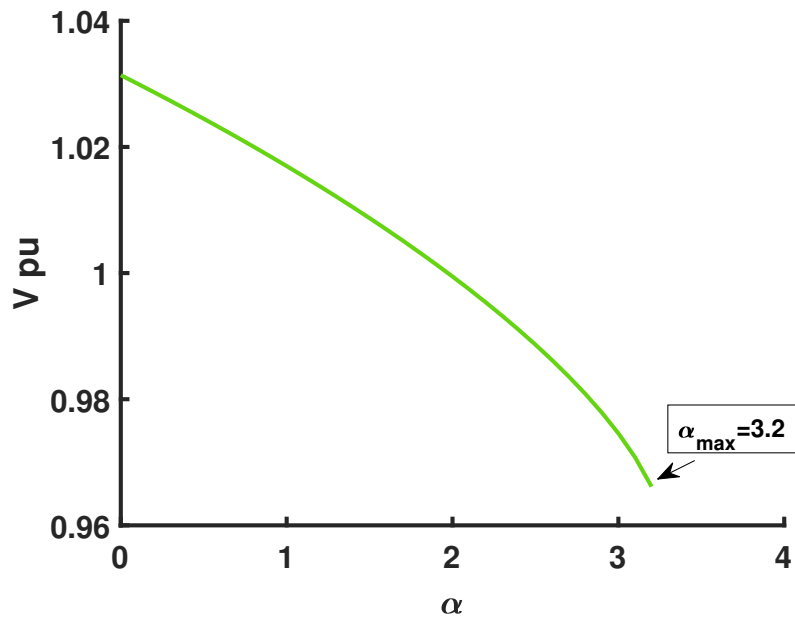


Figure 4.16: Approximate Voltage Stability Margin using MPF.

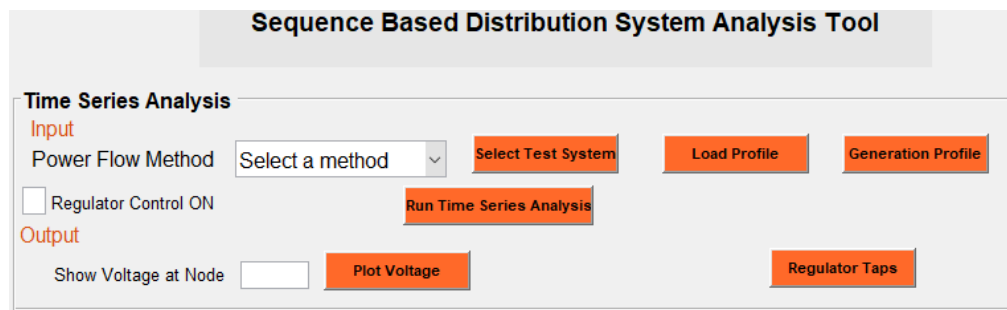


Figure 4.17: Distribution Times Series Analysis Tool

#### 4.6 Three Phase Time Series Analysis Tool

A Graphical User Interface to conduct MPF analysis of unbalanced distribution system utilizing the sequence method is developed as shown in Fig. 4.17. The tool is universal and can be used to analyze any distribution system. The user can select the load flow method, from a drop-down list which will display the list of all load flow methods. The user can also select load and generation profiles from a repository. Regulator tap control option can be turned on as per user requirement. Finally, an option to plot time varying voltage magnitude of a particular node is provided.

## 4.7 Summary

An MPF framework based on injected current sensitivity based load flow is developed in this chapter. Detailed models of discrete control devices like voltage regulators were developed. The framework was used to study the impact of a power factor controlled (PQ) distributed energy resources on the grid. Also the effect of the location of DERs on control devices and how their operation impacts the grid is also analyzed. The MPF framework is used to calculate the approximate voltage stability margin of the system. Comprehensive tests were conducted on IEEE-123 bus test distribution systems.

## CHAPTER 5: FAULT ANALYSIS OF UNBALANCED DISTRIBUTION SYSTEM USING SEQUENCE COMPONENTS

### 5.1 Introduction

Short circuit analysis or fault analysis constitutes a significant part of power system study and the principal aim of fault analysis is to estimate the fault currents and voltages. Faults on power systems are broadly classified into balanced faults such as a line-to-line-to-line fault(LLL) and unbalanced faults such as single line-to-ground fault(SLG), line-to-line fault(LL), and double line-to-ground fault(LLG). The information from fault studies turns out to be useful for proper relay setting and coordination. Information from the three-phase balanced fault and the line-to-ground fault is used for selecting and setting phase relays and ground relays respectively [65]. Insights from fault studies also help in obtaining the rating of the protective switchgear. While circuit-breaker capacity and protective relay performance are deduced from the fault analysis results, the fault analysis is also a pre-requisite for many types of power system researches like voltage sag analyses [66] and transient stability. The magnitude of the fault currents depends on the internal impedance of the generators along with that of the intervening circuit. The bus impedance matrix is formulated and employed for the systematic computation of bus voltages and line currents during the fault. The fault analysis is conventionally conducted based on the symmetrical sequence networks. In a vast majority of the software packages made use of today by the industry, it is evidently the sequence components based fault analysis algorithm which is employed; primarily, on account of its computational efficiency and simplicity in modeling its system elements like generators and transformers, and supplementarily, the availability of the transmission and distribution networks data in

their sequence values [47]. In the case of a power transmission system, the loads are balanced and lines are transposed which would result in a balanced system. One of the main advantages of using the sequence component method is that the three sequences are independent. This situation only holds when the system is balanced. On the other hand, the distribution systems consist of untransposed lines, voltage control devices such as regulators with unequal taps, different transformer connections, and multi-phase laterals. Therefore the application of symmetrical sequence networks for fault analysis is made complicated by these factors and if the existing sequence components methodology is used for distribution fault analysis, it will result in deviations from actual values. A method to perform fault analysis using sequence based methods for unbalanced distribution systems is discussed in [47]. Quantification of errors when using a sequence component based fault analysis on distribution system is discussed in [67] where fault currents using sequence component based method is compared with results obtained using three-phase fault analysis method. In both the papers, the mutual sequence elements were neglected which is the main source of error.

The last decade has seen a rapid growth of inverter-based resources (IBR) and this has led to change in the dynamics of short circuit current on the bulk power systems(BPS), as well as calls to attention new issues for consideration while setting relay elements. In contrast to conventional generators which have universal short-circuit response characteristics, the inverter fault response is based on specific inverter control system designs [12]. During faults, the inverter acts as a constant current source irrespective of the control strategy (Voltage Source Inverters or Current Source Inverters) used. Inverter control systems also restrict the maximum short-circuit current to limit thermal overloads of power electronics. Even though some of the wind turbine generators and static compensators are capable of injecting negative sequence currents, most of the currently existing inverter-based DGs are only capable of injecting positive sequence currents even in case of unbalanced faults [68]- [69].

Hence, the negative sequence current from an inverter-based generating resource may either have a magnitude too low or have an undefined phase angle relationship to the negative sequence voltage. In general, the protective relays utilize this angular relationship between negative sequence voltage and current along with some safety margin to confirm the unbalanced fault direction, provided the magnitudes of the negative sequence currents and voltages are above a certain magnitude. Hence a lower magnitude and undefined phase angle relationship cause reliability issues in relaying applications, including negative sequence directional relaying [70]. Detailed impacts of IBRs on the performance of traditional protection schemes is discussed in [71], [72].

Novel circuit models of Inverter-Interfaced distributed generators are discussed in [73], [74], [75]. The control systems associated with the inverters are responsible for the current injected by the inverter-based resources (IBRs). Therefore, with modification of the controls, some amount of negative sequence current can be injected by IBRs. It would be beneficial to analyze the IBR contribution of negative sequence current during unbalanced faults to support protection systems corresponding to selectivity, dependability, and reliability, as discussed in [76]. Negative sequence current improves the reliability of system operation and also helps in balancing voltages avoiding overvoltage of unfaulted phases. There is very little standardization procedure available for inverter-based resources that can be programmed to inject some amount of negative sequence current. One among them is the German grid code (VDE) requirements [77]. As per VDE, the negative sequence current injection should be programmed (using a K-factor) in such a way that its injection magnitude should be proportional to the measured negative sequence voltage. Also, the negative sequence voltage should lead negative sequence current injected by a minimum of 90 degrees.

This paper proposes a novel method that extends the existing sequence based

method to include mutual sequence elements also thereby reducing the source of error as discussed in [67]. Sequence currents for all ten types of faults, single line to ground (AG, BG, CG) fault, line to line (AB, BC, CA) fault, double line to ground fault (ABG, BCG, CAG), and three phase (ABCG) faults are derived from basic equations. The results are then compared with results obtained from phase based fault analysis. The effectiveness and accuracy of the algorithm are validated using IEEE 13,34 and 123 bus test distribution feeders. Some of the advantages of using the proposed sequence based analysis are as follows. Most of the power system data which are available in terms of sequence quantities (for eg. data for lines, transformers, generators) can be directly used to do steady fault analysis without transforming to phase components to do analysis using phase coordinates methods. The existing sequence component based methods used for distribution fault analysis neglects mutual coupling and will result in deviations from actual values. Neglecting mutual impedance leads to errors in fault current values and also in node voltage during fault. Most of the inverter-based DGs produce positive sequence current during a fault which can be easily modeled if fault analysis is done in sequence domain than phase domain. During an unbalanced fault event, one of the main challenges involved is the overvoltage in unfaulted phases. If DERs are capable of injecting negative sequence current during the fault, it would lead to a reduction in this overvoltage of unfaulted phases. Accurate negative sequence voltage at PCC during fault is required to find the amount of negative sequence current that DER should inject during fault [78]. The proposed method can provide accurate node voltage during fault.

## 5.2 Research Contribution

- A novel fault analysis based on three sequence approach considering mutual sequence coupling.

- Fault Analysis of a unbalanced distribution system with multi-phase laterals.
- Fault Analysis of a DER integrated distribution system.

### 5.3 Power System Modeling

In the proposed approach, first, a  $Y_{bus}$  model considering, distribution lines, voltage regulators, transformers, loads, and distributed energy resources, are developed. Formulation of  $Y_{bus}$  considers various power grid elements including distribution lines, voltage regulators, and transformers. The  $Y_{bus}$  of the three phase distribution line can be written as

$$Y_{abc}^{dl} = \begin{bmatrix} Z_{abc}^{ser}(l)^{-1} + \frac{1}{2}B_{abc}^{sh}(l) & -Z_{abc}^{ser}(l)^{-1} \\ -Z_{abc}^{ser}(l)^{-1} & \frac{1}{2}B_{abc}^{sh}(l) + Z_{abc}^{ser}(l)^{-1} \end{bmatrix} \quad (5.1)$$

where  $Z_{abc}^{ser}(l)$  is three phase series impedance and  $B_{abc}^{sh}(l)$  is three phase shunt admittance matrix of the line  $l$ . The  $Y_{bus}$  of a three phase Yg-Yg type load tap changer in series with a distribution line with admittance  $Y_{abc}(r)$  is given by

$$Y_{abc}^{reg} = \begin{bmatrix} RY_{abc}(r)R^T & -RY_{abc}(r) \\ -Y_{abc}(r)R^T & Y_{abc}(r) \end{bmatrix} \quad (5.2)$$

where  $R = \begin{bmatrix} \frac{1}{a_t} & 0 & 0 \\ 0 & \frac{1}{a_t} & 0 \\ 0 & 0 & \frac{1}{a_t} \end{bmatrix}$  and  $a_t = 1 \mp d_V tp$  where  $tp$  is the tap setting and  $d_V$  is

the per unit voltage change per tap. The  $Y_{bus}$  for a transformer connected between node  $m$  and  $n$  with  $\alpha, \beta$  being off-nominal tap ratios on the primary and second sides respectively can be represented as

$$Y_{abc}^{trf} = \begin{bmatrix} \frac{Y_{nn}}{\alpha^2} & \frac{Y_{nm}}{\alpha\beta} \\ \frac{Y_{mn}}{\alpha\beta} & \frac{Y_{mm}}{\beta^2} \end{bmatrix} \quad (5.3)$$

The loads are modeled as a combination of constant power, constant current, and constant impedance loads (ZIP). With ZIP load modeling [2], the net specified nodal current injection of phase  $s$  at node  $i$  can be represented as

$$(I_i^{sp})^s = - \left[ \left( \frac{|S_i^s| \angle \theta^s}{|V_i^s| \angle \delta^s} \right)^* + \left( \frac{|S_i^s|}{|V_{0i}^s|} \right) \angle (\delta^s - \theta^s) + \left( \frac{V_i^s}{Z_i^s} \right) \right] \quad (5.4)$$

where  $S_i^s$  is scheduled power,  $\delta$  is the voltage angle and  $\theta$  is the power factor angle,  $V_{0i}$  is the nominal voltage,  $Z_i$  is impedance of the load. The shunt capacitance for reactive power support is modelled as a constant impedance load in the proposed method.

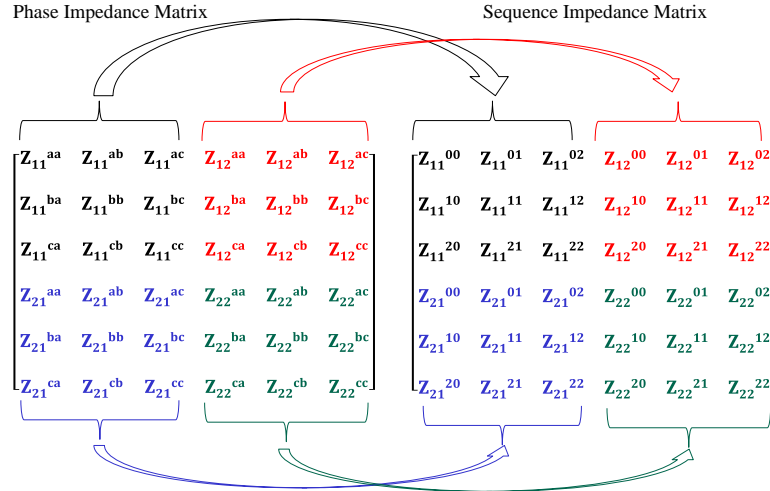


Figure 5.1: Sequence component of impedance submatrices.

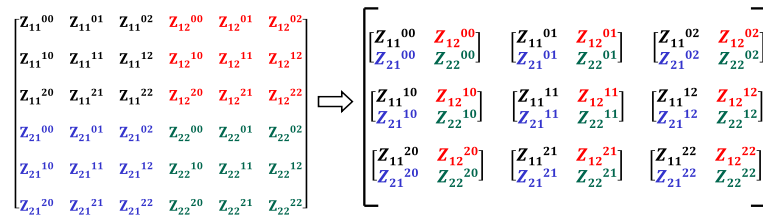


Figure 5.2: Grouping of Sequence impedance submatrices.

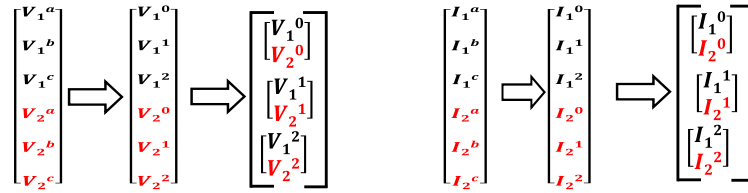


Figure 5.3: Grouping of Sequence current and voltage submatrices.

### 5.3.1 Formation of Sequence Bus Impedance Matrix

The bus impedance matrix is used to find the Thevenin impedance to the point of fault. For a fault at bus  $k$ , the diagonal element in the  $k$  axis impedance matrix gives the Thevenin impedance. Using the models developed for distribution lines, voltage regulators, and transformers, a three-phase bus admittance matrix  $Y^{abc}$  is formed. This is inverted to obtain the bus impedance matrix  $Z^{abc}$ . Each of the phase impedance submatrices can be converted to sequence submatrices using an equation similar to (3.95). Consider a 2 bus system with both buses being 3 phase buses. The phase impedance matrix will be a  $6 \times 6$  matrix and each  $3 \times 3$  submatrix is converted to sequence components as shown in Fig. 5.1. These sequence submatrices are grouped into positive, negative, and zero sequence matrices  $Z^{012}$  as shown in Fig. 5.2. Similarly, the voltage and current submatrices can be converted to sequence submatrices using (5.19) and grouped as shown in Fig. 5.3. One of the challenges while calculating sequence impedance matrix occurs when there are single or two-phase laterals. This leads to buses with missing phases. Two approaches to obtain  $Z^{012}$  for such kinds of systems are tested. Consider a 2 bus system with one three phase bus and the other 2 phase bus with phase b missing. The  $Y^{abc}$  calculated will have a row and column full of zeros as shown in Fig. 5.4. This matrix cannot be inverted as it is singular. But each of the  $3 \times 3$  submatrices can be converted to sequence submatrices. A single non-zero value in the phase admittance submatrix will lead to a full  $3 \times 3$  submatrix in the sequence domain. The sequence admittance

matrix obtained can be inverted to obtain impedance matrix and then grouped to obtain  $Z^{012}$ . This method worked well for smaller test systems but failed as the size of the system and the number of laterals increased. So method 2 is adopted. Here  $Y^{abc}$  is first reduced by removing row and column of zeros (row/column 5 in this case) and then inverted to obtain  $Z^{abc}$ . This matrix is not a square matrix and thus sequence conversion of  $3 \times 3$  submatrices are impossible. To overcome this problem, zeros are added back to rows and columns (row/column 5 in this case). The resulting  $(3N \times 3N)$  matrix can be converted to sequence domain to obtain  $Z^{012}$ . This method was successful in all the systems tested irrespective of size or number of multi-phase laterals.

### 5.3.2 Buses with Missing Phases

To do fault analysis on single and two-phase buses, a fault impedance method is used. For an SLG fault on a bus  $A$ , the self impedance of the line (of respective phase) connecting bus  $A$  to nearest three phase bus  $B$  is calculated and taken as fault impedance  $z_f$ . Now an SLG fault at bus  $B$  with fault impedance  $z_f$  is performed to get fault current. In the case of LL fault,  $z_f$  is calculated using self impedance and mutual impedance of lines in both the phases. Consider bus  $A$  has b and c phases present. The fault impedance is calculated as

$$z_f = z_{AB}^{bb} + z_{AB}^{cc} - (z_{AB}^{bc} + z_{AB}^{cb}) \quad (5.5)$$

In case of LLG fault, separate fault impedance for each phase is calculated as

$$z_{fb} = z_{AB}^{bb} - z_{AB}^{bc} \quad (5.6)$$

$$z_{fc} = z_{AB}^{cc} - z_{AB}^{cb} \quad (5.7)$$

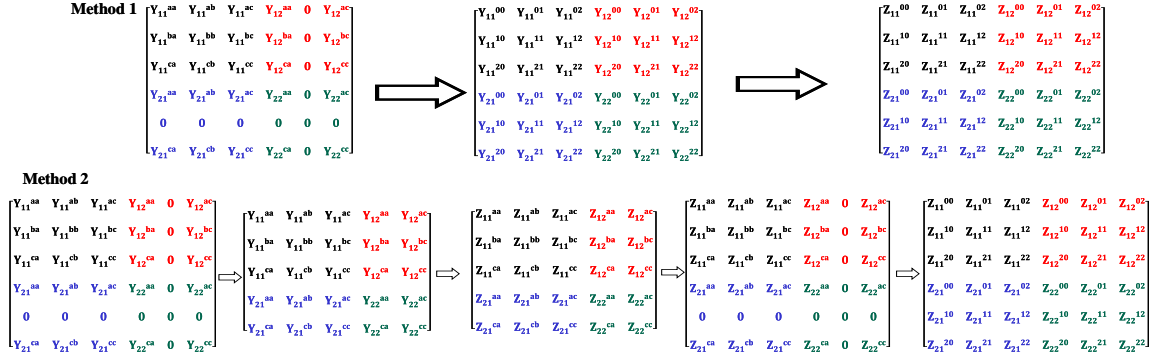


Figure 5.4: Formation of sequence impedance matrix for system having nodes with missing phases.

## 5.4 State of the Art Fault Analysis Methods

### 5.4.1 Phase based fault Analysis

A detailed discussion of phase based fault analysis for distribution system is provided in [79]. First the three phase bus impedance matrix ( $Z_T$ ) is obtained from bus admittance matrix. For a SLG fault at node  $p$  with fault impedance  $z_f$  and pre fault voltage  $E_p$  the fault current is given by

$$I_f = \frac{E_p}{Z_T(p, p) + z_f} \quad (5.8)$$

For a LL fault between nodes  $q$  and  $r$  with fault impedance  $z_f$  and pre fault voltages  $E_q$  and  $E_r$  the fault current is given by

$$I_f = \frac{E_q - E_r}{Z_T(q, q) + \frac{z_f}{2} + Z_T(r, r) + \frac{z_f}{2} - 2Z_T(q, r)} \quad (5.9)$$

For a LLG fault between nodes  $q$  and  $r$  with fault impedance  $z_{fq}$ ,  $z_{fr}$  and pre fault voltages  $E_q$  and  $E_r$  the fault current is given by

$$\begin{bmatrix} I_{fq} \\ I_{fr} \end{bmatrix} = \begin{bmatrix} Z_T(q, q) + z_{fq} & Z_T(q, r) \\ Z_T(r, q) & Z_T(r, r) + z_{fr} \end{bmatrix}^{-1} \begin{bmatrix} E_q \\ E_r \end{bmatrix} \quad (5.10)$$

For a LLLG fault between nodes  $p$ ,  $q$  and  $r$  with fault impedance  $z_{fp}$ ,  $z_{fq}$ ,  $z_{fr}$  and pre fault voltages  $E_p$ ,  $E_q$  and  $E_r$  the fault current is given by

$$\begin{bmatrix} I_{fp} \\ I_{fq} \\ I_{fr} \end{bmatrix} = \begin{bmatrix} Z'_{Tp} & Z_T(p, q) & Z_T(p, r) \\ Z_T(q, p) & Z'_{Tq} & Z_T(q, r) \\ Z_T(r, p) & Z_T(r, q) & Z'_{Tr} \end{bmatrix}^{-1} \begin{bmatrix} E_p \\ E_q \\ E_r \end{bmatrix} \quad (5.11)$$

where

$$Z'_{Ti} = Z_T(i, i) + z_{fi}, i \in p, q, r \quad (5.12)$$

#### 5.4.2 Existing Sequence based fault Analysis

In this section a summary of for different type of fault using existing sequence component based method [65] is summarized. The positive, negative and zero sequence impedance matrices ( $z^{11}$ ,  $z^{22}$ ,  $z^{00}$ ) are obtained by inverting the bus admittance matrix. For a SLG fault on phase a with fault impedance  $z_f$  and pre fault voltage  $E^1$ , the sequence components of fault current is given by

$$I^0 = I^1 = I^2 = \frac{E^1}{z^{00} + z^{11} + z^{22} + 3z_f} \quad (5.13)$$

For a LL fault between phase b and c the zero sequence component is zero and positive and negative sequence components have same magnitude and opposite direction. The components of fault current is given by

$$I^1 = -I^2 = \frac{E^1}{z^{11} + z^{22} + z_f} \quad (5.14)$$

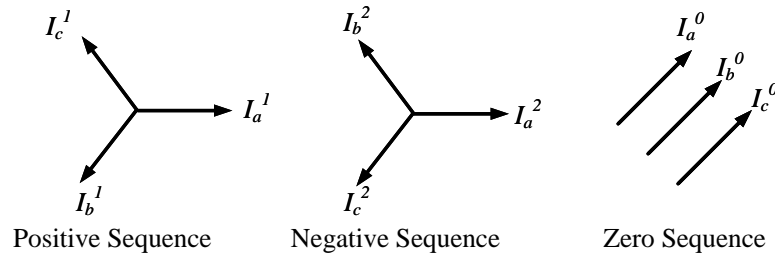


Figure 5.5: Sequence Components.

For a DLG fault on phase b and c with fault impedance  $z_f$  and pre fault voltage  $E^1$ , the sequence components of fault current is given by

$$\begin{aligned}
 I^0 &= -\frac{E^1 - z^{11}I^1}{z^{00} + 3z_f} \\
 I^2 &= -\frac{E^1 - z^{11}I^1}{z^{22}} \\
 I^1 &= \frac{E^1}{z^{11} + \frac{z^{22}(z^{00} + 3z_f)}{z^{22} + z^{00} + 3z_f}}
 \end{aligned} \tag{5.15}$$

For a LLLG fault the zero sequence and negative sequence component is zero. The positive sequence component of fault current is given by

$$I^1 = \frac{E^1}{z^{11} + z_f} \tag{5.16}$$

## 5.5 Proposed Sequence based fault Analysis

### 5.5.1 Sequence Components

Any unbalanced vector can be represented as a combination of 3 balanced vectors as shown in Fig. 5.5.

This can be written in matrix form as

$$\begin{bmatrix} I^a \\ I^b \\ I^c \end{bmatrix} = \begin{bmatrix} 1 & 1 & 1 \\ 1 & a^2 & a \\ 1 & a & a^2 \end{bmatrix} \begin{bmatrix} I^0 \\ I^1 \\ I^2 \end{bmatrix} \quad (5.17)$$

where  $\mathbf{a} = \mathbf{1} < 120$       $\mathbf{a}^2 = \mathbf{1} < 240$

Therefore we can transform a current vector from sequence representation to phase representation as

$$\mathbf{I}^{abc} = \mathbf{C}_a \mathbf{I}^{012} \quad (5.18)$$

Here phase a is taken as reference. Such a transformation would provide us with faults AG, BC, BCG and ABCG. The sequence components can be obtained from phase components as

$$\mathbf{I}^{012} = \mathbf{C}_a^{-1} \mathbf{I}^{abc} \quad (5.19)$$

$$\begin{bmatrix} I^0 \\ I^+ \\ I^- \end{bmatrix} = \frac{1}{3} \begin{bmatrix} 1 & 1 & 1 \\ 1 & a^2 & a \\ 1 & a & a^2 \end{bmatrix} \begin{bmatrix} I^a \\ I^b \\ I^c \end{bmatrix} \quad (5.20)$$

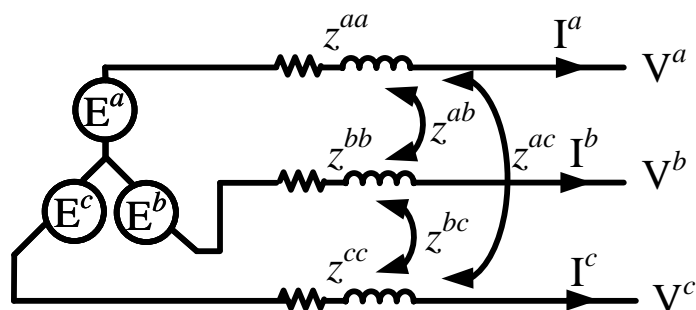


Figure 5.6: Short circuit Analysis with Mutual Coupling.

Applying Kirchoff's voltage law to each phase in Fig.5.6 , we can write

$$\begin{bmatrix} V^a \\ V^b \\ V^c \end{bmatrix} = \begin{bmatrix} E^a \\ E^b \\ E^c \end{bmatrix} - \begin{bmatrix} z^{aa} & z^{ab} & z^{ac} \\ z^{ba} & z^{bb} & z^{bc} \\ z^{ca} & z^{ca} & z^{ca} \end{bmatrix} \begin{bmatrix} I^a \\ I^b \\ I^c \end{bmatrix} \quad (5.21)$$

In compact form we can write

$$\mathbf{V}^{abc} = \mathbf{E}^{abc} - \mathbf{Z}^{abc}\mathbf{I}^{abc} \quad (5.22)$$

Transforming currents and voltages to sequence component, we can write

$$\mathbf{C}_a V^{012} = \mathbf{C}_a E^{012} - \mathbf{Z}^{abc} \mathbf{C}_a I^{012} \quad (5.23)$$

Premultiplying by  $C^{-1}$  we get

$$\begin{aligned} \mathbf{V}^{012} &= \mathbf{E}^{012} - \mathbf{C}^{-1} \mathbf{Z}^{abc} \mathbf{C} I^{012} \\ \mathbf{V}^{012} &= \mathbf{E}^{012} - \mathbf{Z}^{012} \mathbf{I}^{012} \end{aligned} \quad (5.24)$$

where

$$\mathbf{Z}^{012} = \mathbf{C}_a^{-1} \mathbf{Z}^{abc} \mathbf{C}_a \quad (5.25)$$

Therefore

$$\begin{bmatrix} V^0 \\ V^1 \\ V^2 \end{bmatrix} = \begin{bmatrix} E^0 \\ E^1 \\ E^2 \end{bmatrix} - \begin{bmatrix} z^{00} & z^{01} & z^{02} \\ z^{10} & z^{11} & z^{12} \\ z^{20} & z^{21} & z^{22} \end{bmatrix} \begin{bmatrix} I^0 \\ I^1 \\ I^2 \end{bmatrix} \quad (5.26)$$

(5.26) is most prominently used in short circuit analysis including mutual coupling.

It can be see here that, if the voltages  $E^0$ ,  $E^2$  is zero and a transposed system is

considered ( $z^{aa} = z^{bb} = z^{cc}$  and  $z^{ab} = z^{ac} = z^{bc}$ ) (5.26) will reduce to

$$\begin{bmatrix} V^0 \\ V^1 \\ V^2 \end{bmatrix} = \begin{bmatrix} 0 \\ E^1 \\ 0 \end{bmatrix} - \begin{bmatrix} z^{00} & 0 & 0 \\ 0 & z^{11} & 0 \\ 0 & 0 & 0 \end{bmatrix} \begin{bmatrix} I^0 \\ I^1 \\ I^2 \end{bmatrix} \quad (5.27)$$

This is the basic equation for existing sequence based fault analysis [65]. The fault current equations for different type of faults are derived now.

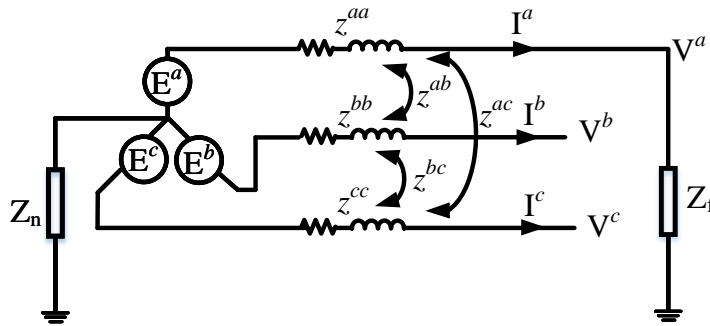


Figure 5.7: Single Line to Ground Fault.

### 5.5.2 Single Line to ground fault

Consider a line to ground fault on phase a through impedance  $Z_f$  as shown in Fig.5.7. The boundary conditions at fault point can be written as

$$\begin{aligned} V^a &= Z_f I^a \\ I^b &= I^c = 0 \end{aligned} \quad (5.28)$$

The symmetrical components of current can be written as

$$\begin{bmatrix} I^0 \\ I^1 \\ I^2 \end{bmatrix} = \frac{1}{3} \begin{bmatrix} 1 & 1 & 1 \\ 1 & a & a^2 \\ 1 & a^2 & a \end{bmatrix} \begin{bmatrix} I^a \\ 0 \\ 0 \end{bmatrix} \quad (5.29)$$

Therefore

$$I^0 = I^1 = I^2 = \frac{1}{3}I^a \quad (5.30)$$

The phase a voltage can be written in terms of symmetrical components similar to (5.17) as

$$V^a = V^0 + V^1 + V^2 \quad (5.31)$$

The sequence voltages can be obtained using (5.26) and thus (5.31) can be written as

$$\begin{aligned} V^a = E^0 - (z^{00}I^0 + z^{01}I^1 + z^{02}I^2) + E^1 - (z^{10}I^0 + z^{11}I^1 \\ + z^{12}I^2) + E^2 - (z^{20}I^0 + z^{21}I^1 + z^{22}I^2) \end{aligned} \quad (5.32)$$

Using (5.30) we can write

$$\begin{aligned} V^a = (E^0 + E^1 + E^2) - (z^{00} + z^{01} + z^{02} + z^{10} + z^{11} + z^{12} \\ + z^{20} + z^{21} + z^{22})I^0 \end{aligned} \quad (5.33)$$

Substituting  $V^a$  from (5.28) we can write

$$\begin{aligned} 3Z_f I^0 = (E^0 + E^1 + E^2) - (z^{00} + z^{01} + z^{02} + z^{10} + \\ z^{11} + z^{12} + z^{20} + z^{21} + z^{22})I^0 \end{aligned} \quad (5.34)$$

Therefore zero sequence current

$$I^0 = \frac{E^0 + E^1 + E^2}{z^{00} + z^{11} + z^{22} + 3Z_f + Z_m} \quad (5.35)$$

where

$$Z_m = z^{01} + z^{02} + z^{10} + z^{12} + z^{20} + z^{21} \quad (5.36)$$

The fault current ( $I^a$ ) can be obtained as

$$\begin{bmatrix} I^a \\ I^b \\ I^c \end{bmatrix} = \begin{bmatrix} 1 & 1 & 1 \\ 1 & a^2 & a \\ 1 & a & a^2 \end{bmatrix} \begin{bmatrix} I^0 \\ I^0 \\ I^0 \end{bmatrix} \quad (5.37)$$

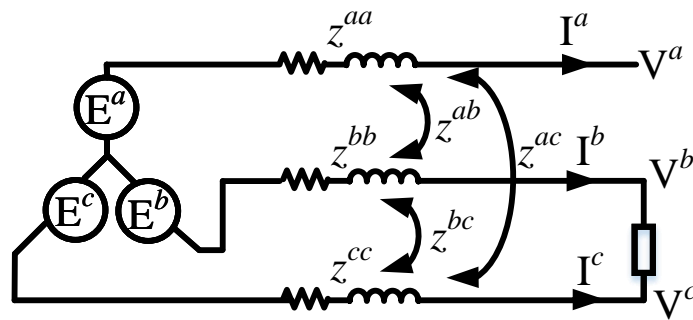


Figure 5.8: Line to Line Fault.

### 5.5.3 Line to Line fault

Consider a fault between phase b and c through impedance  $Z_f$  as shown in Fig.5.8. The boundary conditions at fault point can be written as

$$\begin{aligned} V^b - V^c &= Z_f I^b \\ I^c &= -I^b \\ I^a &= 0 \end{aligned} \quad (5.38)$$

The symmetrical components of current can be written as

$$\begin{bmatrix} I^0 \\ I^1 \\ I^2 \end{bmatrix} = \frac{1}{3} \begin{bmatrix} 1 & 1 & 1 \\ 1 & a & a^2 \\ 1 & a^2 & a \end{bmatrix} \begin{bmatrix} 0 \\ I^b \\ -I^b \end{bmatrix} \quad (5.39)$$

From above equation we get

$$\begin{aligned} I^0 &= 0 \\ I^1 &= -I^2 \\ I^b &= \frac{3I^1}{(a - a^2)} \end{aligned} \quad (5.40)$$

The phase b and c voltage can be written in terms of symmetrical components using (5.17) as

$$\begin{aligned} V^b &= V^0 + a^2V^1 + aV^2 \\ V^c &= V^0 + aV^1 + a^2V^2 \end{aligned} \quad (5.41)$$

Therefore

$$V^b - V^c = (a^2 - a)(V^1 - V^2) \quad (5.42)$$

The sequence voltages can be obtained using (5.26) and thus(5.42) can be written as

$$\begin{aligned} V^b - V^c &= (a^2 - a)[(E^1 - (z^{10}I^0 + z^{11}I^1 + z^{12}I^2)) - \\ &\quad (E^2 - (z^{20}I^0 + z^{21}I^1 + z^{22}I^2))] \end{aligned} \quad (5.43)$$

Using (5.38) we can write

$$Z_f I^b = (a^2 - a)(E^1 - (z^{11}I^1 - z^{12}I^1)) - (E^2 - (z^{21}I^1 - z^{22}I^1)) \quad (5.44)$$

Substituting for  $I^b$  from (5.40) we get

$$Z_f \frac{3I^1}{(a - a^2)} = (a^2 - a)(E^1 - E^2 - (z^{11} - z^{12} - z^{21} + z^{22})I^1) \quad (5.45)$$

Since  $(a^2 - a)(a - a^2) = 3$  we can write

$$Z_f I^1 = (E^1 - E^2 - (z^{11} - z^{12} - z^{21} + z^{22})I^1) \quad (5.46)$$

Therefore positive sequence current can be given by

$$I^1 = \frac{E^1 - E^2}{z^{11} - z^{12} - z^{21} + z^{22} + Z_f} \quad (5.47)$$

The fault current can be obtained as

$$\begin{bmatrix} I^a \\ I^b \\ I^c \end{bmatrix} = \begin{bmatrix} 1 & 1 & 1 \\ 1 & a^2 & a \\ 1 & a & a^2 \end{bmatrix} \begin{bmatrix} 0 \\ I^1 \\ -I^1 \end{bmatrix} \quad (5.48)$$

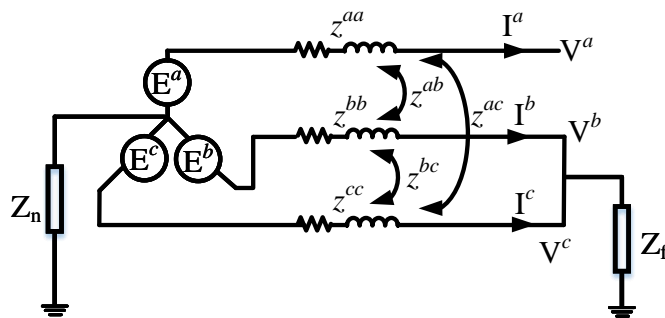


Figure 5.9: Double Line to Ground Fault.

#### 5.5.4 Double Line to Ground fault

##### 5.5.4.1 Double Line to Ground Fault with One Fault Impedance

Consider a fault between phase b and c through impedance  $Z_f$  to ground as shown in Fig.5.9. The boundary conditions at fault point can be written as

$$\begin{aligned} V^b = V^c &= Z_f(I^b + I^c) \\ I^a &= I^0 + I^1 + I^2 = 0 \end{aligned} \quad (5.49)$$

Therefore

$$I^0 = -(I^1 + I^2) \quad (5.50)$$

The phase b and c voltage can be written in terms of symmetrical components using (5.17) as

$$V^b = V^0 + a^2V^1 + aV^2 \quad (5.51)$$

$$V^c = V^0 + aV^1 + a^2V^2$$

Since  $V^b = V^c$  we get

$$V^1 = V^2 \quad (5.52)$$

Substituting (5.52) back in (5.51) we get

$$V^b = V^0 + a^2V^1 + aV^1 = V^0 + (a^2 + a)V^1 \quad (5.53)$$

Since  $(a^2 + a) = -1$ , we can write

$$V^b = V^0 - V^1 \quad (5.54)$$

Similarly the phase b and c current can be written in terms of symmetrical components as

$$I^b = I^0 + a^2I^1 + aI^2$$

$$I^c = I^0 + aI^1 + a^2I^2$$

$$I^b + I^c = I^0 + a^2I^1 + aI^2 + I^0 + aI^1 + a^2I^2 \quad (5.55)$$

$$I^b + I^c = 2I^0 + (a^2 + a)I^1 + (a^2 + a)I^2$$

Since  $(a^2 + a) = -1$  and using (5.50) we can write

$$I^b + I^c = 2I^0 - (I^1 + I^2) \quad (5.56)$$

$$I^b + I^c = 2I^0 + I^0$$

Therefore phase b voltage can be written as

$$V^b = Z_f(I^b + I^c) = 3I^0Z_f \quad (5.57)$$

From (5.54) and (5.57) we can write

$$3I^0 Z_f = V^0 - V^1 \quad (5.58)$$

The sequence voltages can be obtained using (5.26) and thus (5.58) can be written as

$$3I^0 Z_f = (E^0 - (z^{00}I^0 + z^{01}I^1 + z^{02}I^2)) - (E^1 - (z^{10}I^0 + z^{11}I^1 + z^{12}I^2)) \quad (5.59)$$

Grouping coefficients of  $I^0, I^1, I^2$  and on simplification we get

$$(z^{10} - z^{00} - 3Z_f)I^0 + (z^{11} - z^{01})I^1 + (z^{12} - z^{02})I^2 = E^1 - E^0 \quad (5.60)$$

From (5.52) we can write

$$V^1 = V^2$$

$$E^1 - (z^{10}I^0 + z^{11}I^1 + z^{12}I^2) = E^2 - (z^{20}I^0 + z^{21}I^1 + z^{22}I^2) \quad (5.61)$$

Grouping coefficients of  $I^0, I^1, I^2$  and on simplification we get

$$(z^{10} - z^{20})I^0 + (z^{11} - z^{21})I^1 + (z^{12} - z^{22})I^2 = E^1 - E^2 \quad (5.62)$$

Finally from (5.49) we can write

$$I^a = I^0 + I^1 + I^2 = 0 \quad (5.63)$$

The sequence component currents can be calculated by solving (5.63), (5.60) and (5.62) simultaneously. In matrix form this can be written as

$$\begin{bmatrix} 1 & 1 & 1 \\ z^{10} - z^{00} - 3Z_f & z^{11} - z^{01} & z^{12} - z^{02} \\ z^{10} - z^{20} & z^{11} - z^{21} & z^{12} - z^{22} \end{bmatrix} \begin{bmatrix} I^0 \\ I^1 \\ I^2 \end{bmatrix} = \begin{bmatrix} 0 \\ E^1 - E^0 \\ E^1 - E^2 \end{bmatrix} \quad (5.64)$$

The fault current can be obtained as

$$\begin{bmatrix} I^a \\ I^b \\ I^c \end{bmatrix} = \begin{bmatrix} 1 & 1 & 1 \\ 1 & a^2 & a \\ 1 & a & a^2 \end{bmatrix} \begin{bmatrix} I^0 \\ I^1 \\ I^2 \end{bmatrix} \quad (5.65)$$

#### 5.5.4.2 Double Line to Ground Fault with Separate Fault Impedance

Consider a double line to ground fault on phase b and c through impedance  $Z_{fb}$  and  $Z_{fc}$  as shown in Fig.5.10. The boundary conditions at fault point can be written as

$$\begin{aligned} V^b &= Z_{fb}I^b \\ V^c &= Z_{fc}I^c \end{aligned} \quad (5.66)$$

$$I^a = I^0 + I^1 + I^2 = 0$$

The phase b voltage and current can be written in terms of symmetrical components using (5.17). Thus (5.66) can be written as

$$\begin{aligned} V^0 + a^2V^1 + aV^2 &= Z_{fb}(I^0 + a^2I^1 + aI^2) \\ [E^0 - z^{00}I^0 - z^{01}I^1 - z^{02}I^2] + a^2[E^1 - z^{10}I^0 \\ - z^{11}I^1 - z^{12}I^2] + a[E^2 - z^{20}I^0 - z^{21}I^1 - z^{22}I^2] \\ &= Z_{fb}(I^0 + a^2I^1 + aI^2) \end{aligned} \quad (5.67)$$

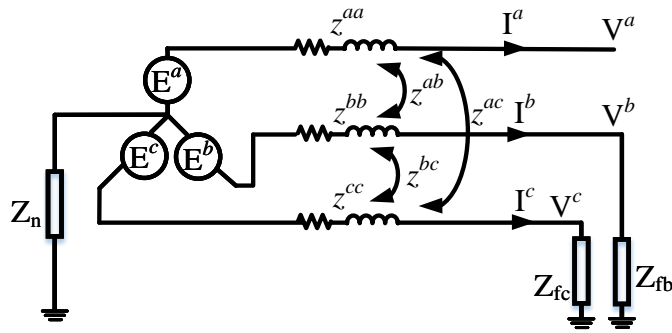


Figure 5.10: Double Line to Ground Fault with separate fault impedance.

Similarly the phase c voltage and current can be written in terms of symmetrical components using (5.17). Thus (5.66) can be written as

$$\begin{aligned}
 V^0 + aV^1 + a^2V^2 &= Z_{fc}(I^0 + aI^1 + a^2I^2) \\
 [E^0 - z^{00}I^0 - z^{01}I^1 - z^{02}I^2] + a[E^1 - z^{10}I^0 - \\
 z^{11}I^1 - z^{12}I^2] + a^2[E^2 - z^{20}I^0 - z^{21}I^1 - z^{22}I^2] & \\
 &= Z_{fc}(I^0 + aI^1 + a^2I^2)
 \end{aligned} \tag{5.68}$$

Finally from (5.66) we can write

$$I^a = I^0 + I^1 + I^2 = 0 \tag{5.69}$$

The sequence component currents can be calculated by grouping coefficients and solving (5.67), (5.68) and (5.69) simultaneously. The fault current can be obtained as

$$\begin{bmatrix} I^a \\ I^b \\ I^c \end{bmatrix} = \begin{bmatrix} 1 & 1 & 1 \\ 1 & a^2 & a \\ 1 & a & a^2 \end{bmatrix} \begin{bmatrix} I^0 \\ I^1 \\ I^2 \end{bmatrix} \tag{5.70}$$

### 5.5.5 Three Phase to Ground fault

Consider a fault between phase a,b and c through impedance  $Z_f$  to ground as shown in Fig.5.11. The sequence currents during a three phase to ground fault is given by

$$\begin{bmatrix} I^0 \\ I^1 \\ I^2 \end{bmatrix} = \begin{bmatrix} z^{00} + 3Z_f & z^{01} & z^{02} \\ z^{10} & z^{11} + Z_f & z^{12} \\ z^{20} & z^{21} & z^{22} + Z_f \end{bmatrix}^{-1} \begin{bmatrix} E^0 \\ E^1 \\ E^2 \end{bmatrix} \quad (5.71)$$

### 5.5.6 Bus Voltages during fault

The faulted bus voltage is calculated by adding the pre-fault voltage with the change in voltage or delta voltage  $\Delta V$  during fault.  $\Delta V$  is calculated by multiplying injected fault current to corresponding impedance.  $\Delta V$  for node  $i$  can be obtained as

$$\begin{aligned} \Delta V^0 &= -(z^{00}I^0 + z^{01}I^1 + z^{02}I^2) \\ \Delta V^1 &= -(z^{10}I^0 + z^{11}I^1 + z^{12}I^2) \\ \Delta V^2 &= -(z^{20}I^0 + z^{21}I^1 + z^{22}I^2) \end{aligned} \quad (5.72)$$

The voltage during fault is given by

$$\begin{bmatrix} V_f^0 \\ V_f^1 \\ V_f^2 \end{bmatrix} = \begin{bmatrix} E^0 \\ E^1 \\ E^2 \end{bmatrix} + \begin{bmatrix} \Delta V^0 \\ \Delta V^1 \\ \Delta V^2 \end{bmatrix} \quad (5.73)$$

### 5.5.7 Faults with B and C phase as Reference

All the equations derived until now are based on phase a as reference during sequence transformation as shown in (5.18). In order to obtain faults such as CG, AB, ABG phase c should be taken as reference and to obtain BG, CA, CAG phase

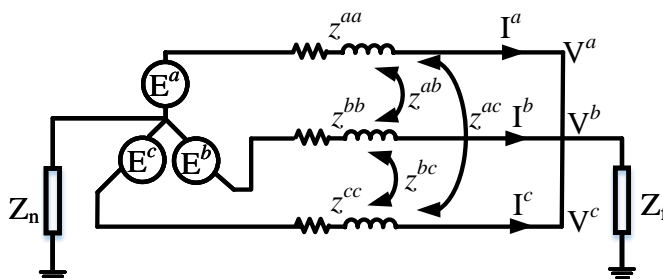


Figure 5.11: Three Phase to Ground Fault.

Table 5.1: Comparison of Per Unit Voltage during LLLG Fault

Bus	Phase Method			Existing Sequence Method			Proposed Sequence Method		
	Va	Vb	Vc	Va	Vb	Vc	Va	Vb	Vc
1	0.910	0.880	0.910	0.900	0.900	0.900	0.910	0.880	0.910
2	0.860	0.840	0.860	0.850	0.850	0.850	0.860	0.840	0.860
3	0.600	0.490	0.580	0.560	0.560	0.560	0.600	0.490	0.580
4	0.000	0.000	0.000	0.000	0.000	0.000	0.000	0.000	0.000

b should be taken as reference during sequence transformation. The transformation matrices are given by

$$C_b = \begin{bmatrix} 1 & a & a^2 \\ 1 & 1 & 1 \\ 1 & a^2 & a \end{bmatrix} \quad C_c = \begin{bmatrix} 1 & a^2 & a \\ 1 & a & a^2 \\ 1 & 1 & 1 \end{bmatrix} \quad (5.74)$$

A detailed flowchart of fault analysis using proposed method is shown in Fig.5.12

## 5.6 Simulation Results

### 5.6.1 Comparison of Proposed Method with Existing Sequence based method and Phase based method

The fault analysis using the proposed method is compared with the existing sequence based method and phase based method as discussed in 5.4 using a modified

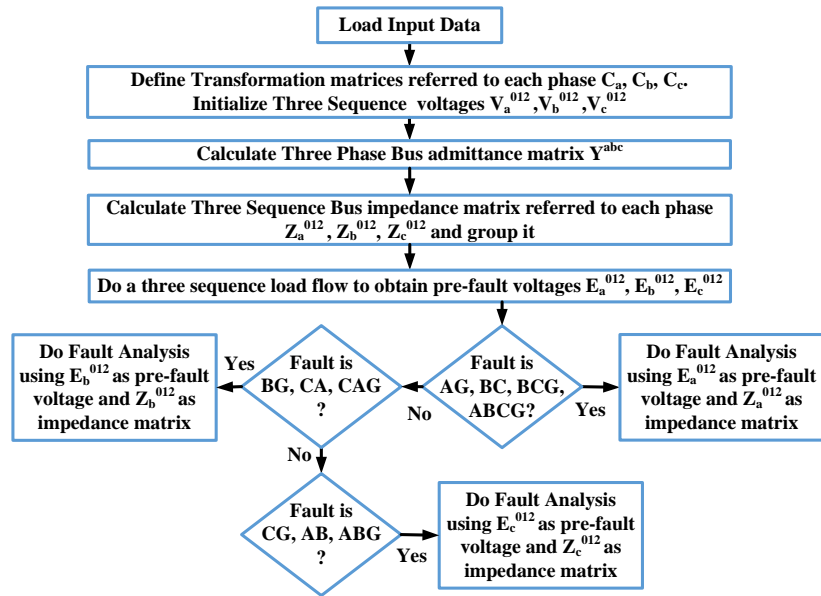


Figure 5.12: Flow chart of Proposed Fault Analysis.

IEEE 4 bus system under no-load condition. Two test scenarios to show the effect of mutual coupling on fault analysis are developed. In case 1, untransposed lines are considered and in case 2 transposed lines ( $z^{aa} = z^{bb} = z^{cc}$  and  $z^{ab} = z^{ac} = z^{bc}$ ) are considered. The fault current values at bus 4 for an LLG and LLLG fault at bus 4 are shown in Fig. 5.13. Also, the voltage during fault is calculated as discussed in 5.5.6 and is shown in Fig. 5.14 and Table. 5.1. Some of the key observations that can be deduced are as follows:

- In case 1, the phase method analysis gives unequal fault current values in three phases even in the case of a symmetric (LLG) fault. This is due to the effect of mutual coupling in untransposed lines. Similar results are obtained using the proposed method. But the existing sequence based method gives equal fault current on all phases. Also, the sequence based method gives different fault currents compared to the phase method.
- In case 2 where transposed lines are considered, the fault current values of all the phases are equal in the case of LLLG fault. Also, fault current values of the

proposed method, sequence method, and phase method are all same for both LLG and LLLG fault.

- Now coming to the voltage during a fault (Table. 5.1), the sequence method gives equal voltage on all phases for case 1. Both phase and the proposed method give unequal voltage values on each phase. The source of error in the sequence method is due to two reasons. One due to wrong fault current calculation and second due to ignoring the mutual impedance during delta voltage calculation.
- If sequence domain voltages during faults are considered, it can be seen from Fig. 5.14 that the negative sequence voltage calculated using the existing sequence method is zero while the true value is non zero. It is clear from this analysis that existing sequence based methods gives inaccurate voltage values during fault and it is not a good option to be used for DER negative current injection controls as discussed in [78]. The proposed method can be used for such controls owing to its accuracy.

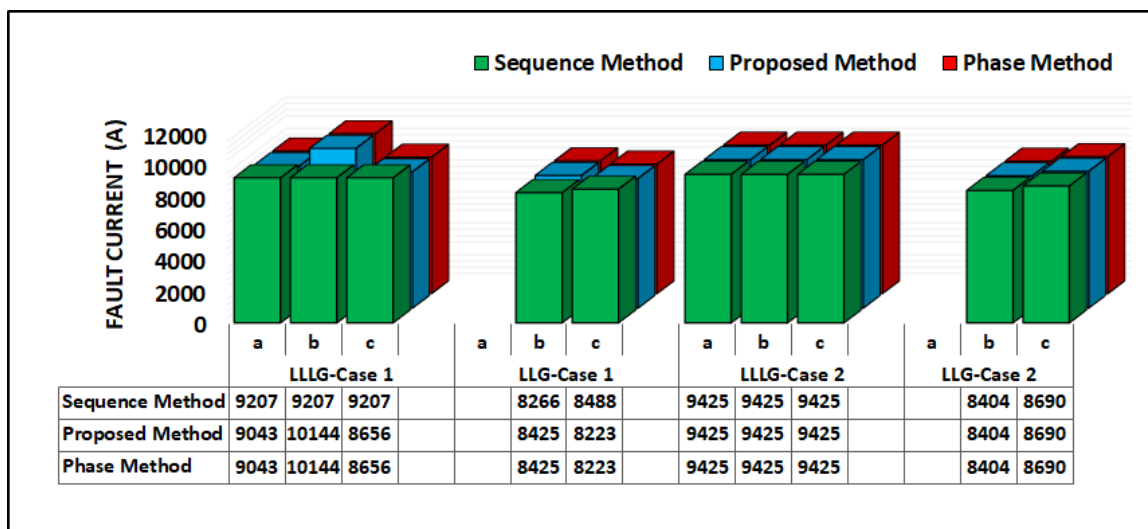


Figure 5.13: Fault Current at Bus 4 for LLG and LLLG fault.

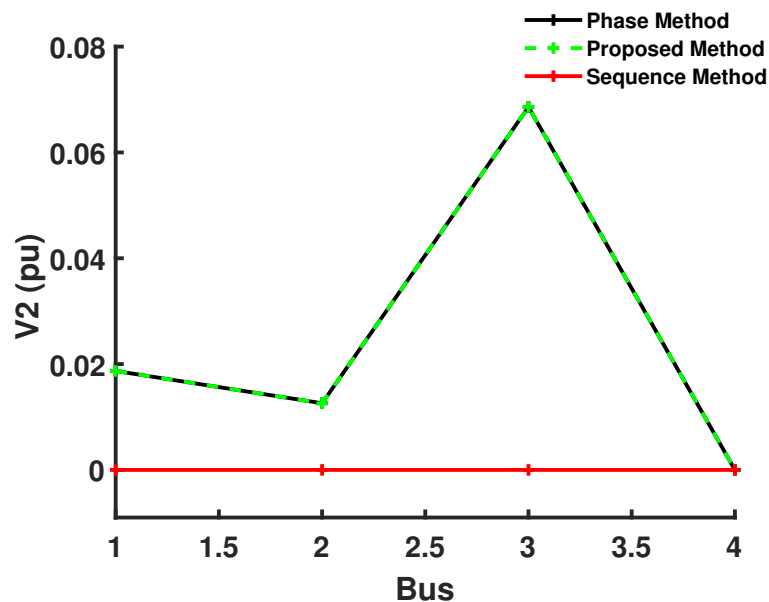


Figure 5.14: Negative sequence Voltage during LLLG fault.

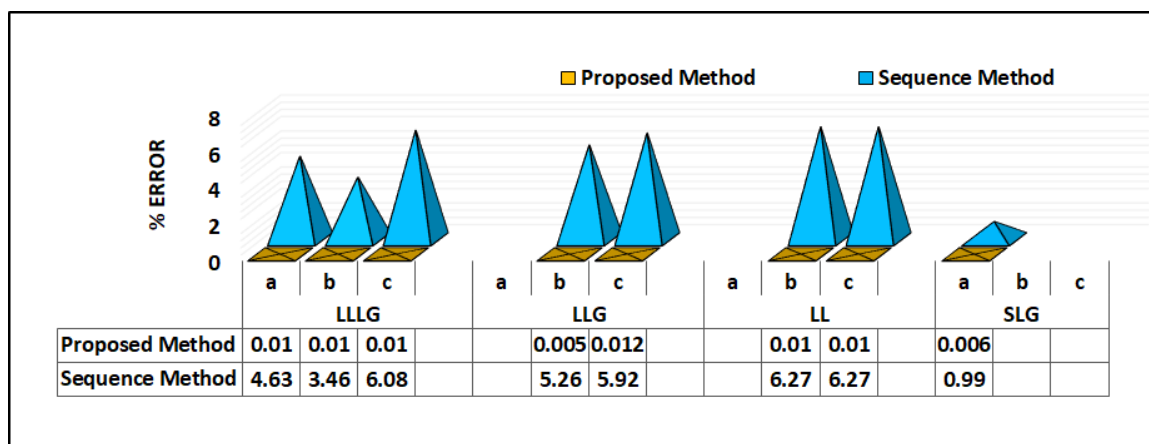


Figure 5.15: Comparison of Maximum % error for IEEE 13 Bus.

### 5.6.2 Validation of Proposed Method with state-of-the-art Fault Analysis results

In this section the results obtained using proposed method is compared with benchmark fault solutions provided in the literature. The source voltage and impedance were taken same as in [80]. Also the short circuit study assumptions on voltage regulator, shunt capacitor, loads and fault impedance were followed as in [80]. A comparison of maximum %error for different types of fault in IEEE 13 bus system is shown in Fig. 5.15. It can be seen that the maximum %error for any fault using

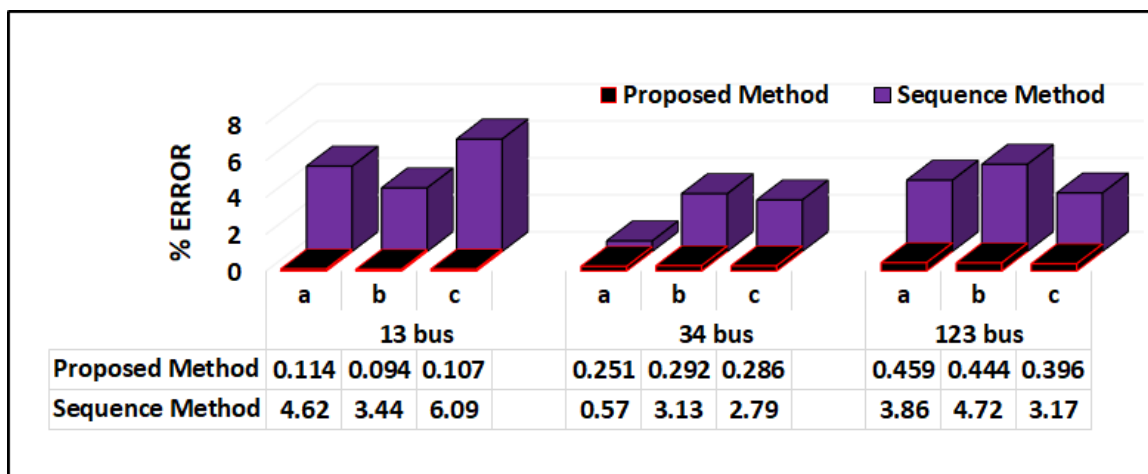


Figure 5.16: Comparison of Fault Analysis with Benchmark.

proposed method is less than 0.01% while that using existing sequence method is 6.2%. In case of IEEE 34 and 123 bus system, results from [81] is taken as reference. Fig. 5.16 shows the comparison of maximum %error for LLLG fault in 13, 34 and 123 bus system. Also fault current values for all the three phase nodes are shown in Fig. 5.17a and Fig. 5.17a.

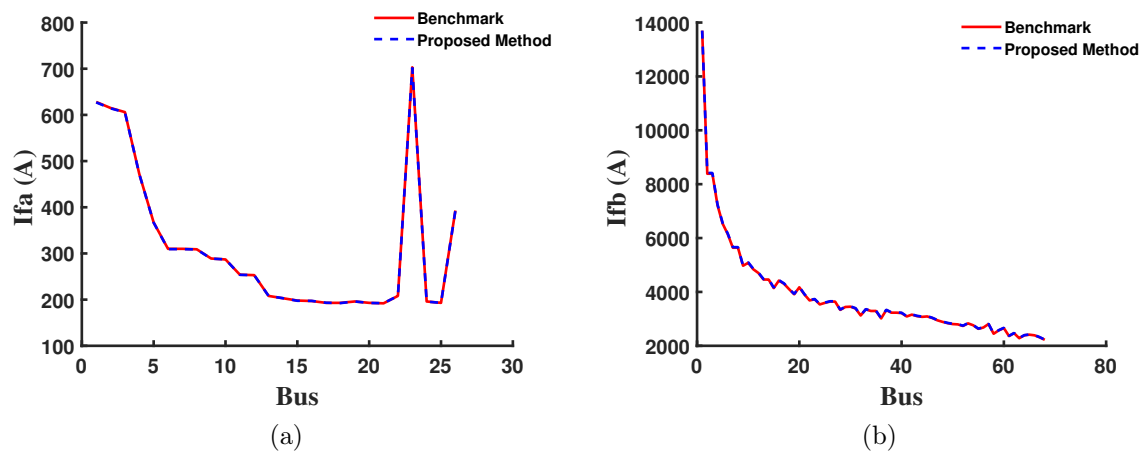


Figure 5.17: (a) A phase Fault current for LLLG Fault on IEEE 34 bus system. (b) B phase Fault current for LLLG Fault on 123 bus system.

Table 5.2: Comparison of Fault Current (Amps) for Buses with missing phases

	Fault Type	Phase Method			Sequence Method			Sequence Method		
		Iap	Ibp	Icp	Ias	Ibs	Ics	Ias	Ibs	Ics
684	SLG	2019			2002			2019		
652	SLG	1796			1784			1796		
645	LL		3191	3191		3068	3068		3191	3191
646	LL		2882	2882		2676	2676		2882	2882
633	DLG		3406	3368		4289	3850		3439	3414
634	DLG		3052	3057		4250	3832		3100	3115

### 5.6.3 Fault analysis on buses with missing phases

The distribution systems consist of multi-phase laterals which can lead to some buses only having 1 or 2 phases present. Short circuit analysis by directly using values from the bus impedance matrix for such nodes showed erroneous fault currents. Therefore a modification on fault analysis is done where fault on such buses is modeled as the fault on the nearest three-phase bus with a fault impedance. The IEEE 13 bus system is used to check the effectiveness of the proposed method in this case. The comparison of per unit fault currents for different types of fault on buses with missing phases is shown in Table. 5.2. In the case of an LLG fault, equations derived in section 5.5.4.2 are used. With this modification, the proposed fault current values were similar to those obtained using phase based method. This is the case if the bus impedance matrix is obtained using method 1 described in 5.3.2. We have observed that if bus impedance matrix is obtained using method 2, then no such modifications are required and the fault current values were accurate compared to phase results even for buses with missing phase.

### 5.6.4 Fault analysis with B and C phase as Reference

The unsymmetrical faults in the power system can occur in any phase, not only on the  $a$  phase. To accommodate that, the phase reference during sequence transformation is changed as explained in 5.5.7. Comparison of fault currents for an LLG

Table 5.3: Comparison of LLG Fault on CA phase on IEEE 13 bus system

Node	LLG - Benchmark [80]		LLG - Proposed Method	
	C	A	C	A
150	8450.7	8446.3	8449.7	8445.9
650	2822.6	2892.2	2822.5	2892.1
692	2616.5	2644.8	2616.4	2644.8
684	2435.2	2489.2	2435.2	2489.2
680	2627.8	2713.8	2627.7	2713.8
675	2822.6	2892.2	2822.5	2892.1
671	14358	14150	14357.5	14150.1
634	3636.9	3673.8	3636.8	3673.7
633	4153.2	4283.8	4152.9	4283.7

fault between phase a and c are shown in Table. 5.3. In this case, phase b is taken as phase reference during sequence transformation. Also, fault current during an SLG fault on phase c is shown in Fig. 5.18. The fault current values for all types of fault

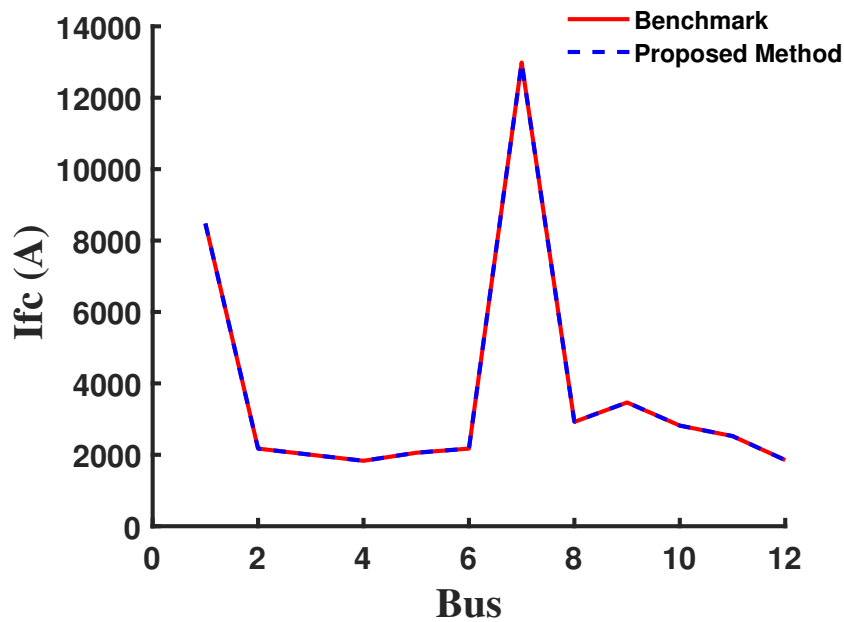


Figure 5.18: SLG fault on phase C.

in case of IEEE 13, IEEE 34 and 123 bus systems are given in appendix.

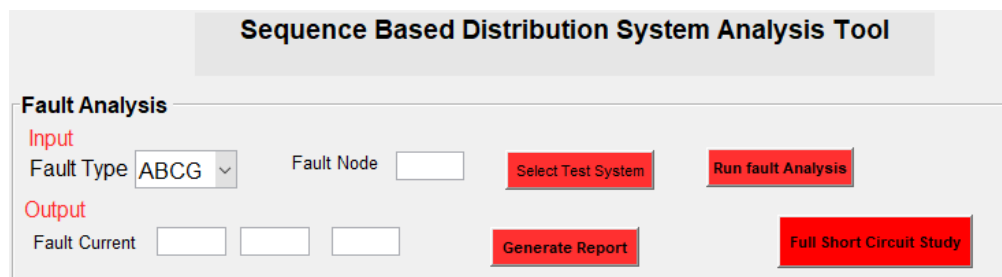


Figure 5.19: Distribution Fault Analysis Tool

### 5.7 Three Phase Fault Analysis Tool

A Graphical User Interface to conduct fault analysis on unbalanced distribution systems utilizing the sequence method is developed as shown in Fig. 5.19. The tool is universal and can be used to analyze any distribution system. The user can select the type of fault, from a drop-down list which will display the list of all 10 types of fault. The user can also select the fault node and fault impedance. Once analysis is complete a report will be generated with node voltages and line currents during fault. In addition to this, a full system-level short circuit study option is provided where fault currents for all 10 types of fault on all nodes of the system are calculated.

### 5.8 Three Sequence Based Distribution System Analysis Tool

Finally, a complete distribution system analysis tool based on sequence based methods derived in chapters 3, 4, and 5 is developed as shown in Fig. 5.20. The tool is universal and can be used to analyze any distribution system. The user can conduct load flow, QSTS, and fault analysis on the system selected. The capabilities of individual sections are already explained in detail in respective sections.

### 5.9 Summary

In this chapter, a novel method to conduct fault analysis using three sequence components considering mutual coupling is proposed. The method is capable of analyzing all 10 types of shunt faults in three phase unbalanced system. The results obtained using the proposed method are validated with phase based fault analysis

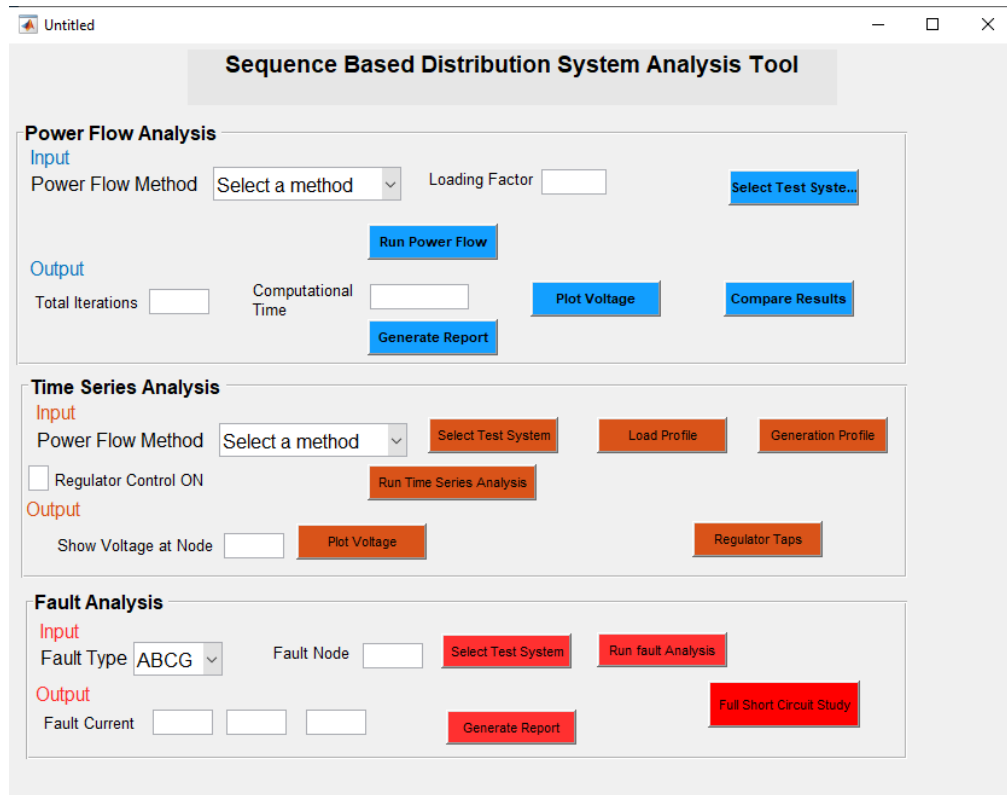


Figure 5.20: Sequence Based Distribution System Analysis Tool.

results as well as with state-of-the-art fault analysis benchmark data. Comprehensive numerical tests on IEEE-4, 13, 34, and 123 bus test distribution systems shows the accuracy and robustness of the proposed approach for distributed lines with missing phases, several voltage regulators, and transformer connection. Owing to its accuracy and based on sequence component frame, the method is very much suitable to be used for steady state fault analysis of DER integrated power distribution system. The method can also be used to conduct short circuit analysis on integrated transmission and distribution systems.

## CHAPTER 6: THREE-SEQUENCE UNIFIED TRANSMISSION AND DISTRIBUTION STEADY STATE ANALYSIS

### 6.1 Introduction

Power grid modernization significantly changes the grid operation and leads to new challenges. Even though smart grid technologies like DERs, energy storage, smart appliances, demand response mechanisms, are deployed at the distribution level, most of the benefits are accumulated at the transmission level. By having a framework of integrated transmission and distribution technologies as a single simulation environment, the benefits of smart grid assets at the transmission level can be quantified [82]. By representing the distributed smart grid assets using reduced-order models, their impacts on the bulk power system with respect to stability and reliability could be analyzed. With active distribution networks, it is important to have transmission system analysis consider distribution level variations and changes. To capture these unprecedented transmission and distribution (T&D) interactions an integrated grid modeling may be required. Furthermore, the impacts of distribution level changes on transmission systems such as reverse power flow can be analyzed with an integrated T&D model. Generally, steady-state and dynamic studies of the bulk power system are conducted assuming a balanced system model. For such studies, transmission lines are assumed to be symmetric and loads are assumed to be balanced. With the rising penetration level of DERs in the distribution system, especially the non-symmetrical placement of single-phase Photo-Voltaic (PV) farms, significant unbalances can occur which can even have an impact on the transmission system. For analysis of such power grids with large penetration of DERs, three-phase modeling of the transmission and distribution system would be useful.

Several efforts have been proposed recently to model an integrated T&D system for power flow and stability assessment such as in [83] and [84]. In most of these approaches, the transmission system is modeled based on a positive sequence framework and the distribution system in three-phase representation. In [85] a large hybrid model(three phase integrated transmission and distribution system models) was presented and steady state analysis on this hybrid system was used to demonstrate insights that were not obtained from the study of transmission and distribution systems separately. An integrated electromechanical and electromagnetic transient simulation of transmission systems was discussed in [86] where the system was divided into sub system and interfaced through Thevenin and Norton equivalents at the boundary. In [87] an electromagnetic transient (EMT)-transient stability (TS) hybrid simulation platform is proposed and its application to fault-induced delayed voltage recovery is presented. [88] discusses an integrated grid modeling System developed for co-simulation of electric power transmission and distribution systems. In [83] a global power flow method that considers transmission and distribution grids as a whole is discussed where a master-slave-splitting iterative method is developed to alleviate boundary mismatches between the transmission and distribution grids. A hybrid power flow formulation unifying three-phase and single phase models were proposed in [89] where unbalance at the interconnecting point is considered and interfacing is done using a single-port three-sequence Norton equivalent. A contingency analysis method based on global power flow analysis which integrates both the transmission and distribution power flow is proposed in [90] where a global transmission contingency analysis is introduced to study contingency in distribution networks that are more frequently looped. In [91] integrated T&D dynamic simulation is done using a Schur-complement based domain decomposition algorithm by representing the transmission and distribution systems in single-phase detail. A simplified distribution system with one feeder was considered used to simulate T&D systems in [92] using

PSSE which is a Positive-sequence based commercial software. A scalable open-source simulation framework was discussed in [93] that runs aggregated simulations using separate distribution and transmission system simulators. It integrates existing simulation tools and blurs the boundaries between generation, transmission, distribution, and markets.

A novel modeling framework is proposed in [94], where the transmission system is modeled as three-sequence detail and the distribution system connected to it is modeled in three-phase detail. A dynamic model of a Combined transmission-distribution System was presented in [95] with all components of the transmission system and distribution system represented with dynamic details and included dynamics of a DG inverter. A new approach for studying the impact of DGPV on power systems using integrated T&D models was presented in [96] where PV was connected to the secondary distribution networks. Also, the impact of change in transmission voltage on distribution voltage profiles and voltage regulator operations is analyzed taking an integrated T&D system. In [84] a large-scale, high-performance integrated transmission-distribution tool was developed to explore the system-wide operational interactions of high-penetration of distributed generation from solar photovoltaics. In [97] an Integrated transmission and distribution model was used to assess impacts of wholesale Photovoltaic systems within distribution circuits, on substation and regional transmission. Finally, some of the current platforms used for integrated T&D modeling Distributed Engineering Workstation(DEW) [98] and Hierarchical Engine for Large-scale Infrastructure Co-Simulation HELIX [99]. The Steady-state analysis using Integrated T&D is challenging because numerical methods used for power flow analysis which are stable for transmission networks may not work as required for distribution networks.

The importance of detailed modeling of an unbalanced distribution system and the importance of T&D co-simulation to accurately assess voltage stability of the grid are

discussed in [100]. The significance of T&D co-simulation for voltage stability analysis is discussed in [101, 102]. PV curve superimposition approach was developed in [101] to analyze the voltage stability of the T&D system, a phasor measurement-based method to assess voltage stability was developed in [102]. For stability purposes, a continuation power flow model for a three-phase unbalanced system is developed in [103] to assess the voltage stability in the presence of an unbalanced network and loads in the system.

## 6.2 Research Contribution

- Developed a unified T&D modeling framework that can serve as a benchmark for existing decoupled approaches.
- Developed an integrated T&D approach where transmission and distribution systems are modeled considering all the three-phases and load flow analysis is conducted using a three sequence approach.
- Developed a multi-period integrated T&D load flow approach that can provide insights on approximate voltage stability margin. Also, the three sequence CPF method is used to obtain a more accurate voltage stability margin.
- Developed a three sequence based fault analysis to do an integrated T&D short circuit analysis.

## 6.3 Methods of modeling Transmission busloads in Integrated T&D framework

In an integrated T&D framework, we consider that loads in a transmission system are due to a collection of distribution systems. So total load in the transmission system can be replaced by a group of distribution systems. It may not be always possible to completely replace transmission system load with distribution systems. The chart in Fig. 6.1 depicts different methods in which the loads in the transmission system can be modeled in a T&D framework. Owing to computational complexity, only 1

distribution system is generally modeled in detail. To bring in the effect of multiple distribution systems, a multiplication factor is used. An integer multiplication factor ( $n$ ) when taken can be thought of as, there are  $n$  distribution systems in total, of which 1 is modeled in detail. In such cases, the total power drawn by all distribution systems may not be equal to transmission system load. So small compensating loads are taken. A detailed description of each method with a numerical example from the 14-123 integrated T&D system is described.

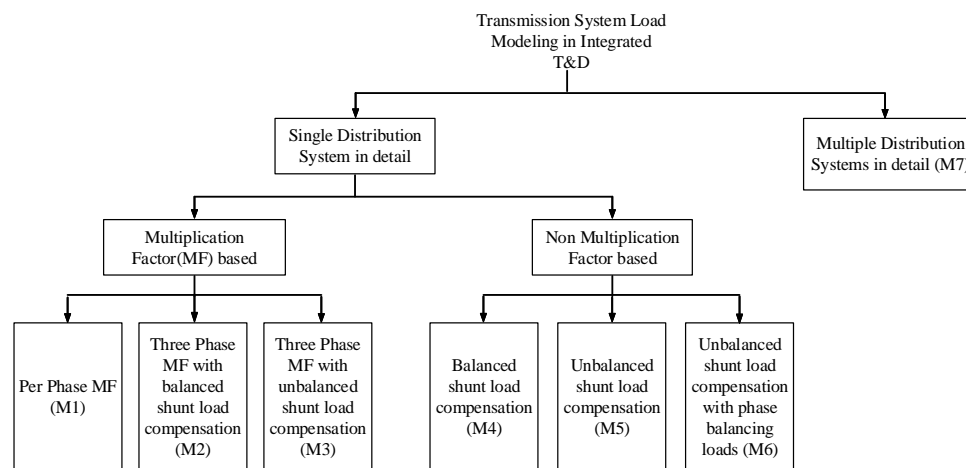


Figure 6.1: Modelling load at boundary bus in transmission system.

### 6.3.1 Multiplication Factor(MF) Based Methods

#### 6.3.1.1 Per phase MF method-M1

This is the simplest method. A multiplication factor is found separately for active and reactive power of each phase as shown in Table. 6.1. The transmission system would see a balanced load if this method is used as shown in Table. 6.2. The integrated T&D system is shown in Fig. 6.2.

#### 6.3.1.2 Three phase MF with balanced shunt load-M2

Assume there are 3 distribution systems. Only 1 system is modelled in detail. To bring in effect of other 2 systems, the substation power obtained by solving detailed

Table 6.1: Multiplication Factor per phase

MF	Ph-1 (P)	Ph-1 (Q)	Ph-2 (P)	Ph-2 (Q)	Ph-3 (P)	Ph-3 (Q)
Pt (a)	4.966667	1.666667	4.966667	1.666667	4.966667	1.666667
Pd 1dist s/m (b)	1.497317	0.68677	0.92121	0.312203	1.21042	0.451413
MF(a/b)	3.317044	2.42681	5.391457	5.338403	4.10326	3.692108

Table 6.2: Transmission boundary bus load distribution using M1

Transmission bus load	Ph-1 (P)	Ph-1 (Q)	Ph-2 (P)	Ph-2 (Q)	Ph-3 (P)	Ph-3 (Q)	Pt (MW)	Qt (MVA <sub>r</sub> )
Distribution system Load	4.96	1.66	4.96	1.66	4.96	1.66		
Shunt Load	0	0	0	0	0	0		
Total	4.96	1.66	4.96	1.66	4.96	1.66	14.9	5

modelled distribution system is multiplied by 3. Therefore Net Distribution system active power P would become 10.88684MW and Net Distribution system reactive power Q=4.351166 MVAR.

Remaining load Pr=14.9 - 10.88684=4.013161MW.

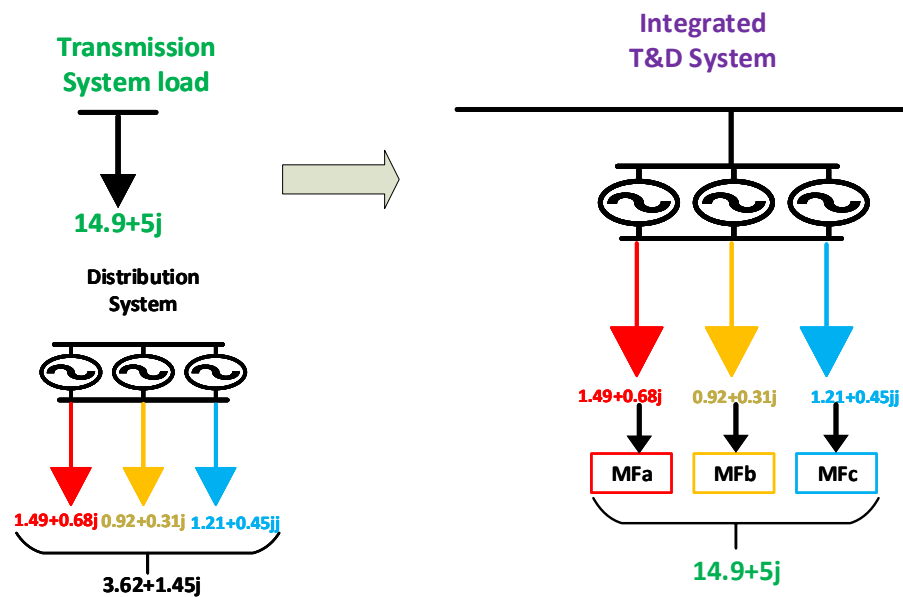


Figure 6.2: Per phase MF method.

Remaining load  $Q_r=5 - 4.351166 = 0.648834$  MVAR.

This is equally divided among 3 phases as a shunt load. So each phase would have a shunt load of  $4.013161/3=1.34$  MW load. The transmission system would see an unbalanced load if this method is used as shown in Table. 6.4. The integrated T&D system is shown in Fig. 6.3.

Table 6.3: Net Load on 3 distribution system

	Ph-1 (P)	Ph-1 (Q)	Ph-2 (P)	Ph-2 (Q)	Ph-3 (P)	Ph-3 (Q)
Pd 1dist s/m	1.497317	0.68677	0.92121	0.312203	1.21042	0.451413
Pd 3dist s/m	4.491952	2.06032	2.763631	0.93661	3.63126	1.35424

Table 6.4: Transmission boundary bus load distribution using M2

Transmission bus load	Ph-1 (P)	Ph-1 (Q)	Ph-2 (P)	Ph-2 (Q)	Ph-3 (P)	Ph-3 (Q)	Pt (MW)	Qt (MVA <sub>r</sub> )
Distribution system Load	4.49	2.06	2.76	0.94	3.63	1.35	10.89	4.36
Shunt Load	1.34	0.22	1.34	0.22	1.34	0.22	4.01	0.64
Total	5.83	2.28	4.1	1.15	4.97	1.57	14.9	5

### 6.3.1.3 Three phase MF with unbalanced shunt load-M3

Assume there are 3 distribution systems. Only 1 system is modelled in detail. To bring in effect of other 2 systems, the substation power obtained by solving detailed modeled distribution system is multiplied by 3. Therefore Net Distribution system active power P would become 10.88684MW and Net Distribution system reactive power  $Q=4.351166$  MVAR.

Remaining load  $P_r=14.9 - 10.88684=4.013161$ MW.

Remaining load  $Q_r=5 - 4.351166 = 0.648834$  MVAR.

This is divided among 3 phases as a shunt load. The load for each phase is calculated as below. The distribution system phase a has 1.497MW of active power which is 41.2% of the total 3 phase active power of 3.69MW and has reactive power is 47.3%

of total 3 phase reactive power. Similar quantities for other phases are obtained. This is used to distribute the total shunt load of 4.013MW 0.684MVAR among 3 phases. So shunt load in phase a would be 41.2% of 4.013MW which is 1.66MW. The transmission system would see an unbalanced load if this method is used as shown in Table. 6.6. The integrated T&D system is shown in Fig. 6.4. These method are

Table 6.5: Net Load on 3 distribution system

	Ph-1 (P)	Ph-1 (Q)	Ph-2 (P)	Ph-2 (Q)	Ph-3 (P)	Ph-3 (Q)
Pd 1dist s/m	1.497317	0.68677	0.92121	0.312203	1.21042	0.451413
Pd 3dist s/m	4.491952	2.06032	2.763631	0.93661	3.63126	1.35424

computationally promising but since only 1 distribution system should be modeled in detail. But it cannot be used for studies like fault analysis since effect of fault at 1 distribution system will be magnified by the multiplication factor as it is transferred to transmission system.

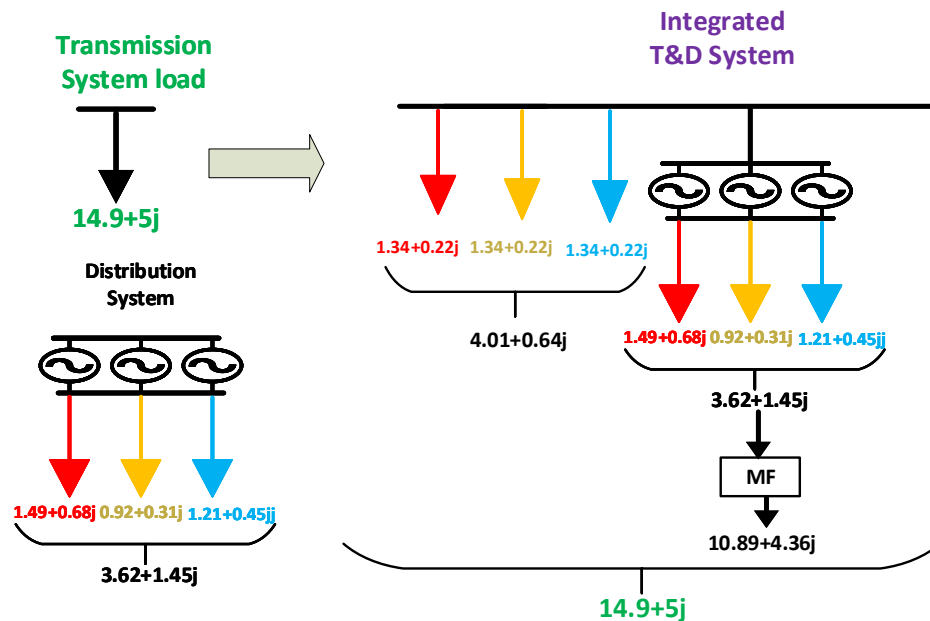


Figure 6.3: Three phase MF with balanced shunt load.

Table 6.6: Transmission boundary bus load distribution using M3

Transmission bus load	Ph-1 (P)	Ph-1 (Q)	Ph-2 (P)	Ph-2 (Q)	Ph-3 (P)	Ph-3 (Q)	Pt (MW)	Qt (MVA <sub>r</sub> )
Distribution system Load	4.49	2.06	2.76	0.94	3.63	1.35	10.89	4.36
Shunt Load	1.66	0.31	1.02	0.14	1.34	0.2	4.01	0.64
Total	6.15	2.37	3.78	1.08	4.97	1.56	14.9	5

### 6.3.2 Non Multiplication Factor Based Methods

#### 6.3.2.1 Balanced shunt load compensation-M4

In this method only 1 distribution system is considered and is modelled in detail. Therefore Net Distribution system active power P would become 3.6289MW and Net Distribution system reactive power Q=1.450MVAR.

Remaining load  $P_r = 14.9 - 3.6289 = 11.271054$  MW.

Remaining load  $Q_r = 5 - 1.450 = 3.549611$  MVAR.

This is equally divided among 3 phases as a shunt load. So each phase would have

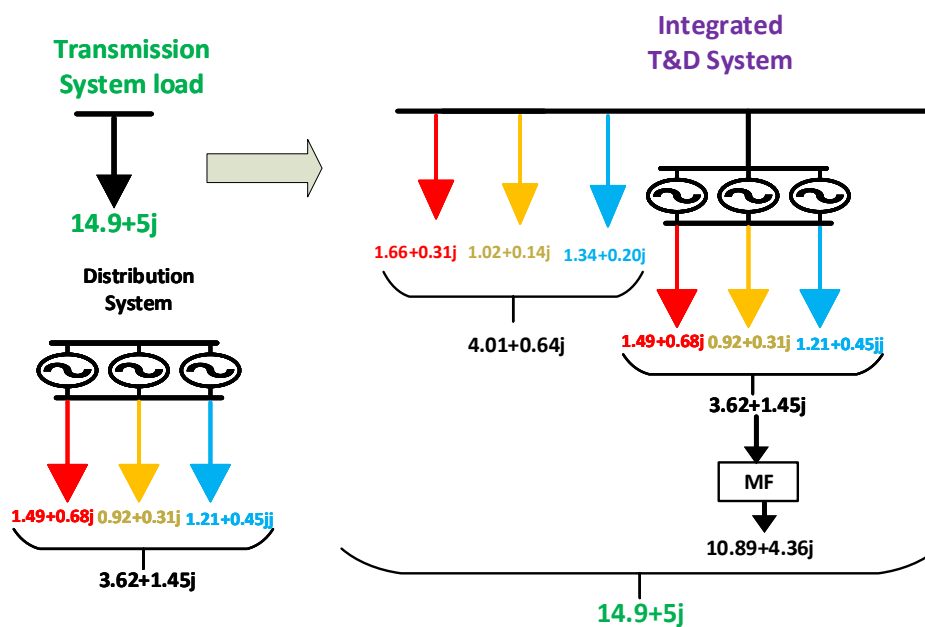


Figure 6.4: Three phase MF with unbalanced shunt load.

a shunt load of  $4.013161/3=1.34$  MW load. The transmission system would see an unbalanced load if this method is used as shown in Table. 6.7. The integrated T&D system is shown in in Fig. 6.5.

Table 6.7: Transmission boundary bus load distribution using M4

Transmission bus load	Ph-1 (P)	Ph-1 (Q)	Ph-2 (P)	Ph-2 (Q)	Ph-3 (P)	Ph-3 (Q)	Pt (MW)	Qt (MVA <sub>r</sub> )
Distribution system Load	1.49	0.68	0.92	0.31	1.21	0.45	3.62	1.45
Shunt Load	3.76	1.18	3.76	1.18	3.76	1.18	11.28	3.55
Total	5.25	1.87	4.68	1.5	4.97	1.63	14.9	5

### 6.3.2.2 Unbalanced shunt load compensation-M5

In this method only 1 distribution system is considered and is modelled in detail. Therefore Net Distribution system active power P would become 3.6289MW and Net Distribution system reactive power Q=1.450MVAR. Remaining load  $P_r=14.9 - 3.6289=11.271054$ MW. Remaining load  $Q_r=5 - 1.450=3.549611$ MVAR.

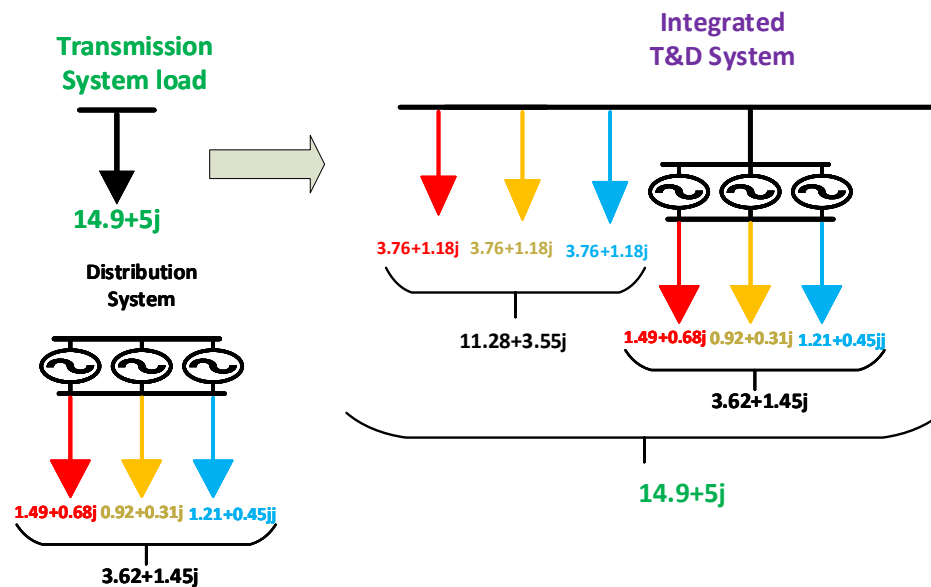


Figure 6.5: Balanced shunt load compensation.

This is divided into 3 phases as a shunt load. The load for each phase is calculated as below. The distribution system phase a has 1.497MW of active power which is 41.2% of the total 3 phase active power of 3.69MW and has reactive power is 47.3% of total 3 phase reactive power. Similar quantities for other phases are obtained and are depicted in table D.3. This is used to distribute the total shunt load of 11.27MW 3.54 MVAR among 3 phases. So shunt load in phase a would be 41.2% of 11.27MW which is 4.65MW. The transmission system would see an unbalanced load if this method is used as shown in Table. 6.8. The integrated T&D system is shown in Fig. 6.6.

Table 6.8: Transmission boundary bus load distribution using M5

Transmission bus load	Ph-1 (P)	Ph-1 (Q)	Ph-2 (P)	Ph-2 (Q)	Ph-3 (P)	Ph-3 (Q)	Pt (MW)	Qt (MVA <sub>r</sub> )
Distribution system Load	1.49	0.68	0.92	0.31	1.21	0.45	3.62	1.45
Shunt Load	4.65	1.68	2.86	0.76	3.76	1.1	11.28	3.55
Total	6.15	2.37	3.78	1.08	4.97	1.56	14.9	5

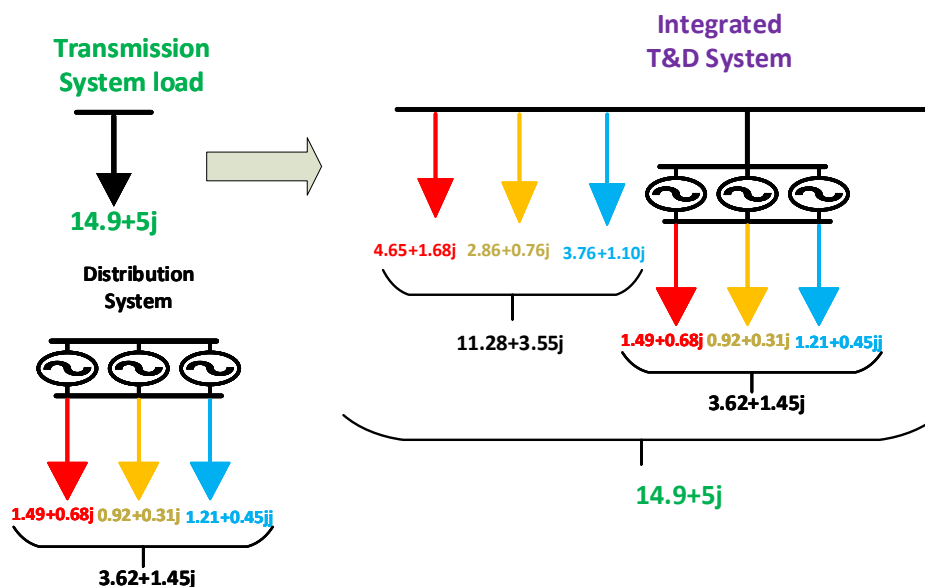


Figure 6.6: Unbalanced shunt load compensation.

### 6.3.2.3 Unbalanced shunt load compensation with phase balancing loads-M6

Assume there are 3 distribution systems. Only 1 system is modeled in detail. To bring in effect of other 2 systems, a shunt load with rating of 2 times net load of distribution system is added. Remaining load for each phase is calculated, assuming that each phase of transmission system had a load of one third of 14.9MW and 5MVAR which is 4.97MW,1.67MVAR.

$$\text{Remaining load Pra}=4.97 - 1.49-2*1.5=0.47\text{MW.}$$

$$\text{Remaining load Qra}=1.67 - 0.68-2*0.69=-0.39 \text{ MVAR.}$$

$$\text{Remaining load Prb}=4.97 - 0.92-2*0.92=2.2\text{MW.}$$

$$\text{Remaining load Qrb}=1.67 - 0.31-2*0.31=0.73 \text{ MVAR.}$$

$$\text{Remaining load Prc}=4.97 - 1.21-2*1.21=1.34\text{MW.}$$

$$\text{Remaining load Qrbc}=1.67 - 0.45-2*0.45=0.31 \text{ MVAR.}$$

The transmission system would see a balanced load if this method is used as shown in Table. 6.9. The integrated T&D system is shown in in Fig. 6.7.

Table 6.9: Transmission boundary bus load distribution using M6

Transmission bus load	Ph-1 (P)	Ph-1 (Q)	Ph-2 (P)	Ph-2 (Q)	Ph-3 (P)	Ph-3 (Q)	Pt (MW)	Qt (MVAR)
Distribution system Load	1.49	0.68	0.92	0.31	1.21	0.45	3.62	1.45
Shunt Load	2.99	1.37	1.84	0.62	2.42	0.9	7.26	2.9
Phase balancing shunt load	0.47	-0.39	2.2	0.73	1.34	0.31	4.02	0.66
Total	4.97	1.67	4.97	1.67	4.97	1.67	14.9	5

### 6.3.2.4 Multiple Distribution System in detail-M7

In this method, all distribution systems considered are modeled in detail. A set of loading factors are randomly selected as shown in Table. 6.10 so that the sum of substation power drawn by all subsystems will be approximately equal to the transmission system boundary bus. The transmission system would see an unbalanced

load if this method is used as shown in Table. 6.11. The integrated T&D system is shown in Fig. 6.8.

Table 6.10: Loading Factor per phase

Loading Factor	Ph-1 (P)	Ph-1 (Q)	Ph-2 (P)	Ph-2 (Q)	Ph-3 (P)	Ph-3 (Q)
Dsub	1.49	0.68	0.92	0.31	1.21	0.45
LF 1	1.3686	1.1491	1.3686	1.1491	1.3686	1.1491
LF 2	1.3562	1.1397	1.3562	1.1397	1.3562	1.1397
LF3	1.3811	1.1586	1.3811	1.1586	1.3811	1.1586

Table 6.11: Transmission boundary bus load distribution using M7

Transmission bus load	Ph-1 (P)	Ph-1 (Q)	Ph-2 (P)	Ph-2 (Q)	Ph-3 (P)	Ph-3 (Q)	Pt (MW)	Qt (MVA <sub>r</sub> )
Distribution system 1 Load	2.05	0.79	1.26	0.36	1.66	0.52	4.97	1.67
Distribution system 2 Load	2.03	0.78	1.25	0.36	1.64	0.51	4.92	1.65
Distribution system 3 Load	2.07	0.8	1.27	0.36	1.67	0.52	5.01	1.68
Total	6.15	2.37	3.78	1.08	4.97	1.56	14.9	5

A comparison of merits and demerits of each method is shown in Table. 6.12

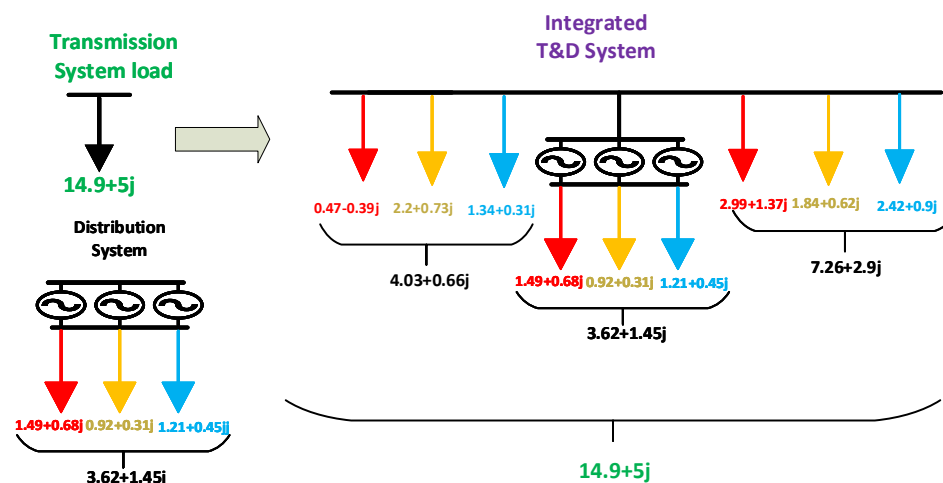


Figure 6.7: Unbalanced shunt load compensation with phase balancing loads.

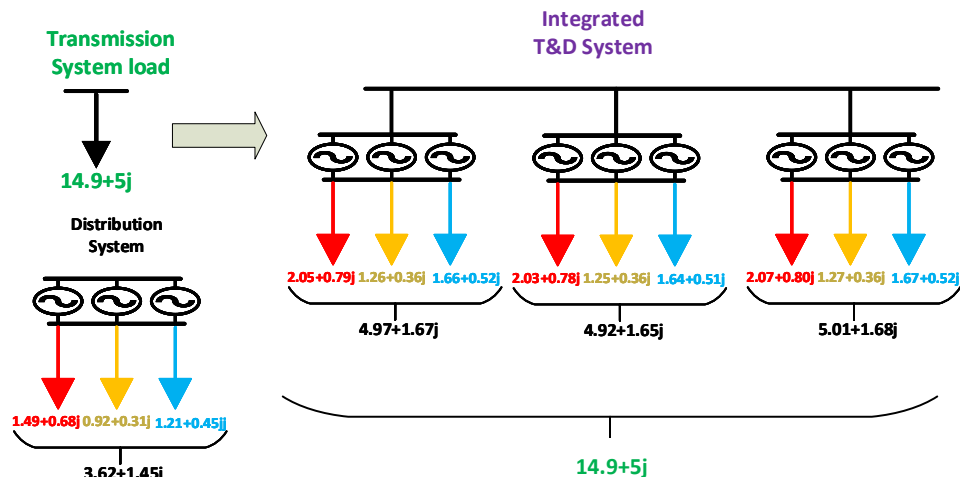


Figure 6.8: Multiple Distribution System in detail.

Table 6.12: Comparison of merits and demerits of each method

Comparison of Methods	M1	M2	M3	M4	M5	M6	M7
Balanced Transmission bus load	Yes	No	No	No	No	Yes	No
Effect of D on T	Best	Good	Good	Bad	Bad	Bad	Best
Computational Burden	Less	Less	Less	Less	Less	Less	More
Fault Analysis on D	No	No	No	Yes	Yes	Yes	Yes
Practical Meaning	No	Yes	Yes	Yes	Yes	Yes	Yes

#### 6.4 State of the art method in Integrated T&D load flow

##### 6.4.1 Decoupled Approach of T&D System

The T&D co-simulation methods in current literature follow a decoupled approach, where transmission and distribution systems are decoupled at interface buses and solved independently either one after other or simultaneously depending on the parallelizing capability of the processing unit used. In the modeling aspect, the transmission system is modeled based on three sequence modeling (some of the works have considered positive sequence alone) and the distribution system is based on three-phase modeling. Most of these decoupled approaches use existing methods or tools in solving respective transmission and distribution models (PSS@E, PSLF for

transmission system and GridlabD, OpenDss for distribution system). An interface should be explicitly built for the exchange of voltage and power flow data between the simulators. A decoupled Integrated T&D method is shown in Fig. 6.9.

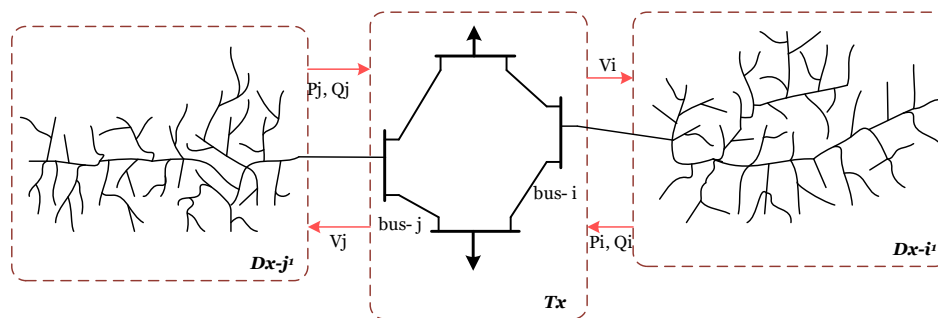


Figure 6.9: Integrated T&D Decoupled System.

#### 6.4.1.1 Disadvantage of solution method

1. Even though, the decoupled approaches exhibit benefits of parallelization, the inherent time delays due to data exchange, data loss, or corruption during data exchange, an inappropriate choice of simulation time step may lead to divergence of the solution during parallel solving of both systems.
2. Even though widely used, it is not known if the power flow solutions of the T&D system using decoupled approach would converge to the true (solution obtained considering T&D system as 1 single system).
3. Since the bench-marking solutions to T&D co-simulation is not available, current works in literature compare the solution against solutions obtained from the EMT solvers. This is not feasible as the system size increases.

#### 6.4.1.2 Disadvantage in modeling approach

1. There will be variations in results with the variation in load type of shunt loads using methods M1 through M6. For example, the voltages obtained with shunt

loads modeled as constant PQ would be different from shunt loads modeled as constant Z load. This would be more prominent in M4, M5, M6 owing to bigger values of loads.

2. The load type of load assumed at transmission boundary bus(for transmission load flow) is normally assumed as PQ type. If all the loads in the distribution system are of PQ type, then after distribution system load flow, the substation power obtained can be modeled as a constant PQ load for transmission system power flow. But If the distribution system has a lot of voltage dependant loads (modeled as ZIP loads), would the net load for transmission system load flow be modeled as constant PQ, Constant Z, or Constant P load?
3. The interactions between distribution and transmission systems cannot be accurately obtained if only 1 distribution system is modeled in detail and using a multiplication factor. Using 1 distribution system and shunt loads may not provide any insights in terms of T&D interactions taking into account the size of 1 distribution system compared to transmission system load is very small. Using a MF assumes that all distribution systems are identical. It is not a good assumption since a fault (or a load change) in 1 distribution system would be modeled as a fault (or a load change) in all distribution systems. In the case of DER integrated distribution systems, multiple distribution systems could have different DER penetrations and hence it cannot be modeled using the MF method. Even though integrated T&D modeling was brought in, not to study interactions between 2 distribution systems, the effect of DER penetration of 1 distribution system may be more prominent on other adjacent distribution systems rather than on transmission systems(especially if the level of DER penetrations are different in each distribution systems).
4. Assuming that more distribution systems are modeled in detail, it is going

to affect the existing advantage in terms of computational burden as well as parallel operation of decoupled load flow method. With all distribution systems modeled in detail, distribution solvers should be invoked for each distribution system. Calling such solvers simultaneously for all these distribution systems would lead to a more complex interface.

### 6.5 Proposed Unified Approach of T&D System

A unified T&D co-simulation can primarily serve as an approach to produce benchmark solutions that can aid in validating the results obtained using other co-simulation approaches. It can also be used to conduct T&D load flow, fault analysis, and voltage stability analysis, provided, there exists a computationally efficient solution methodology that can take care of systems with loops and a large number of radial laterals. The T&D system is considered as a single unit (unified system) and solved using a single method. A unified integrated T&D system is shown in Fig. 6.10. Consider an

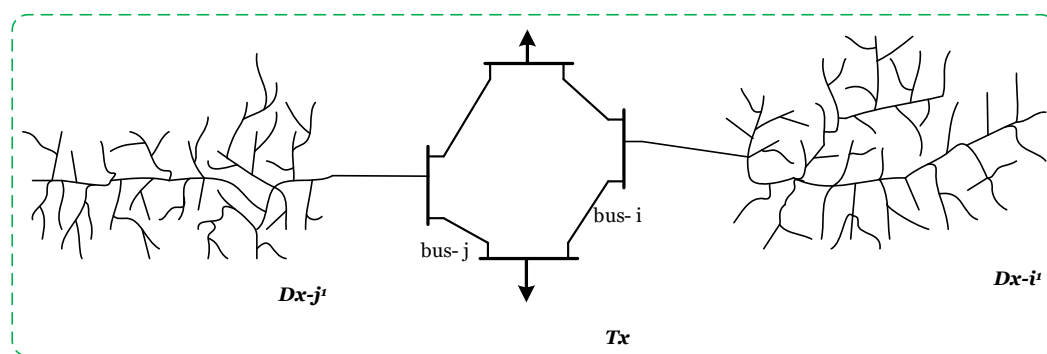


Figure 6.10: Integrated T&D Unified System.

$N$ -bus transmission system, where the first  $m$  buses have lumped loads, and buses  $m + 1$  through  $N$  have distribution feeders connected downstream the buses. The

power flow model of the transmission system can be written as,

$$\mathbf{V}_j^t = \sum_{k \in N} \mathbf{Y}_{j,k}^t \mathbf{I}_k^t \quad \forall j \in 1, 2, \dots, N \quad (6.1)$$

$$\mathbf{P}_j^t = \mathbf{Real} \left( \mathbf{V}_j^t \mathbf{I}_j^{t*} \right) \quad \forall j \in 1, 2, \dots, m \quad (6.2)$$

$$\mathbf{Q}_j^t = \mathbf{Imag} \left( \mathbf{V}_j^t \mathbf{I}_j^{t*} \right) \quad \forall j \in 1, 2, \dots, m \quad (6.3)$$

where  $\mathbf{V}^t$ ,  $\mathbf{I}^t$ ,  $\mathbf{P}^t$  and  $\mathbf{Q}^t$  represent bus voltage, injection current, active power injection, reactive power injection, and bus admittance matrix, respectively.  $\mathbf{Y}^t$  represents the bus admittance matrix of transmission system. Consider a  $M$ -bus distribution system connected to arbitrary bus of the transmission network. The distribution power flow analysis can be formulated as

$$\mathbf{V}_i^d = \sum_{r \in M} \mathbf{Y}_{i,r}^d \mathbf{I}_r^d \quad \forall i \in 1, 2, \dots, M \quad (6.4)$$

$$\mathbf{P}_i^d = \mathbf{Real} \left( \mathbf{V}_i^d \mathbf{I}_i^{d*} \right) \quad \forall i \in 1, 2, \dots, M \quad (6.5)$$

$$\mathbf{Q}_i^d = \mathbf{Imag} \left( \mathbf{V}_i^d \mathbf{I}_i^{d*} \right) \quad \forall i \in 1, 2, \dots, M \quad (6.6)$$

where  $\mathbf{V}^d$ ,  $\mathbf{I}^d$ ,  $\mathbf{P}^d$ ,  $\mathbf{Q}^d$  represents node voltage, injection current, active power injection and reactive power injection respectively.  $\mathbf{Y}^d$  represents the bus admittance matrix of distribution system.

An integrated T&D system with one  $M$ -node distribution systems can be formed and power flow model of the combined system can be written as,

$$\mathbf{V}_j^U = \sum_{k \in N+M} \mathbf{Y}_{j,k}^U \mathbf{I}_k^U \quad \forall j \in 1, 2, \dots, N + M \quad (6.7)$$

$$\mathbf{P}_j^U = \mathbf{Real} \left( \mathbf{V}_j^U \mathbf{I}_j^{U*} \right) \quad \forall j \in 1, 2, \dots, N + M \quad (6.8)$$

$$\mathbf{Q}_j^U = \mathbf{Imag} \left( \mathbf{V}_j^U \mathbf{I}_j^{U*} \right) \quad \forall j \in 1, 2, \dots, N + M. \quad (6.9)$$

where

$$\mathbf{V}^U = [\mathbf{V}^t \ \mathbf{V}^d]^T \quad \mathbf{I}^U = [\mathbf{I}^t \ \mathbf{I}^d]^T \quad (6.10)$$

$$\mathbf{P}^U = [\mathbf{P}^t \ \mathbf{P}^d]^T \quad \mathbf{Q}^U = [\mathbf{Q}^t \ \mathbf{Q}^d]^T \quad (6.11)$$

$\mathbf{Y}^U$  represents the bus admittance matrix of unified system.

### 6.5.1 Stacked Ybus Approach for Unified Ybus

A coalescing Ybus approach is used to obtain the bus admittance matrix of the combined T&D system, where the bus admittance matrix of the transmission system and all distribution systems are grouped in a certain way. Three matrices namely Starting Bus Vector  $\mathbf{SBV}$ , Position Vector  $\mathbf{PV}$ , and Tie Line Vector  $\mathbf{TLV}$  are used in coalescing the Ybus approach. With the knowledge of the number of transmission buses and total buses for each distribution system, a renumbered unified T&D system is formed.

The Starting Bus Vector stores information regarding starting node of each distribution system. The Position Vector has two columns, of which the first column stores information regarding starting node of each distribution system, and the second column stores information regarding the total number of buses available in the distribution system of the respective row. The Tie Line Vector stores information regarding line connecting transmission and distribution systems. The first column stores information regarding starting node of each distribution system and the second column stores information regarding the corresponding transmission bus (called Boundary Bus) that the distribution system in the respective row is connected. An example shown in Fig. 6.11(b) is used to illustrate coalescing Ybus approach. Let  $\mathbb{S}_b(x)$  is starting bus of distribution system  $x$ ,  $\mathbb{N}_b(x)$  is total number of buses available in distribution system  $x$  and  $\mathbb{B}_b(x)$  is transmission bus where distribution system  $x$

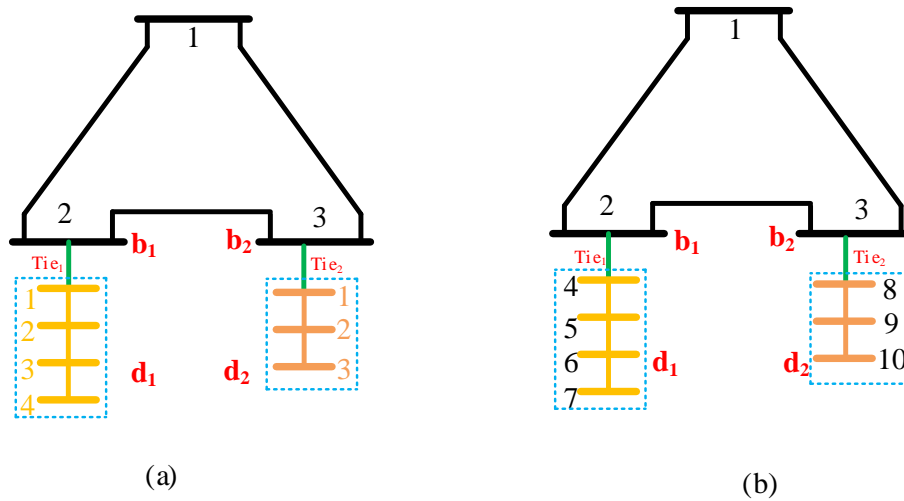


Figure 6.11: (a) T&D Unified system (b) Renumbered T&D Unified System.

is connected. Therefore the **SBV**, **PV** and **TLV** matrices can be written as

$$\mathbf{SBV} = \begin{bmatrix} \mathbb{S}_b(d_1) \\ \mathbb{S}_b(d_2) \end{bmatrix} = \begin{bmatrix} 4 \\ 8 \end{bmatrix} \quad (6.12)$$

$$\mathbf{PV} = \begin{bmatrix} \mathbb{S}_b(d_1) & \mathbb{N}_b(d_1) \\ \mathbb{S}_b(d_2) & \mathbb{N}_b(d_2) \end{bmatrix} = \begin{bmatrix} 4 & 4 \\ 8 & 3 \end{bmatrix} \quad (6.13)$$

$$\mathbf{TLV} = \begin{bmatrix} \mathbb{S}_b(d_1) & \mathbb{B}_b(d_1) \\ \mathbb{S}_b(d_2) & \mathbb{B}_b(d_2) \end{bmatrix} = \begin{bmatrix} 4 & 2 \\ 8 & 3 \end{bmatrix} \quad (6.14)$$

Let  $n_t$  be number of transmission buses,  $n_{d1}$  and  $n_{d2}$  be number of buses in distribution system 1 and 2 respectively and the total number of buses in unified system be  $n_T$ . Let  $\mathbf{Y}^t$ ,  $\mathbf{Y}^{d1}$  and  $\mathbf{Y}^{d2}$  be bus admittance matrix of transmission and distribution system 1 and 2 respectively. A matrix  $\mathbf{Y}^U$  of dimension  $(n_T \times n_T)$  is initialized with

zeros. The first  $n_t$  rows and columns of  $\mathbf{Y}^U$  is stacked with  $\mathbf{Y}^t$ . The  $\mathbf{P}\mathbf{V}$  matrix is used to populate rest of  $\mathbf{Y}^U$ , travelling through each row. The Ybus corresponding to distribution system present in first row of  $\mathbf{P}\mathbf{V}$  matrix is taken and stacked from row (column) $\mathbf{P}\mathbf{V}(1)$  to row (column) $\mathbf{P}\mathbf{V}(1) + \mathbf{P}\mathbf{V}(2) - 1$ . In this example, the Ybus corresponding to  $d1$  ( $\mathbf{Y}^{d1}$ ) is taken and stacked from row (column)4 to row (column)7. Similarly  $\mathbf{Y}^{d2}$  is taken and stacked from row (column)8 to row (column)10.

The unified Ybus is missing the values corresponding to tie lines which connects transmission and distribution system. So a tie line correction step should be implemented. This is done using  $\mathbf{TLV}$  matrix travelling through each row. Let  $\mathbf{Y}^{tie1}$  be bus admittance component of tie line connecting distribution system 1 to transmission system and  $\mathbf{Y}^{tie2}$  be tie line connecting distribution system 2 to transmission system. The  $Y^{tie}$ , corresponding to distribution system present in first row of  $\mathbf{TLV}$  matrix is taken and the components of  $\mathbf{Y}^U$  are modified as below

$$\mathbf{Y}^U(TLV(1), TLV(1)) = Y^U(TLV(1), TLV(1)) + \mathbf{Y}^{tie1} \quad (6.15)$$

$$\mathbf{Y}^U(TLV(2), TLV(2)) = Y^U(TLV(2), TLV(2)) + \mathbf{Y}^{tie1} \quad (6.16)$$

$$\mathbf{Y}^U(TLV(1), TLV(2)) = Y^U(TLV(1), TLV(2)) - \mathbf{Y}^{tie1} \quad (6.17)$$

$$\mathbf{Y}^U(TLV(2), TLV(1)) = Y^U(TLV(2), TLV(1)) - \mathbf{Y}^{tie1} \quad (6.18)$$

In this example  $\mathbf{Y}^U(4, 4), \mathbf{Y}^U(2, 2), \mathbf{Y}^U(4, 2), \mathbf{Y}^U(2, 4)$  will be updated for tie line correction. The final unified Ybus  $\mathbf{Y}^U$  is shown in Fig. 6.12.

### 6.5.2 Challenges and Solutions

1. One of the challenges involved in building a unified system arises due to the fact that a transmission system is generally represented in sequence frame and distribution system in phase frame. So, a unified system should either be in phase frame or sequence frame. Since distribution systems are mostly unbalanced, representing a unified system in phase frame provides a solution that

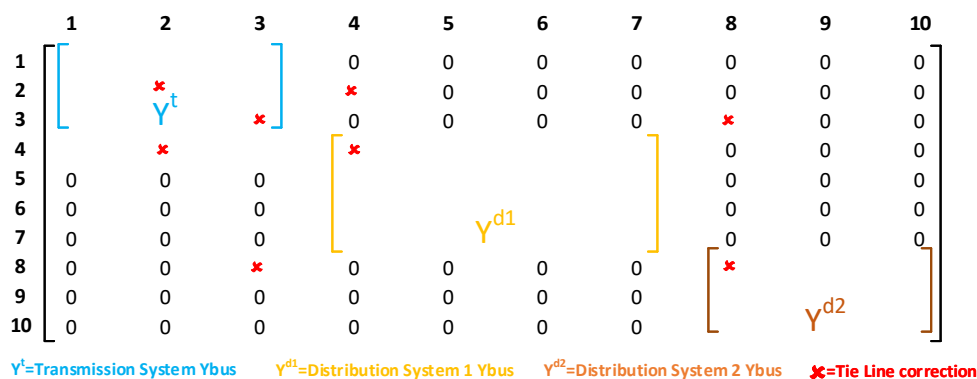


Figure 6.12: T&amp;D Unified Ybus

can capture the unbalanced nature of the system. Moreover, with a very large number of distribution systems connected, the transmission system would also become slightly unbalanced. So a unified T&D system in phase frame is used.

2. The second challenge is concerning the selection of the method/solver that can be used for the unified system. The steady-state response of power systems (power flow analysis) using integrated T&D is challenging because numerical methods used for power flow analysis which are stable for transmission networks may not work as required for distribution networks. For example, the Newton Raphson method that is efficient for transmission systems may fail if used in distribution systems owing to the higher R/X ratio and sparse nature of the system. Similarly, distribution system analysis methods like Forward Backward sweep would fail (or require system-dependent modifications) when a transmission system is analyzed.

A Current Injection method is a promising candidate which can solve weakly meshed systems as well as radial systems effectively.

3. The third challenge involved is attributed to the computational burden since the unified approach requires the solution of a fairly large system compared to

smaller transmission or each of individual distribution systems. This gets aggravated when more distribution systems are added to the transmission system. A method based on the sequence components frame can be utilized where three-phase unbalanced power flow is decomposed into three separate subproblems as discussed in chapter 3. The sequence component based methods can also be used to conduct voltage stability analysis using three sequence CPF and short circuit analysis using three sequence fault analysis discussed in chapter 5. Another approach is to use the parallel architecture of GPUs to accelerate the analysis of the unified system. Owing to its better performances on memory bandwidth and float-pointing calculation, the GPUs can aid in alleviating the computational burden of the unified approach.

## 6.6 Power Flow Analysis

### 6.6.1 Single Phase Integrated T&D System

An integrated transmission and distribution system model is developed and a unified load flow that runs for the combined system is discussed in this section. The distribution system represented using three phase parameters is converted to sequence frame and combined with transmission system parameters to develop an integrated T&D system. A flow chart of the unified simulation of single phase integrated T&D system is presented in Fig. 6.13. An integrated T&D system is formed by combining a 14-bus transmission system and a 33-node balanced distribution system connected to as shown in Fig. 6.14. The 14-bus transmission system consists of 5 generators and 11 loads with a net load of 260MW (75MVAR). The 33-node distribution system has a net-connected load of 3.7MW (2.3MVAR). First, the transmission system model and distribution system model are separately verified for the distributed approach. The transmission system model is also solved with the spot load approach, where all the loads on distribution feeders are lumped at a corresponding transmission bus. Then, the combined T&D model is solved using distributed and unified approach

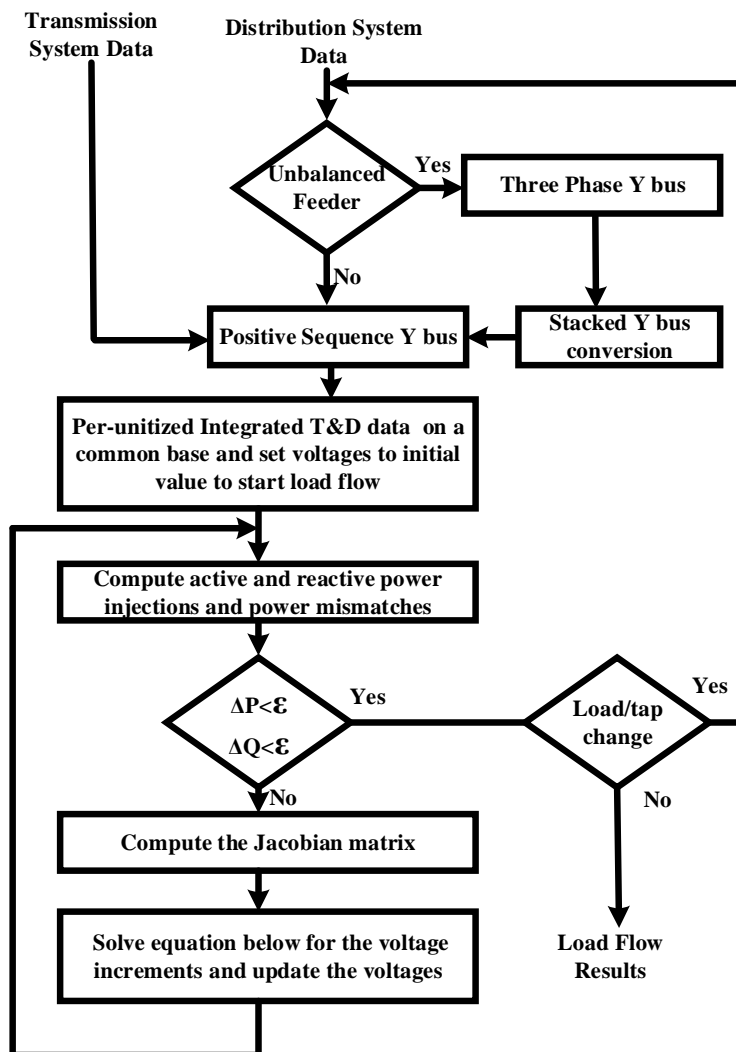


Figure 6.13: Flowchart of Unified T&D Simulation.

and the results are shown in Fig.6.15. The error plot shows that the decoupled and unified approaches produce similar results. The augmented 47-bus system is further used to compare the performance of voltage and power angle solution on the transmission as well as distribution part of the circuit. The load flow voltage and angle obtained from the unified approach and decoupled approach are shown in Fig. 6.16a and Fig. 6.16b. The plots clearly show that the voltage and angle solutions from both approaches are very close with errors less than  $6 \times 10^{-6}$  on voltages and  $2.5 \times 10^{-3}$  on

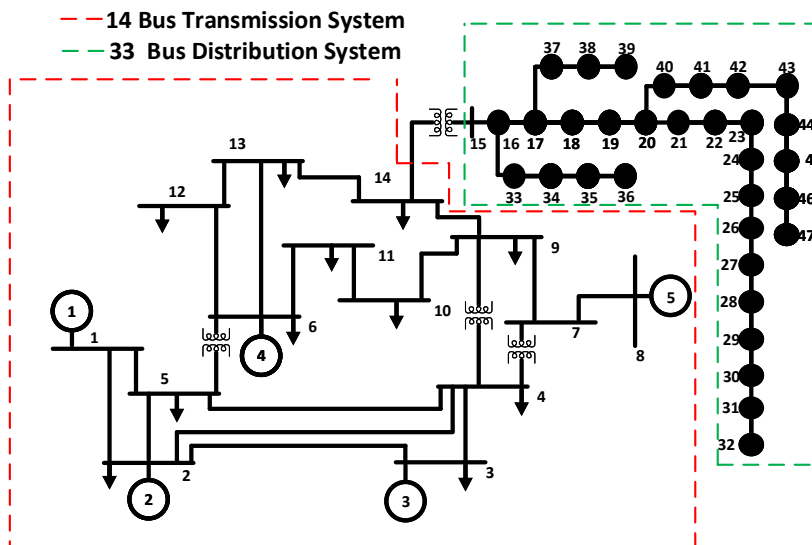


Figure 6.14: One line diagram of 47-bus T&D system.

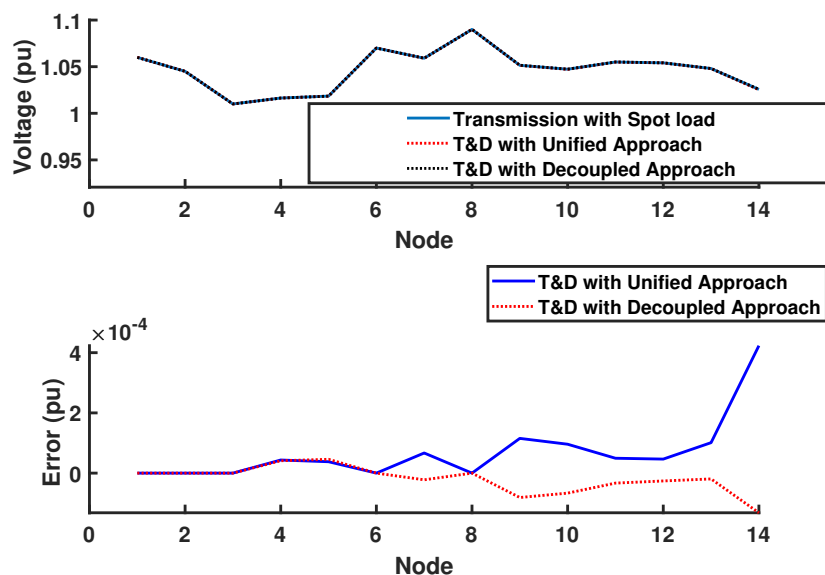


Figure 6.15: Voltage solution and error on transmission circuits.

angles. Two augmented 113-bus systems are also created by using three sections of a 33-node distribution feeder (see Fig. 6.17). The load flow voltage and angle obtained from the unified approach and decoupled approach for the first case of the circuit configuration (Case a) is shown in Fig. 6.18a and Fig. 6.18b. The plots clearly show

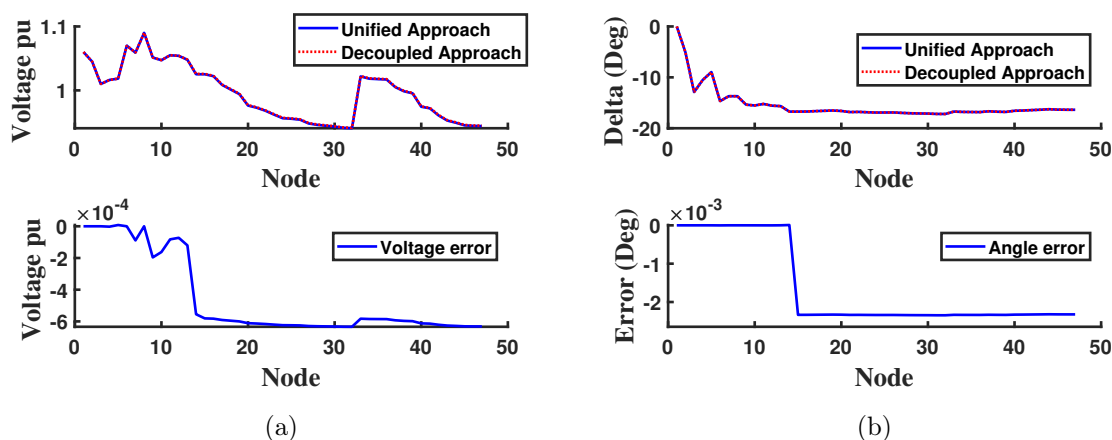


Figure 6.16: (a) Voltage solution (b) Angle solution (and error) of 47-bus T&D system obtained from decoupled and unified approaches.

that the voltage and angle solutions from both approaches are very close with errors less than  $3 \times 10^{-5}$  on voltages and  $2.5 \times 10^{-3}$  on angles. For the second case of the circuit configuration (Case b), the voltage and angle solution obtained are shown in Fig. 6.19a and Fig. 6.19b. The plots clearly show that the voltage and angle solutions from both approaches are very close with errors less than  $3 \times 10^{-5}$  on voltages and  $2.5 \times 10^{-3}$  on angles. The case studies demonstrate that the distributed and unified approaches for solving the T&D model yield the same solutions.

### 6.6.2 Three Phase Integrated T&D System

An integrated T&D system is formed by combining a 14-bus transmission system and a 123-node distribution system connected to as shown in Fig. 6.20. The 14-bus transmission system consists of 5 generators and 11 loads with net load of 260MW (75MVar). The 123-node distribution system has net connected load of 3.7MW (1.3MVar). First, the transmission system model and distribution system model are separately verified for the decoupled approach. The transmission system model is also solved with spot load approach, where all the loads on distribution feeders are lumped at a corresponding transmission bus. Then, the combined T&D model is solved using distributed and unified approach. The error plot shows that the decoupled

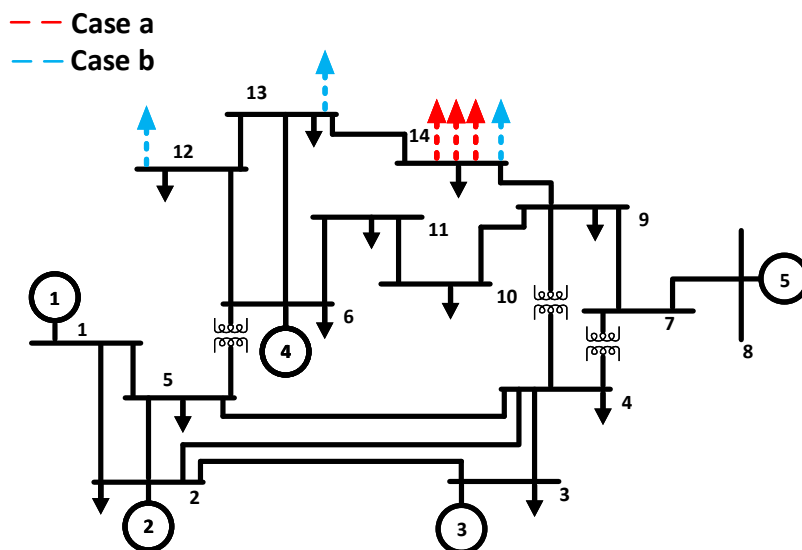


Figure 6.17: Two configuration of 113-bus T&D system.

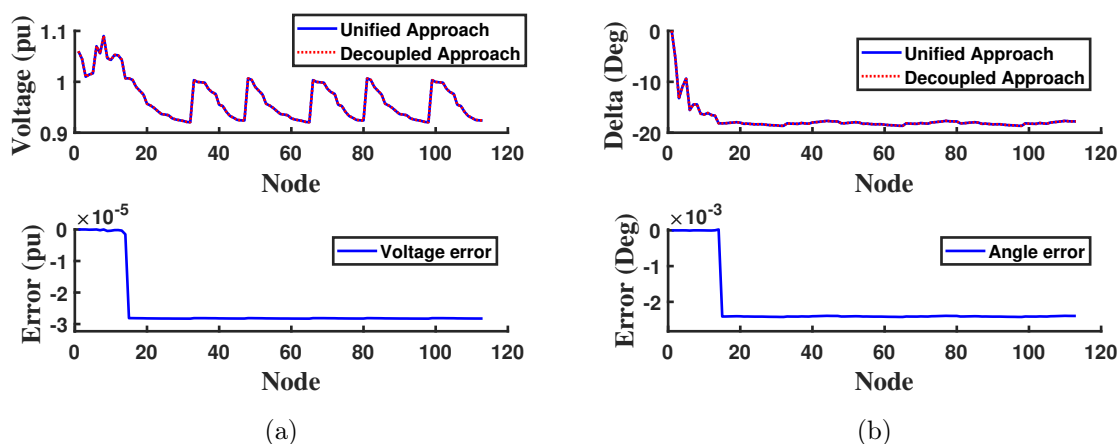


Figure 6.18: (a) Voltage solution (b) Angle solution (and error) of 113-bus T&D system (Case a) obtained from decoupled and unified approaches.

approach results is the same solution as the unified approach. The augmented 127-bus system (see Fig. 6.20) is used to compare the performance of voltage and angle solution on the transmission as well as distribution part of the circuit. First, the transmission system load flow voltage results with distribution system connected at a particular node are compared with transmission system load flow voltage results with an equivalent spot load connected to the same node as shown in Fig. 6.21. The

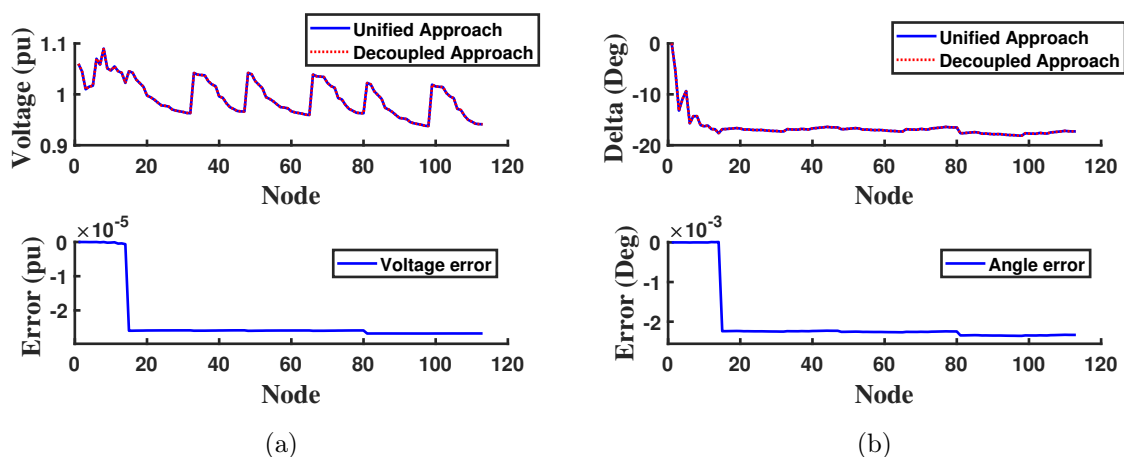


Figure 6.19: (a) Voltage solution (b) Angle solution (and error) of 113-bus T&D system (Case b) obtained from decoupled and unified approaches.

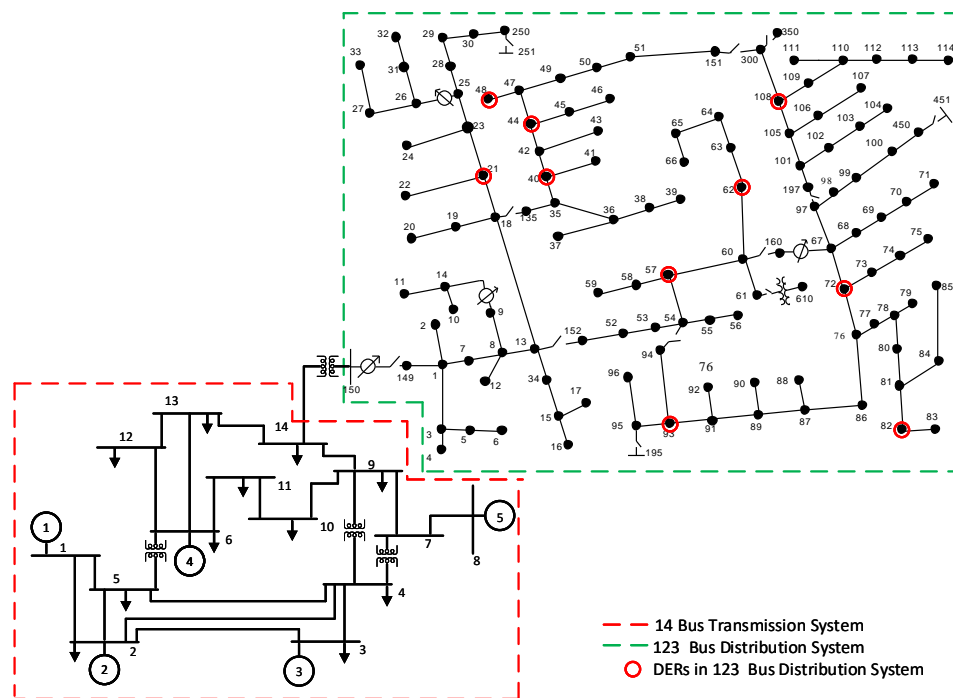


Figure 6.20: One line diagram of 3phase T&D system.

difference in voltages is due to the line losses in the distribution system as well as due to unbalance nature brought in by the distribution system. The load flow voltage and angle of the integrated T&D system obtained from the unified approach and decoupled approach are shown in Fig. 6.22a to Fig. 6.24b. The plots clearly show

that the voltage and angle solutions from both approaches are very close with errors less than  $6 \times 10^{-6}$  on voltages and  $2.5 \times 10^{-3}$  on angles.

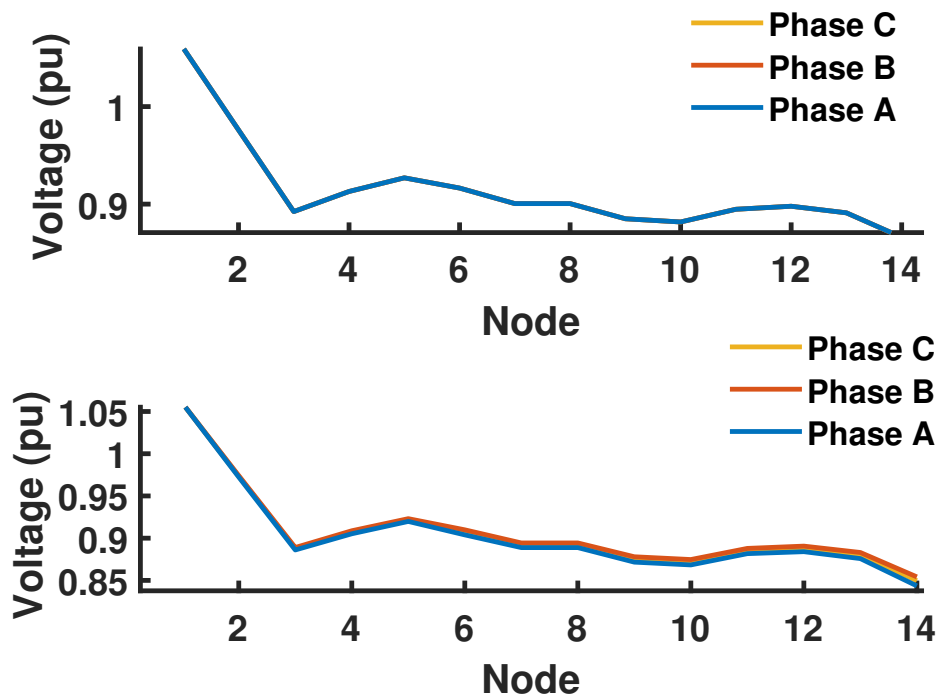


Figure 6.21: Phase Voltage solution of Transmission system with spot load and distribution system

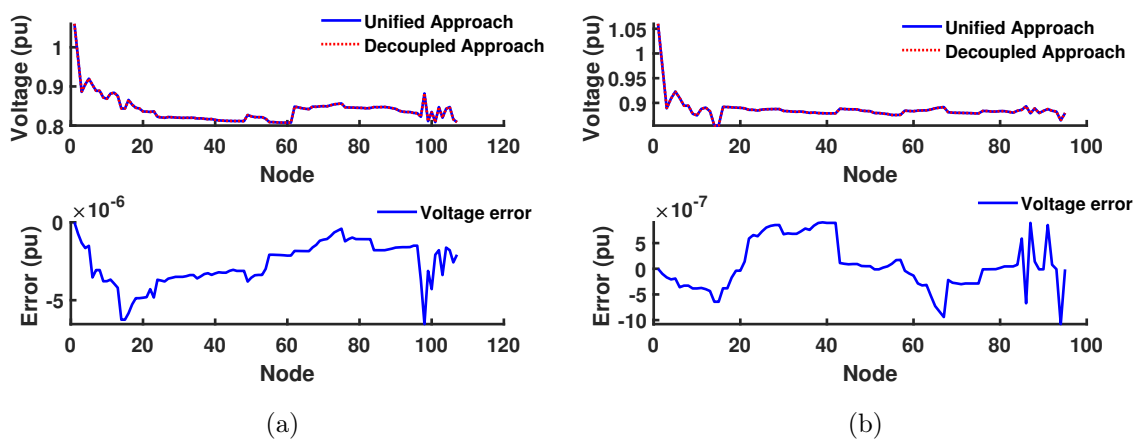


Figure 6.22: (a) Phase A Voltage (b) Phase B Voltage solution (and error) of T&D system obtained from decoupled and unified approaches

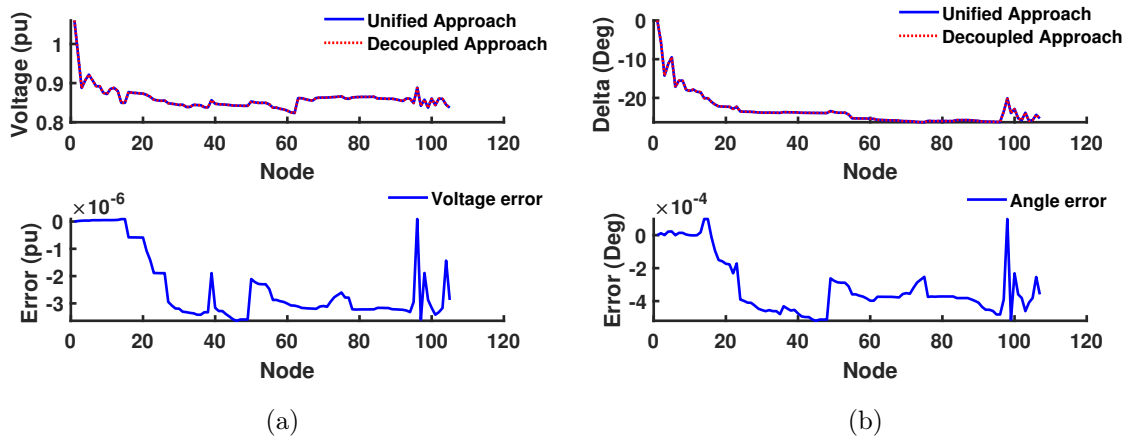


Figure 6.23: (a) Phase C Voltage (b) Phase A Angle solution (and error) of T&D system obtained from decoupled and unified approaches

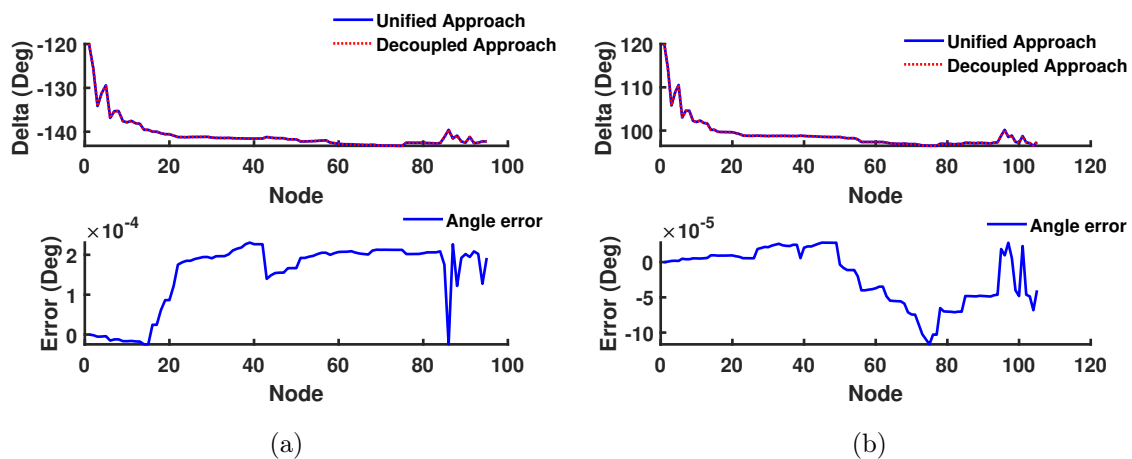


Figure 6.24: (a) Phase B Angle (b) Phase C Angle solution (and error) of T&D system obtained from decoupled and unified approaches

T&D modeling for load flow is proposed in [94], where the transmission system is modeled as three-sequence detail and the distribution system connected to it is modeled in three-phase detail. The power flow of the integrated T&D system is solved by iteratively solving a three-sequence power flow for the transmission system and a three-phase power flow for each distribution system. For validating the proposed unified approach, a load flow is performed with baseload, and the results are compared

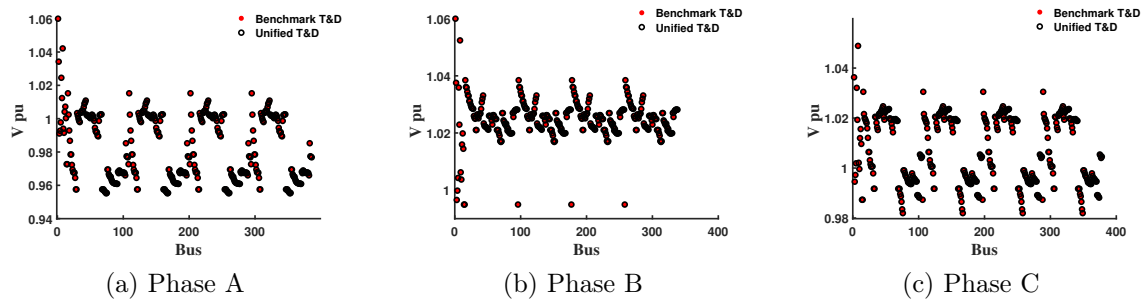


Figure 6.25: Comparison of Unified Sequence T&D Load Flow with state of the art T&D load flow method

with results obtained using the approach in [94]. It is observed that the voltage variations are very close to each other as shown in Fig. 6.25.

## 6.7 Voltage Stability Assessment

The voltage stability of a system is expressed in terms of voltage stability margin(VSM). VSM is defined as the difference between the critical loadability limit and the current operating load level. For static voltage stability analysis of an interconnected system, power flow models have been considered. It has been proved that near the system maximum loading point the load flow diverges as power flow Jacobian becomes singular. An injection current sensitivity based multi-period power flow is used for solving integrated T&D power flow and finding VSM of the system.

The existence of a solution in a power flow problem can be attributed to a successful transfer of active and reactive power from all available sources to loads. For a distribution system with the generator at the swing bus being only the source, the load flow will diverge when the swing bus is not able to support the loads and losses of the system. The voltage of the swing bus, as well as the type of loads used, affects the losses and hence convergence of load flow. During an integrated T&D load flow, the substation voltage for each loading will be varying depending on boundary bus voltage. To see the effect of this, a series of load flows were performed on IEEE 123 bus distribution system(all loads assumed as constant power loads) using load

increment factor  $\lambda$ . The loads were varied from baseload ( $\lambda = 0$ ) to a loading where load flow diverged ( $\lambda = \lambda_{max}$ ). Two test scenarios were performed where the swing bus voltage was held at a fixed value (1.05 pu) as well as the swing bus voltage was slightly decreased as loading was increased. The voltage profile of phase A of node 1 of the 123 bus system is shown in Fig. 6.26. For the same set of load variations, it can be concluded that the divergence occurs at a lower loading when swing bus voltage was varying. This is because the line losses with lower substation voltage are much higher than fixed substation voltage. It was also observed that when swing bus voltages were unbalanced, ( $\lambda_{max}$ ) further decreased compared to the case with balanced swing bus voltages.

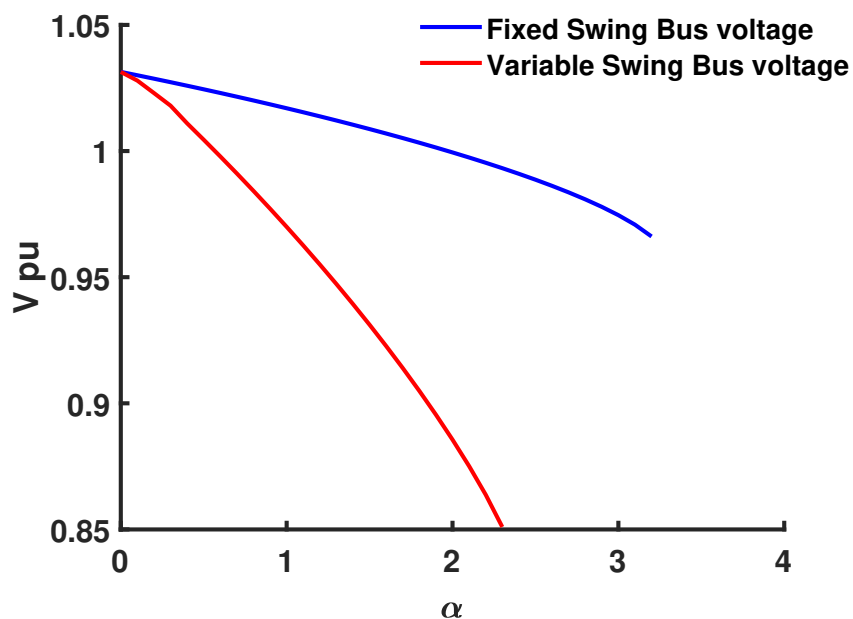


Figure 6.26: Distribution load flow with different swing bus voltage.

### 6.7.1 Integrated T&D Multi-Period Power Flow Model(MPF)

The three-phase integrated T&D multi-period power flow is based on a master-slave approach where transmission and distribution systems are decoupled at a boundary bus and solved independently. The injection current sensitivity based power flow discussed in chapter 2 is used for transmission system load flow. Since transmission

system lines are considered to be transposed lines, the mutual coupling between them is negligible and a three-phase power flow solution can be obtained by solving 3 phases independently. Three phase injection current sensitivity based power flow is used to solve distribution system load flow.

The process is initiated with a transmission load flow where three phases are solved independently. For each boundary bus(B), the voltage magnitude and angle of three phases are passed to the corresponding distribution system solvers. The per-phase net power injections obtained after solving all distribution system load flow are passed back to the transmission system solver. When the voltage magnitude at the boundary bus between consecutive iterations is less than a tolerance threshold value, T&D power flow is converged. The iteration count(k) is reset and T&D power flow with the next loading factor( $\lambda(p)$ ) is initiated. If T&D iterations are going beyond a maximum iteration count( $k_{max}$ ), the T&D load flow is assumed to be diverging. This iterative process is stopped when either transmission or distribution or T&D load flow diverges. The corresponding loading factor ( $\lambda_{max}$ ) is taken as the VSM of the system. A detailed flowchart of the proposed T&D load flow for VSM assessment is shown in Fig. 6.27.

An integrated power grid model is developed that includes the IEEE 14 bus for the transmission side and four IEEE 123 bus test distribution feeder [104] on the distribution side connected to the bus# 14 of the transmission system as shown in Fig. 6.28. Modified versions of the IEEE 123 bus system are developed where the loads on all 3 phases are varied such that the combination of all four feeders would result in approximately the same loading on each phase of load at bus 14 of the transmission system. This is referred to as a balanced distribution system in further discussions. For validating the proposed approach, a distribution load-flow is performed with the same load variation. Then the three-phase distribution part of the proposed architecture is compared with the distribution load flow. It is observed that the voltage variations are very close to each other (difference of  $6 \times 10^{-5}$ ). This

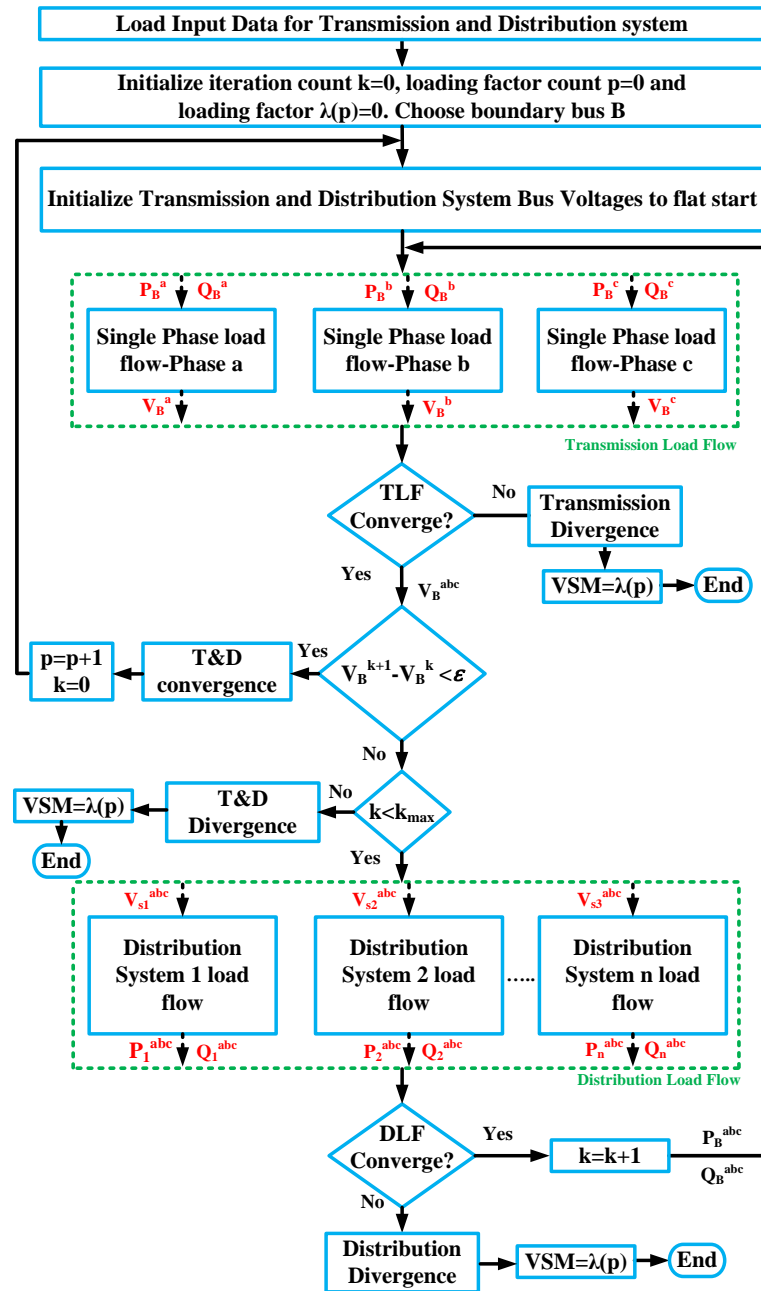


Figure 6.27: Proposed Integrated T&D Load flow.

proves the accuracy of the proposed architecture.

#### 6.7.1.1 VSM Comparison with existing methods

The VSM obtained using the proposed method is compared with VSM obtained using a.) Transmission system with spot loads, b.) Transmission system with equiv-

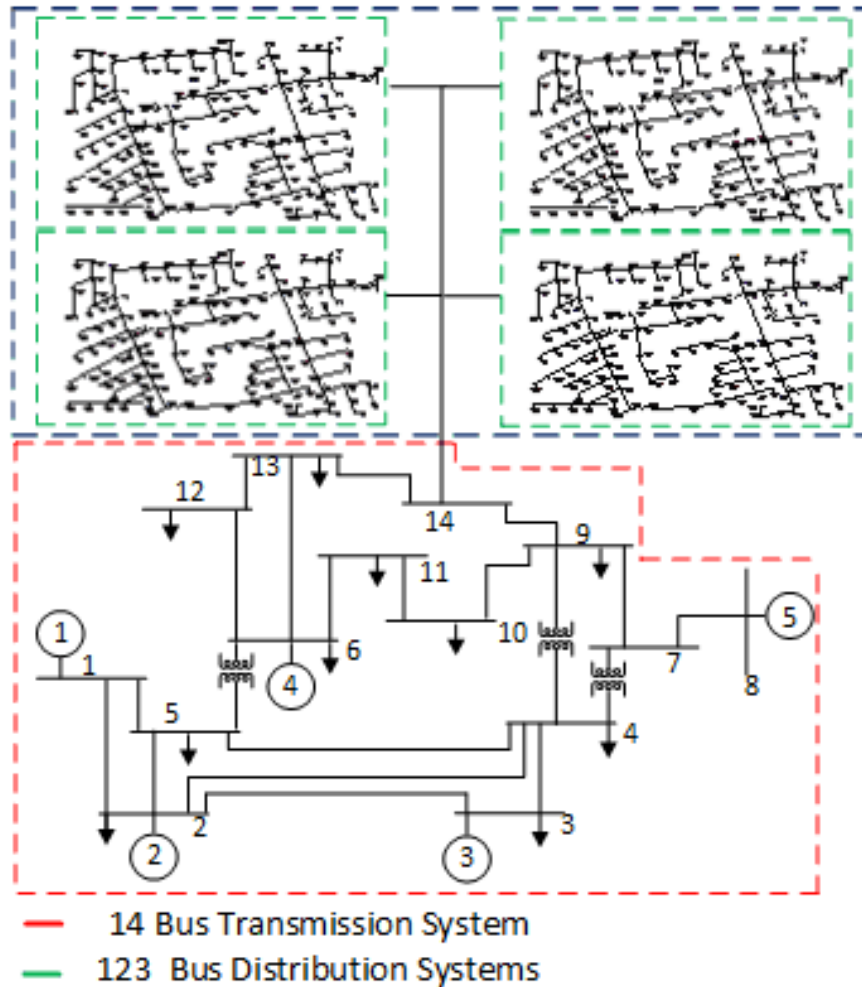


Figure 6.28: One line diagram of T&D system.

alent distribution system and c.) Integrated T&D system with the transmission system modeled in a positive sequence. For the transmission system with spot loads, the spot loads represent the total load and losses of distribution systems connected. These loads are varied using loading factor  $\lambda$ . The load at bus  $i$  with base power  $S_{0i}$  can be represented by

$$S_{Li} = S_{0i}(1 + \lambda) \quad \forall \lambda \in 0, 1, \dots, \lambda_{max} \quad (6.19)$$

To model losses in a better way, the equivalent distribution feeder method is used where the distribution system is modeled as a distribution line connected to a spot load representing the net load of the distribution system. To find the parameters of

equivalent distribution feeder ( $R_{eq}, X_{eq}$ ), a distribution system load flow is performed, and the net losses and injected current at the substation are used. The  $R_{eq}, X_{eq}$  parameters should be computed for each loading level of the system.

$$R_{eq} + jX_{eq} = \frac{S_{loss}}{I_{sub}^2} \quad (6.20)$$

An integrated T&D system with a transmission system modeled in a positive sequence for VSM assessment is discussed in [100]. The active and reactive power injection at each phase of the substation bus obtained after distribution system load flow is added to represent a three-phase load value for the boundary bus which is then used for positive sequence transmission power flow in the next iteration.

The VSM obtained with positive sequence T&D for a balanced and unbalanced distribution system is depicted in Fig.6.29a and the proposed approach is depicted in Fig.6.29b. With the proposed approach, the PV curves for each phase are different with phase a being the most vulnerable. It can be observed that when a balanced distribution system is replaced with an unbalanced system, the reduction in  $\lambda_{max}$  was from 1.2 to 0.9 when a three-phase transmission power flow is done. The reduction was from 1.5 to 1.4 with positive sequence transmission power flow. The effect of distribution system unbalance on stability margin is captured prominently in the proposed approach compared to the positive sequence T&D approach. Thus it can be proved that the proposed architecture is extremely critical for evaluating the long-term voltage stability margin especially with unbalanced load and proliferation of multi-phase DERs in the distribution network.

#### 6.7.1.2 Analysis of PV curves With Different Load Types

The comparison of all methods for a balanced distribution system with constant power loads is depicted in Fig. 6.30a and ZIP loads are depicted in Fig. 6.30b. It can be seen that  $\lambda_{max}$  decreases drastically from 3.6 to 1.5 when spot load is replaced

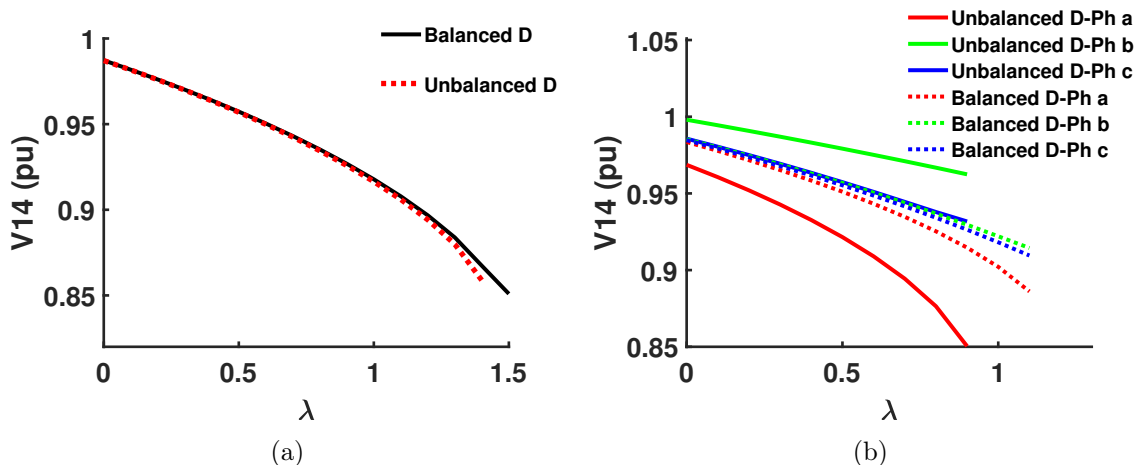


Figure 6.29: (a) PV curves using Positive Sequence T&D method (b) PV curves using Proposed Three Phase T&D method

by distribution system in 3 phase detail while transmission system still represented in positive sequence. Furthermore, even with an approximately balanced net load at

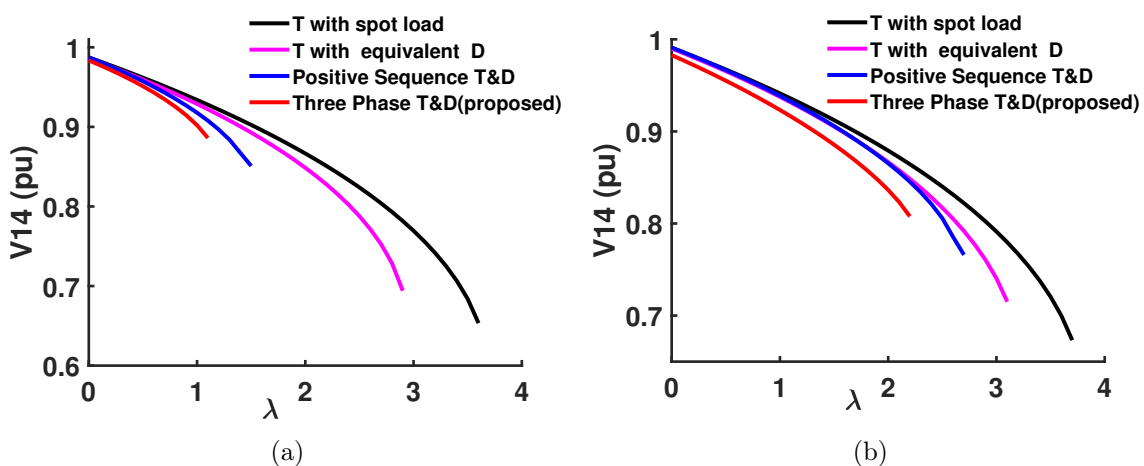


Figure 6.30: (a) PV curves of T&D system with constant power load (b) PV curves of T&D system with ZIP load

the boundary bus, the  $\lambda_{max}$  is further reduced to 1.1 when the transmission system is represented in 3 phase detail. The distribution system consists of untransposed lines and a large number of single-phase laterals. This will lead to different line losses in each phase which results in unbalanced substation power even if total loads in

all the phases are approximately the same. These slight unbalance in power when used for transmission load flow would lead to unbalance boundary bus voltage. When this is used as a source bus voltage in distribution load flow, it would lead to more unbalance in losses and leads to faster divergence as loading is increased. The  $\lambda_{max}$  when all loads considered as constant power loads are lower than when ZIP loads are considered. This is because, in the case of constant power loads, the lower bus voltage during heavy loading will lead to higher current flow to maintain the constant power drawn by the load. This higher current leads to higher line losses and hence lower  $\lambda_{max}$  or faster divergence. A detailed comparison of  $\lambda_{max}$  for all the cases are depicted in Fig. 6.31. The average time required for convergence of proposed T&D load flow for different values of  $\lambda$  is shown in Table 6.13. The computational load when the three-phase T&D method is used is very close to the positive sequence T&D method. It is also observed that, as loading is increased, the number of T&D iteration required in three-phase T&D method is more, which is also the reason for higher values of computational time.

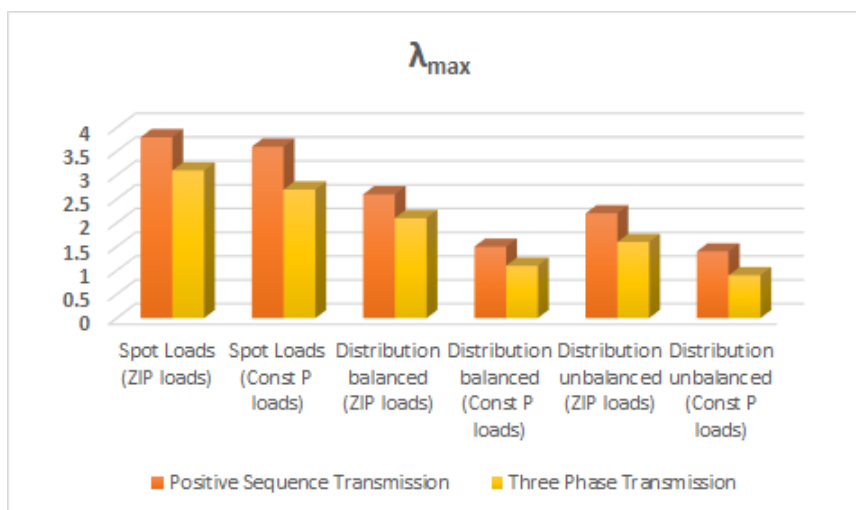


Figure 6.31: Maximum loading factor.

All these test cases are repeated by using a sequence based MPF developed in chapter 4 on the unified T&D systems. The results are not presented again as it is

Table 6.13: Average Computational Time for Convergence

$\lambda$	Avg Time(s)		% Increase in Time
	Positive Sequence T&D	Three phase T&D	
0	0.1995	0.2069	3.709273
0.5	0.2621	0.2795	6.638688
1	0.2705	0.2912	7.652495
1.5	0.3763	0.4097	8.875897

Table 6.14: Iterations to converge.

$\lambda$	Sequence Power Flow (flat start)		Sequence Continuation Power Flow	
	Iteration	Time	Iteration	Time
0.1	4	4.2	2	2.8
0.3	5	5.1	3	3.4
0.5	9	8.2	5	5.6
0.8	14	15.4	8	9.2
0.9	50	30	15	25.
0.921	100	50	20	32.5

similar to the one obtained using decoupled MPF.

### 6.7.2 Integrated T&D Continuation Power Flow Model

A continuation power flow (CPF) is a method based on predictor-corrector scheme with a continuation parameter (voltage or power). It is generally used to trace the PV curve or nose curve which traces the voltage as load is increased from base value until it reaches the loadability limit and then back to base value. The Jacobian will become singular at nose point and due to which the system become ill conditioned Therefore the normal power flow diverges at nose point. This problem of ill-conditioning can be solved using continuation power flow. The continuation power flow introduces an additional parameter and an equation to the power flow equation so that the augmented Jacobian is not singular at the nose point. The basic approach in CPF is to first predict the power flow solution using a chosen continuation parameter. This is mostly accomplished using linear approximations. Then a corrector step is implemented where augmented power flow equations are solved using these predicted

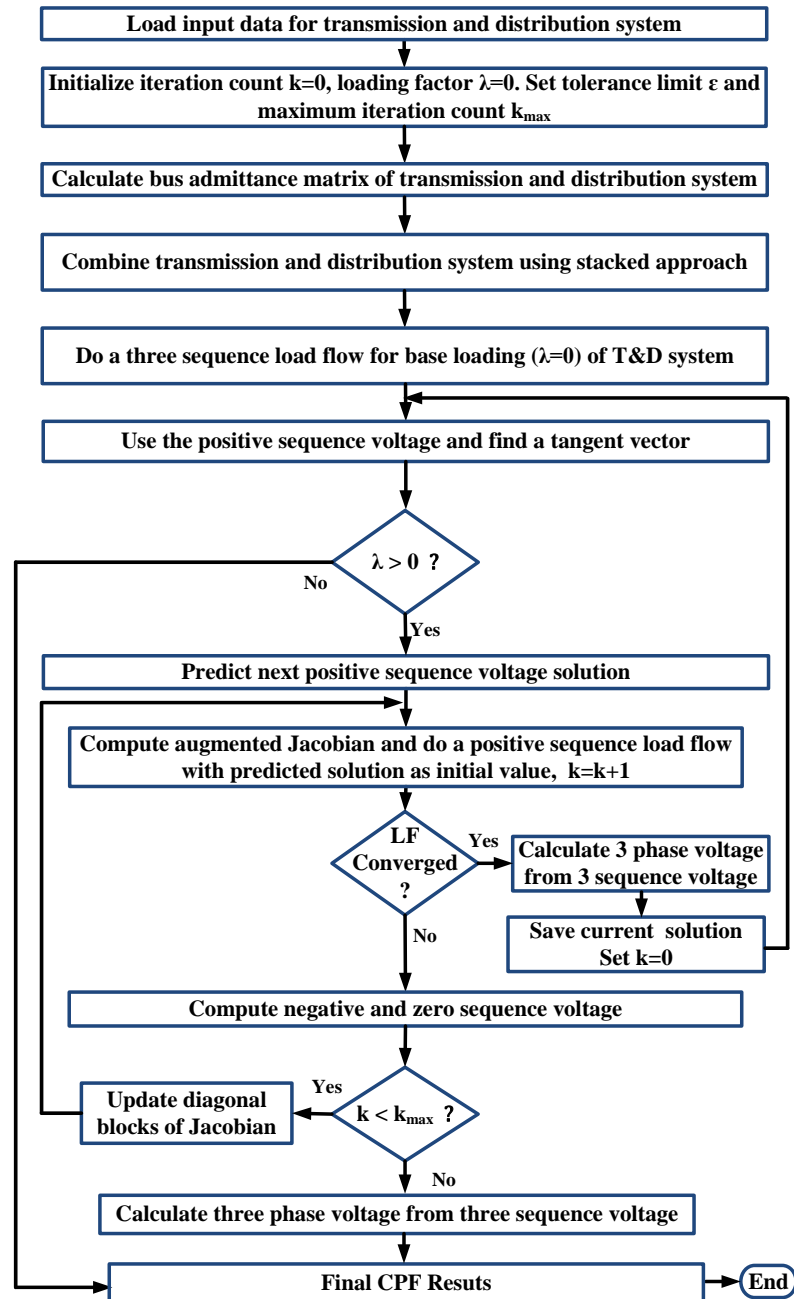


Figure 6.32: Three sequence T&D continuation power flow.

values as the initial condition.

An integrated power grid model is developed that includes the IEEE 14 bus for the transmission side and four IEEE 123 bus test distribution feeders on the distribution side connected to the bus# 14 of the transmission system as shown in Fig. 6.28. Also,

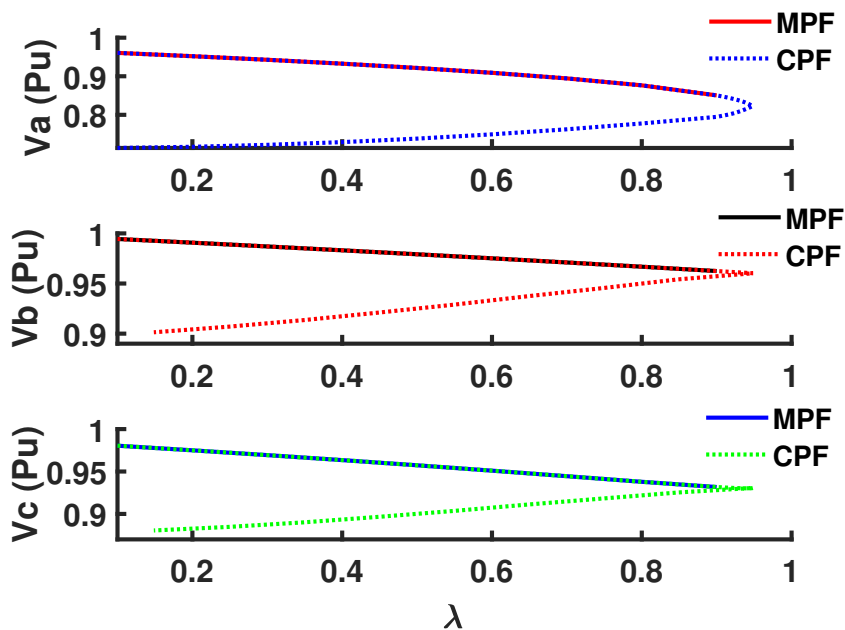


Figure 6.33: Comparison of CPF and MPF.

a larger T&D system with the 8500 node distribution system is developed to assess the scalability of the proposed approach.

#### 6.7.2.1 Comparison of MPF Approach with Unified Sequence CPF Approach

In this section, sequence based multi-period power flow (MPF) is compared with proposed sequence based continuation power flow. It can be seen from Fig. 6.33 that CPF is stable while MPF diverges as the nose point is reached. Therefore more accurate results are obtained using the proposed CPF approach. While MPF uses a flat start to initialize load flow, the CPF utilizes a predictor-corrector approach where solutions from the prediction step are used as initial conditions for correction. This can lead to lower computation when CPF is used compared to MPF. A table depicting the number of iterations to converge and time required for three sequence power flow and three sequence CPF is shown in table 6.14. It can be observed that the CPF takes lesser iterations to converge for any the values of  $\lambda$ . It can also be seen that MPF failed to converge (maximum iterations of 100) for  $\lambda = 0.921$ , whereas CPF still converged. Therefore CPF has higher computational efficiency and convergence

capability compared to MPF.

### 6.7.2.2 Effect of Regulator tap operation on VSM

The effect of regulator operation on voltage stability margin is discussed in this section. As loading is increased, the voltage at regulating point will reduce which results in , tap up operation of regulator. This will continue until regulator hits upper limit of 16. The VSM margin of system increased from 0.921 to 1.118 when regulator control was enabled. A comparison pf PV curve with and without regulator control is shown in Fig. 6.34.

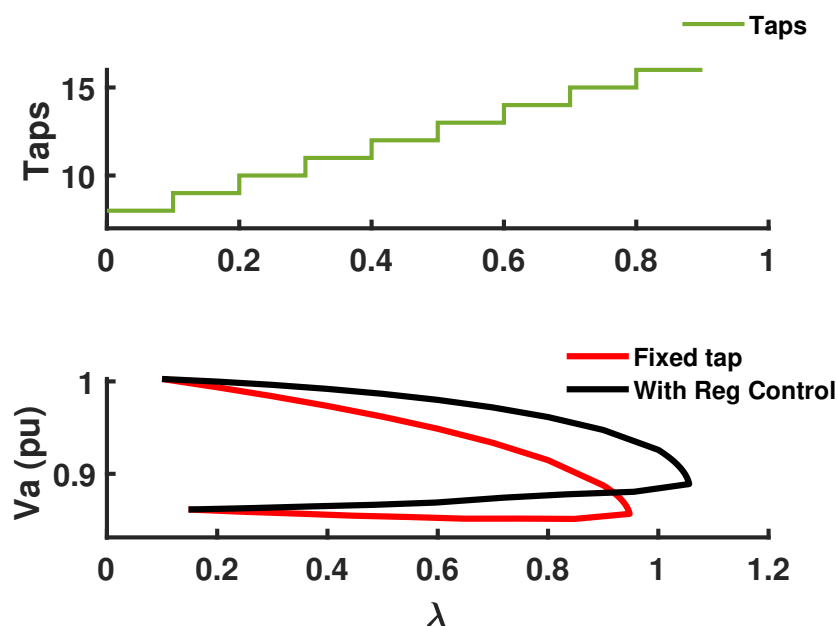


Figure 6.34: VSM with Regulator Control.

### 6.7.2.3 Scalability Assessment

To assess the effect of the system size on the execution of the proposed CPF approach, a T&D system with 8500 node distribution system connected to 14 bus transmission system is used. The PV curve of bus 14 is for this T&D system is shown in Fig. 6.35.

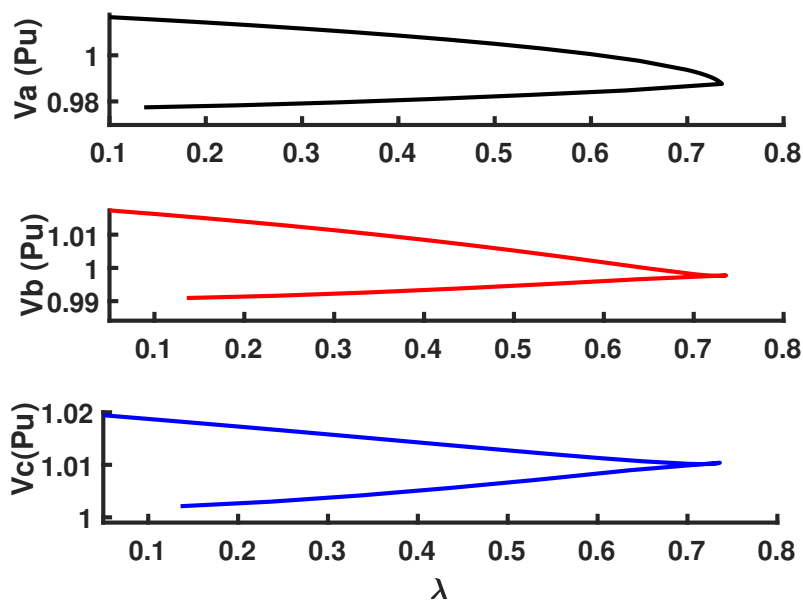


Figure 6.35: PV Curves of 14-8500 T&D System.

## 6.8 Fault Analysis

Steady-state fault analysis is used to estimate the fault currents and voltages which are then used for proper relay setting and coordination. Even though there are proven methods to do fault analysis on transmission systems and distribution systems, there are no specific methods in literature to do fault analysis on T&D systems. Most of the existing works related to fault analysis rely on EMT softwares such as PSCAD. Another approach to analyze fault events is to have a dynamic T&D modeling similar to the work in [94]. Both these approaches are computationally demanding and unnecessary if the final aim is to find the steady-state fault currents and not the dynamics during fault. The three sequence based fault analysis method developed in chapter 5 is used to do fault analysis for the unified T&D system. A T&D system with 9 bus transmission and a 123 bus distribution system is considered. Different faults are simulated at bus 7 of the distribution system. The results are compared with results obtained from the EMT solver (SIMULINK). It is evident from Fig. 6.37 and Table. 6.15 that the proposed method is accurate with a maximum error of less

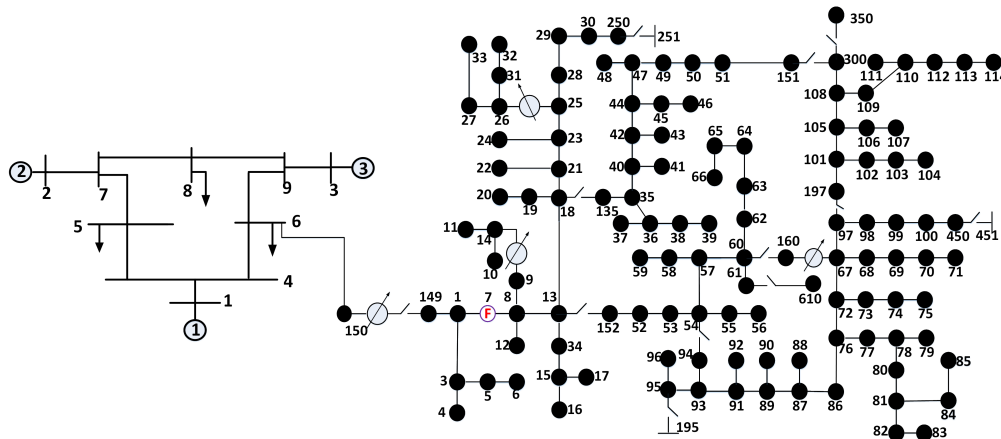


Figure 6.36: IEEE 9-123 T&D system

than 1.8%. This method can be further extended to do steady state fault analysis of T&D systems with large DER penetrations.

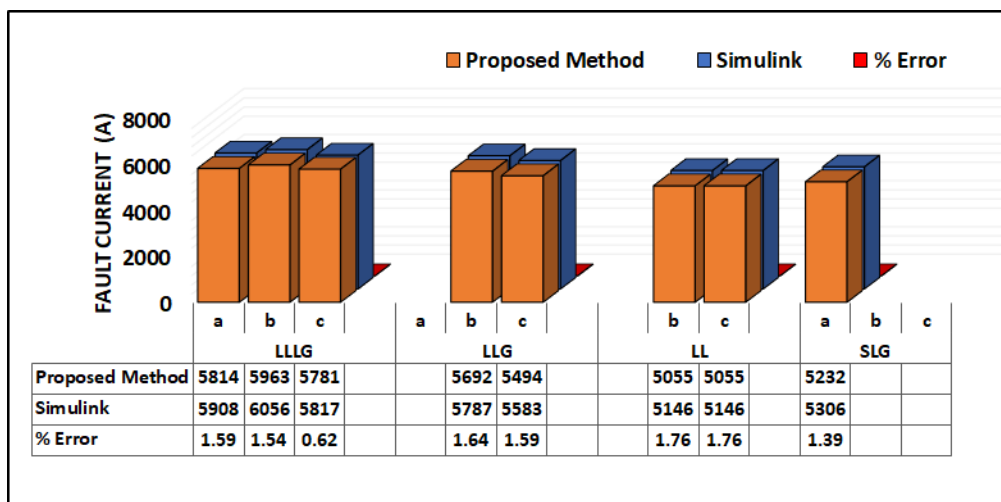


Figure 6.37: Comparison of different faults currents at bus 7 Distribution system

### 6.9 Sequence Based Integrated T&D System Analysis Tool

Finally a sequence based integrated T&D system analysis tool is developed as shown in Fig. 6.38. The tool is universal and can be used to analyze any T&D system. The tool is capable of conducting a load flow analysis, voltage stability analysis and fault analysis on the system selected.

Table 6.15: Fault Currents in Amps for 9-123 T&amp;D System.

Bus	Fault Type	Proposed Method			Simulink (EMT)			% Error		
		Iap	Ibp	Icp	Ias	Ibs	Ics	Ias	Ibs	Ics
D7	LLLG	5814	5963	5781	5908	6056	5817	-1.59	-1.54	-0.62
D7	SLG	5232.1	0	0	5306	0	0	-1.39		
D7	LL	0	5055.37	5055.37		5146	5146		-1.76	-1.76
D7	LLG	0	5692.3	5494.3		5787	5583		-1.64	-1.59

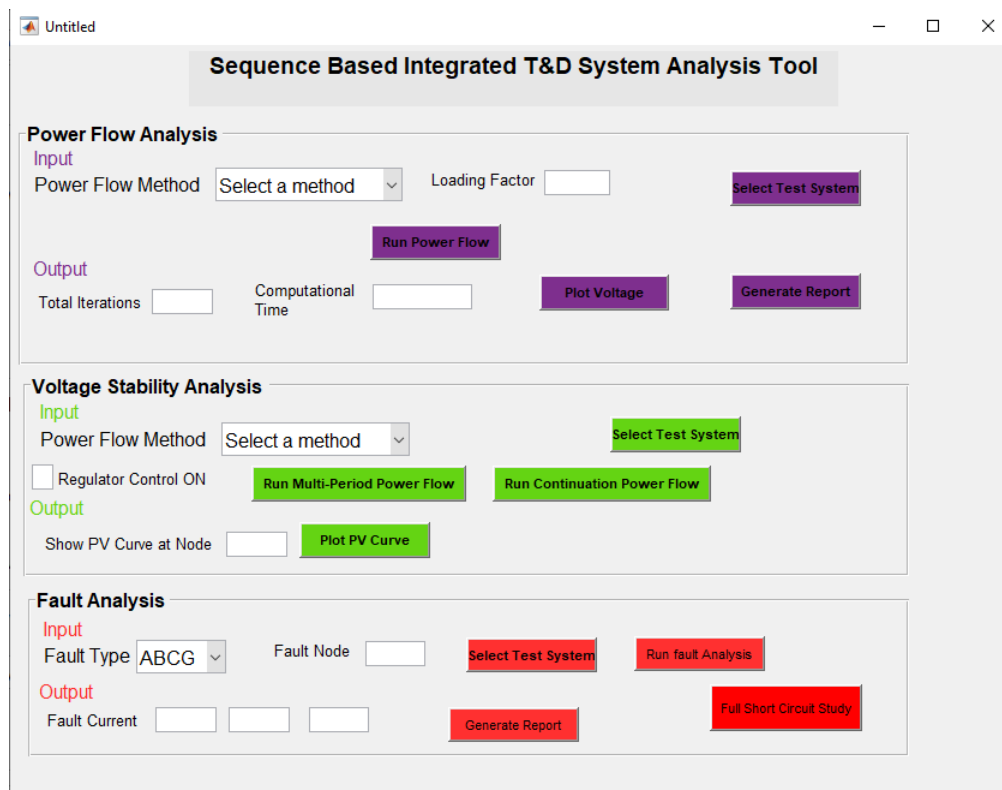


Figure 6.38: Sequence Based Distribution System Analysis Tool.

## 6.10 Summary

In the chapter, a new model for integrated transmission and distribution system in three phase modeling framework is proposed which can successfully capture the interactions between transmission and distribution systems. The three sequence load flow methods developed are used for the load flow of the unified T&D system. Also, a sequence based multi-period load flow approach and three sequence continuation power flow methods are used to obtain accurate voltage stability margin of integrated

T&D system. Finally, the steady state short circuit analysis of the T&D system is computed using the three sequence fault analysis approach. The results are compared with EMT simulations and error is less than 1.8%. All the sequence based approach discussed in this chapter are novel approaches with a computational advantage over three-phase methods and is best suited for T&D systems owing to their large size.

## CHAPTER 7: SENSITIVITY BASED DYNAMIC COORDINATED CONTROL FOR GRID SUPPORT USING DISTRIBUTED ENERGY RESOURCES

### 7.1 Introduction

There has been a significant increase recently, in the penetration of distributed generations (DGs) especially through Distributed Energy Resources (DERs) at medium voltage and low voltage distribution power grid. One main problem that has been discussed leading to a low penetration level of DG is the uneven voltage profile attributed to intermittent DER output. The penetration level can be fairly increased if voltage profiles can be optimally balanced. Moreover, if the voltage profile is kept at an optimal level, the losses in the distribution network can be reduced as well. As the integration of DERs causes bidirectional power flow, conventional voltage and reactive power management may not be effective at all operating conditions. Several research works have focused on this problem considering various factors ranging from reactive power management, coordination of reactive power, studying power output from the renewable energy source that could be harnessed to provide stability for the grid in addition to meeting electrical demand. A comprehensive review of controlling DER output using various inverter control schemes is presented in [105]. Ref. [106] has studied the impact of DER penetration on the static voltage stability of the system. For a distribution network, being in direct contact with the user, the power supply reliability and quality is of prime importance. The reactive power compensation in the distribution network can lead to improved power quality of users, a better utilization rate of the power transformer, and reduced network losses.

There are two main control methods for DG units to balance the power. The first one is local or decentralized control and the second one is coordinated or centralized

control [13]. The local control is achieved by controlling the reactive power of the DG unit locally, without coordination with other DGs connected in the grid. Here, communication infrastructure and delays associated with it are reduced which results in faster response, easy installation, and reduced cost [107, 108]. Centralized control on the other hand is based on optimal power flow and takes into account optimum sharing of reactive power between different DG units which in turn requires communication infrastructure. This can lead to high installation cost [109]. but have better controllability. Some examples include work in [110], where coordination between reactive power from DGs at the MV level and active power output from DG sources at the LV level is proposed. Similarly, a coordinated control with adaptive zoning is proposed in [111], where the distribution grid is divided into zones with individual reactive support schemes which leads to reduced system complexity and data handling capability. With proper control strategies implemented, the inverter-based DG units could be utilized for instantaneous voltage support during system contingencies. A reactive power management scheme using coordinated secondary voltage control was developed in [112] to achieve efficient voltage regulation and to maximize the dynamic reactive power reserve. Also, an inverter control strategy was proposed in [113] where DGs were controlled to provide voltage support during voltage sags.

Local inverter controllers for grid-tied operations have been covered in the previous work of the authors [114], which elaborates on the interaction of inverters with the utility/power grid. Enhanced power management and control techniques for grid supporting features were developed in [115, 116], which focused on mitigation of voltage anomalies and power unbalances locally. In this paper, a coordinated control architecture for multiphase DERs using measurement-based transfer function identification is proposed. The sensitivity between voltage deviation and the reactive power injection is captured by transfer function identification which is further used for coordinated control of DERs. The main advantage of this method is that, since

the method is based on measurements, any changes to the system variables can be dynamically captured by the algorithm.

## 7.2 Research Contribution

- A coordinated control architecture for multiphase DERs using measurement-based transfer function identification is proposed.
- A transfer function identification scheme using ADMM is used to obtain sensitivity between voltage deviation and the reactive power injection and is further used for coordinated control of DERs.
- Since the method is based on measurements, any changes to the system variables can be dynamically captured by the algorithm.
- The algorithm can be used for dynamic DER selection where scenarios like loss of one or more DERs during operation can be analyzed.

## 7.3 Realtime DER Integrated Distribution System Modeling

For DER integrated distribution system modeling, the distribution lines are modeled in three-phase detail using a distributed parameter line model. The models include unbalanced lines, voltage regulators, and inline transformers unbalanced loads. The substation is assumed as a rigid voltage source with infinite capacity. Most of the loads are modeled as spot loads and some of them as distributed loads. Multiple DERs are integrated to IEEE test distribution systems developed in Simulink software. The test systems used are IEEE 13 node test feeder, IEEE 34 node test feeder, and IEEE 123 node test feeder.

### 7.3.1 Voltage Regulators

Voltage regulators are assumed to be step-type and can be connected in the substation or to a specified line segment. In the case of 3 phase regulators, three single phase regulators of Y type are developed. Regulators can either control the voltage

Figure 7.1: Voltage comparison at test node.

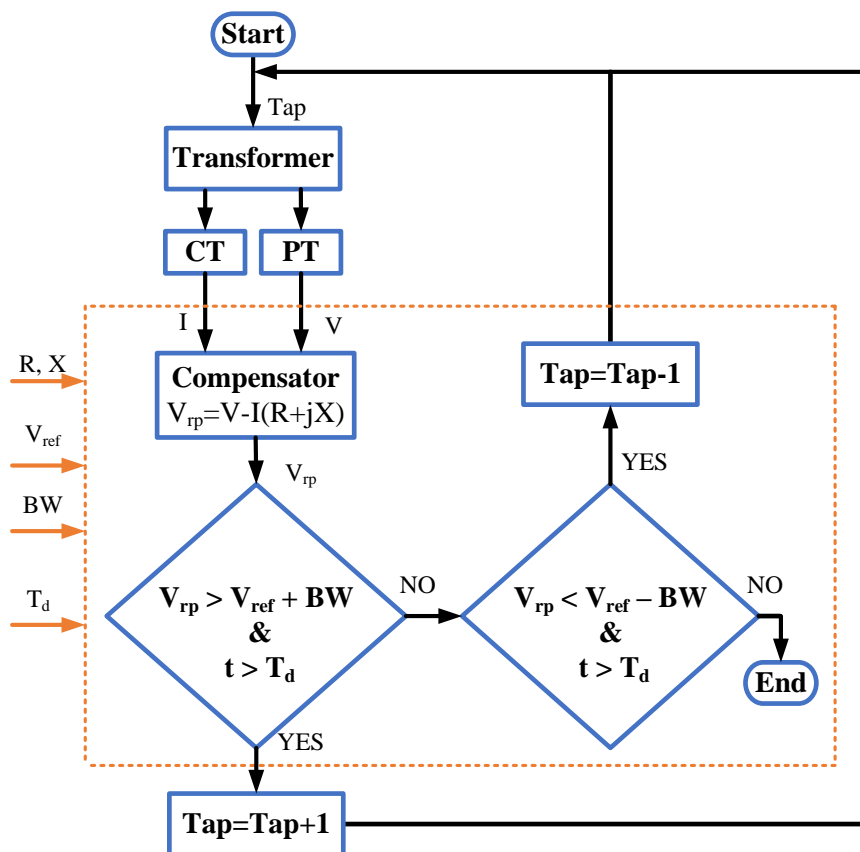


Figure 7.2: Voltage Regulator Control

at its output node, or they can control the voltage at a remote node downstream. A line drop compensator is used to regulate the voltage at a remote node. There are four settings for the compensator circuit. They are compensator R and X settings, voltage level setting ( $V_{ref}$ ), bandwidth setting (BW), and time delay ( $T_d$ ) setting. The per-unit R and X settings are chosen to be equal to the per-unit equivalent line impedance from the regulator output to the regulation point. The voltage setting gives the desired voltage to hold at the regulation point and bandwidth defines the allowed variance of the regulation point voltage centered at the desired voltage level. The time delay is the delay before a tap change is made when the voltage is not

within the bandwidth. When the voltage at the remote node is higher than the upper voltage level setting  $V_{ref} + BW$  and it stays there for a time greater than  $T_d$ , a raise operation is initiated and tap is increased. This process is continued until the tap reaches its maximum limit. Similarly, when the voltage at the remote node is lower than the lower voltage level setting  $V_{ref} - BW$  and it stays there for a time greater than  $T_d$ , a lower operation is initiated and tap is decreased as shown in Fig 7.2. The developed regulator model is validated using a dynamic load variation. A case is shown in Fig 7.3 in which a load is added to IEEE 13 node test feeder at 3 seconds resulting in a drop in voltage. The regulator taps raise after a delay of 2sec as shown in Fig 7.3. The voltage on phase C goes out of bounds. So a tap change occurs in regulator C and with that the voltage comes back to within the band.

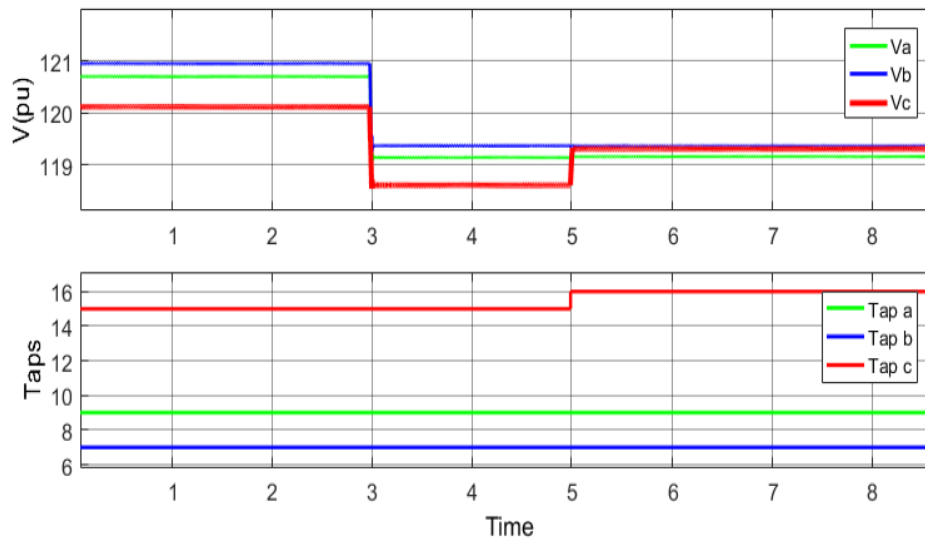


Figure 7.3: Regulator Taps

### 7.3.2 Realtime Implementation with OPAL-RT

All the distribution systems with DERs integrated are built to run in real-time using a real-time simulator called Opal-Rt [117]. They run in a "model in the loop" real-time simulation and can be extended in the future to do "hardware in the loop" simulations [118]. In RT-Lab, ARTEMiS-SSN is the solvers specifically designed

for microgrid, distribution systems that provide fast and accurate real-time simulation without introducing artificial delays. ARTEMiS-SSN optimizes all electric system models using an advanced decoupling technique called the state-space nodal method. It virtually decouples large systems of state-space equations into smaller groups, whose solutions can be obtained simultaneously by using a nodal admittance method similar to the one found in other real-time software such as EMTP-RV. The resulting algorithm is much similar to EMTP-type ones except that part of the algorithms can be solved in parallel, on different processors, without adding any artificial delays in the solution [119].

The models are initially created in SIMULINK which has Opal Rt libraries. Then the RT-Lab GUI is used to run the model in real-time using a 3 step process namely build, load, and execute. The build process converts the model into a Linux executable code. The load process uploads the executable code to the simulator and the execute process starts the real-time simulation in the simulator as shown in Fig 7.4. In this

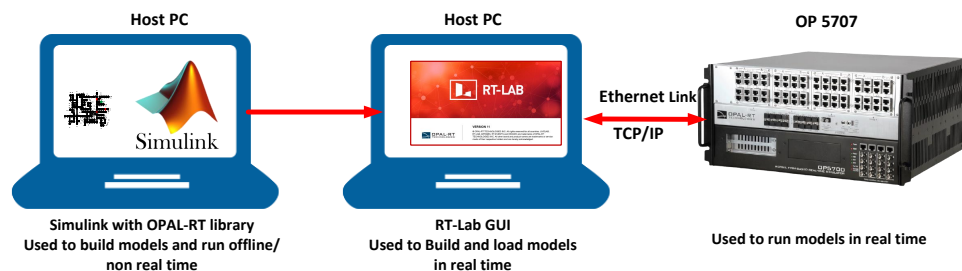


Figure 7.4: Real Time Implementation using OP 5707

work, the IEEE 123 bus system with multiple DERs is modeled to run in real-time. The real-time simulator OP 5707 is used which has 16 cores. The models are first designed in Simulink and then partitioned into multiple subsystems as shown in Fig 7.5 to run it in different cores and leverage the parallel computing capability of RT-Lab.

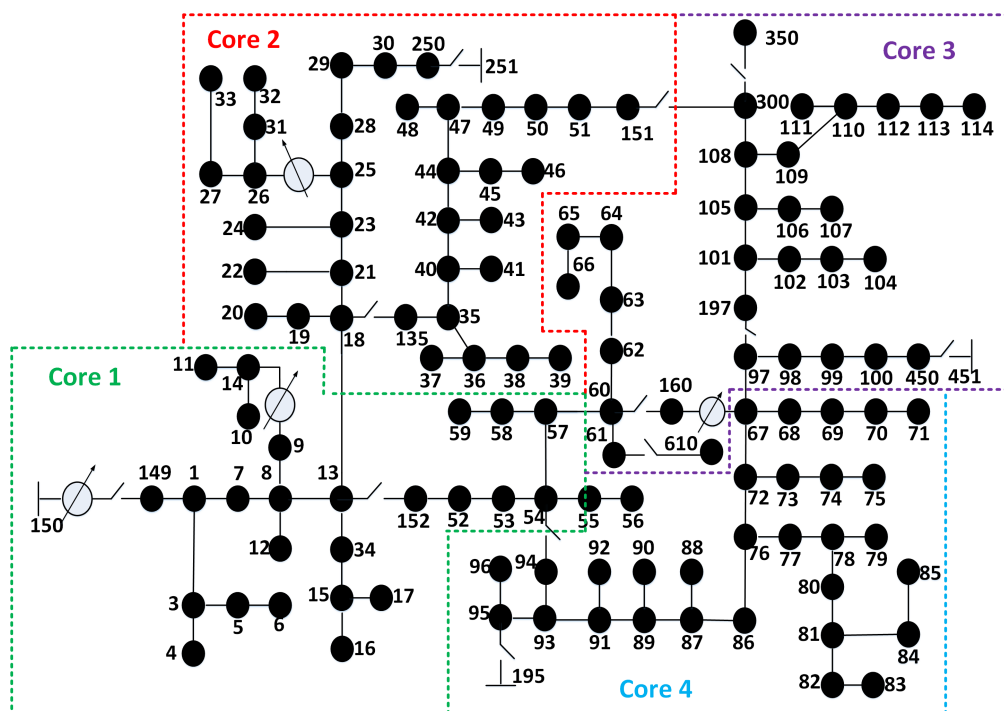


Figure 7.5: IEEE 123 Bus Distribution Test Feeder

### 7.3.3 DER Integration to Distribution Grid

PV farms of rating 500kW, 1MW, 2MW are designed on both 4160 V and 24900 V levels. Design parameters of 1MW PV farm are shown in fig7.6. Table 7.1 shows details of PV integration in 13,34 and 123 bus test feeders. The PV array is connected to the grid via a DC-DC boost converter and a three-phase three-level voltage source converters (VSC). Maximum Power Point Tracking (MPPT) is implemented in the boost converter using a Perturb and Observe technique. The VSC converts the 500 V DC link voltage to 260 V AC. The VSC control system uses two control loops, an external control loop that regulates DC link voltage to 500 V and an internal control loop that regulates  $I_d$  (active current component) and  $I_q$  (reactive current components) grid currents.  $I_d$  current reference is the output of the DC voltage external controller. The output of the current controller is voltages  $V_d$  and  $V_q$  which are converted to three modulating signals for the inverter. The control topology is shown in Fig 7.7. The voltage at PCC and nodes near by would see a rise in voltage

PV PLANT DESIGN			
Power Rating (MW)	2	PV Module	SunPower SPR-305E-WHT-D
AC Voltage (Volts, L-L)	480	PV Plant Output Voltage (Volts)	820.5
PV Plant Output Voltage (Volts)	820.5	Approximate String Voltage	820
Modulation Index (Ma)	0.7838	Number of Modules in String NM	10
Voltage at MPP (Vmpp)	54.7	String Power SP (MW)	0.00305226
Current at MPP (Impp)	5.58	String Voltage (SV)	820
Power at MPP (Pmpp)	305.226	Number of Strings NS	437
Open-circuit voltage (Voc)	64.2	Number of arrays NA	15
Short-circuit current (Isc)	5.96	Total Number of Modules TNM	4370
Module Efficiency (%)	16.4		
Array Power Rating (MW)	2		

INVERTER DESIGN		<i>Average Model</i>	
AC frequency (Hz)	60	Inverter Input DC Voltage Vin (V)	1000
Inverter Power Rating (MW)	2	Interfacing Capacitor Cdc	0.0798
Number of Inverters NI	1	Acceptable Voltage Ripple %	5
Switching Frequency fsw (kHz)	10	Inverter Output Voltage Vout (V,L-L)	480
Frequency Modulation Index Mf	90	DC Power Pdc (MW)	3
Id	5103.7242	Em	391.9183588
Series Inductor Filter L ac (mH)	0.15		

DC BOOST CONVERTER DESIGN		<i>Average Model</i>	
Number of Converters	1	Converter Inductor Lconv (mH)	0.1208
Converter Input Voltage (Vin)	820	Converter Input Capacitor Cconv (uF)	1100
Converter Power Rating (MW)	2	Acceptable Current Ripple %	5
Converter Output Voltage (Vout)	1000		
Duty Cycle (D)	0.1795		

Figure 7.6: PV farm design

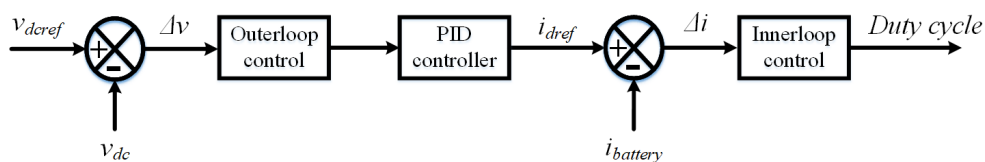


Figure 7.7: Control Topology

Table 7.1: PV integration to Test Feeders

Test Feeder	PCC Nodes	Rating
13	Node 680,682,634	2MW
34	Node 814,854,840	500KW
123	Node 44,65,160	2MW

due to PV integration. Since there is no explicit control of voltage at PCC, the voltage regulator would regulate the voltage by changing taps.

#### 7.3.4 Control of DERs

A modern power distribution system requires deep and comprehensive visibility, distribution automation and outage management, and coordination and control of distributed resources. For a distribution network, being in direct contact with the user, the power supply reliability and power quality is of prime importance. The reactive power compensation in distribution networks can lead to improved power quality of users, a better utilization rate of the power transformer, and reduced network losses. A comprehensive review of controlling DER output using various inverter control schemes is presented in [105]. Ref. [120] has studied the impact of RER-based DG penetration on the static voltage stability of the system.

There are two main control methods for DG units to balance the power. The first one is local or decentralized control and the second one is coordinated or centralized control [13]. The local control is achieved by controlling the reactive power of the DG unit locally, without coordination with other DGs connected in the grid. In this sense, communication infrastructure and delays associated with it are reduced which results in higher response speed, easy installation, and reduced cost [107]. Centralized control on the other hand is based on optimal power flow and takes into account optimum sharing of reactive power between different DG units which in turn requires communication infrastructure. This can lead to high installation cost [109, 121] but have better controllability. Some examples include work in [110], where coordination between reactive power from DGs at MV level and active power output from DG sources at LV level is proposed. Similarly, a coordinated control with adaptive zoning is proposed in [111], where the distribution grid is divided into zones with individual reactive support schemes which leads to reduced system complexity and data handling capability. With proper control strategies implemented, the inverter-based DG units

could be utilized for instantaneous voltage support during system contingencies. A reactive power management scheme using coordinated secondary voltage control was developed in [112] to achieve efficient voltage regulation and to maximize the dynamic reactive power reserve in a distribution network. Also, an inverter control strategy was proposed in [113] where DGs were controlled to provide voltage support during voltage sags.

With the PV farm, if a battery Energy storage is included, the inverter of the battery could be controlled to regulate the voltage at the node of interest. Here the voltage at the node of interest is measured and a reference for active and reactive power is generated for the inverter of the battery. Since the distribution system has a higher R/X ratio, the active power also can be used to regulate the voltage at a node if necessary. Therefore Either active power ( $\Delta P$  control), or reactive power ( $\Delta Q$  control) or both could be controlled to regulate voltage ( $\Delta P + \Delta Q$  control).

#### 7.4 Voltage Control using ADMM

In this method, an input-output signal selection based control using ADMM is implemented. Using measured data, a black-box transfer function model is estimated based on Lagrange multipliers [122] which is further utilized to control reactive power and regulate the voltage at the node of interest. The measurements of voltage and reactive power at the node of interest are used to estimate the transfer function which is then used to find the required Q to maintain a reference voltage at Node of Interest.

The proposed algorithm initially identifies the sensitivity of DERs to control the voltage at the node of interest using an Alternating direction method of multipliers (ADMM) based transfer function identification. The states of transfer functions obtained are estimated using a Kalman Filter. Finally, the reactive power reference for DERs is generated using a linear quadratic regulator (LQR) controller.

The closed-loop control architecture depicted in Fig. 7.8, show the reactive power outputs ( $Q_1, Q_2$ , and  $Q_3$ ) from three DERs measured at the PCC and deviation of

target node voltage from a reference voltage ( $\Delta V$ ) are used to identify the transfer functions using ADMM. The state-space matrices (ABCD) corresponding to each transfer function are calculated. The states are then used to find the states of the transfer function. This is used to formulate the optimal control signals ( $Q_{ref1}$ ,  $Q_{ref2}$ , and  $Q_{ref3}$ ) for each DER to reduce the voltage deviation. The reference signal generated is sent to each DER. The overall proposed architecture flow chart is shown in Fig. 7.9.

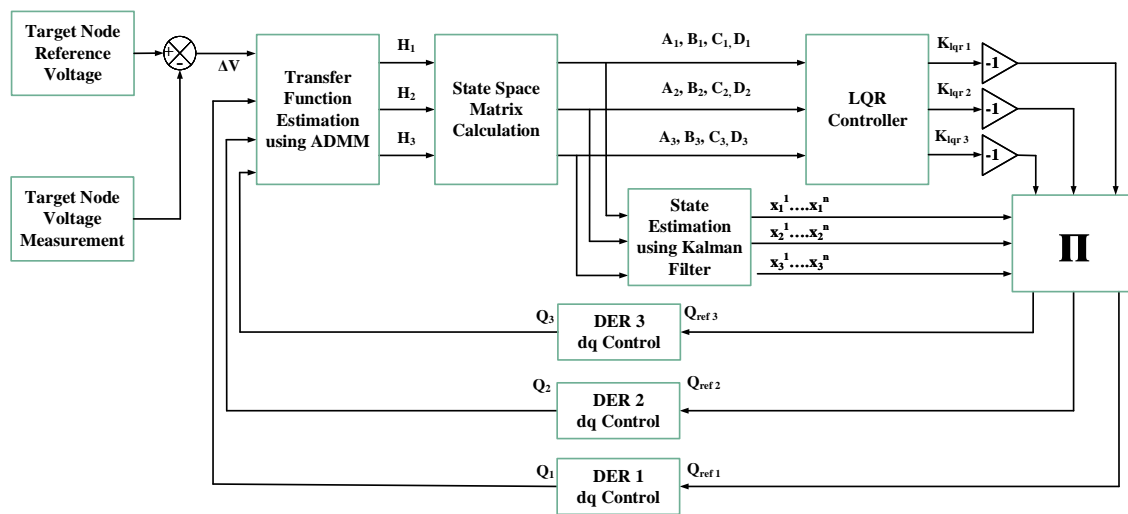


Figure 7.8: Closed-loop control architecture.

#### 7.4.1 ADMM based Transfer Function Identification

Alternating direction method of multipliers (ADMM) is an optimization algorithm that combines the advantages of the dual ascent method and method of multipliers. The optimization problem shown in (7.1) is solved with the primal variable split into two parts,  $x$  and  $z$ .

$$\begin{aligned} & \text{minimize} && f(x) + g(z) \\ & \text{subject to} && Ax + Bz = c \end{aligned} \tag{7.1}$$

The augmented Lagrangian for optimization is developed similarly to the method of multipliers and is given by.

$$L_\rho(x, z, y) = f(x) + g(z) + y^T(Ax + Bz - c) + \frac{\rho}{2}\|Ax + Bz - c\|^2 \quad (7.2)$$

The ADMM optimization routine consists of 3 main steps, an  $x$ -minimization step, a  $z$ -minimization step and a dual variable update step as discussed in [123] and shown in

$$x^{k+1} := \underset{x}{\operatorname{argmin}} L_\rho(x, z^k, y^k) \quad (7.3)$$

$$z^{k+1} := \underset{z}{\operatorname{argmin}} L_\rho(x^{k+1}, z, y^k) \quad (7.4)$$

$$y^{k+1} := y^k + \rho(Ax^{k+1} + Bz^{k+1} - c) \quad (7.5)$$

where  $\rho$  is augmented Lagrangian parameter.

A method of identifying transfer functions using ADMM is proposed in [124]. The multiple-input multiple-output(MIMO) transfer function relating deviation of voltage at a target node with the reactive power output from DERs can be written as

$$\begin{bmatrix} \Delta V \end{bmatrix} = \begin{bmatrix} H_1(z) & H_2(z) & H_3(z) \end{bmatrix} \begin{bmatrix} Q_1 \\ Q_2 \\ Q_3 \end{bmatrix} \quad (7.6)$$

where  $\Delta V$  is the deviation of the voltage from reference voltage at a node of interest, and  $Q_1$ ,  $Q_2$  and  $Q_3$  are the three phase reactive power output of each DER. The individual transfer functions ( $H_1$ ,  $H_2$  and  $H_3$ ) in MIMO can be represented as

$$H_1 = \frac{\Delta V}{Q_1} = \frac{b_0^1 + b_1^1 z^{-1} + \dots + b_k^1 z^{-k}}{1 + a_1^1 z^{-1} + a_2^1 z^{-2} + \dots + a_k^1 z^{-k}} \quad (7.7)$$

$$H_2 = \frac{\Delta V}{Q_2} = \frac{b_0^2 + b_1^2 z^{-1} + \dots + b_k^2 z^{-k}}{1 + a_1^2 z^{-1} + a_2^2 z^{-2} + \dots + a_k^2 z^{-k}} \quad (7.8)$$

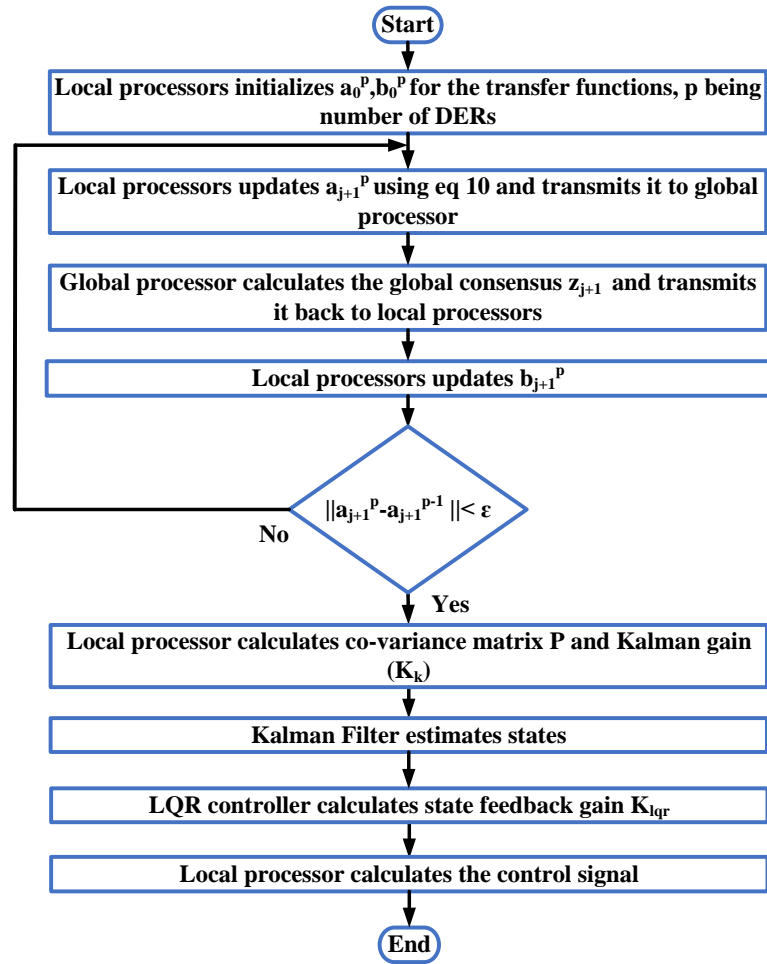


Figure 7.9: Overall algorithm flowchart.

$$H_3 = \frac{\Delta V}{Q_3} = \frac{b_0^3 + b_1^3 z^{-1} + \dots + b_k^3 z^{-k}}{1 + a_1^3 z^{-1} + a_2^3 z^{-2} + \dots + a_k^3 z^{-k}} \quad (7.9)$$

Here  $a_1, a_2, \dots, a_k$  are the denominator coefficients of the transfer functions and  $b_0, b_1, \dots, b_k$  are the numerator coefficients of the transfer functions. A global consensus optimization problem can be formulated as

$$\min_{a^1 \dots a^n} \frac{1}{2} \|[L][a] - [B] + [M][b]\|^2 \quad (7.10)$$

where  $a, b$  are vectors of all the denominator and numerator coefficients respectively.

$B$  is the matrix of the current samples of  $\Delta V$ ,  $L$  is the matrix of the previous samples of  $\Delta V$  and  $M$  is the matrix of the current and previous samples of  $Q_1$ ,  $Q_2$  and  $Q_3$ . The state-space matrices(ABCD) are calculated from identified coefficients of each transfer function.

#### 7.4.2 Kalman Filter based State Estimation

The states of system are estimated with a Kalman Filter using state space matrices and output measurement. The state and measurement equations can be written as

$$x_k = Ax_{k-1} + Bu_{k-1} + w_{k-1} \quad (7.11)$$

$$z_k = Hx_k + v_k \quad (7.12)$$

where  $H$  is the transformation matrix that maps the state vector to measurement.  $w_k$  and  $v_k$  represent the process and measurement noise respectively. They are set to zero as we ignore process and measurement noise during state estimation. The error co-variance matrix ( $P$ ) can be calculated as

$$P_k = AP_{k-1}A' + BQB' \quad (7.13)$$

The gain ( $K$ ) is given by

$$K_k = P_k H' (H P_k H' + R)^{-1} \quad (7.14)$$

where  $R$  is the measurement noise covariance matrix and  $Q$  is the process noise covariance matrix. The estimated states are given by (7.15)

$$\hat{x}_k = \hat{x}_k^- + K_k(z_k - Hx_k^-) \quad (7.15)$$

where  $\hat{x}_k^-$  is a priori state estimate at step k.

### 7.4.3 Discrete Linear Quadratic Regulator Control

A discrete time quadratic problem is used to minimize the objective function given by

$$\sum (x^T Q_{lqr} x + u^T R_{lqr} u) \quad (7.16)$$

The state transition matrix (A), input matrix (B), positive definite weights on state and input vectors  $Q_{lqr}$  and  $R_{lqr}$  respectively are utilized to solve the discrete-time algebraic Riccati equation given by

$$A^T S A - (A^T S B)(R + B^T S B)^{-1}(B^T S A) + Q - S = 0 \quad (7.17)$$

The state-feedback gain  $K_{lqr}$  is given by

$$K_{lqr} = (R_{lqr} + B^T S B)^{-1}(B^T S A) \quad (7.18)$$

Finally the control signal  $u$  is given by (7.19).

$$u = -K_{lqr} * \hat{x} \quad (7.19)$$

The overall proposed architecture flow chart is shown in Fig. 7.9.

### 7.4.4 Simulation Results

The algorithm is tested on IEEE 123 node test distribution feeder as shown in Fig. 7.10. The feeder consists of a substation load tap changer, 3 inline step voltage regulators, and 1 inline transformer. The loads are unbalanced and all types of loads (constant impedance, constant current, and constant power) are used. The feeder has a lot of single-phase and 2 phase laterals which make it a good candidate for testing multi-phase DER integration studies. The three-phase DERs are connected to nodes 67, 450, and 108 with a rating of 300KVA as shown in Fig.7.10.

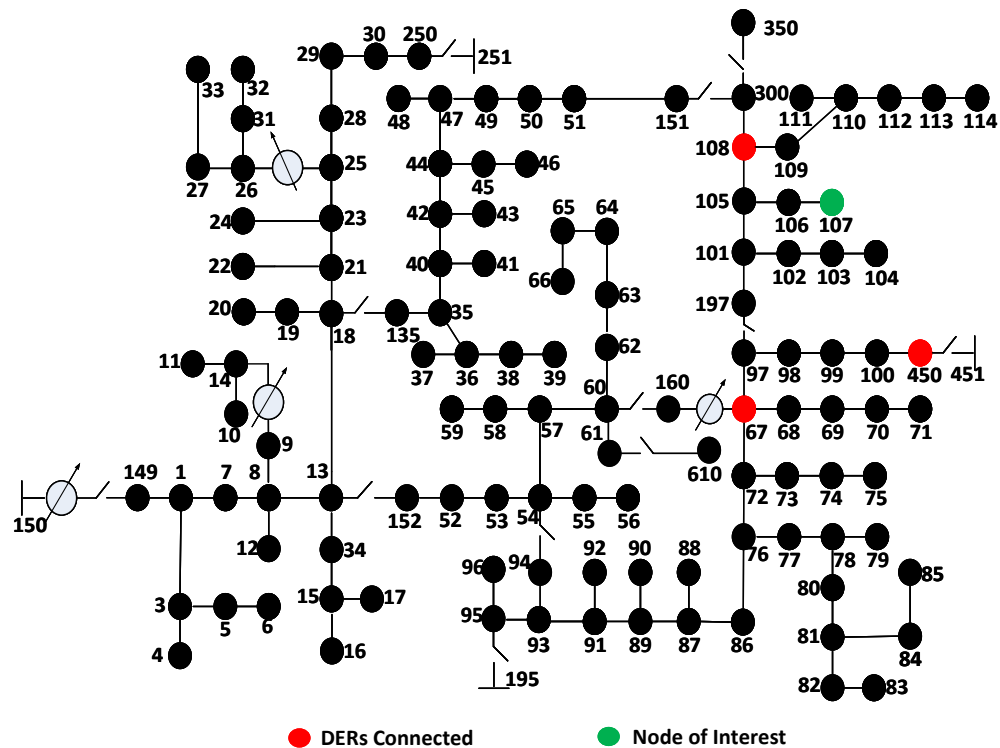


Figure 7.10: IEEE 123 Bus Distribution Test Feeder with DERs.

#### 7.4.4.1 Voltage Support

In this case, a remote node at 107 is chosen as a node of interest, and the reference voltage is chosen to be 1pu. It can be seen from Fig. 7.11 that voltage with ADMM is closer to 1pu. It can also be seen that a sudden voltage dip due to the addition of load is reduced effectively with the proposed architecture. Unlike other control methods that compare the output with the reference, the state feedback control methods compare states multiplied by the control ( $Kx$ ) with the reference. This will lead to a steady-state error. A linear quadratic regulator (LQR) with integral action (LQI) can be used to improve the steady-state response. Since the objective here is to bring voltage closer to the reference voltage and not equal to it the small steady-state error can be ignored.

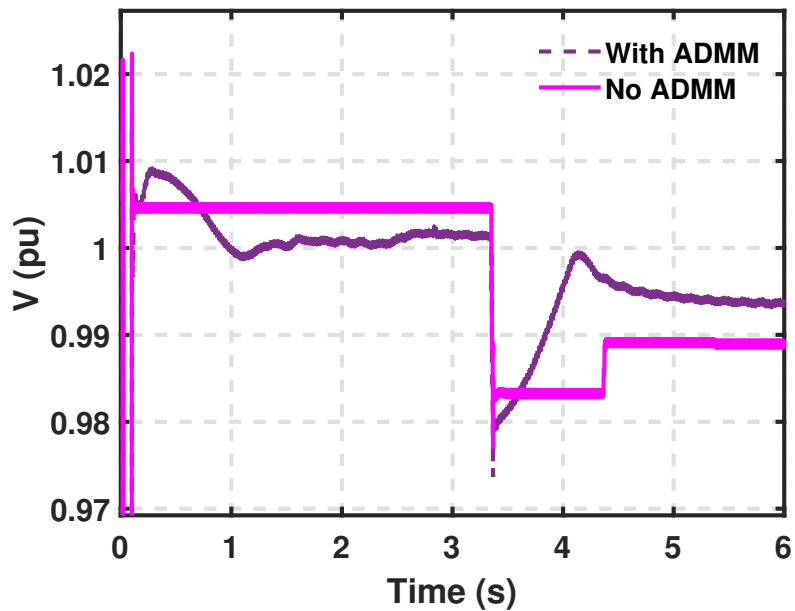


Figure 7.11: Voltage at test node.

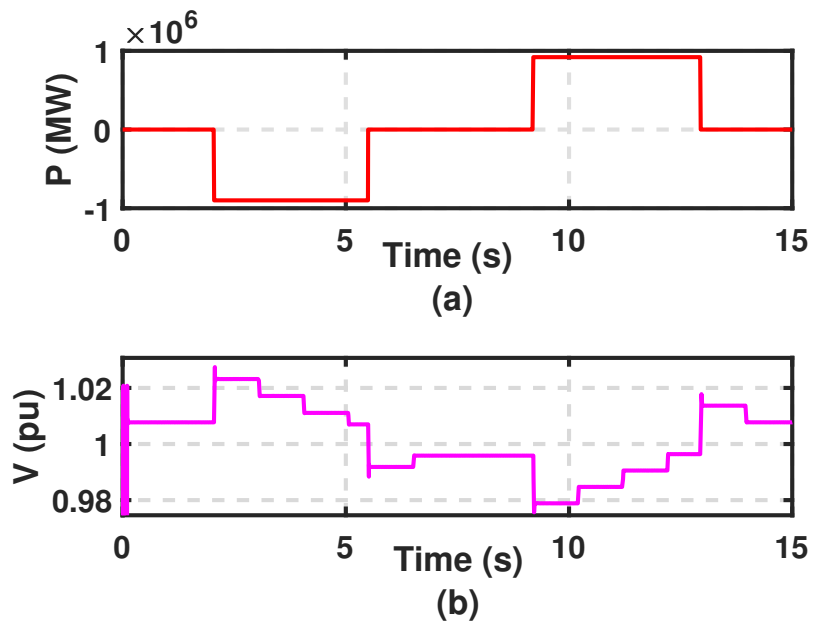


Figure 7.12: (a) Load variation(b) Voltage variation with load variation.

#### 7.4.4.2 Voltage Regulation and Tap Improvement

In this case, a scenario is created where load variation as shown in Fig. 7.12a is initiated which leads to both rising and drop of voltages. The voltage regulators will

adjust the taps after the voltage is out of bounds for a time greater than the delay setting of the regulator. The delay setting of the regulator is set to 1 sec and therefore

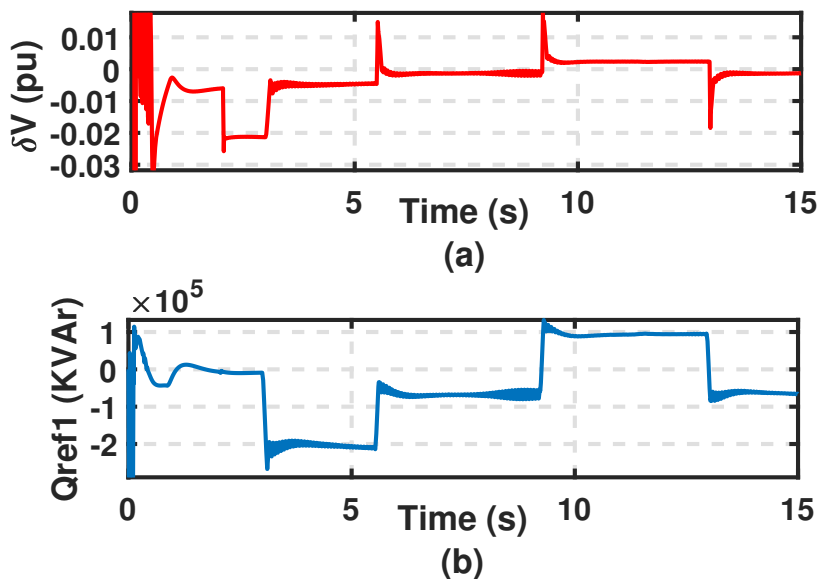


Figure 7.13: (a)  $\Delta V$  at target node (b) Reactive power reference of DER1.

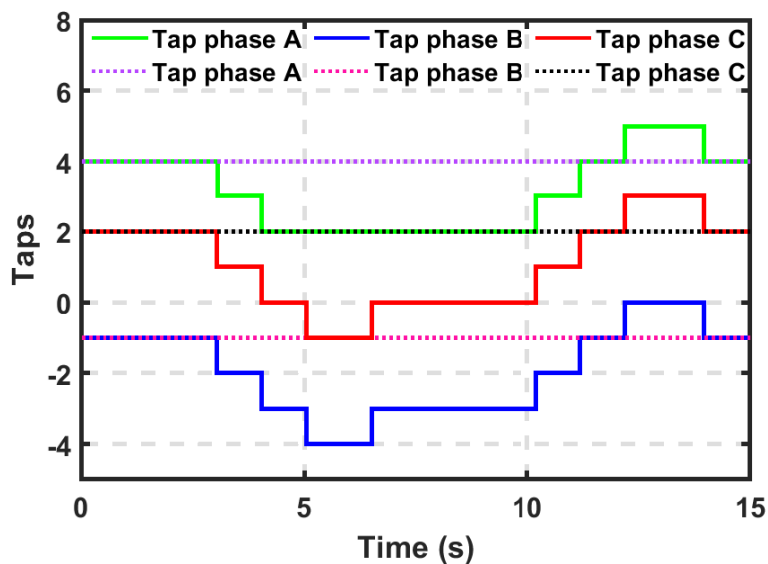


Figure 7.14: Taps operation of Regulator 160-67.

with a load change at 2 sec, a tap-down operation is initiated at 3 sec as shown in

Fig. 7.14. The tap down operation continues with the interval of 1sec each until the voltage at the regulating point is within the bandwidth. The resultant voltage can be observed in Fig. 7.12b. A target node voltage higher than the reference voltage leads

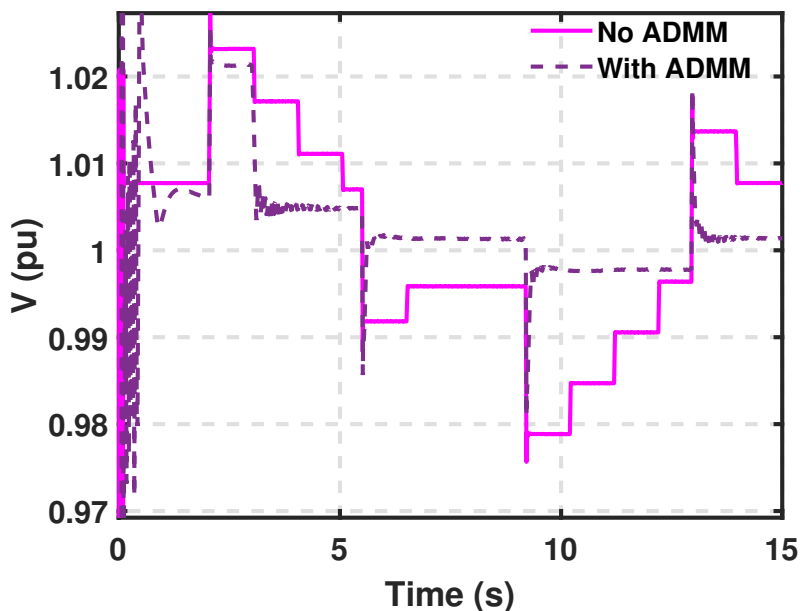


Figure 7.15: Voltage comparison at test node.

to a negative  $\Delta V$ . It can be seen from Fig. 7.13b that the reactive power reference generated by the LQR controller is negative which means the controller is asking the DER to absorb reactive power to reduce the voltage. Therefore, the deviation in voltage at a target node is utilized to generate reactive power setpoints which can reduce the voltage variations. It can be seen from Fig. 7.15 that with reactive power support, voltages stay closer to 1 pu leading to no tap operation when ADMM control is activated compared to 21 tap operations without ADMM control. This is shown in Fig. 7.14 where solid lines are tap variation for the case without ADMM and dotted lines are tap variation for the case with ADMM.

Several scenarios are used to test the efficacy of proposed controller. The location of DERs for each test cases are shown Fig. 7.16 in where a group of DERs connected to different nodes of IEEE 123 bus system are used to regulate voltage of a target

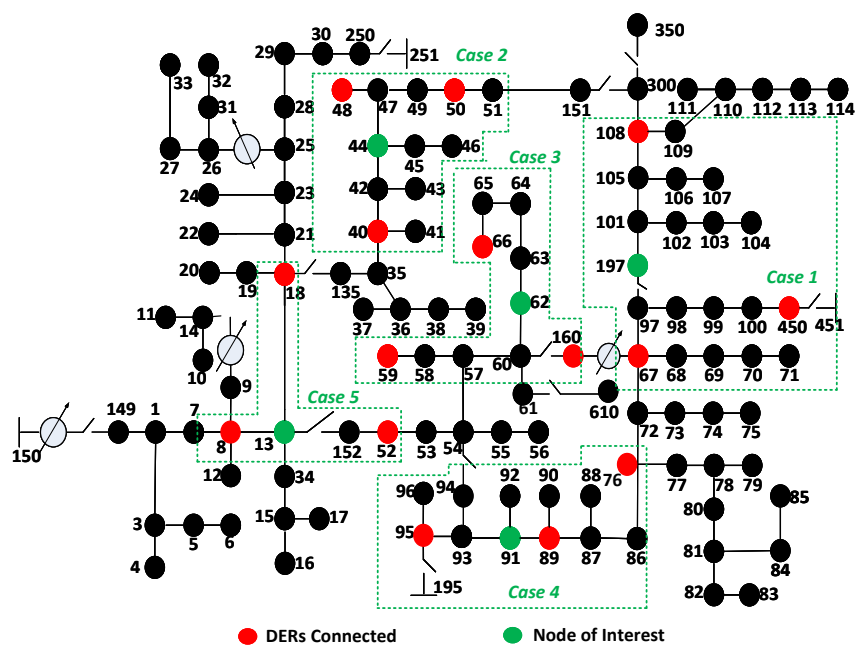


Figure 7.16: Location of DERs for different test cases.

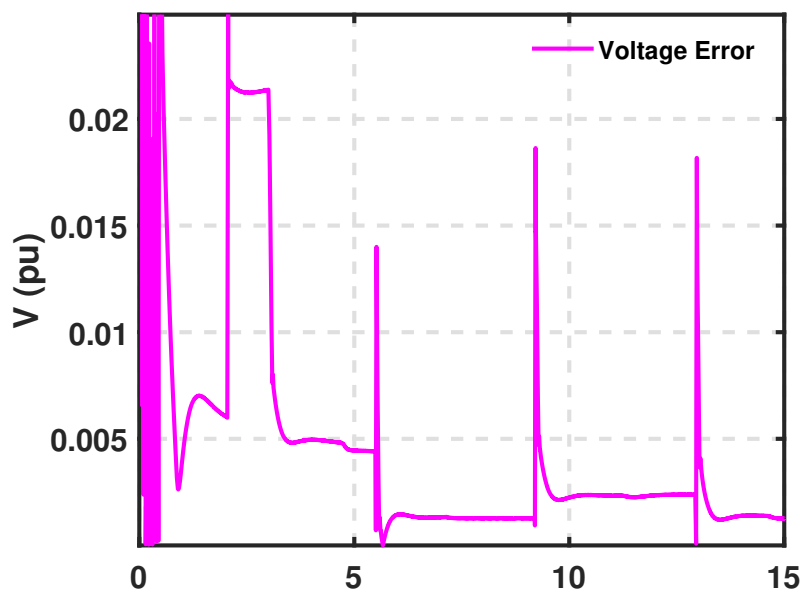


Figure 7.17: Voltage error at target node for case 1.

node. The effectiveness of controller to regulate voltage close to a reference voltage is obtained by calculating the area under the voltage error curve as shown in Fig.

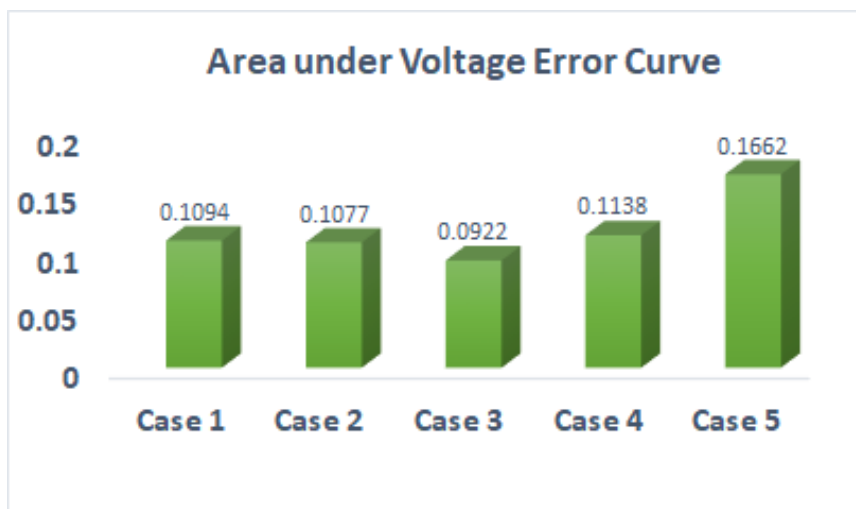


Figure 7.18: Voltage error area comparison for different cases.

7.17. The comparison of area for different test cases are depicted in Fig. 7.18 and it can be seen that voltage error area is almost similar for all the cases. Thus it can be concluded that the controller is capable of regulating target node voltages irrespective of location of the DERs in the feeder.

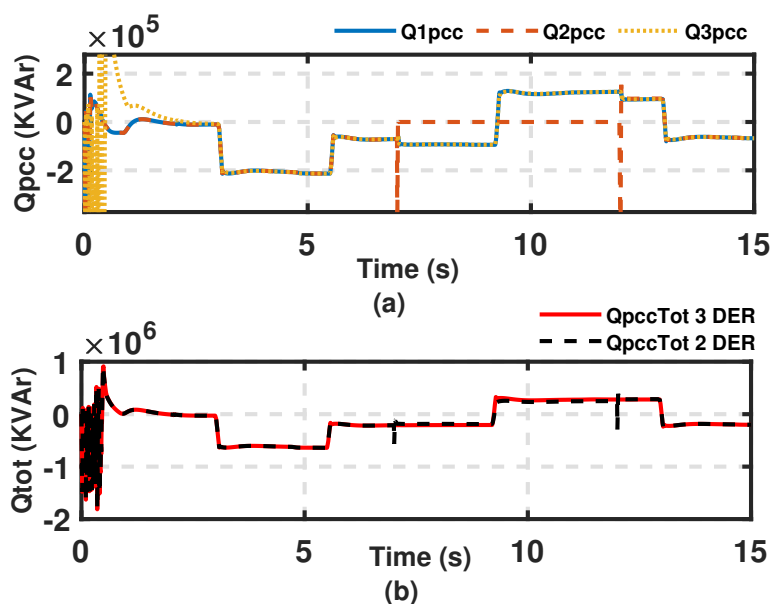


Figure 7.19: (a) Reactive power of each DER (b) Total Reactive power of DERs.

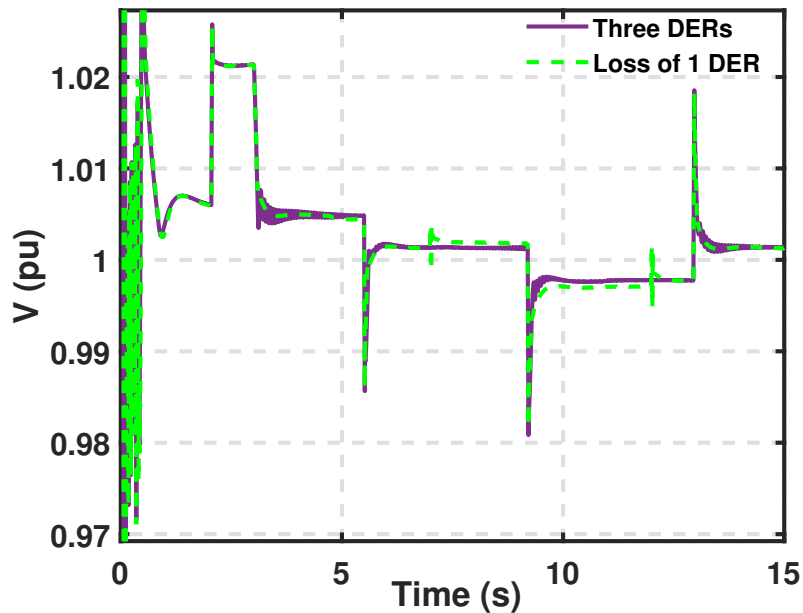


Figure 7.20: Voltage comparison at test node.

#### 7.4.4.3 Loss of DERs

In this case, effectiveness of controller during a condition with sudden loss of one or more DERs is studied. Three DERs are utilized for reactive power support to regulate voltage at node 197 to 1pu. The DER 2 is taken out at 7 sec and brought back at 12 sec. The reactive power contribution from DER 2 falls to zero at 7 sec and comes back at 12 sec as shown in Fig. 7.19a. The tertiary controller dynamically changes the output of other 2 DERs during this time. The output from DER 1 and 3 are increased at 7 sec as soon as DER 2 is lost and DER 1 and 3 outputs are reduced as soon as DER 2 comes back at 12 sec as shown in Fig. 7.19a. Also it can be seen from Fig. 7.19b that the total reactive power of all DERs remain almost same due to this change. The target voltage variation is minimal and is maintained closer to reference voltage even with the loss of 1 DER as shown in Fig. 7.20.

## 7.5 Summary

In this chapter, an algorithm that calculates the effectiveness of DER to control voltage at a particular node of interest is developed. Real-time compatible models of the IEEE 123 bus test distribution feeder with 3 DERs is used to perform case studies. The effectiveness of the algorithm is validated in simulation results, where voltage control using reactive power support results in lower voltage regulator operations and tighter voltage profiles. Also effectiveness of proposed method during scenarios like the loss of one or more DERs are analyzed.

## CHAPTER 8: CONCLUSIONS AND FUTURE WORK

This dissertation presents advanced three sequence based steady state analysis algorithms that can be used to conduct load flow, voltage stability and short circuit analysis of unbalanced distribution system. A computationally efficient load flow algorithm based on injected current sensitivity is proposed. This sequence based methodologies are then extended to analyze integrated transmission and distribution system. A multi-period power flow analysis to capture the time-varying aspects of the system is also proposed. The accuracy of proposed approaches are highlighted by comparing it with existing methods. The efficacy of these methods are validated by using a diverse array of test feeders with different scenarios. The scalability of proposed methods were proved using very large test systems like 8500 node feeder. The contributions of this thesis are as follows:

- A load flow algorithm based on injected current sensitivity (ICS) for 1 phase distribution systems with high penetration of DERs is proposed where PV type DERs can be modeled.
- The ICS-based load flow algorithm is then extended to a three-phase distribution network. Multiphase DERs with voltage control capability is modeled using a reactive power sensitivity based approach.
- An unbalanced power flow based on the sequence components frame is proposed where three-phase unbalanced power flow is decomposed into three separate sub problems. Also a three sequence continuation power flow to analyze voltage stability of distribution system is proposed.

- A multi-period power flow analysis is proposed to accurately capture the time-varying aspects of the system. A QSTS framework with detailed modeling of voltage regulators and distributed energy resources is proposed that can be used to study the impacts of DERs on the grid.
- A three sequence based fault analysis method for unbalanced distribution system is proposed.
- A universal distribution system analysis tool based on sequence component is designed.
- A unified three phase T&D modelling approach based on stacked Y-bus method is proposed. The sequence based methods developed were then used to conduct load flow, voltage stability and fault analysis of T&D system.
- A coordinated control architecture for distribution systems with multiple DERs is proposed. The method uses an ADMM based transfer function identification scheme. The algorithm is utilized for dynamic DER selection and can be used for voltage regulation using reactive power support.

This dissertation also proposes some future research directions which includes

- The three sequence based power flow approaches can be extended to optimal power flow for unbalanced distribution system.
- The multi-period method which currently can take care of load and generation variations can be extended to include fault scenarios. Even though transient may not be analyzed, this would provide a better visualization on how DER integrated power grid behaves during fault scenarios.
- The three sequence based fault analysis can be extended to analyze fault scenarios in DER integrated system with Type II, III and IV DERs.

- The effectiveness of LQR control in the proposed sensitivity based transfer function identification technique deteriorates in presence of input and state constraints. A model predictive control (MPC) framework is a good candidate which can deal with these constraints.

## LIST OF PUBLICATIONS

1. A. Suresh, S. J. Hossain, S. Abdelrazek and S. Kamalasan, "Online Power Profile Based Universal Battery Degradation Methodology Suitable for Various Battery Types," 2019 IEEE Power & Energy Society General Meeting (PESGM), Atlanta, GA, USA, 2019
2. A. Suresh, R. Bisht, and S. Kamalasan, "ADMM Based LQR for Voltage Regulation Using Distributed Energy Resources," 2020 Power Electronics, Drives and Energy Systems (PEDES), Jaipur, India
3. A. Suresh, S. Paudyal and S. Kamalasan, "A Novel Three-Phase Transmission and Unbalance Distribution Co-Simulation Power Flow Model For Long Term Voltage Stability Margin Assessment," 2021 IEEE Power & Energy Society General Meeting (PESGM) Washington, DC, USA, 2021
4. A. Suresh, K. Murari and S. Kamalasan, "Injected Current Sensitivity Based Load Flow Algorithm for Multi-Phase Distribution System in the Presence of Distributed Energy Resources," in IEEE Transactions on Power Delivery, (Under Review)
5. M. A. I. Khan, A. Suresh, S. Paudyal and S. Kamalasan, "Decoupled and Unified Approaches for Solving Transmission and Distribution Co-Simulations," 2019 North American Power Symposium (NAPS), Wichita, KS, USA, 2019
6. R. Bisht, A. Suresh and S. Kamalasan, "Multiple Single Phase Inverters Based Combined Active Power Management and Voltage Regulation of Power Distribution System Based on A Novel Optimal Control Architecture," 2019 North American Power Symposium (NAPS), Wichita, KS, USA, 2019
7. R. Bisht, A. Suresh, and S. Kamalasan, "Higher Order Identification and Control of Single Phase Inverters for Volt-Var Compensation," 2019 IEEE Power &

Energy Society General Meeting (PESGM), Montreal, Canada.

8. S. J. Hossain, T. G. Paul, R. Bisht, A. Suresh and S. Kamalasan, "An Integrated Battery Optimal Power Dispatch Architecture for End-User-Driven Microgrid in Islanded and Grid-Connected Mode of Operation," in IEEE Transactions on Industry Applications, vol. 54, no. 4, pp. 3806-3819, July-Aug. 2018,
9. A. Joshi, A. Suresh and S. Kamalasan, "Control and Dispatch of Distributed Energy Resources with Improved Frequency Regulation using Fully Active Hybrid Energy Storage System," 2020 IEEE International Conference on Power Electronics, Smart Grid and Renewable Energy (PESGRE2020), Cochin, India, 2020.
10. A. Joshi, A. Suresh and S. Kamalasan, "Grid Frequency Regulation Based on Point of Common Coupling Angle Deviation Control of Distributed Energy Resources With Fully Active Hybrid Energy Storage System," in IEEE Transactions on Industry Applications, vol. 57, no. 5, pp. 4473-4485, Sept.-Oct. 2021.
11. A. Suresh, S. Paudyal and S. Kamalasan, "A Novel Fault Analysis for Unbalanced Distribution System using Sequence Components," in IEEE Transactions on Power Delivery, (Submitted)
12. A. Suresh, S. Paudyal and S. Kamalasan, "A Novel Integrated Transmission and Distribution Continuation Power Flow Model using Sequence Components," in IEEE Transactions on Power Delivery, (Submitted)

## REFERENCES

- [1] T. . Chen, M. . Chen, T. Inoue, P. Kotas, and E. A. Chebli, “Three-phase cogenerator and transformer models for distribution system analysis,” *IEEE Transactions on Power Delivery*, vol. 6, pp. 1671–1681, Oct 1991.
- [2] H. Saadat, *Power system analysis*. CRC-Press, 2018.
- [3] V. Jalili-Marandi and J. Bélanger, “Real-time transient stability simulation of confederated transmission-distribution power grids with more than 100,000 nodes,” in *Proc. IEEE Power Energy Society General Meeting*, pp. 1–5, Aug 2018.
- [4] H. Sun, Q. Guo, B. Zhang, Y. Guo, Z. Li, and J. Wang, “Master–slave-splitting based distributed global power flow method for integrated transmission and distribution analysis,” *IEEE Transactions on Smart Grid*, vol. 6, pp. 1484–1492, May 2015.
- [5] Q. Huang and V. Vittal, “Integrated transmission and distribution system power flow and dynamic simulation using mixed three-sequence/three-phase modeling,” *IEEE Transactions on Power Systems*, vol. 32, pp. 3704–3714, Sep. 2017.
- [6] Z. Li, J. Wang, H. Sun, and Q. Guo, “Transmission contingency analysis based on integrated transmission and distribution power flow in smart grid,” *IEEE Transactions on Power Systems*, vol. 30, pp. 3356–3367, Nov 2015.
- [7] W. Kersting, *Distribution System Modeling and Analysis*. WCB/McGraw-Hill, 1999.
- [8] J. A. Martinez and J. Mahseredjian, “Load flow calculations in distribution systems with distributed resources. A review,” *IEEE Power and Energy Soety General Meeting*, pp. 1–8, 2011.
- [9] K. L. Lo and C. Zhang, “Decomposed three-phase power flow solution using the sequence component frame,” *IEE Proceedings C - Generation, Transmission and Distribution*, vol. 140, no. 3, pp. 181–188, 1993.
- [10] M. Abdel-Akher, K. M. Nor, and A. H. A. Rashid, “Improved three-phase power-flow methods using sequence components,” *IEEE Transactions on Power Systems*, vol. 20, no. 3, pp. 1389–1397, 2005.
- [11] M. J. Reno, J. Deboever, and B. Mather, “Motivation and requirements for quasi-static time series (qsts) for distribution system analysis,” in *2017 IEEE Power Energy Society General Meeting*, pp. 1–5, 2017.
- [12] R. Mahmud, A. Hoke, and D. Narang, “Fault response of distributed energy resources considering the requirements of ieee 1547-2018,” in *2020 IEEE Power Energy Society General Meeting (PESGM)*, pp. 1–5, 2020.

- [13] F. A. Viawan and D. Karlsson, "Combined local and remote voltage and reactive power control in the presence of induction machine distributed generation," *IEEE Transactions on Power Systems*, vol. 22, pp. 2003–2012, Nov 2007.
- [14] W. F. Tinney and C. E. Hart, "Power flow solution by newton's method," *IEEE Transactions on Power Apparatus and Systems*, vol. PAS-86, no. 11, pp. 1449–1460, 1967.
- [15] B. Stott and O. Alsac, "Fast decoupled load flow," *IEEE Transactions on Power Apparatus and Systems*, vol. PAS-93, no. 3, pp. 859–869, 1974.
- [16] L. Srivastava, S. Srivastava, and L. Singh, "Fast decoupled load flow methods in rectangular coordinates," *International Journal of Electrical Power & Energy Systems*, vol. 13, no. 3, pp. 160–166, 1991.
- [17] J. Nanda, D. Kothari, and S. Srivastava, "A novel second order fast decoupled load flow method in polar coordinates," *Electric Machines & Power Systems*, vol. 14, no. 5, pp. 339–351, 1988.
- [18] V. M. da Costa, N. Martins, and J. L. R. Pereira, "Developments in the newton raphson power flow formulation based on current injections," *IEEE Transactions on Power Systems*, vol. 14, no. 4, pp. 1320–1326, 1999.
- [19] P. A. N. Gara, J. L. R. Pereira, S. Carneiro, V. M. da Costa, and N. Martins, "Three-phase power flow calculations using the current injection method," *IEEE Transactions on Power Systems*, vol. 15, no. 2, pp. 508–514, 2000.
- [20] P. A. N. Gara, J. L. R. Pereira, S. Carneiro, M. P. Vinagre, and F. V. Gomes, "Improvements in the representation of pv buses on three-phase distribution power flow," *IEEE Transactions on Power Delivery*, vol. 19, no. 2, pp. 894–896, 2004.
- [21] V. M. [da Costa], M. L. [de Oliveira], and M. R. Guedes, "Developments in the analysis of unbalanced three-phase power flow solutions," *International Journal of Electrical Power Energy Systems*, vol. 29, no. 2, pp. 175 – 182, 2007.
- [22] P. A. N. Gara, J. L. R. Pereira, and S. Carneiro, "Voltage control devices models for distribution power flow analysis," *IEEE Transactions on Power Systems*, vol. 16, no. 4, pp. 586–594, 2001.
- [23] T. . Chen, M. . Chen, K. . Hwang, P. Kotas, and E. A. Chebli, "Distribution system power flow analysis-a rigid approach," *IEEE Transactions on Power Delivery*, vol. 6, no. 3, pp. 1146–1152, 1991.
- [24] J.-H. Teng, "A modified gauss–seidel algorithm of three-phase power flow analysis in distribution networks," *International Journal of Electrical Power Energy Systems*, vol. 24, no. 2, pp. 97 – 102, 2002.

- [25] J. C. M. Vieira, W. Freitas, and A. Morelato, "Phase-decoupled method for three-phase power-flow analysis of unbalanced distribution systems," *IEE Proceedings - Generation, Transmission and Distribution*, vol. 151, no. 5, pp. 568–574, 2004.
- [26] S. Ghosh and D. Das, "Method for load-flow solution of radial distribution networks," *IEE Proceedings - Generation, Transmission and Distribution*, vol. 146, no. 6, pp. 641–648, 1999.
- [27] S. Khushalani, J. M. Solanki, and N. N. Schulz, "Development of three-phase unbalanced power flow using pv and pq models for distributed generation and study of the impact of dg models," *IEEE Transactions on Power Systems*, vol. 22, no. 3, pp. 1019–1025, 2007.
- [28] K. Mahmoud and N. Yorino, "Robust quadratic-based bfs power flow method for multi-phase distribution systems," *IET Generation, Transmission Distribution*, vol. 10, no. 9, pp. 2240–2250, 2016.
- [29] Y. Ju, W. Wu, B. Zhang, and H. Sun, "An extension of fbs three-phase power flow for handling pv nodes in active distribution networks," *IEEE Transactions on Smart Grid*, vol. 5, no. 4, pp. 1547–1555, 2014.
- [30] D. Shirmohammadi, H. W. Hong, A. Semlyen, and G. Luo, "A compensation-based power flow method for weakly meshed distribution and transmission networks," *IEEE Transactions on power systems*, vol. 3, no. 2, pp. 753–762, 1988.
- [31] C. S. Cheng and D. Shirmohammadi, "A three-phase power flow method for real-time distribution system analysis," *IEEE Transactions on Power Systems*, vol. 10, no. 2, pp. 671–679, 1995.
- [32] X. Wang, M. Shahidehpour, C. Jiang, W. Tian, Z. Li, and Y. Yao, "Three-phase distribution power flow calculation for loop-based microgrids," *IEEE Transactions on Power Systems*, vol. 33, no. 4, pp. 3955–3967, 2018.
- [33] R. Verma and V. Sarkar, "Active distribution network load flow analysis through non-repetitive fbs iterations with integrated dg and transformer modelling," *IET Generation, Transmission Distribution*, vol. 13, no. 4, pp. 478–484, 2019.
- [34] T. Alinjak, I. Pavić, and M. Stojkov, "Improvement of backward/forward sweep power flow method by using modified breadth-first search strategy," *IET Generation, Transmission Distribution*, vol. 11, no. 1, pp. 102–109, 2017.
- [35] K. Murari, "Graph-theoretic based approach for the load-flow solution of three-phase distribution network in the presence of distributed generations," *IET Generation, Transmission Distribution*, vol. 14, pp. 1627–1640(13), May 2020.
- [36] U. Ghatak and V. Mukherjee, "An improved load flow technique based on load current injection for modern distribution system," *International Journal of Electrical Power & Energy Systems*, vol. 84, pp. 168–181, 2017.

- [37] J.-H. Teng, "A direct approach for distribution system load flow solutions," *IEEE Transactions on power delivery*, vol. 18, no. 3, pp. 882–887, 2003.
- [38] J.-H. Teng, "Modelling distributed generations in three-phase distribution load flow," *IET generation, transmission & distribution*, vol. 2, no. 3, pp. 330–340, 2008.
- [39] A. Marini, S. Mortazavi, L. Piegari, and M.-S. Ghazizadeh, "An efficient graph-based power flow algorithm for electrical distribution systems with a comprehensive modeling of distributed generations," *Electric Power Systems Research*, vol. 170, pp. 229–243, 2019.
- [40] K. Murari and N. P. Padhy, "A network-topology-based approach for the load-flow solution of ac–dc distribution system with distributed generations," *IEEE Transactions on Industrial Informatics*, vol. 15, no. 3, pp. 1508–1520, 2018.
- [41] A. Bokhari, A. Alkan, R. Dogan, M. Diaz-Aguiló, F. De Leon, D. Czarkowski, Z. Zabar, L. Birenbaum, A. Noel, and R. Uosef, "Experimental determination of the ZIP coefficients for modern residential, commercial, and industrial loads," *IEEE Transactions on Power Delivery*, vol. 29, no. 3, pp. 1372–1381, 2014.
- [42] EPRI, "The open distribution system simulator, openss version 7.6.5." <https://sourceforge.net/projects/electricdss/>, 2017.
- [43] W. H. Kersting and W. H. Phillips, "Distribution feeder line models," *IEEE Transactions on Industry Applications*, vol. 31, pp. 715–720, July 1995.
- [44] M. J. Gorman and J. J. Grainger, "Transformer modelling for distribution system studies. ii. addition of models to y/sub bus/ and z/sub bus/," *IEEE Transactions on Power Delivery*, vol. 7, no. 2, pp. 575–580, 1992.
- [45] M. Bazrafshan and N. Gatsis, "Comprehensive Modeling of Three-Phase Distribution Systems via the Bus Admittance Matrix," *IEEE Transactions on Power Systems*, vol. 33, no. 2, pp. 2015–2029, 2018.
- [46] W. W. Price, C. W. Taylor, G. J. Rogers, K. Srinivasan, C. Concordia, M. K. Pal, Bess, P. Kundur, B. L. Agrawal, J. F. Luini, E. Vaahedi, and B. K. Johnson, "Standard Load Models for Power Flow and Dynamic Performance Simulation," *IEEE Transactions on Power Systems*, vol. 10, no. 3, pp. 1302–1313, 1995.
- [47] M. Abdel-Akher and K. M. Nor, "Fault analysis of multiphase distribution systems using symmetrical components," *IEEE Transactions on Power Delivery*, vol. 25, no. 4, pp. 2931–2939, 2010.
- [48] Wikipedia, "Gaussian elimination." [https://en.wikipedia.org/wiki/Gaussian\\_elimination#Computational\\_efficiency](https://en.wikipedia.org/wiki/Gaussian_elimination#Computational_efficiency), 2017.
- [49] R. Broderick, J. Quiroz, M. Reno, A. Ellis, J. Smith, and R. Dugan, "Time series power flow analysis for distribution connected pv generation," 01 2013.

- [50] "Ieee approved draft guide to conducting distribution impact studies for distributed resource interconnection," *IEEE P1547.7/D11, June 2013*, pp. 1–129, 2014.
- [51] J. W. Smith, R. Dugan, and W. Sunderman, "Distribution modeling and analysis of high penetration pv," in *2011 IEEE Power and Energy Society General Meeting*, pp. 1–7, 2011.
- [52] B. A. Mather, "Quasi-static time-series test feeder for pv integration analysis on distribution systems," in *2012 IEEE Power and Energy Society General Meeting*, pp. 1–8, 2012.
- [53] M. Baggu, R. Ayyanar, and D. Narang, "Feeder model validation and simulation for high-penetration photovoltaic deployment in the arizona public service system," in *2014 IEEE 40th Photovoltaic Specialist Conference (PVSC)*, pp. 2088–2093, 2014.
- [54] A. Khoshkbar-Sadigh and K. M. Smedley, "The necessity of time-series simulation for investigation of large-scale solar energy penetration," in *2015 IEEE Power Energy Society Innovative Smart Grid Technologies Conference (ISGT)*, pp. 1–5, 2015.
- [55] M. AbdelWarth, M. Abdel-Akher, and M. Aly, "Quasi-static time-series simulation of congested power systems with wind power plant," 12 2015.
- [56] M. Kleinberg, J. Harrison, and N. Mirhosseini, "Using energy storage to mitigate pv impacts on distribution feeders," in *ISGT 2014*, pp. 1–5, 2014.
- [57] Y. P. Agalgaonkar, B. C. Pal, and R. A. Jabr, "Distribution voltage control considering the impact of pv generation on tap changers and autonomous regulators," *IEEE Transactions on Power Systems*, vol. 29, no. 1, pp. 182–192, 2014.
- [58] J. E. Quiroz, M. J. Reno, and R. J. Broderick, "Time series simulation of voltage regulation device control modes," in *2013 IEEE 39th Photovoltaic Specialists Conference (PVSC)*, pp. 1700–1705, 2013.
- [59] M. Cohen and D. Callaway, "Effects of distributed pv generation on california's distribution system, part 1: Engineering simulations," *Solar Energy*, vol. 128, pp. 126 – 138, 2016. Special issue: Progress in Solar Energy.
- [60] A. Pagnetti and G. Delille, "A simple and efficient method for fast analysis of renewable generation connection to active distribution networks," *Electric Power Systems Research*, vol. 125, pp. 133 – 140, 2015.
- [61] D. Paradis, F. Katiraei, and B. Mather, "Comparative analysis of time-series studies and transient simulations for impact assessment of pv integration on reduced ieee 8500 node feeder," in *2013 IEEE Power Energy Society General Meeting*, pp. 1–5, 2013.

- [62] P. K. Sen and S. L. Larson, "Fundamental concepts of regulating distribution system voltages," in *Proceedings of 1994 IEEE Rural Electric Power Conference*, pp. C1/1–C110, April 1994.
- [63] W. H. Kersting, "Distribution feeder voltage regulation control," *IEEE Transactions on Industry Applications*, vol. 46, pp. 620–626, March 2010.
- [64] W. Kersting, *Distribution System Modeling and Analysis*. The Electric Power System Engineering Series, CRC Press, 2002.
- [65] H. Saadat, *Power system analysis*. WCB/McGraw-Hill, 1999.
- [66] J. M. C. Filho, R. C. Leborgne, P. M. da Silveira, and M. H. Bollen, "Voltage sag index calculation: Comparison between time-domain simulation and short-circuit calculation," *Electric Power Systems Research*, vol. 78, no. 4, pp. 676–682, 2008.
- [67] K. Gampa, S. A. Vemprala, and S. M. Brahma, "Errors in fault analysis of power distribution systems using sequence components approach," in *IEEE PES T D 2010*, pp. 1–6, 2010.
- [68] K. H. Oon, C. Tan, A. Bakar, H. S. Che, H. Mokhlis, and H. Illias, "Establishment of fault current characteristics for solar photovoltaic generator considering low voltage ride through and reactive current injection requirement," *Renewable and Sustainable Energy Reviews*, vol. 92, pp. 478–488, 2018.
- [69] S. Report, J. R. Williams, and B. Karlson, "Wind power plant short-circuit modeling guide," 2012.
- [70] A. Haddadi, M. Zhao, I. Kocar, U. Karaagac, K. W. Chan, and E. Farantatos, "Impact of inverter-based resources on negative sequence quantities-based protection elements," *IEEE Transactions on Power Delivery*, vol. 36, no. 1, pp. 289–298, 2021.
- [71] A. Haddadi, E. Farantatos, I. Kocar, and U. Karaagac, "Impact of inverter based resources on system protection," *Energies*, vol. 14, no. 4, 2021.
- [72] A. Haddadi, I. Kocar, J. Mahseredjian, U. Karaagac, and E. Farantatos, "Negative sequence quantities-based protection under inverter-based resources challenges and impact of the german grid code," 06 2020.
- [73] L. V. Strezoski, B. Dumnic, B. Popadic, M. Prica, and K. A. Loparo, "Novel fault models for electronically coupled distributed energy resources and their laboratory validation," *IEEE Transactions on Power Systems*, vol. 35, no. 2, pp. 1209–1217, 2020.
- [74] W.-M. Guo, L.-H. Mu, and X. Zhang, "Fault models of inverter-interfaced distributed generators within a low-voltage microgrid," *IEEE Transactions on Power Delivery*, vol. 32, no. 1, pp. 453–461, 2017.

- [75] L. V. Strezoski, M. D. Prica, and K. A. Loparo, "Generalized  $\delta$ -circuit concept for integration of distributed generators in online short-circuit calculations," *IEEE Transactions on Power Systems*, vol. 32, pp. 3237–3245, 2017.
- [76] NERC, "Distributed energy resources connection, modeling and reliability considerations," 11 2016.
- [77] V.-A.-N. 4120, "Technical requirements for the connection and operation of customer installations to the high voltage network," 2015.
- [78] I. Erlich, T. Neumann, F. Shewarega, P. Schegner, and J. Meyer, "Wind turbine negative sequence current control and its effect on power system protection," in *2013 IEEE Power Energy Society General Meeting*, pp. 1–5, 2013.
- [79] E. Makram, M. Bou-Rabee, and A. Girgis, "Three-phase modeling of unbalanced distribution systems during open conductors and/or shunt fault conditions using the bus impedance matrix," *Electric Power Systems Research*, vol. 13, no. 3, pp. 173–183, 1987.
- [80] W. H. Kersting and G. Shirek, "Short circuit analysis of ieeec test feeders," in *PES T D 2012*, pp. 1–9, 2012.
- [81] R. F. Arritt and R. C. Dugan, "Matching the ieeec test feeder short circuit results," in *PES T D 2012*, pp. 1–7, 2012.
- [82] K. Kalsi, J. Fuller, F. Tuffner, J. Lian, W. Zhang, L. Marinovici, A. Fisher, F. Chassin, and M. Hauer, "Integrated transmission and distribution control (pacific northwest nat. lab., richland, wa, usa, pnnl- 22157.)," 01 2013.
- [83] H. Sun, Q. Guo, B. Zhang, Y. Guo, Z. Li, and J. Wang, "Master–slave-splitting based distributed global power flow method for integrated transmission and distribution analysis," *IEEE Transactions on Smart Grid*, vol. 6, pp. 1484–1492, May 2015.
- [84] B. Palmintier, E. Hale, T. Hansen, W. Jones, D. Biagioni, K. Baker, H. Wu, J. Giraldez, H. Sorensen, M. Lunacek, N. Merket, J. Jorgenson, and B.-M. Hodge, "Integrated distribution-transmission analysis for very high penetration solar pv (final technical report)," 01 2016.
- [85] H. Jain, K. Rahimi, A. Tbaileh, R. P. Broadwater, A. K. Jain, and M. Dilek, "Integrated transmission and distribution system modeling and analysis: Need and advantages," in *2016 IEEE Power and Energy Society General Meeting (PESGM)*, pp. 1–5, July 2016.
- [86] L. Wen-zhuo, H. Jun-xian, T. Yong, W. Lei, S. Xin-li, and F. Sheng-tao, "An electromechanical/electromagnetic transient hybrid simulation method that considers asymmetric faults in an electromechanical network," in *2011 IEEE/PES Power Systems Conference and Exposition*, pp. 1–7, March 2011.

- [87] Q. Huang and V. Vittal, "Application of electromagnetic transient-transient stability hybrid simulation to fidvr study," *IEEE Transactions on Power Systems*, vol. 31, pp. 2634–2646, July 2016.
- [88] B. Palmintier, E. Hale, B. Hodge, K. Baker, and T. M. Hansen, "Experiences integrating transmission and distribution simulations for ders with the integrated grid modeling system (igms)," in *2016 Power Systems Computation Conference (PSCC)*, pp. 1–7, June 2016.
- [89] J. M. Marinho and G. Taranto, "A hybrid three-phase single-phase power flow formulation," in *2009 IEEE Power Energy Society General Meeting*, pp. 1–1, July 2009.
- [90] Z. Li, J. Wang, H. Sun, and Q. Guo, "Transmission contingency analysis based on integrated transmission and distribution power flow in smart grid," *IEEE Transactions on Power Systems*, vol. 30, pp. 3356–3367, Nov 2015.
- [91] P. Aristidou and T. V. Cutsem, "A parallel processing approach to dynamic simulations of combined transmission and distribution systems," *International Journal of Electrical Power Energy Systems*, vol. 72, pp. 58 – 65, 2015. The Special Issue for 18th Power Systems Computation Conference.
- [92] Y. Zhang, A. Allen, and B. Hodge, "Impact of distribution-connected large-scale wind turbines on transmission system stability during large disturbances," in *2014 IEEE PES General Meeting | Conference Exposition*, pp. 1–5, July 2014.
- [93] K. Anderson, J. Du, A. Narayan, and A. E. Gamal, "Gridspice: A distributed simulation platform for the smart grid," *IEEE Transactions on Industrial Informatics*, vol. 10, pp. 2354–2363, Nov 2014.
- [94] Q. Huang and V. Vittal, "Integrated transmission and distribution system power flow and dynamic simulation using mixed three-sequence/three-phase modeling," *IEEE Transactions on Power Systems*, vol. 32, pp. 3704–3714, Sept 2017.
- [95] R. Venkatraman, S. K. Khaitan, and V. Ajjarapu, "A combined transmission-distribution system dynamic model with grid-connected dg inverter," in *2017 IEEE Power Energy Society General Meeting*, pp. 1–5, July 2017.
- [96] H. Jain, B. Palmintier, I. Krad, and D. Krishnamurthy, "Studying the impact of distributed solar pv on power systems using integrated transmission and distribution models," in *2018 IEEE/PES Transmission and Distribution Conference and Exposition (T D)*, pp. 1–5, April 2018.
- [97] P. Evans, "Integrated transmission and distribution model for assessment of distributed wholesale photovoltaic generation," 4 2013.
- [98] M. Dilek, F. de Leon, R. Broadwater, and S. Lee, "A robust multiphase power flow for general distribution networks," *IEEE Transactions on Power Systems*, vol. 25, pp. 760–768, May 2010.

- [99] B. Palmintier, D. Krishnamurthy, P. Top, S. Smith, J. Daily, and J. Fuller, "Design of the helics high-performance transmission-distribution-communication-market co-simulation framework," in *2017 Workshop on Modeling and Simulation of Cyber-Physical Energy Systems (MSCPES)*, pp. 1–6, April 2017.
- [100] A. K. Bharati and V. Ajjarapu, "Investigation of relevant distribution system representation with dg for voltage stability margin assessment," *IEEE Transactions on Power Systems*, vol. 35, no. 3, pp. 2072–2081, 2020.
- [101] A. Singhal and V. Ajjarapu, "Long-term voltage stability assessment of an integrated transmission distribution system," in *2017 North American Power Symposium (NAPS)*, pp. 1–6, 2017.
- [102] A. R. R. Matavalam, A. Singhal, and V. Ajjarapu, "Identifying long term voltage stability caused by distribution systems vs transmission systems," 2018.
- [103] Xiao-Ping Zhang, Ping Ju, and E. Handschin, "Continuation three-phase power flow: a tool for voltage stability analysis of unbalanced three-phase power systems," *IEEE Transactions on Power Systems*, vol. 20, no. 3, pp. 1320–1329, 2005.
- [104] IEEE, "Distribution test feeders." <https://site.ieee.org/pes-testfeeders/>, 2017.
- [105] M. A. Hossain, H. R. Pota, W. Issa, and J. Hossain, "Overview of ac microgrid controls with inverter-interfaced generations," 2017.
- [106] S. Okada and S. Masuda, "Data-driven minimum variance control using regulatory closed-loop data based on the frit method," in *2017 56th Annual Conference of the Society of Instrument and Control Engineers of Japan (SICE)*, pp. 253–254, Sep. 2017.
- [107] T. Sansawatt, L. F. Ochoa, and G. P. Harrison, "Smart decentralized control of dg for voltage and thermal constraint management," *IEEE Transactions on Power Systems*, vol. 27, pp. 1637–1645, Aug 2012.
- [108] H. J. Liu, W. Shi, and H. Zhu, "Dynamic decentralized voltage control for power distribution networks," in *2016 IEEE Statistical Signal Processing Workshop (SSP)*, pp. 1–5, June 2016.
- [109] T. M. Sobhy, N. G. A. Hemdan, M. M. Hamada, and M. A. A. Wahab, "Coordinated reactive power management in distribution networks with renewable energy resources," in *2016 Eighteenth International Middle East Power Systems Conference (MEPCON)*, pp. 837–842, Dec 2016.
- [110] A. G. Madureira and J. A. P. Lopes, "Coordinated voltage support in distribution networks with distributed generation and microgrids," *IET Renewable Power Generation*, vol. 3, pp. 439–454, December 2009.

- [111] J. Barr and R. Majumder, "Integration of distributed generation in the volt/var management system for active distribution networks," *IEEE Transactions on Smart Grid*, vol. 6, pp. 576–586, March 2015.
- [112] K. Alobeidli and M. S. E. Moursi, "Novel coordinated secondary voltage control strategy for efficient utilisation of distributed generations," *IET Renewable Power Generation*, vol. 8, pp. 569–579, July 2014.
- [113] J. Miret, A. Camacho, M. Castilla, L. G. de Vicuna, and J. Matas, "Control scheme with voltage support capability for distributed generation inverters under voltage sags," *IEEE Transactions on Power Electronics*, vol. 28, no. 11, pp. 5252–5262, 2013.
- [114] R. Bisht, S. Subramaniam, R. Bhattarai, and S. Kamalasan, "Active and reactive power control of single phase inverter with seamless transfer between grid-connected and islanded mode," in *2018 IEEE Power and Energy Conference at Illinois (PECI)*, pp. 1–8, 2018.
- [115] R. Bisht, R. Bhattarai, S. Subramaniam, and S. Kamalasan, "A novel synchronously rotating reference frame based adaptive control architecture for enhanced grid support functions of single-phase inverters," *IEEE Transactions on Industry Applications*, vol. 56, no. 4, pp. 4288–4298, 2020.
- [116] R. Bisht, A. Suresh, and S. Kamalasan, "Multiple single phase inverters based combined active power management and voltage regulation of power distribution system based on a novel optimal control architecture," in *2019 North American Power Symposium (NAPS)*, pp. 1–6, 2019.
- [117] H. Hooshyar, L. Vanfretti, and C. Dufour, "Delay-free parallelization for real-time simulation of a large active distribution grid model," in *IECON 2016 - 42nd Annual Conference of the IEEE Industrial Electronics Society*, pp. 6278–6284, Oct 2016.
- [118] H. Hooshyar, F. Mahmood, L. Vanfretti, and M. Baudette, "Specification, implementation, and hardware-in-the-loop real-time simulation of an active distribution grid," *Sustainable Energy, Grids and Networks*, vol. 3, pp. 36 – 51, 2015.
- [119] C. Hani.Saad, Jean.Mahseredjian, and Jean.Bélanger, "Custom-coded models in the state space nodal solver of artemis," in *International Conference on Power Systems Transients*, pp. 6278–6284, Jul 2013.
- [120] N. Roy, H. Pota, and M. Hossain, "Reactive power management of distribution networks with wind generation for improving voltage stability," *Renewable Energy*, vol. 58, pp. 85 – 94, 2013.
- [121] A. Abessi, V. Vahidinasab, and M. S. Ghazizadeh, "Centralized support distributed voltage control by using end-users as reactive power support," *IEEE Transactions on Smart Grid*, vol. 7, pp. 178–188, Jan 2016.

- [122] A. Thakallapelli and S. Kamalasadán, “Alternating direction method of multipliers (admm) based distributed approach for wide-area control,” in *2017 IEEE Industry Applications Society Annual Meeting*, pp. 1–7, Oct 2017.
- [123] S. Boyd, N. Parikh, E. Chu, B. Peleato, and J. Eckstein, “Distributed optimization and statistical learning via the alternating direction method of multipliers,” *Foundations and Trends in Machine Learning*, vol. 3, no. 1, pp. 1–122, 2010.
- [124] A. Thakallapelli and S. Kamalasadán, “Alternating direction method of multipliers (admm) based distributed approach for wide-area control,” *IEEE Transactions on Industry Applications*, vol. 55, pp. 3215–3227, May 2019.
- [125] W. H. Kersting, “Radial distribution test feeders,” in *2001 IEEE Power Engineering Society Winter Meeting. Conference Proceedings (Cat. No.01CH37194)*, vol. 2, pp. 908–912 vol.2, Jan 2001.

## APPENDIX A: Fault Analysis on IEEE Test Distribution Feeders

The complete data for IEEE radial distribution feeders discussed here has been presented in [125]. The one line diagram of each are shown in Figs A.1, A.2, and A.3.

The fault current values of all 10 types of faults are discussed in this section.

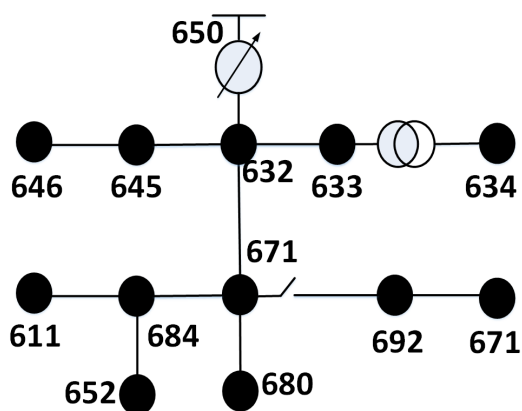


Figure A.1: IEEE 13 Bus Distribution Test Feeder

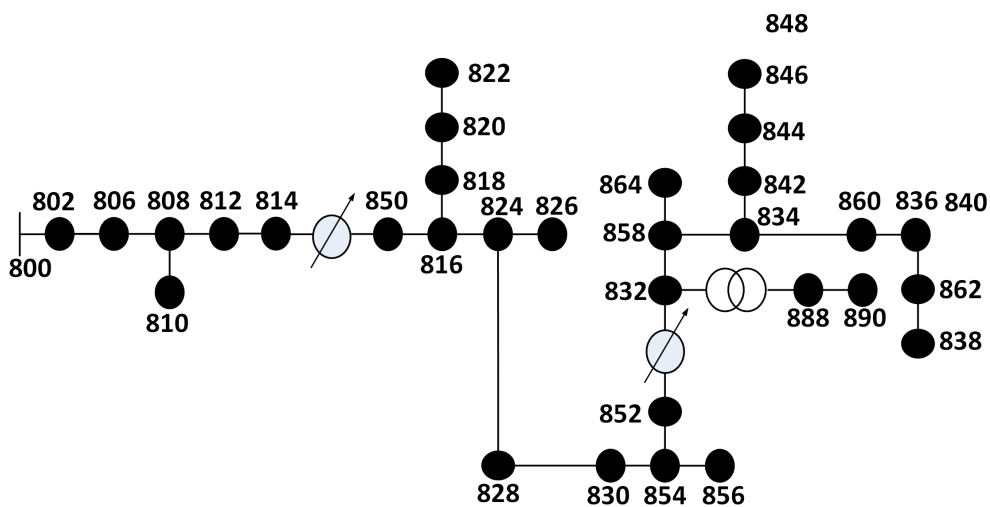


Figure A.2: IEEE 34 Bus Distribution Test Feeder

Table A.1: LLLG and SLG Fault currents in Amps for IEEE 13 bus system

Node	Phase	LLLG			SLG		
		A	B	C	A	B	C
150	ABC	13700.2	13700.2	13700.2	10952.7	10952.7	10952.7
650	ABC	8416.0	8416.0	8416.0	8478.8	8478.8	8478.8
692	ABC	3317.4	3268.0	3009.5	2196.4	2156.9	2173.9
684	AC	-	-	-	2019.5	-	2001.7
680	ABC	2880.6	2836.8	2589.5	1851.9	1817.0	1832.0
675	ABC	3091.5	3087.0	2816.3	2076.9	2049.9	2057.5
671	ABC	3317.4	3268.0	3009.5	2196.4	2156.9	2173.9
652	A	-	-	-	1795.7	-	-
634	ABC	15190.8	15149.6	14796.1	13046.4	12961.6	12985.8
633	ABC	4115.5	4028.2	3837.0	2950.5	2910.3	2921.7
632	ABC	4759.0	4698.0	4449.1	3495.4	3444.4	3466.4
645	BC	-	-	-	-	2806.5	2817.8
646	BC	-	-	-	-	2516.5	2524.2
611	C	-	-	-	-	-	1852.0

Table A.2: LL Fault currents in Amps for IEEE 13 bus system

Node	Phase	LL (AB)		LL (BC)		LL (CA)	
		A	B	B	C	A	C
150	ABC	11865	11865	11865	11865	11865	11865
650	ABC	7289	7289	7289	7289	7289	7289
692	ABC	2938	2938	2600	2600	2735	2735
684	AC	-	-	-	-	2518	2518
680	ABC	2555	2555	2239	2239	2364	2364
675	ABC	2752	2752	2456	2456	2552	2552
671	ABC	2938	2938	2600	2600	2735	2735
652	A	-	-	-	-	-	-
634	ABC	13236	13236	12782	12782	13057	13057
633	ABC	3586	3586	3298	3298	3469	3469
632	ABC	4195	4195	3836	3836	3982	3982
645	BC	-	-	3191	3191	-	-
646	BC	-	-	2882	2882	-	-
611	C	-	-	-	-	-	-



Table A.4: LLLG and SLG Fault currents in Amps for IEEE 34 bus system

Node	Phase	LLLG			SLG		
		A	B	C	A	B	C
150	ABC	1733.0	1732.9	1733.2	1262.0	1261.9	1262.0
800	ABC	627.1	627.2	627.2	655.6	655.5	655.6
802	ABC	614.2	614.1	613.6	634.1	633.7	633.8
806	ABC	605.7	605.6	604.7	620.2	619.6	619.8
808	ABC	471.7	473.7	465.2	431.4	429.7	430.4
810	B	-	-	-	-	397.5	-
812	ABC	366.7	371.1	358.6	312.9	311.3	311.9
814	ABC	309.3	314.7	301.4	255.8	254.5	255.0
850	ABC	309.3	314.6	301.4	255.8	254.4	255.0
816	ABC	308.7	314.0	300.8	255.2	253.9	254.4
818	A	-	-	-	251.3	-	-
820	A	-	-	-	172.5	-	-
822	A	-	-	-	157.9	-	-
824	ABC	288.8	294.5	281.4	237.2	235.9	236.4
826	B	-	-	-	-	230.0	-
828	ABC	287.2	293.0	279.9	235.8	234.6	235.0
830	ABC	253.7	259.8	247.4	206.3	205.3	205.7
854	ABC	252.9	259.1	246.6	205.7	204.7	205.0
852	ABC	208.0	214.2	203.0	167.5	166.8	167.0
832	ABC	207.9	214.2	203.0	167.5	166.8	167.0
858	ABC	203.1	209.3	198.3	163.4	162.7	162.9
834	ABC	197.5	203.7	192.9	158.8	158.2	158.4
842	ABC	197.3	203.4	192.7	158.6	158.0	158.2
844	ABC	196.0	202.2	191.5	157.6	157.0	157.1
846	ABC	192.8	198.9	188.3	154.9	154.3	154.4
848	ABC	192.3	198.4	187.8	154.5	153.9	154.1
860	ABC	195.7	201.8	191.1	157.3	156.7	156.8
836	ABC	193.3	199.4	188.8	155.3	154.7	154.9
840	ABC	192.5	198.6	188.0	154.7	154.1	154.2
862	ABC	193.0	199.2	188.5	155.1	154.5	154.7
838	B	-	-	-	-	151.0	-
864	A	-	-	-	161.8	-	-
888	ABC	702.4	711.1	691.4	615.0	612.5	612.8
890	ABC	392.5	403.6	382.4	315.7	314.1	314.3
856	B	-	-	-	-	173.3	-

Table A.5: LL Fault currents in Amps for IEEE 34 bus system

Node	Phase	LL (AB)		LL (BC)		LL (CA)	
		A	B	B	C	A	C
150	ABC	1500.7	1500.7	1500.8	1500.8	1501.0	1501.0
800	ABC	543.1	543.1	543.2	543.2	543.2	543.2
802	ABC	532.4	532.4	531.1	531.1	531.7	531.7
806	ABC	525.3	525.3	523.2	523.2	524.2	524.2
808	ABC	412.6	412.6	402.0	402.0	406.7	406.7
810	B	-	-	-	-	-	-
812	ABC	322.7	322.7	310.4	310.4	315.9	315.9
814	ABC	273.1	273.1	261.3	261.3	266.6	266.6
850	ABC	273.1	273.1	261.3	261.3	266.6	266.6
816	ABC	272.5	272.5	260.8	260.8	266.0	266.0
818	A	-	-	-	-	-	-
820	A	-	-	-	-	-	-
822	A	-	-	-	-	-	-
824	ABC	255.2	255.2	244.1	244.1	249.1	249.1
826	B	-	-	-	-	-	-
828	ABC	253.8	253.8	242.8	242.8	247.8	247.8
830	ABC	224.6	224.6	214.9	214.9	219.3	219.3
854	ABC	223.9	223.9	214.2	214.2	218.6	218.6
852	ABC	184.4	184.4	176.6	176.6	180.2	180.2
832	ABC	184.4	184.4	176.6	176.6	180.2	180.2
858	ABC	180.1	180.1	172.5	172.5	176.0	176.0
834	ABC	175.3	175.3	167.9	167.9	171.3	171.3
842	ABC	175.0	175.0	167.7	167.7	171.0	171.0
844	ABC	173.9	173.9	166.6	166.6	170.0	170.0
846	ABC	171.1	171.1	163.9	163.9	167.2	167.2
848	ABC	170.7	170.7	163.5	163.5	166.8	166.8
860	ABC	173.6	173.6	166.3	166.3	169.7	169.7
836	ABC	171.5	171.5	164.3	164.3	167.6	167.6
840	ABC	170.8	170.8	163.7	163.7	167.0	167.0
862	ABC	171.3	171.3	164.1	164.1	167.4	167.4
838	B	-	-	-	-	-	-
864	A	-	-	-	-	-	-
888	ABC	616.3	616.3	599.0	599.0	607.2	607.2
890	ABC	347.9	347.9	332.7	332.7	339.6	339.6
856	B	-	-	-	-	-	-

Table A.6: LLG Fault currents in Amps for IEEE 34 bus system

Node	Phase	LLG (AB)		LLG (BC)		LLG (CA)	
		A	B	B	C	A	C
806	ABC	611.1	615.7	610.1	614.6	615.3	610.5
808	ABC	456.3	457.7	450.5	447.8	452.4	453.0
810	B	-	-	-	-	-	-
812	ABC	344.0	355.2	337.2	342.1	347.8	340.2
814	ABC	285.8	300.9	279.4	287.7	293.4	282.2
850	ABC	285.8	300.9	279.4	287.7	293.4	282.2
816	ABC	285.2	300.3	278.8	287.1	292.8	281.6
818	A	-	-	-	-	-	-
820	A	-	-	-	-	-	-
822	A	-	-	-	-	-	-
824	ABC	265.2	282.0	259.4	269.3	274.8	261.9
826	B	-	-	-	-	-	-
828	ABC	263.6	280.6	257.9	268.0	273.4	260.4
830	ABC	230.6	249.6	225.9	238.0	243.0	228.0
854	ABC	229.8	248.9	225.2	237.3	242.3	227.3
852	ABC	186.5	206.6	183.2	196.8	201.1	184.7
832	ABC	186.5	206.6	183.2	196.8	201.1	184.7
858	ABC	181.9	202.0	178.7	192.4	196.5	180.2
834	ABC	176.7	196.7	173.7	187.4	191.4	175.0
842	ABC	176.4	196.5	173.4	187.1	191.2	174.8
844	ABC	175.2	195.3	172.3	186.0	190.0	173.7
846	ABC	172.2	192.2	169.3	183.0	187.0	170.6
848	ABC	171.7	191.8	168.9	182.6	186.6	170.2
860	ABC	174.9	195.0	172.0	185.7	189.7	173.3
836	ABC	172.6	192.7	169.8	183.5	187.5	171.1
840	ABC	171.9	192.0	169.1	182.8	186.8	170.4
862	ABC	172.4	192.4	169.5	183.3	187.2	170.9
838	B	-	-	-	-	-	-
864	A	-	-	-	-	-	-
888	ABC	656.7	688.7	649.2	668.9	678.3	652.2
890	ABC	352.3	389.2	345.5	370.4	378.9	348.2
856	B	-	-	-	-	-	-

Table A.7: LLLG and SLG Fault currents in Amps for IEEE 123 bus system

Node	Phase	LLLG			SLG		
		A	B	C	A	B	C
650	ABC	13700.2	13700.2	13700.2	10952.7	10952.7	10952.7
150	ABC	8416.0	8416.0	8416.0	8478.8	8478.8	8478.8
149	ABC	8416.0	8416.0	8416.0	8478.8	8478.8	8478.8
1	ABC	7123.9	7246.1	7092.9	6501.6	6538.5	6517.5
7	ABC	6381.3	6560.3	6335.4	5525.1	5571.1	5544.9
8	ABC	5964.3	6169.7	5912.3	5020.2	5068.6	5041.1
13	ABC	5429.5	5662.2	5372.2	4413.5	4462.8	4434.7
152	ABC	5429.5	5662.2	5372.2	4413.5	4462.8	4434.7
52	ABC	4846.8	5100.5	4787.3	3799.5	3847.6	3820.2
53	ABC	4599.1	4858.7	4539.7	3551.9	3599.1	3572.2
54	ABC	4456.4	4718.8	4397.5	3412.9	3459.3	3432.9
55	ABC	4171.4	4437.1	4113.7	3142.1	3186.8	3161.3
56	ABC	3920.0	4186.8	3864.0	2910.9	2953.9	2929.4
57	ABC	4083.4	4318.4	4089.1	3078.4	3112.8	3098.4
60	ABC	3464.0	3653.1	3554.2	2543.4	2562.3	2562.4
160	ABC	3464.0	3653.1	3554.2	2543.4	2562.3	2562.4
67	ABC	3255.0	3396.7	3335.9	2350.7	2368.5	2370.8
72	ABC	3094.1	3226.6	3191.8	2219.8	2234.4	2239.1
76	ABC	2986.9	3113.1	3094.5	2133.3	2146.0	2152.2
77	ABC	2810.4	2899.1	2905.3	1977.8	1990.0	1997.1
78	ABC	2769.6	2850.0	2861.6	1942.4	1954.5	1961.7
79	ABC	2682.0	2745.5	2768.0	1867.2	1879.0	1886.6
80	ABC	2591.1	2637.9	2670.9	1790.1	1801.6	1809.5
81	ABC	2434.6	2455.0	2504.1	1660.0	1671.0	1679.2
82	ABC	2359.7	2368.5	2424.5	1598.8	1609.5	1617.9
83	ABC	2289.3	2287.8	2349.8	1541.9	1552.4	1560.8
86	ABC	2664.1	2771.8	2796.0	1877.3	1884.9	1894.7
87	ABC	2506.7	2580.3	2622.2	1741.7	1749.4	1759.2
89	ABC	2419.5	2475.8	2526.3	1668.0	1675.7	1685.6
91	ABC	2352.6	2396.3	2452.9	1612.2	1619.9	1629.8
93	ABC	2289.4	2321.7	2383.7	1560.0	1567.7	1577.5
95	ABC	2210.3	2229.1	2297.3	1495.4	1503.0	1512.9
97	ABC	3108.1	3241.3	3204.4	2231.1	2245.9	2250.5
197	ABC	3108.1	3241.3	3204.4	2231.1	2245.9	2250.5
101	ABC	2974.0	3099.5	3082.8	2123.0	2135.4	2141.8
105	ABC	2839.3	2957.1	2959.2	2015.6	2025.8	2033.8
108	ABC	2695.2	2804.7	2825.2	1901.8	1909.8	1919.3
300	ABC	2331.6	2420.7	2479.5	1620.3	1623.8	1635.8
98	ABC	2961.2	3086.0	3071.1	2112.8	2125.0	2131.5
99	ABC	2705.8	2815.9	2835.1	1910.1	1918.3	1927.6

Table A.8: LLLG and SLG Fault currents in Amps for IEEE 123 bus system(cont.)

Node	Phase	LLLG			SLG		
		A	B	C	A	B	C
100	ABC	2584.3	2687.5	2721.0	1815.1	1821.6	1832.0
450	ABC	2308.3	2396.0	2456.9	1602.5	1605.8	1617.9
61	ABC	3151.9	3304.6	3186.4	2258.7	2267.9	2270.4
611	ABC	3151.9	3304.6	3186.4	2258.7	2267.9	2270.4
610	ABC	4924.9	4969.2	4946.6	4603.1	4607.2	4608.3
62	ABC	3274.9	3465.0	3367.8	2395.8	2415.2	2412.0
63	ABC	3149.5	3339.0	3243.9	2298.5	2317.8	2312.9
64	ABC	2916.8	3102.8	3013.3	2119.0	2137.7	2130.5
65	ABC	2665.9	2845.1	2763.4	1927.3	1944.9	1936.2
66	ABC	2496.0	2668.8	2593.2	1798.6	1815.0	1806.0
18	ABC	4444.2	4475.2	4300.3	3327.8	3344.3	3320.9
135	ABC	4444.2	4475.2	4300.3	3327.8	3344.3	3320.9
35	ABC	4047.7	4115.8	3965.3	2988.3	3005.4	2979.9
40	ABC	3830.3	3917.8	3751.6	2796.1	2815.0	2790.5
42	ABC	3634.8	3737.9	3559.8	2627.1	2647.3	2623.7
44	ABC	3492.1	3605.4	3419.8	2505.9	2526.7	2503.9
47	ABC	3328.7	3452.2	3259.7	2369.2	2390.6	2368.6
48	ABC	3232.8	3361.2	3178.7	2294.8	2315.7	2293.6
49	ABC	3171.9	3303.1	3127.0	2247.7	2268.3	2246.1
50	ABC	3029.1	3166.4	3004.9	2138.1	2158.0	2135.6
51	ABC	2898.5	3040.5	2892.1	2038.6	2057.8	2035.5
151	ABC	2668.2	2816.6	2690.3	1865.0	1882.9	1860.9
21	ABC	4169.5	4157.0	4009.2	3053.8	3064.4	3042.4
23	ABC	3965.3	3924.2	3795.0	2857.5	2864.4	2843.5
25	ABC	3762.5	3696.2	3584.2	2668.7	2672.5	2652.7
28	ABC	3627.6	3546.3	3445.0	2546.3	2548.3	2529.2
29	ABC	3442.4	3342.9	3255.2	2382.3	2382.1	2364.0
30	ABC	3248.8	3133.0	3058.5	2215.7	2213.6	2196.6
250	ABC	3147.6	3024.5	2956.4	2130.6	2127.6	2111.2

Table A.9: SLG Fault currents in Amps for IEEE 123 bus system

SLG								
Node	Phase		Node	Phase		Node	Phase	
68	A	2210	2	B	5704	3	C	5386
69	A	2040	12	B	4408	4	C	4703
70	A	1868	58	B	2817	5	C	4350
71	A	1742	59	B	2569	6	C	3775
88	A	1672	90	B	1594	73	C	2066
94	A	1474	96	B	1444	74	C	1878
109	A	1702	106	B	1907	75	C	1699
110	A	1590	107	B	1656	84	C	1452
111	A	1408	36	AB	2551	85	C	1324
112	A	1547	38	B	2348	92	C	1527
113	A	1388	39	B	2124	102	C	2010
114	A	1304	43	B	2242	103	C	1844
36	AB	2535	22	B	2514	104	C	1561
37	A	2298				41	C	2486
45	A	2347				24	C	2344
46	A	2140				26	AC	2446
19	A	2994				27	AC	2304
20	A	2641				31	C	2276
26	AC	2457				32	C	2081
27	AC	2313				34	C	4078
33	A	1997				15	C	3867
9	A	4373				16	C	3225
14	A	3487				17	C	3262
10	A	3106						
11	A	3106						

Table A.10: LL Fault currents in Amps for IEEE 123 bus system

Node	Phase	LL (AB)		LL (BC)		LL (CA)	
		A	B	B	C	A	C
650	ABC	11864.7	11864.7	11864.7	11864.7	11864.7	11864.7
150	ABC	7288.5	7288.5	7288.5	7288.5	7288.5	7288.5
149	ABC	7288.5	7288.5	7288.5	7288.5	7288.5	7288.5
1	ABC	6285.0	6285.0	6185.1	6185.1	6112.4	6112.4
7	ABC	5689.2	5689.2	5548.1	5548.1	5447.0	5447.0
8	ABC	5348.6	5348.6	5189.8	5189.8	5076.8	5076.8
13	ABC	4905.7	4905.7	4729.6	4729.6	4605.6	4605.6
152	ABC	4905.7	4905.7	4729.6	4729.6	4605.6	4605.6
52	ABC	4415.2	4415.2	4227.4	4227.4	4096.7	4096.7
53	ABC	4204.1	4204.1	4013.7	4013.7	3881.8	3881.8
54	ABC	4082.0	4082.0	3890.7	3890.7	3758.4	3758.4
55	ABC	3836.2	3836.2	3644.4	3644.4	3512.5	3512.5
56	ABC	3617.9	3617.9	3427.2	3427.2	3296.6	3296.6
57	ABC	3720.7	3720.7	3610.8	3610.8	3470.5	3470.5
60	ABC	3126.8	3126.8	3126.7	3126.7	2979.9	2979.9
160	ABC	3126.8	3126.8	3126.7	3126.7	2979.9	2979.9
67	ABC	2909.8	2909.8	2923.4	2923.4	2812.1	2812.1
72	ABC	2759.2	2759.2	2794.4	2794.4	2680.5	2680.5
76	ABC	2659.1	2659.1	2707.4	2707.4	2592.2	2592.2
77	ABC	2479.2	2479.2	2532.7	2532.7	2446.5	2446.5
78	ABC	2437.9	2437.9	2492.5	2492.5	2412.6	2412.6
79	ABC	2349.9	2349.9	2406.5	2406.5	2339.6	2339.6
80	ABC	2259.3	2259.3	2317.6	2317.6	2263.4	2263.4
81	ABC	2105.0	2105.0	2165.6	2165.6	2131.3	2131.3
82	ABC	2032.0	2032.0	2093.3	2093.3	2067.8	2067.8
83	ABC	1963.8	1963.8	2025.6	2025.6	2007.9	2007.9
86	ABC	2359.4	2359.4	2441.0	2441.0	2324.0	2324.0
87	ABC	2199.9	2199.9	2281.2	2281.2	2192.1	2192.1
89	ABC	2112.6	2112.6	2193.4	2193.4	2118.5	2118.5
91	ABC	2046.2	2046.2	2126.4	2126.4	2061.9	2061.9
93	ABC	1983.8	1983.8	2063.4	2063.4	2008.2	2008.2
95	ABC	1906.3	1906.3	1985.0	1985.0	1940.7	1940.7
97	ABC	2772.2	2772.2	2805.6	2805.6	2691.9	2691.9
197	ABC	2772.2	2772.2	2805.6	2805.6	2691.9	2691.9
101	ABC	2647.1	2647.1	2696.9	2696.9	2581.5	2581.5
105	ABC	2521.8	2521.8	2586.5	2586.5	2470.1	2470.1
108	ABC	2388.2	2388.2	2467.0	2467.0	2350.1	2350.1
300	ABC	2053.4	2053.4	2159.5	2159.5	2044.1	2044.1
98	ABC	2635.2	2635.2	2686.5	2686.5	2571.0	2571.0
99	ABC	2398.0	2398.0	2475.8	2475.8	2358.9	2358.9

Table A.11: LL Fault currents in Amps for IEEE 123 bus system(cont.)

Node	Phase	LL (AB)		LL (BC)		LL (CA)	
		A	B	B	C	A	C
100	ABC	2285.8	2285.8	2374.1	2374.1	2257.2	2257.2
450	ABC	2032.0	2032.0	2139.5	2139.5	2024.4	2024.4
61	ABC	2845.9	2845.9	2798.6	2798.6	2699.3	2699.3
611	ABC	2845.9	2845.9	2798.6	2798.6	2699.3	2699.3
610	ABC	4301.1	4301.1	4288.9	4288.9	4262.1	4262.1
62	ABC	2963.4	2963.4	2963.3	2963.3	2818.6	2818.6
63	ABC	2854.3	2854.3	2854.3	2854.3	2711.8	2711.8
64	ABC	2650.6	2650.6	2650.5	2650.5	2513.7	2513.7
65	ABC	2429.1	2429.1	2429.1	2429.1	2300.4	2300.4
66	ABC	2278.1	2278.1	2278.0	2278.0	2155.7	2155.7
18	ABC	3908.8	3908.8	3742.5	3742.5	3790.9	3790.9
135	ABC	3908.8	3908.8	3742.4	3742.4	3790.9	3790.9
35	ABC	3577.0	3577.0	3465.6	3465.6	3457.3	3457.3
36	AB	3088.3	3088.3	-	-	-	-
40	ABC	3403.0	3403.0	3285.4	3285.4	3265.5	3265.5
42	ABC	3244.9	3244.9	3122.9	3122.9	3093.8	3093.8
44	ABC	3128.4	3128.4	3003.9	3003.9	2968.8	2968.8
48	ABC	2910.8	2910.8	2798.2	2798.2	2746.7	2746.7
49	ABC	2857.8	2857.8	2754.0	2754.0	2696.2	2696.2
50	ABC	2733.5	2733.5	2649.3	2649.3	2577.8	2577.8
51	ABC	2619.5	2619.5	2552.1	2552.1	2469.3	2469.3
151	ABC	2417.7	2417.7	2377.5	2377.5	2277.6	2277.6
21	ABC	3638.8	3638.8	3477.6	3477.6	3560.3	3560.3
23	ABC	3440.5	3440.5	3283.8	3283.8	3388.1	3388.1
25	ABC	3245.7	3245.7	3093.9	3093.9	3216.7	3216.7
28	ABC	3117.2	3117.2	2969.0	2969.0	3102.4	3102.4
29	ABC	2942.4	2942.4	2799.3	2799.3	2945.2	2945.2
30	ABC	2761.5	2761.5	2624.2	2624.2	2780.5	2780.5
250	ABC	2667.8	2667.8	2533.6	2533.6	2694.3	2694.3
26	AC	-	-	-	-	2987.6	2987.6
27	AC	-	-	-	-	2829.2	2829.2

Table A.12: LLG Fault currents in Amps for IEEE 123 bus system

Node	Phase	LLG (AB)G		LLG (BC)		LLG (CA)	
		A	B	B	C	A	C
650	ABC	12311.4	13093.8	12311.4	13093.8	13093.8	12311.4
150	ABC	8445.9	8449.7	8445.9	8449.7	8449.7	8445.9
149	ABC	8445.9	8449.7	8445.9	8449.7	8449.7	8445.9
1	ABC	6992.0	6899.2	6970.9	6781.9	6721.5	6913.0
7	ABC	6206.9	6139.0	6164.0	5969.1	5879.7	6081.9
8	ABC	5778.1	5732.7	5722.9	5539.9	5437.2	5630.4
13	ABC	5238.2	5224.1	5168.7	5009.2	4893.3	5066.3
152	ABC	5238.2	5224.1	5168.7	5009.2	4893.3	5066.3
52	ABC	4660.1	4678.8	4578.1	4449.2	4324.0	4469.2
53	ABC	4417.0	4448.3	4330.7	4215.4	4087.8	4220.4
54	ABC	4277.6	4315.7	4189.3	4081.7	3953.2	4078.6
55	ABC	4000.2	4050.7	3908.4	3816.1	3686.8	3797.7
56	ABC	3756.7	3816.7	3662.9	3583.5	3454.5	3553.0
57	ABC	3895.8	3923.9	3851.2	3784.4	3639.5	3744.1
60	ABC	3269.1	3285.6	3286.2	3274.8	3113.3	3185.0
160	ABC	3269.1	3285.6	3286.2	3274.8	3113.3	3185.0
67	ABC	3038.4	3055.6	3064.0	3060.7	2934.7	2990.4
72	ABC	2880.1	2895.2	2918.2	2925.9	2795.7	2844.4
76	ABC	2775.0	2788.7	2820.7	2835.1	2702.6	2746.9
77	ABC	2584.3	2599.0	2633.3	2651.6	2549.2	2581.9
78	ABC	2540.7	2555.5	2590.3	2609.4	2513.5	2543.7
79	ABC	2447.7	2462.8	2498.5	2519.1	2436.9	2461.8
80	ABC	2352.0	2367.4	2403.8	2425.9	2357.0	2376.9
81	ABC	2189.3	2205.1	2242.3	2266.6	2218.9	2230.9
82	ABC	2112.4	2128.3	2165.6	2190.8	2152.6	2161.0
83	ABC	2040.7	2056.7	2094.1	2120.0	2090.1	2095.4
86	ABC	2460.3	2470.9	2525.6	2557.1	2420.7	2452.5
87	ABC	2291.6	2303.3	2356.7	2389.4	2282.5	2304.7
89	ABC	2199.4	2211.6	2264.1	2297.2	2205.5	2222.9
91	ABC	2129.3	2141.8	2193.6	2227.0	2146.3	2160.2
93	ABC	2063.5	2076.4	2127.4	2160.9	2090.2	2100.9
95	ABC	1981.9	1995.0	2045.0	2078.7	2019.8	2026.9
97	ABC	2893.8	2909.0	2930.9	2937.7	2807.7	2857.1
197	ABC	2893.8	2909.0	2930.9	2937.7	2807.7	2857.1
101	ABC	2762.3	2776.0	2808.9	2824.1	2691.4	2735.2
105	ABC	2630.8	2643.0	2686.1	2708.9	2574.1	2612.5

Table A.13: LLG Fault currents in Amps for IEEE 123 bus system(cont.)

Node	Phase	LLG (AB)		LLG (BC)		LLG (CA)	
		A	B	B	C	A	C
108	ABC	2490.6	2501.4	2554.2	2584.3	2448.1	2481.0
300	ABC	2139.5	2147.5	2219.2	2263.7	2127.7	2148.3
98	ABC	2749.8	2763.3	2797.3	2813.2	2680.3	2723.5
99	ABC	2500.8	2511.8	2563.9	2593.5	2457.3	2490.6
100	ABC	2383.1	2393.0	2452.3	2487.4	2350.7	2379.6
450	ABC	2117.1	2125.0	2197.6	2242.8	2107.0	2126.9
61	ABC	2961.8	2984.2	2934.0	2929.5	2818.7	2866.9
611	ABC	2961.8	2984.2	2934.0	2929.5	2818.7	2866.9
610	ABC	4779.3	4834.1	4779.6	4819.0	4788.1	4772.1
62	ABC	3098.5	3107.9	3117.9	3095.6	2937.3	3015.6
63	ABC	2984.3	2990.2	3004.6	2977.4	2821.8	2902.6
64	ABC	2770.0	2771.9	2791.4	2758.8	2609.4	2691.8
65	ABC	2536.5	2536.5	2557.9	2524.1	2382.9	2463.2
66	ABC	2377.1	2376.9	2398.1	2365.3	2230.5	2307.8
18	ABC	4133.5	4117.4	4036.4	3927.1	3992.8	4047.3
135	ABC	4133.5	4117.4	4036.4	3927.1	3992.8	4047.3
35	ABC	3766.2	3761.7	3708.5	3626.6	3635.2	3676.9
36	AB	3240.1	3242.3	-	-	-	-
40	ABC	3567.2	3576.9	3505.8	3434.2	3429.0	3467.4
42	ABC	3388.3	3409.6	3324.1	3261.4	3245.2	3280.4
44	ABC	3257.7	3286.6	3191.8	3135.3	3111.8	3144.7
47	ABC	3108.1	3144.9	3040.5	2990.8	2959.8	2990.0
48	ABC	3019.5	3056.8	2961.9	2917.9	2876.1	2903.4
49	ABC	2963.2	3000.8	2911.8	2871.2	2823.0	2848.4
50	ABC	2831.1	2869.4	2793.7	2760.9	2698.3	2719.6
51	ABC	2710.3	2749.0	2684.9	2658.8	2584.1	2601.9
151	ABC	2497.0	2536.2	2491.1	2475.8	2382.6	2394.6
21	ABC	3838.3	3824.9	3738.3	3642.8	3745.4	3774.0
23	ABC	3622.5	3611.4	3521.5	3435.8	3561.9	3573.5
25	ABC	3411.4	3402.8	3310.2	3234.0	3380.0	3376.5
28	ABC	3272.6	3265.7	3171.8	3101.5	3259.1	3246.5
29	ABC	3084.2	3079.7	2984.6	2922.1	3093.2	3069.5
30	ABC	2890.1	2888.0	2792.3	2737.5	2919.8	2886.1
250	ABC	2789.7	2788.8	2693.1	2642.2	2829.2	2790.9
26	AC	-	-	-	-	3135.3	3133.2
27	AC	-	-	-	-	2966.6	2965.2